IMPERIAL COLLEGE OF SCIENCE, TECHNOLOGY AND MEDICINE
UNIVERSITY OF LONDON

Identification of Cracks in Operating Rotors via Vibration Analysis

by

Jeonghoon Kim

A thesis submitted for the degree of Doctor of Philosophy
of University of London and for the
Diploma of Imperial College

May 2000

DYNAMICS SECTION
MECHANICAL ENGINEERING DEPARTMENT

Abstract

The research described in this thesis deals with the development of new crack detection methods based on vibration analysis for operating rotor systems with a transverse crack.

The thesis starts with a brief review of past investigations regarding the cracked rotor problem. According to this, most of the existing crack detection strategies have been focused on dealing with transient vibration data to detect a crack as more information is available in transient operating conditions than in steady state. During a run-up (or run-down) period, sub-resonances caused by crack-induced harmonic components have been monitored with a view to detecting a crack. However, in analysing the transient data, the existing methods based on signal processing techniques impose unwanted resolution problems in both time and frequency domains, as discussed in the thesis. For steady-state conditions, the possibility of crack detection has always been limited mainly by relying on the inspection of 2Ω harmonic component caused by a crack, although considerable $\pm 1\Omega$ vibrations are also induced in the cracked rotor systems.

Following the review, comparative research on the dynamic behaviour of cracked rotors and equivalent normal rotor systems with various different configurations is presented to provide a better understanding of the problem.

To form the basis for an improved crack detection strategy, a multi-degree-of-freedom (MDOF) rotor system with a transverse crack has been modelled based on the finite element method (FEM), and its dynamic characteristics have been investigated for both transient and steady-state conditions. In particular, effects of various vibration measurement positions and crack locations have been investigated.

Based on the predicted results obtained from the mathematical models, improved crack detection techniques have been developed for measurements made under both transient and steady-state running conditions. For transient-state vibrations, a new

directional harmonic wavelet transform (DHWT) technique has been introduced and developed together with the existing versatile tool for time-frequency analysis, i.e. short-time Fourier transform (STFT). For steady-state conditions, a new directional-difference vibration signature analysis (DDVSA) has been developed as an improved technique for this operating condition.

The enhanced performance of these new techniques has been shown via experiments with a 2-disk cracked rotor system. For transient data, the crack-induced resonances have been accurately detected by applying the DHWT, and for steady-state data, DDVSA enables the isolation of crack-related harmonic components, leading to reliable crack detection. In both methods, the performance has been greatly enhanced by decomposing the vibration components from rotating machinery into co- and counter-rotating components, which is a major feature that enables one to overcome the limitations of existing conventional methods.

Finally, the field-applicability of the developed methods has been confirmed by demonstrating the improved performance with the vibration data (simulated) of an industrial 250 MW high & intermediate pressure (HIP) steam turbine rotor model, where the fluid-film bearings play an important role in vibration characteristics due to strong bearing stiffness anisotropy and substantial damping.

Throughout the research, it is concluded that the developed MDOF cracked rotor models are capable of accurately predicting the dynamic behaviour of cracked rotor systems, and the cracks in operating rotors can be identified reliably by applying the improved crack detection techniques (DHWT & DDVSA).

Acknowledgements

I am very grateful to my supervisor, Professor D. J. Ewins, for his encouragement, interest, stimulus, and guidance throughout this project. It was due to his initiatives and valuable instructions that helped me to develop this work.

Thanks go to all members of the staff in Dynamics Section who helped me so much during these years. Also, I would like to thank my colleagues who provided friendly cooperations and useful discussions throughout the period of this research.

Special thanks are due to my parents in Seoul, my wife Heesook, and two sons Dongheon and Taeheon, for their love and sacrifices. Without their love, this thesis would have not been completed.

Finally, I would like to thank Korea Electric Power Corporation (KEPCO) and GEC ALSTHOM for their joint financial support, and the British Council for the sincere administrative supports.

Nomenclature

Basic Terms and Dimensions

x, y, z	translational displacements/coordinates in inertial frame of reference
χ, ξ, η	translational displacements/coordinates in rotating frame of reference
q	generalised coordinate
N	total number of degrees of freedom/coordinates
ω ; f	frequency of vibration (in rad/s ; Hz)
t	time
T	period ($T = 1/f$)
Ω	speed of rotation
i	$\sqrt{-1}$

Super- and Subscripts

*	complex conjugate
i, j, k	integers
f, b	forward, backward direction

Prefixes

$+, -$	forward, backward direction

Matrices, Vectors, and Scalars

$[\ ]$	matrix
$[\ ]^{-1}$	inverse of a matrix
$[\ ]^{T}$	transpose of a matrix
$\boldsymbol{M}$	mass matrix
$\boldsymbol{K}$	stiffness matrix
$\boldsymbol{C}$	damping matrix
$\boldsymbol{G}$	gyroscopic matrix

A	cross-sectional area
C_a, C_m	assembled, machined bearing clearance
D	diameter
E	Young's modulus
F	excitation force
I	transverse moment of inertia of a cross-sectional area
J	polar moment of inertia of a cross-sectional area
L	length
Q	generalised force
S	magnitude of harmonic frequency component
S_o	Sommerfeld number
T	kinetic energy (in Chapter 3)
V	strain energy (or elastic potential energy)
W	(i) virtual work (in Chapter 3), or (ii) bearing load (in Chapter 6)
a	crack depth
r	radius
$h(t)$	breathing function of a crack
α	phase angle
ζ	damping factor
ρ	density
γ	stiffness reduction ratio
ε	eccentricity
ϵ	journal eccentricity ratio
ϕ	attitude angle
μ	viscosity of lubricant (in Pa·s)

Abbreviations

DHWT	directional harmonic wavelet transform
DDVSA	directional-difference vibration signature analysis

Table of Contents

Title 1
Abstract 2
Acknowledgements 4
Nomenclature 5
Table of Contents 7

Chapter 1 Introduction 10
1.1 Introduction 10
1.2 Definition of the Cracked Rotor Problem 13
1.3 Literature Review 15
1.3.1 Dynamic Models of Cracked Rotor Systems 15
1.3.2 Existing Crack Detection Methods 17
1.3.3 Concluding Remarks 23
1.4 Scope of the Thesis 24

Chapter 2 Simple Rotor System with a Transverse Crack 26
2.1 Introduction 26
2.2 Whirl in Rotating Machinery 27
2.3 The Equations of Motion of a Cracked Rotor System 30
2.3.1 The Breathing Crack Model 31
2.3.2 The Open Crack Model 37
2.4 Vibration Response Analysis 38
2.4.1 Transient-State Vibration Response Analysis 40
2.4.2 Steady-State Vibration Response Analysis 51
2.5 Conclusions 59

Chapter 3 MDOF Rotor System with a Transverse Crack 60
3.1 Introduction 60
3.2 Modelling a MDOF Cracked Rotor System via the Finite Element Approach 61
3.2.1 Shaft 62
3.2.2 Disk 65

3.2.3 Bearings 66
3.2.4 Mass Unbalance 66
3.2.5 Transverse Crack 67
3.2.6 System Equations of Motion 72
3.3 Vibration Response Analysis 74
3.3.1 Transient-State Vibration Response Analysis 76
3.3.2 Steady-State Vibration Response Analysis 82
3.4 Conclusions 92

Chapter 4 Improved Crack Detection Techniques 94
4.1 Introduction 94
4.2 Spectral Analysis 95
4.2.1 Fourier Analysis 95
4.2.2 Considerations on Digital Signal Processing 98
4.2.2.1 Sampling 99
4.2.2.2 Windowing 100
4.3 Transient State 102
4.3.1 Short-Time Fourier Transform 102
4.3.2 Wigner Distribution 104
4.3.3 Directional Harmonic Wavelet Transform (DHWT) 107
4.4 Steady State 120
4.4.1 The FFT for Complex-valued Data 120
4.4.2 Directional-Difference Vibration Signature Analysis (DDVSA) 124
4.5 Conclusions 128

Chapter 5 Experimental Studies 129
5.1 Introduction 129
5.2 Experimental Test Rig 130
5.2.1 Modified Rotor Assembly 131
5.2.2 Slotted Shaft for Simulating Cracked Condition 131
5.3 Instrumentation 132
5.3.1 Non-contact Displacement Transducers 134
5.3.2 Data Acquisition and Signal Processing Equipment 138
5.4 Modal Testing of the Rotor Rig 141
5.4.1 Test Model 141

5.4.2 Test Instrumentation and Set-up 143
5.4.3 Test Procedure 143
5.4.4 Modal Analysis 144
5.5 Experimental Procedures and Results 146
5.5.1 Effect of Crack Extent 146
5.5.2 Effect of Crack Location 155
5.5.3 Application of New Methods 158
5.5.4 Effect of Unbalance on the Cracked Rotor System 166
5.6 Conclusions 173

Chapter 6 Industrial Application Case Study 176
6.1 Introduction 176
6.2 Model Description 177
6.3 Fluid-Film Bearing Characteristics 180
6.3.1 Static Equilibrium of Journal supported by Fluid-Film Bearings 180
6.3.2 Linearised Bearing Force Coefficients 182
6.3.3 Characteristics of Elliptical Bearing 184
6.4 Effect of Fluid-Film Bearings on Rotor Dynamics 187
6.5 Transient Vibration 191
6.6 Steady Vibration 195
6.7 Conclusions 198

Chapter 7 Conclusions 200
7.1 Conclusions 200
7.2 Summary of Comparison with Existing Methods 204
7.3 List of Contributions 205
7.4 Recommendations for Further Research 208

References 209

Chapter 1
Introduction

1.1 Introduction

The research described in this thesis deals with the development of new crack detection methods based on vibration analysis for operating rotor systems with a transverse crack.

Rotating machinery represented by turbines or generators are categorised as **critical machinery** within an operating power plant (refer to Fig 1.1.1 & 1.1.2) as the plant cannot function without these machines in most cases. As there are usually no spare units available for these machines, any unexpected operating problem can lead to huge economic loss. Generally, rotating machines are subject to several types of malfunction (refer to Fig 1.1.3) that range from internal forcing functions due to self-excitation mechanisms, to external forces that may impose dynamic loads upon the machinery. These various excitations are common for all working machine elements, and they affect the dynamic behaviour of specific parts of the machinery. If the forces due to these excitations increase beyond normal conditions, the integrity of the equipment is significantly affected. In this regard, machines of this class are typically equipped with permanently-installed proximity probe transducer systems for vibration measurements (together with other transducer systems for measuring temperature, pressure, etc) to monitor the mechanical condition of the machinery and to warn of any anticipated problems.

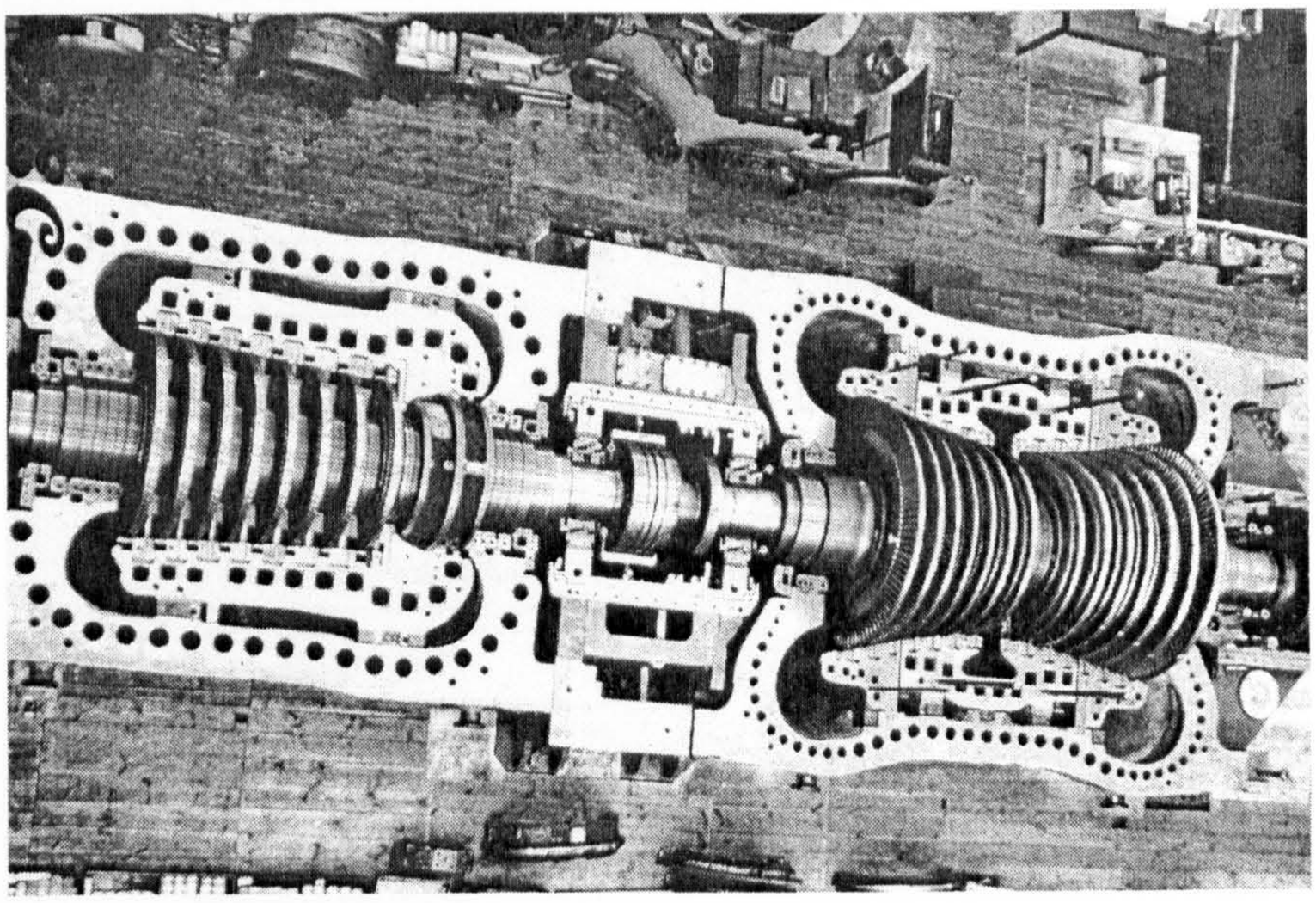


Fig 1.1.1 Rotor System for Power Generation: In Overhaul [from GEC]

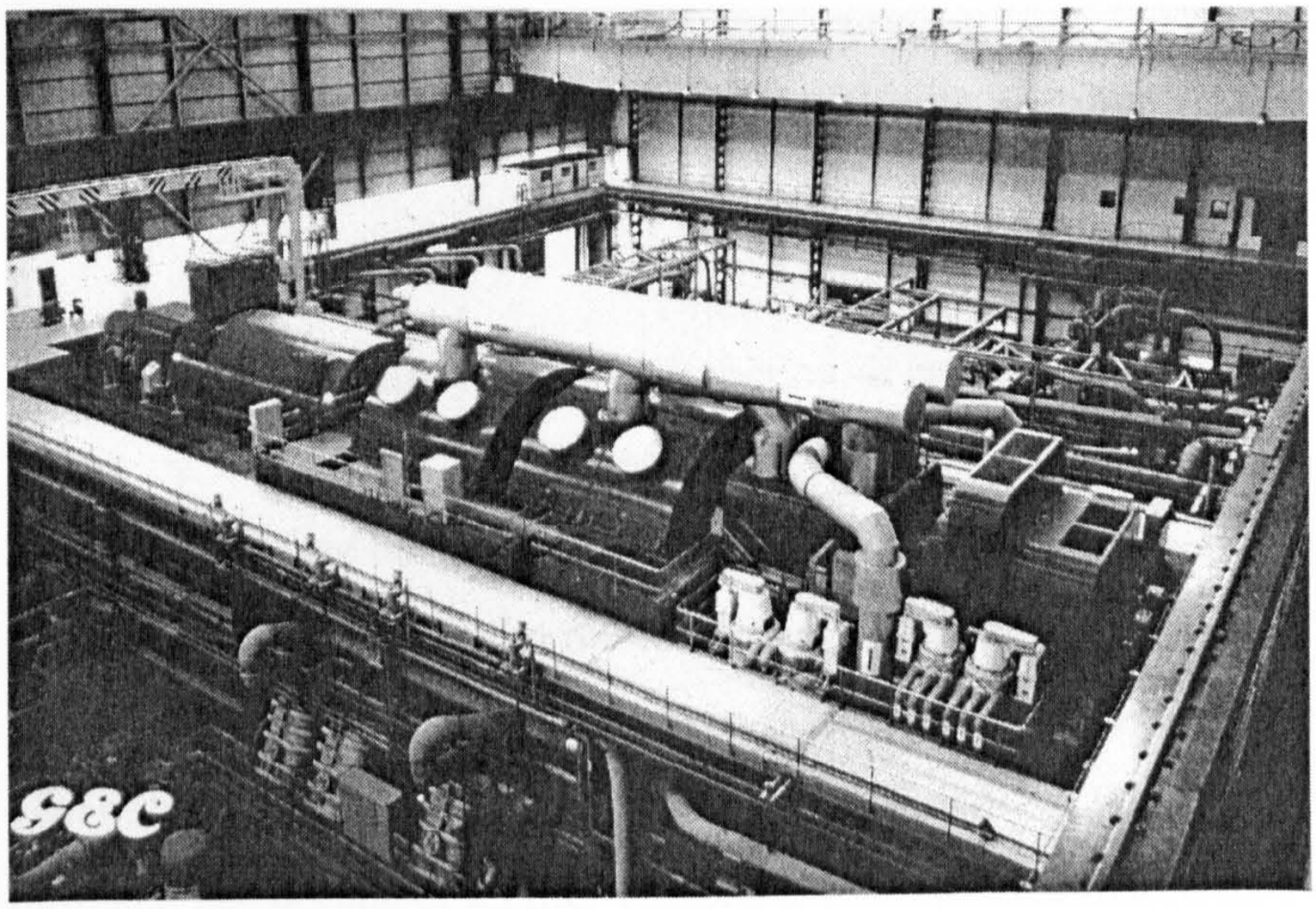


Fig 1.1.2 Rotor System for Power Generation: In Operation [from GEC]

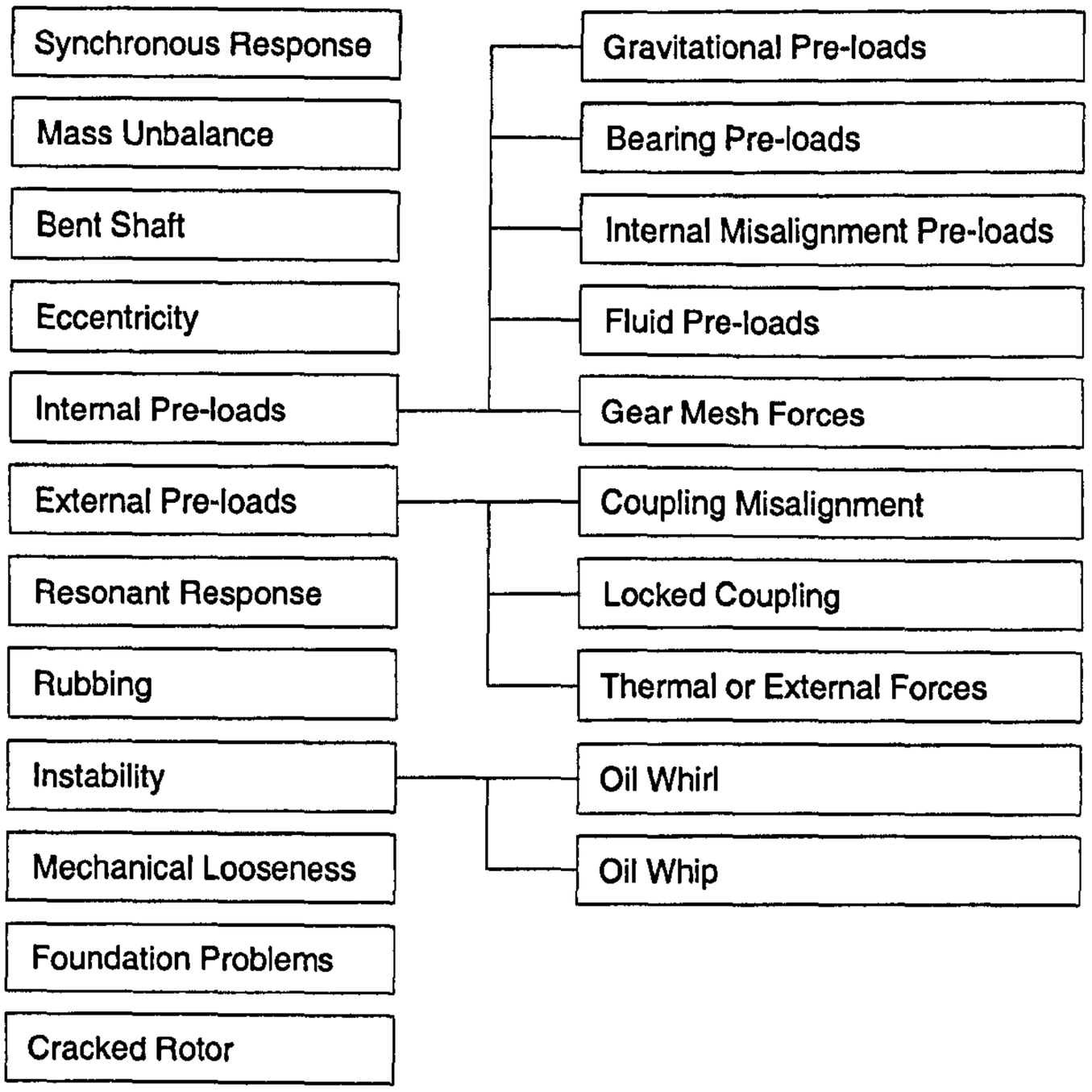


Fig 1.1.3 Vibration Problems in Rotating Machinery

Among these various types of malfunction, a cracked rotor can lead to catastrophic failure if undetected during normal operating conditions. Consequently, crack detection has long been regarded as a critical need by the power industry. Although it can be argued that cracks in rotors are rare phenomena, still, cracks sometimes occur in new rotors after only a few months of operation. Most turbomachinery for power generation has a design life of 30 years and the bulk of this equipment is now in the third and last decade of its life. Therefore, it is expected that fatigue cracks can be one of the major causes of machine failure in this coming decade. As an industrial case history on cracked rotor problems, there were at least 6 major types of shaft cracks on

large turbo-units in the CEGB (Central Electricity Generating Board) during the 10 years (1975-1984). These have not been confined to one plant design, or to either old or new plant. CEGB assumed the probability of a further cracked rotor, somewhere on a large unit to be 0.6/year. When considering the benefit-to-cost ratio in vibration monitoring for turbomachinery in power plants, CEGB provided 10:1 excluding the crack detection, and 17:1 including the crack detection, [140].

For modern complex rotor designs, the well-established non-destructive crack detection techniques such as the DC potential method and ultrasonic sound techniques [28] are impractical for field operations of turbomachinery. This is because such methods cannot clearly indicate the existence of a crack due to significant noise levels produced by multiple wave reflections from the complicated structural geometry of a rotor. Hence, condition monitoring based on vibration measurement has, certainly, the greatest potential since it can be executed without dismantling any part of the machine and usually without even taking the machine out of operation.

1.2 Definition of the Cracked Rotor Problem

Cracks in rotors are initiated from the coupled influence of tensile loads, varying stresses, and plastic strains that eventually cause micro- and macro-structural discontinuities. Also, high- and low-cycle fatigues, creep, and stress corrosion are considered to be important crack-propagating mechanisms.

In most cases, transverse cross-sectional cracks due to fatigue failures are found in high-speed and heavy-duty rotor shafts at some time during their life. Once the crack is initiated and increases to the extent that the bending stiffness is influenced, then the stiffness of the rotor will influence the dynamic behaviour of such a system.

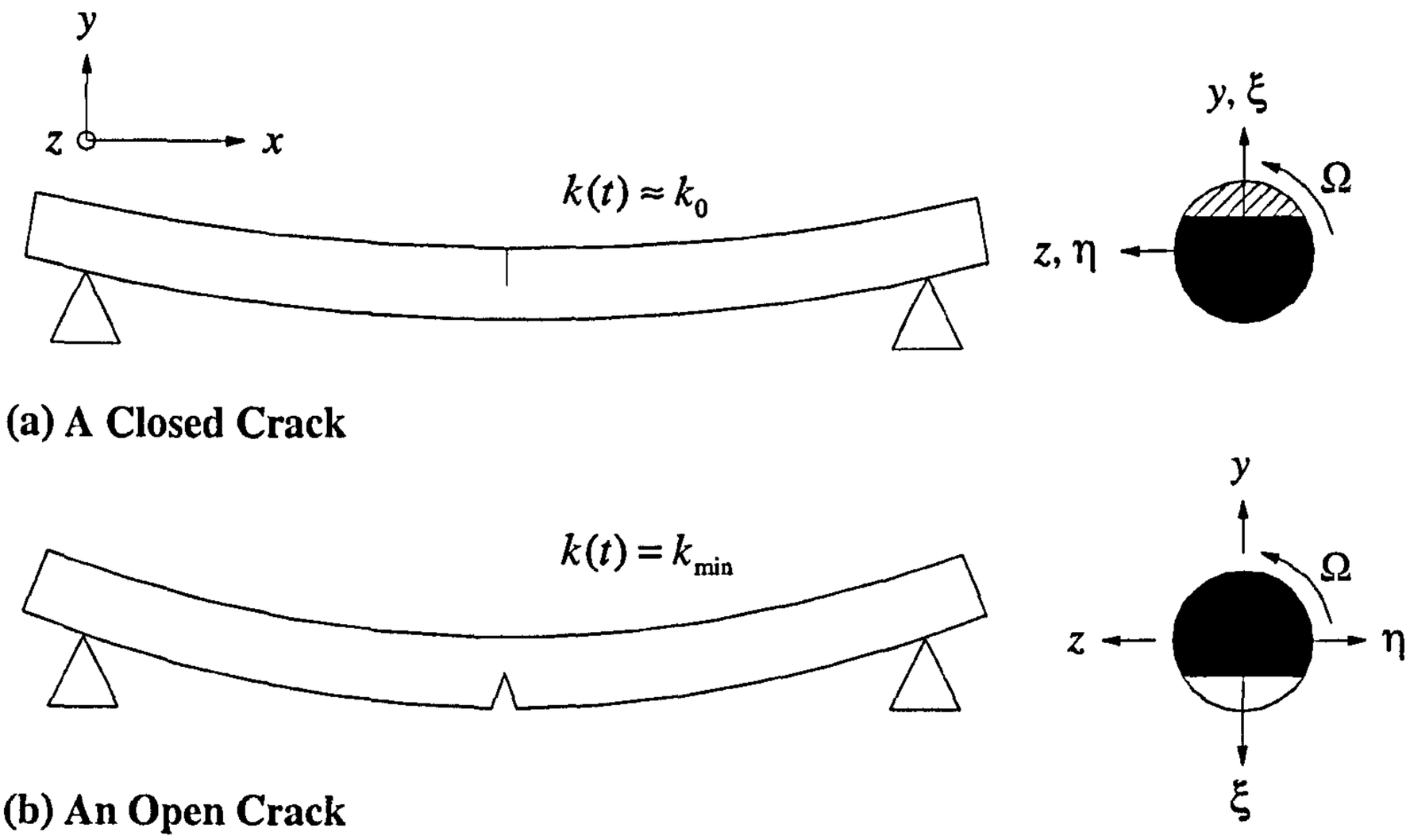


Fig 1.2.1 Breathing Crack in a Rotor

Fig 1.2.1 shows a simply-supported flexible shaft with a transverse cross-sectional crack. Let k_0 be the bending stiffness between 2 supports of the uncracked original shaft; the stiffness of the shaft is reduced because of the crack, and becomes time-dependent when the shaft rotates. When the crack is located at the 0° position relative to the y-axis, the cracked region is under compressive load caused by the self-weight of the shaft, and behaves as if it has no crack. As the shaft rotates, the crack becomes located in the 180° position. Due to the tension caused by the self-weight of the shaft, the cracked part opens and the stiffness of the shaft is reduced to its minimum value. This periodic closing and opening of the crack is called 'breathing' and causes a complicated non-linear dynamic behaviour of the rotor due to the continuously-varying effective stiffness of the rotor. However, this phenomenon also gives valuable information for the diagnosis of the cracked rotors, as will be discussed.

1.3 Literature Review

The field of monitoring rotating machinery vibrations to detect rotor cracks has been developed in parallel with investigations on the dynamics of cracked rotors. Also, the study on the dynamics of cracked rotors has been closely associated with the investigations on the dynamics of rotors with asymmetric shaft stiffness [141] as the cracked rotor system can be considered as an extended form of such rotor systems due to opening and closing of the cracked region causing time-varying stiffness. In an early paper in 1976, Gasch [42] modelled a breathing crack by a spring-loaded hinge. In spite of the fact that his crack model simplified the variation of stiffness to a step change, it still incorporates all the essential dynamics regarding flexural vibrations of cracked rotating structures. His simple but practical crack modelling approach has been adopted and applied, sometimes in modified form, by many subsequent researchers.

1.3.1 Dynamic Models of Cracked Rotor Systems

The majority of analytical and experimental studies on cracked rotor systems have been performed basically with a Jeffcott rotor model (a simply-supported, massless flexible shaft carrying a rigid disk at mid-span) with various modifications. Probably, the main reason for this was the fact that, even for simple rotor systems, the dynamic behaviour of the system is very complicated due to the non-linearity caused by the 'breathing' effect of the crack.

Gasch [42], and Henry & Okah-Avae [59] incorporated the bending stiffness change due to a crack into the equations of motion. They considered the non-linear mechanism of a breathing crack of a Jeffcott rotor with different flexibilities for open and closed cases, described in body-fixed, rotating coordinates. By transforming to stationary coordinates, they obtained equations of motion with periodically time-

varying stiffness coefficients. On the other hand, Mayes & Davies [88] derived an approximate analytical estimation of the cracked region flexibility based on the virtual work method and worked directly in space-fixed coordinates. In order to obtain analytical solutions, they introduced some simplifications, especially with regard to the stiffness properties in stationary coordinates, which were considered as a time-periodic step function and also reported the first experimental results on the dynamics of cracked rotors.

Grabowski [49] applied a modal formulation to investigate the dynamic characteristics of single and coupled flexible rotors containing a transverse crack. By performing a numerical integration of the equations of motion, the independence of vibrations excited by the crack with the unbalance has been identified.

Inagaki et al [64] have used the transfer matrix method, modelling the crack open/close mechanism by a step function for the bending moment. The non-linear equations have been linearised using a Fourier series expansion for the step function. They concluded that their experimental results confirmed their theoretical predictions and that phase of unbalance with respect to the location of the crack is extremely important.

A finite element method study of the cracked rotor system was made by Nelson & Nataraj [97] to deal with practical rotor models. They formulated the system equations of motion in complex coordinate form and employed static condensation method to reduce the number of degrees of freedom. The presence of a crack in the elements has been considered as a parametrically exciting perturbation term. Since their work, the finite element method has become the major tool for analysing the multi-degree-of-freedom cracked rotor systems.

Based on the work of Papadopoulos & Dimarogonas [105], Theis [138] developed a finite crack element where the additional flexibility of the shaft due to a crack is calculated via the energy release rate. Although it is mostly the flexural vibrations that are of primary concern, the finite crack element has a meaning in that it enables the vibration analysis of all degrees of freedom for cracked rotors. With this crack element, Seibold & Weinert [124] proposed a time-domain method for the localisation of cracks in rotors by applying an extended Kalman filter.

1.3.2 Existing Crack Detection Methods

• Crack Detection based on Changes in Modal Properties

It is a well-known fact that a crack reduces the stiffness of a structure by affecting a local flexibility, consequently reducing the natural frequency of the structure. Hence, attempts to detect cracks in structures naturally have been started by using changes in natural frequencies, [1, 12, 65]. This is also because an estimate of the natural frequency can be made from vibration measurement even at only one point of the structure. However, in spite of its relative convenience in measurement, natural frequency change is now known to be insufficient for most practical crack identification demands due to the limitation that the decrease in natural frequency is proportional to the square of ratio of crack depth to height of structure, [82]. Hence, complementarily, the use of dynamically-measured stiffness or its reverse i.e. flexibility matrix [57, 118], mode shape or its derivatives such as mode shape curvature [38, 101, 117, 126, 151], and non-linear effects of structures [83, 137] have been investigated and incorporated into crack (or damage) identification procedures.

In applying the frequency response functions for crack detection, the excitations are usually applied to different planes of the structures. Due to different stiffnesses in the orthogonal planes with the presence of a crack, reduced natural frequencies that differ

from the uncracked rotor natural frequencies have been used as an indication of a crack. For non-contact excitation, Joh & Lee [67] applied electromagnetic exciter to the rotating structure and they decomposed the frequency response function into forward and backward directional components to identify rotor stiffness asymmetry.

Among the modal properties, probably the damping has not been focused on due to the practical difficulties in measuring damping properties in operating rotor systems. However, it is known that the damping may increase in cracked structures [145], and this can be explained by the fact that the compressed crack faces induce dry friction, so an additional damping is introduced.

On the other hand, there have been attempts to detect a crack using external periodic forces [17, 66], although this method is mostly used in laboratory environments. In this method, an external periodic force of frequency ω_p is applied to a rotating rotor. Usually, a slow rotation speed (Ω) is adopted to reduce the effects of unbalance. The existence of a combination harmonics ($\Omega \pm \omega_p$) has been used to identify the cracked rotors.

Although some of these techniques have been successfully applied to detect cracks in non-rotating structures, unfortunately, most of them are not applicable to operating rotor systems due to the following problems:

(i) the rotor is not easily accessible for many measurement points required to describe its mode shapes,

(ii) in addition to the controlled excitation forces, intrinsic excitation forces exist in the operational system. The rotor response generated by the intended excitation must be separated from the overall response, and

(iii) measurements must be taken at speed because the dynamic properties of the rotor depends on speed.

• Crack Detection based on the Existence of Coupled Vibrations

According to fracture mechanics theory, a transverse crack in a structural member introduces local flexibility due to the strain energy concentration in the vicinity of the crack tip under load, [75]. With this concept, Papadopoulos & Dimarogonas [105], and Haisty et al [54] introduced a complete local flexibility matrix for a transverse crack on a shaft with arbitrary loading. Papadopoulos & Dimarogonas [103] also considered the off-diagonal terms in the local stiffness matrix obtained by inverse transforming the local flexibility matrix, and analysed for coupled longitudinal and bending vibrations of cracked rotating shaft. They concluded that the on-line analysis of the longitudinal vibration signal could yield valuable information for the development of surface cracks on rotors and shafts because the longitudinal vibration of such members was usually associated with a low level of noise.

The coupling of modes of vibration of a clamped-free Timoshenko shaft with a transverse crack was investigated analytically by Papadopoulos & Dimarogonas [104]. Coupling between the longitudinal, torsional, and bending vibrations caused by the non-diagonal terms of the local stiffness matrix was apparent in all spectra obtained with a harmonic excitation swept throughout the frequency range. Although the calculation results showed sensitive results even for small cracks, their work was confined to the clamped-free circular cross-sectional beam and no further work has been provided for the rotating structures.

The problem of coupled lateral/torsional vibrations due to shaft asymmetry with radial constant pre-load force was discussed by Muszynska et al [95]. The experimental results obtained on a laboratory rotor rig exhibited the existence of significant torsional vibrations due to coupling with the lateral modes. They concluded that the torsional vibrations, monitored along with lateral vibrations, were found to be useful

in early detection of cracked shafts even though the rotor had relatively thin and long rectangular cross-section in the mid-span to produce the coupling effect.

• Model-based Diagnosis

With the progress of the modelling techniques for complicated rotor systems, the concept of model-based diagnosis has been established recently, [96]. Using the pre-estimated fault symptoms usually obtained from analytical models, the model-based diagnosis aims to develop a method to detect, localise, and assess the damage, although for operating rotating machinery in particular, the localisation problem has long been regarded as virtually impossible mainly due to the relatively sophisticated geometry of the rotor than other engineering structures.

Probably the first model-based method for detecting cracks in rotors has been presented in 1993 by Söffker et al [135]. By using the state observer based on system information about normal rotor system, the specific non-linear crack excitation forces were reconstructed and compared with a predefined crack model to identify the damage. Seibold et al [123] presented crack detection procedures based on the extended Kalman filter, and the instrumental variables method. Also, a finite element model of the rotor was used to assess the severity of the crack. Seibold [122] extended this work further to localise the position of the crack along the shaft-line. Model condensation technique has been used to reduce the size of the finite element model in order to avoid time-consuming computations. Bach & Markert [3] proposed a fault model-based method for identification of malfunctions in rotor systems by using equivalent loads, or fault models representing the specific malfunctions, such as an unbalance or a transverse crack. They established the procedures of reconstructing the state of a system with limited measured data using a state observer based on the undamaged linear rotor model. The suggested method was tested on simulated

vibration data from a cracked shaft with simple geometry to identify the position and the extent of the crack.

Conventionally, the dynamic modelling techniques have been developed for the purpose of predicting the vibration behaviour of structures, but probably not for the diagnostic use. However, with the developments in system identification techniques and the successful modelling of some interaction effects between the rotor and stator, the possibility of model-based diagnostics of rotating machinery is now emerging.

• Crack detection based on Vibration Signatures

Vibration signature analysis is by far the most widely-accepted methodology for detecting cracked rotors. This is hardly surprising, considering the fact that most turbomachinery is equipped with standard vibration measurement instrumentation for condition monitoring of these expensive machines. The technique involves acquiring vibration data from the machine under normal operating conditions, and subsequent spectral analysis. With a view to detecting a cracked rotor, vibration signatures for the suspect case are compared to those of a normal rotor. Initial appearances of specific symptoms related with cracks have been specifically monitored. Among many symptoms related with cracked rotors, the most representative vibration symptoms are:

(i) the existence of harmonics, which is usually applied in steady-state crack detection methods, and

(ii) due to the existence of harmonics, the subsequent resonances and changes in phase angle in the resonance regions during run-up or run-down period of a rotor system, which are applied in transient-state crack detection methods.

Generally, most of the detection strategies have been focused on dealing with transient vibration data [4, 20, 27, 41, 49, 58, 64, 87, 97, 103, 121, 127] to detect a crack as

more information is available in transient operating conditions than in steady state. Customarily, the vibrational behaviour during run-up or run-down operations of rotating machinery is recorded and plotted in a time-frequency domain [16, 56] by applying short-time Fourier transform [2] or Wigner distribution [92], sometimes in the form of Campbell diagram [45], with a view to monitoring the structural health condition of the machinery. In particular, to get more sensitive measures for the presence of a crack, Gasch [41] proposed the inspection of harmonic components in rotor vibration response decomposed into forward and backward whirl directions. For a simple rotor system with a transverse crack, he investigated analytically both forward whirl and backward whirl components of the shaft orbit and suggested a strong backward whirl component (-1Ω vibration) excited by the crack as an important hint to the existence of a crack. Bucher et al [10] developed an improved method for the decomposition and visualisation of transient vibration signals measured on rotating structures using signals obtained from several sensors. With the analytical demonstration with a cracked Jeffcott rotor, they confirmed the existence of a crack via a forward/backward directional Campbell diagram.

On the other hand, crack detection methods in the steady-state running condition [61, 62, 71, 114] have been developed mainly based on the inspection of 2Ω harmonic component, although significant synchronous vibration is also generated by a crack, [41, 94]. Due to this, the possibility of crack detection has always been limited as the lack of parameters for crack identification caused an ambiguity problem with other types of faults such as misalignment.

In spite of modern developments in instrumentations, the fact still remains that crack detection using vibration signatures is by far the most applicable to industrial rotating machinery as the available instrumentations are quite limited on those machines. Also, this methodology can be applied in an 'on-line' condition which is an essential requirement for most process industry represented by power generation. However, the

fault diagnosis must be made very carefully to assure that the other fault conditions are not incorrectly identified as a cracked rotor.

1.3.3 Concluding Remarks

The existing literature on crack detection methods can be briefly summarised as follows:

(i) Most of the research on cracked rotors has been dedicated to develop methods to predict and to detect the existence of a crack in the rotor via flexural vibration response analysis. This trend is based not only on the fact that the flexural modes are the lowest, and the existing forcing frequencies excite flexural vibrations much more easily than the longitudinal or torsional ones, but also because the possibility of high-amplitude flexural vibrations represents more dangerous modes for the machine integrity. However, it should be noted that the flexural vibration response is usually highly affected by inherent masking effects, mainly from the bearing damping, and the symptoms of a crack in the rotor during operation are very often similar to those of other common malfunctions.

(ii) Under the circumstances that up to now the vibration signature-based approaches are the most field-applicable, the existing crack detection strategies have been focused mainly on dealing with transient vibration data rather than in steady state. During a run-up (or run-down) period, sub-resonances caused by crack-induced harmonic components have been monitored with a view to detecting a crack. However, in analysing transient data, the existing methods based on signal processing techniques impose unwanted resolution problems in both time and frequency domains, as will be discussed in the relevant chapter here. For steady-state conditions, the possibility of crack detection has always been limited mainly by relying on the inspection of 2Ω harmonic component caused by a crack, although considerable $\pm 1\Omega$ vibrations are also induced in the cracked rotor systems.

1.4 Scope of the Thesis

To overcome the limitations identified from the existing techniques for crack detection in rotors, the following items need to be studied, and they form the basis of research in this thesis:

(i) thorough understanding of the vibration characteristics of cracked rotating structures,
(ii) practical modelling of cracked rotor systems which can accurately predict the dynamic behaviour of such systems, and
(iii) development of new crack detection method which is sensitive to the problem and unambiguous in diagnosing stage.

These tasks constitute the major elements of the research reported in this thesis, which is structured as follows:

In Chapter 2, comparative research on the dynamic behaviour of cracked rotors and equivalent normal rotor systems with various different configurations is presented to provide a thorough understanding of the problem.
In Chapter 3, a multi-degree-of-freedom (MDOF) rotor system with a transverse crack has been modelled based on the finite element method (FEM) and its dynamic characteristics have been investigated to form the basis for an improved crack detection strategy.
In Chapter 4, based on the predicted results obtained from the mathematical models developed in Chapter 3, improved crack detection techniques have been developed for measurements made under both transient and steady-state running conditions.
In Chapter 5, the performance of these new techniques has been evaluated via laboratory experiments with a 2-disk cracked rotor system.

In Chapter 6, the field-applicability of the developed methods has been verified using the vibration data (simulated) for an industrial 250 MW high & intermediate pressure (HIP) steam turbine rotor model.

Finally, in Chapter 7, a brief review of the research performed and overall conclusions are presented together with suggestions for further research.

It should be mentioned here that among various possible forms in the crack geometry, the cross-sectional transverse crack has been considered as it happens in most cases of cracked rotor incidents. Also, a study of *initiation* of crack has not been dealt with in this thesis as it is a separate subject in itself.

Chapter 2
Simple Rotor System with a Transverse Crack

2.1 Introduction

In this chapter, the dynamic characteristics of a simple rotor system with a transverse crack have been investigated to provide a basic understanding of the problem, i.e. cracked rotors in general.

Ahead of the main topic of cracked rotor problem, the whirl motion of a rotating machine will be introduced due to its importance as one of the most characteristic features in rotating machinery dynamics. Following this, the equations of motion of a cracked simple rotor system have been derived for both the breathing and open crack cases, including a comparison of existing crack models.

Using the Mayes & Davies' breathing crack assumption, vibration characteristics of the cracked simple rotor system have been investigated for both transient and steady-state running conditions. Moreover, various typical rotor systems with different physical configurations (rotor asymmetry, bearing anisotropy, etc) have been considered and compared with the cracked rotor case for thorough understanding of the cracked rotor problem.

2.2 Whirl in Rotating Machinery

Before considering the cracked rotor system, it seems appropriate to introduce the concept of rotor whirl as it is one of the most characteristic features of rotating structures.

The basic vibrational behaviour of a rotor system can be described by considering motion at certain nodes of the rotor, as illustrated in Fig 2.2.1. The vertical and horizontal displacement components of the motion (usually harmonic due to unbalance) with whirl frequency, Ω, are, respectively:

$$y(t) = c_1 \cos \Omega t + s_1 \sin \Omega t \tag{2.2.1}$$

$$z(t) = c_2 \cos \Omega t + s_2 \sin \Omega t \tag{2.2.2}$$

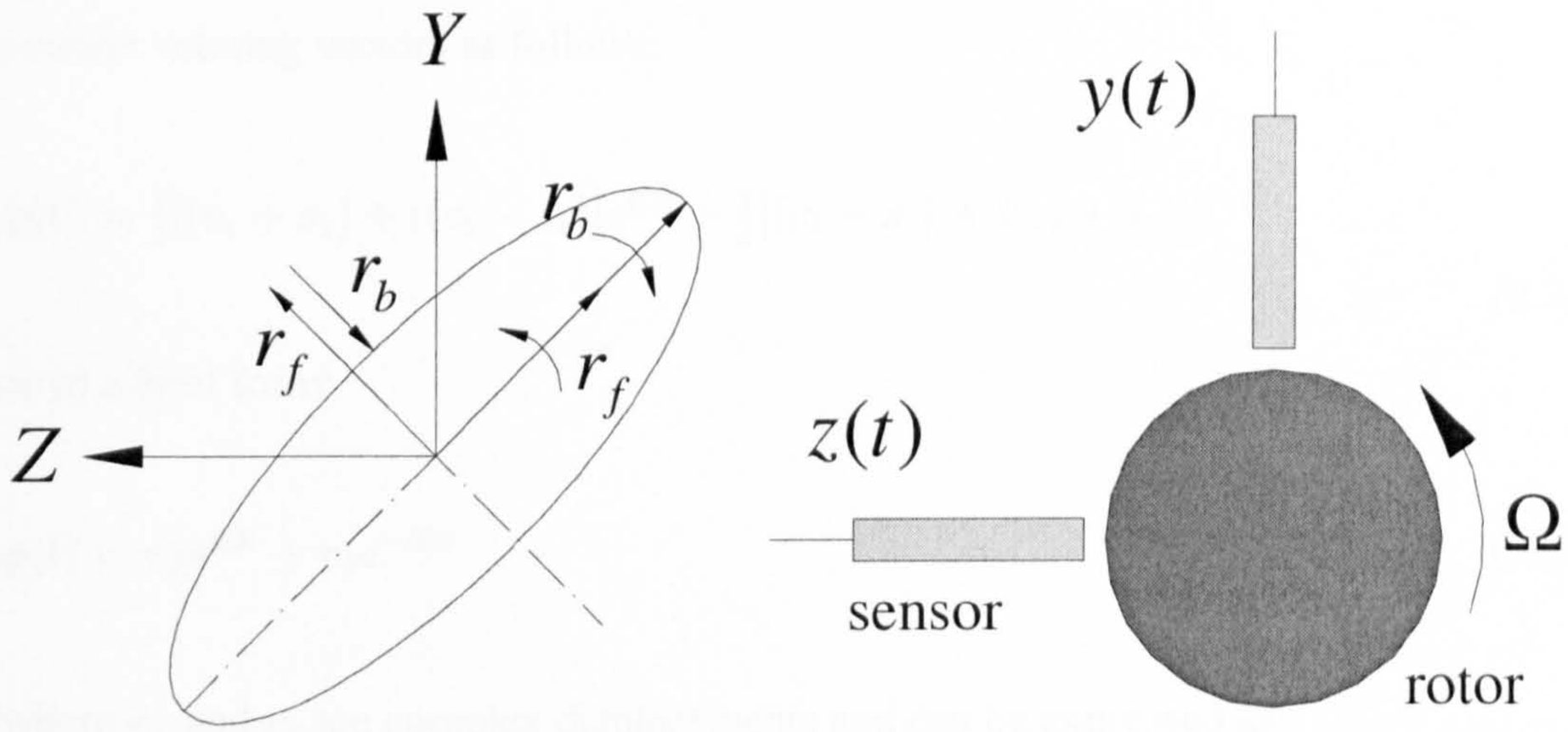


Fig 2.2.1 Elliptical Whirl Orbit of a Rotor

Together, the response components $y(t)$ and $z(t)$ describe an elliptical path, which can be either forward or backward relative to the direction of rotation of the rotor. To find the direction of rotation, the attitude angle, and the half-axes of the ellipse (in particular, the length of the semimajor axis, which has a practical importance of indicating largest possible clearance at certain nodal position), these vibration components need to be combined into one complex vector by considering the YZ plane as a complex plane with real axis along the Y-axis and imaginary axis along the Z-axis:

$$\boldsymbol{q}(t) = y(t) + iz(t) \tag{2.2.3}$$

Using equations (2.2.1) & (2.2.2) and the following relations (2.2.4) from Euler formula:

$$\sin \Omega t = -\tfrac{i}{2}(e^{i\Omega t} - e^{-i\Omega t}),\ \cos \Omega t = \tfrac{1}{2}(e^{i\Omega t} + e^{-i\Omega t}) \tag{2.2.4}$$

the elliptical orbit can be represented with the co-rotating (with shaft rotation) and counter-rotating vectors as follows:

$$\boldsymbol{q}(t) = \tfrac{1}{2}[(c_1 + s_2) + i(c_2 - s_1)]e^{i\Omega t} + \tfrac{1}{2}[(c_1 - s_2) + i(c_2 + s_1)]e^{-i\Omega t} \tag{2.2.5}$$

or in a brief form:

$$\boldsymbol{q}(t) = \boldsymbol{r}_f e^{i\Omega t} + \boldsymbol{r}_b e^{-i\Omega t} \tag{2.2.6}$$

where $\boldsymbol{r}_f$ and $\boldsymbol{r}_b$ are complex displacements and can be expressed as:

$$\boldsymbol{r}_f = |\boldsymbol{r}_f| e^{i\alpha} \tag{2.2.7}$$

$$\boldsymbol{r}_b = |\boldsymbol{r}_b| e^{i\beta} \tag{2.2.8}$$

each with magnitude and phase angle:

$$|r_f| = \tfrac{1}{2}\sqrt{(c_1 + s_2)^2 + (c_2 - s_1)^2}, \quad \alpha = \arctan\tfrac{c_2 - s_1}{c_1 + s_2}$$
$$|r_b| = \tfrac{1}{2}\sqrt{(c_1 - s_2)^2 + (c_2 + s_1)^2}, \quad \beta = \arctan\tfrac{c_2 + s_1}{c_1 - s_2}$$

In this format, it is convenient to recognise that the elliptical path consists of the summation of two rotating vectors r_f and r_b where the vector r_f rotates in the co-rotating (or forward whirl) direction and the other vector r_b rotates in the counter-rotating (or backward whirl) direction with same angular frequency Ω. Also, by estimating the relative magnitudes of two vectors, the dominating whirl direction of a shaft centre on the elliptical orbit against the shaft rotational direction can be identified, i.e.:

$|r_f| > |r_b|$ forward whirl orbit
$|r_f| < |r_b|$ backward whirl orbit
$|r_f| = |r_b|$ motion on a straight line

Most vibration signals commonly occurring in rotating machinery consist of the superposition of several elliptical vibrations of the general form (2.2.6):

$$q_k = r_{fk}e^{i\omega_k t} + r_{bk}e^{-i\omega_k t}, \quad k = 1, 2, \cdots, N \tag{2.2.9}$$

with the total response given by:

$$q = \sum_{k=1}^{N}(r_{fk}e^{i\omega_k t} + r_{bk}e^{-i\omega_k t}) \tag{2.2.10}$$

Generally, this total response is not periodic, nor is it an elliptical vibration. Also, simultaneous forward and backward whirls can exist on a rotor at different nodal positions for a given operating condition. In this case, the rotor moves along a straight line at the position of the change of whirl direction along the shaft-line.

2.3 The Equations of Motion of a Cracked Rotor System

Certainly, the simplest type of crack found in rotors is an open transverse crack, so that the stiffness of the shaft in a body-fixed (or rotating) coordinate system does not change. In this sense, the rotor with an open crack can be treated as a sort of asymmetrical rotor which has two different inertias in orthogonal axes. However, a real fatigue crack will have more complicated properties. As there would be almost no gap between the crack faces, so it will repeatedly open and close with the shaft rotation, especially in the case of heavy rotors such as those used in steam turbines for power generation. Hence, the crack will breathe with a certain form, sometimes referred to as the 'breathing (or switching) function'. As the breathing crack model needs to represent the more general case, it will be introduced ahead of the open crack model.

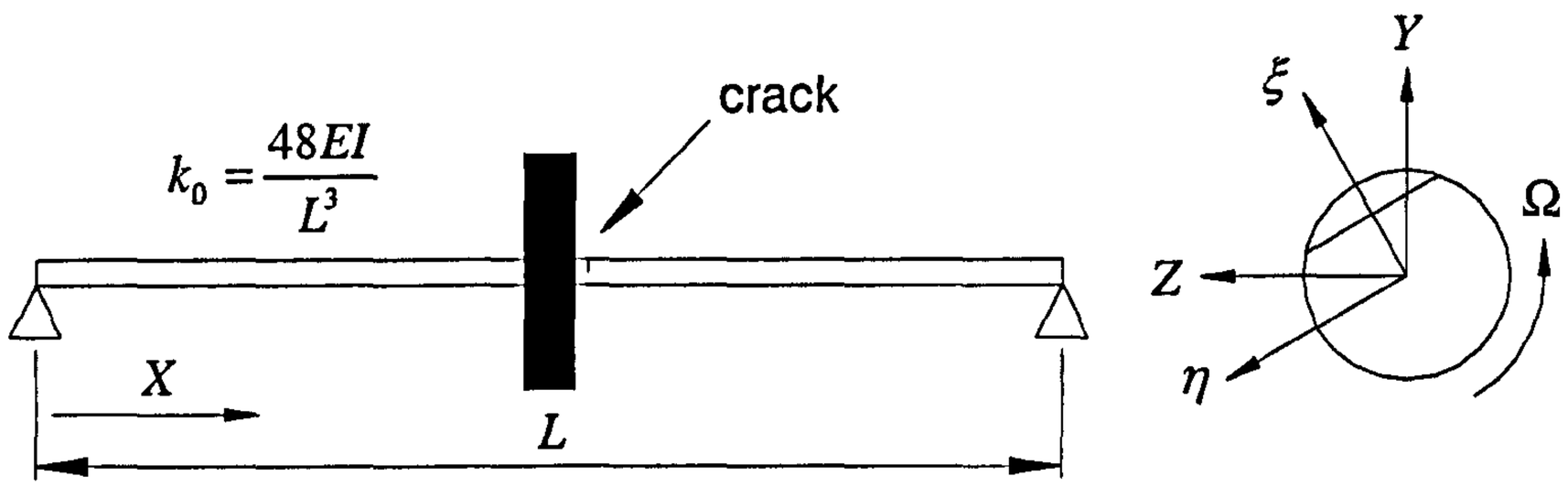


Fig 2.3.1 Simple Rotor System with a Transverse Crack

2.3.1 The Breathing Crack Model

For the cracked rotor system shown in Fig 2.3.1, the equations of motion without a crack will have the following form, defined in terms of stationary coordinate system X, Y, and Z:

$$\begin{bmatrix} m & 0 \\ 0 & m \end{bmatrix}\begin{bmatrix} \ddot{y} \\ \ddot{z} \end{bmatrix} + \begin{bmatrix} c & 0 \\ 0 & c \end{bmatrix}\begin{bmatrix} \dot{y} \\ \dot{z} \end{bmatrix} + \begin{bmatrix} k & 0 \\ 0 & k \end{bmatrix}\begin{bmatrix} y \\ z \end{bmatrix} = \begin{bmatrix} -mg \\ 0 \end{bmatrix}$$

$$+ m\varepsilon\Omega^2 \begin{bmatrix} \cos(\Omega t + \alpha) \\ \sin(\Omega t + \alpha) \end{bmatrix} \tag{2.3.1}$$

With a transverse crack, the stiffness of the shaft is reduced and is time-varying with the shaft rotation. Hence,

$$[K]_{normal} = \begin{bmatrix} k & 0 \\ 0 & k \end{bmatrix} \text{ becomes } [K]_{cracked} = [K(q,t)] \tag{2.3.2}$$

where

$q = \begin{bmatrix} y(t) \\ z(t) \end{bmatrix}$: displacement vector of the rotor

If weight-dominance is assumed for the elastic deflection of the rotor, i.e.:

$$q_{static} \gg \Delta q \tag{2.3.3}$$

where

q_{static} : static deflection of the rotor

Δq : additional vibrational deflection due to the crack

then the opening and the closing of the crack is only related to the rotation of the shaft, i.e.:

$$[\boldsymbol{K}(q,t)] \rightarrow [\boldsymbol{K}(t)] \tag{2.3.4}$$

This assumption is considered to be reasonable, since even the static sag of the rotor is usually large: e.g. in turbo-generators, it is often more than 1 mm.

Hence, the equations of motion become:

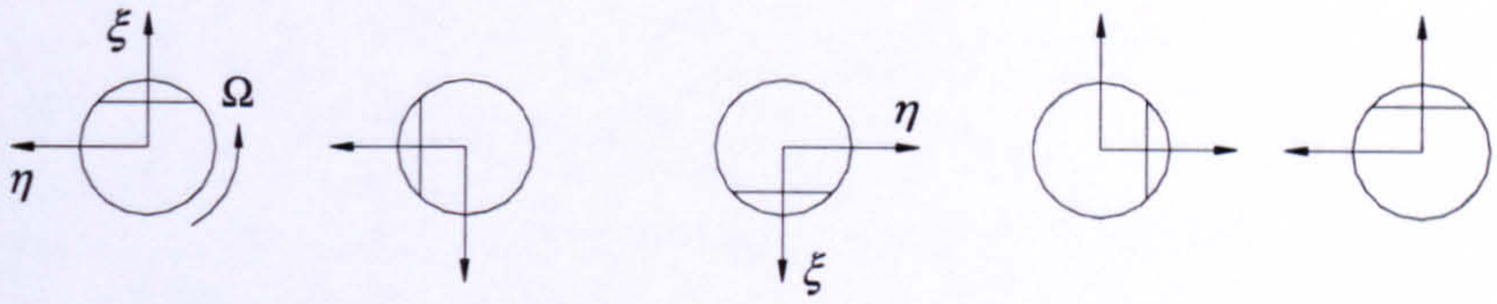
$$\begin{bmatrix} m & 0 \\ 0 & m \end{bmatrix}\begin{bmatrix} \ddot{y} \\ \ddot{z} \end{bmatrix} + \begin{bmatrix} c & 0 \\ 0 & c \end{bmatrix}\begin{bmatrix} \dot{y} \\ \dot{z} \end{bmatrix} + \begin{bmatrix} k_{11}(t) & k_{12}(t) \\ k_{21}(t) & k_{22}(t) \end{bmatrix}\begin{bmatrix} y \\ z \end{bmatrix} = \begin{bmatrix} -mg \\ 0 \end{bmatrix}$$
$$+ m\epsilon\Omega^2 \begin{bmatrix} \cos(\Omega t + \alpha) \\ \sin(\Omega t + \alpha) \end{bmatrix} \tag{2.3.5}$$

To describe the variation of stiffness $[\boldsymbol{K}(t)]$ in equation (2.3.5) with shaft rotation, essentially, two breathing (or switching) models have been proposed for the breathing crack and have been studied theoretically and experimentally by Gasch [42] and Mayes & Davies [87] respectively, i.e.:

(i) Gasch's hinge model

(ii) Mayes & Davies' model

In spite of the fact that Gasch's hinge model for a crack simplifies the variation of stiffness to a step change, it still incorporates all the essential dynamics regarding flexural vibrations and is known to be valid for small crack depths ($a/r < 0.5$).



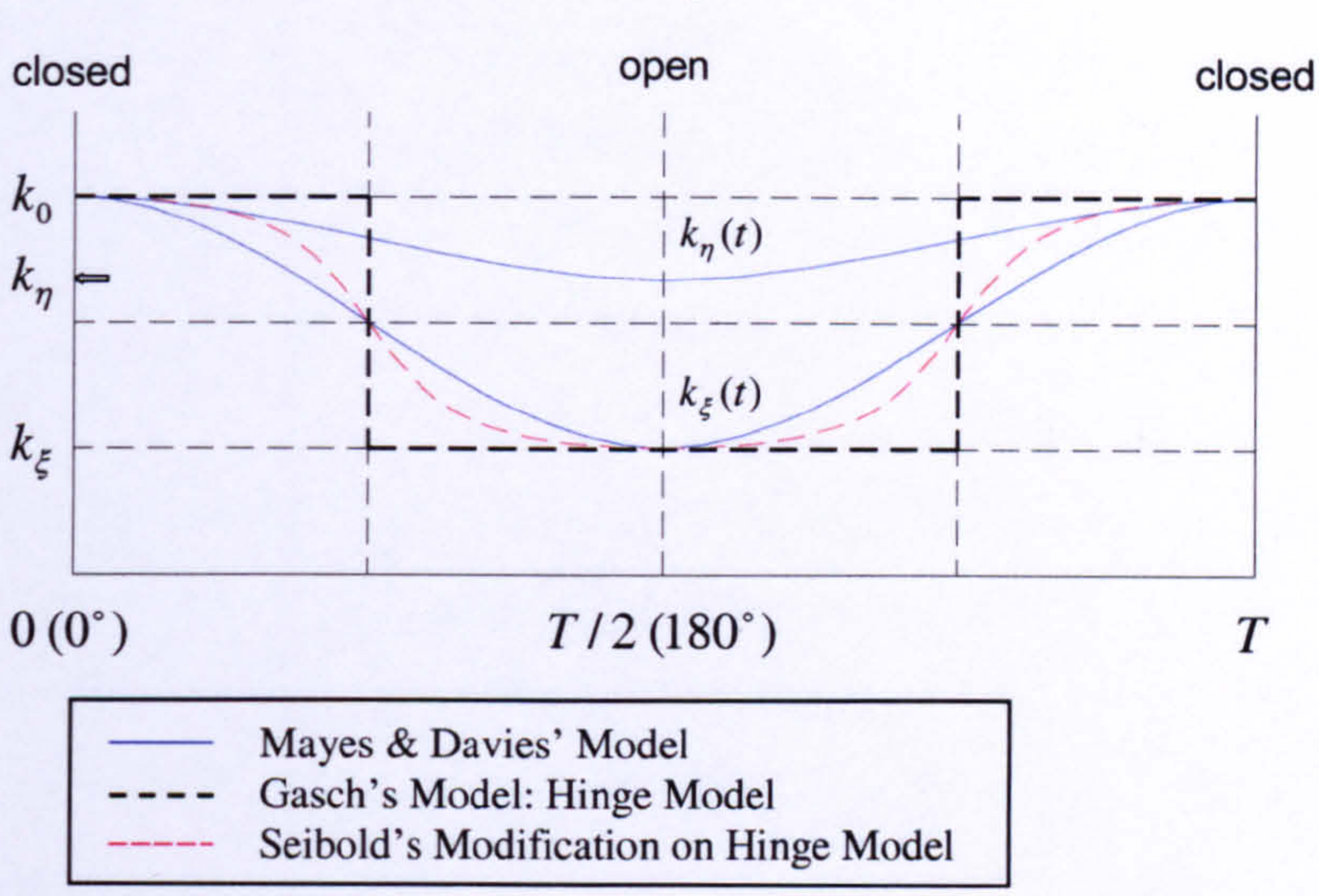


Fig 2.3.2 Variation of Stiffness for a Breathing Crack

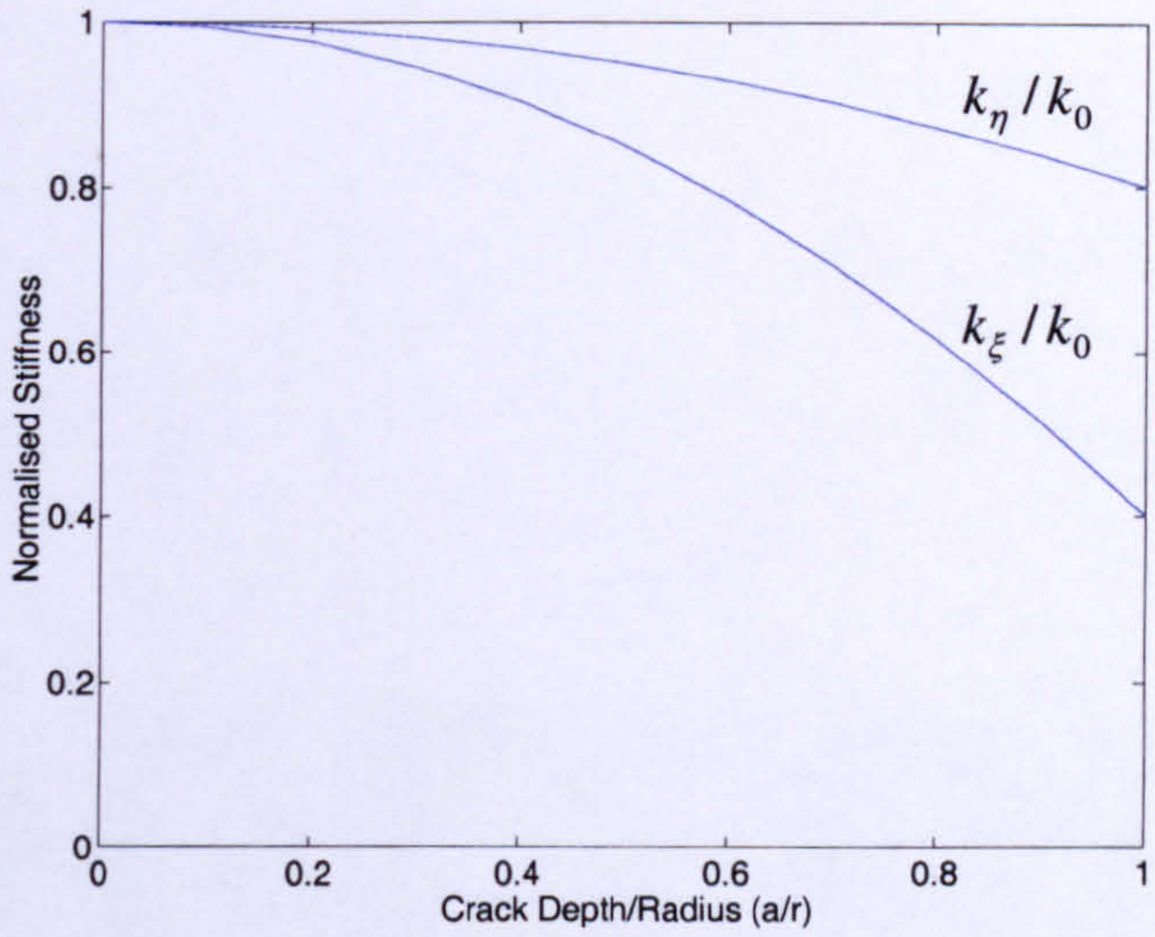


Fig 2.3.3 Stiffness Reduction Ratio to the Depth of Crack

On the other hand, Mayes & Davies, on the basis of their own experimental investigation of rotors including deep cracks ($a/r > 0.5$), assumed a harmonic stiffness variation with period T ($= 2\pi/\Omega$) due to the rotation and self-weight of the rotor, as shown in Fig 2.3.2, and they also considered the cross-stiffness (k_η) reduction which has not been considered in Gasch's hinge modelling. These two representative breathing crack models have been used by many subsequent researchers without any modification. Only recently, have Seibold et al [123] modified Gasch's hinge model slightly, also as shown in Fig 2.3.2, and used it in their work for crack detection.

In this research, due to the availability of experimental data for the stiffness reduction ratio (refer to Fig 2.3.3 presented in interpolated form), Mayes & Davies' breathing crack assumption has been adopted for vibration analysis of simple rotor system with a transverse crack. Fig 2.3.4 shows a cross-section of a cracked shaft in both inertial and rotating coordinates.

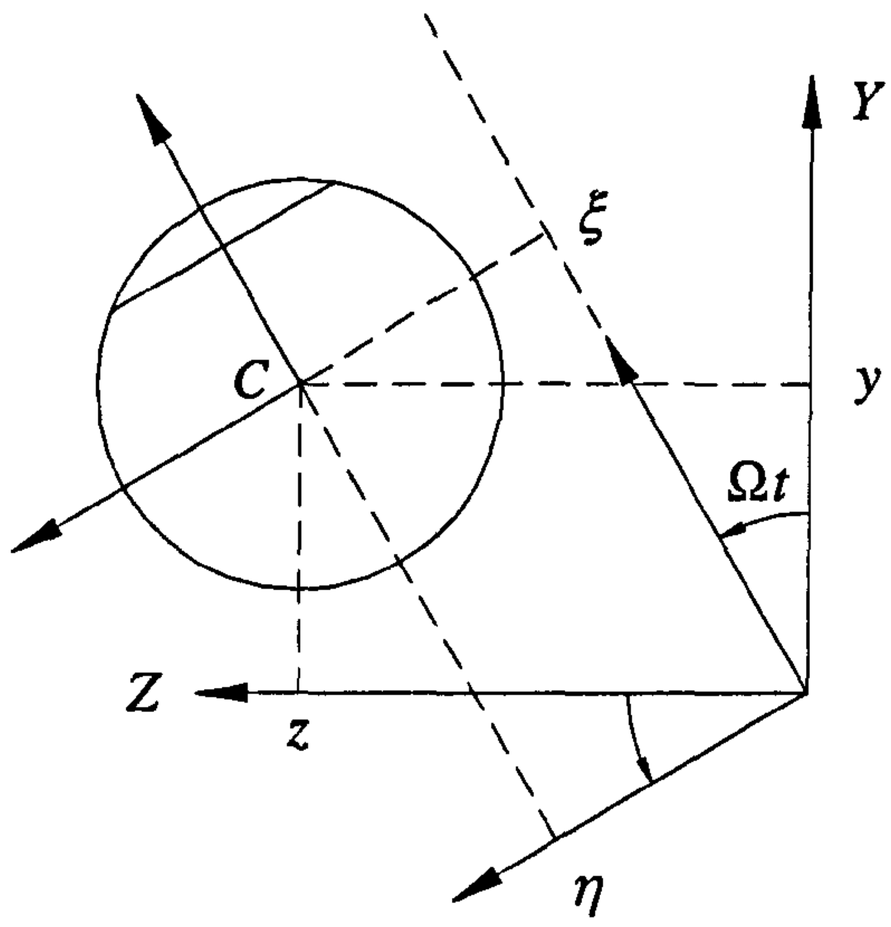


Fig 2.3.4 Inertial Coordinates $Y-Z$ and Rotating Coordinates $\xi-\eta$

By using the rotating axes coordinate system as in Fig 2.3.4, the corresponding stiffness matrix $[\boldsymbol{K}(t)]_R$ will have the following form:

$$[\boldsymbol{K}(t)]_R = \begin{bmatrix} k_\xi(t) & 0 \\ 0 & k_\eta(t) \end{bmatrix} \tag{2.3.6}$$

where

$$k_\xi(t) = \frac{k_0 + k_\xi}{2} + \frac{k_0 - k_\xi}{2}\cos\Omega t$$

$$k_\eta(t) = \frac{k_0 + k_\eta}{2} + \frac{k_0 - k_\eta}{2}\cos\Omega t$$

The transformation matrix relating the rotational and inertial coordinates (Fig 2.3.4) is:

$$\begin{bmatrix} \xi \\ \eta \end{bmatrix} = \begin{bmatrix} \cos\Omega t & \sin\Omega t \\ -\sin\Omega t & \cos\Omega t \end{bmatrix} \begin{bmatrix} y \\ z \end{bmatrix} \text{ or } [\boldsymbol{q}]_R = [\boldsymbol{T}][\boldsymbol{q}] \tag{2.3.7}$$

Hence the stiffness matrix expressed in the inertial coordinate system, $[\boldsymbol{K}(t)]$, becomes:

$$[\boldsymbol{K}(t)] = [\boldsymbol{T}]^{\mathrm{T}}[\boldsymbol{K}(t)]_R[\boldsymbol{T}] = \begin{bmatrix} k_m + \Delta k\cos 2\Omega t & \Delta k\sin 2\Omega t \\ \Delta k\sin 2\Omega t & k_m - \Delta k\cos 2\Omega t \end{bmatrix} \tag{2.3.8}$$

where

$$k_m = \frac{1}{2}[k_\xi(t) + k_\eta(t)]\,,\ \Delta k = \frac{1}{2}[k_\xi(t) - k_\eta(t)]$$

Hence,

$$[\boldsymbol{K}(t)] = \begin{bmatrix} k' & 0 \\ 0 & k' \end{bmatrix} + \frac{k_\xi - k_\eta}{8}\begin{bmatrix} f_1(t) & f_3(t) \\ f_3(t) & f_2(t) \end{bmatrix} \tag{2.3.9}$$

where

$$k' = \frac{2k_0 + k_\xi + k_\eta}{4}$$

$$f_1(t) = \frac{4 - 3k_\xi - k_\eta}{k_\xi - k_\eta}\cos\Omega t + 2\cos 2\Omega t - \cos 3\Omega t$$

$$f_2(t) = \left[2 + \frac{4 - 3k_\xi - k_\eta}{k_\xi - k_\eta}\right]\cos\Omega t - 2\cos 2\Omega t + \cos 3\Omega t$$

$$f_3(t) = -\sin\Omega t + 2\sin 2\Omega t - \sin 3\Omega t$$

Finally, the equations of motion of the cracked simple rotor become, i.e. in a brief form:

$$[M][\ddot{q}] + [C][\dot{q}] + [K(t)][q] = [F(t)] \qquad (2.3.10)$$

It should be remembered that this mathematical model applies to a crack which breathes during the shaft rotation. As mentioned earlier, this assumption is valid if the static deflection of the shaft is large, compared with the vibration amplitude. In this case, the crack opens and closes periodically with the shaft rotation. If the static deflection of the shaft is small, as in most light shafts, the crack remains open if the unbalance is in the direction of the crack, as usually happens. Or if the unbalance is in the opposite direction (although this may be quite a rare case), the crack remains closed and does not affect the shaft behaviour, except in the case of violent transients. However, the versatility of the present analysis is maintained even in the case of an open crack because most of the features of rotor behaviour under a breathing crack are qualitatively maintained in the case of a rotor with an open crack.

2.3.2 The Open Crack Model

As mentioned earlier, a rotor system with an open crack introduces local dissimilar moments of inertia at the location of a crack. Due to this local asymmetry in stiffness, the dynamic behaviour of open-cracked rotors has the similar characteristics to that of asymmetric rotors. On some occasions, open cracks can be assumed for small vibration amplitudes and static deflections that are not substantial.

Hence, in the open cracked case, the rotor will have different transverse moments of inertia, I_ξ & I_η, due to the existence of the crack. The stiffnesses k_y & k_z depend upon the rotation (or angle Ωt) while k_ξ & k_η remain constant. Therefore, it is more convenient to set up stiffness matrix in rotating coordinates, and then transform to inertial coordinates, as was the case in the breathing crack model without consideration of the breathing function.

Then, the equations of motion in the inertial frame of reference can be described as follows:

$$\begin{bmatrix} m & 0 \\ 0 & m \end{bmatrix}\begin{bmatrix} \ddot{y} \\ \ddot{z} \end{bmatrix} + \begin{bmatrix} c & 0 \\ 0 & c \end{bmatrix}\begin{bmatrix} \dot{y} \\ \dot{z} \end{bmatrix} + \begin{bmatrix} k_1 + k_2\cos 2\Omega t & k_2\sin 2\Omega t \\ k_2\sin 2\Omega t & k_1 - k_2\cos 2\Omega t \end{bmatrix}\begin{bmatrix} y \\ z \end{bmatrix}$$

$$= \begin{bmatrix} -mg \\ 0 \end{bmatrix} + m\varepsilon\Omega^2\begin{bmatrix} \cos(\Omega t + \alpha) \\ \sin(\Omega t + \alpha) \end{bmatrix} \qquad (2.3.11)$$

where

$$k_1 = \frac{k_\xi + k_\eta}{2}\ ,\ k_2 = \frac{k_\xi - k_\eta}{2}\ ,\ k_\xi = 48\frac{EI_\xi}{L^3}\ ,\ k_\eta = 48\frac{EI_\eta}{L^3}$$

As can be noticed in equation (2.3.11), the stiffness variation has a less complicated form than the breathing crack model.

2.4 Vibration Response Analysis

To investigate the dynamic behaviour of a cracked rotor system, the specifications presented in Table 2.4.1 have been used in the calculations. The system has been modelled using MATLAB SIMULINK (Fig 2.4.2) according to the formulations of the breathing crack model, and the simulation has been performed for both transient and steady-state conditions. The equations of motion, which are non-linear due to the time-varying terms in stiffness caused by the crack, have been solved using a 4th-order Runge-Kutta numerical integration algorithm [150] with variable time step option.

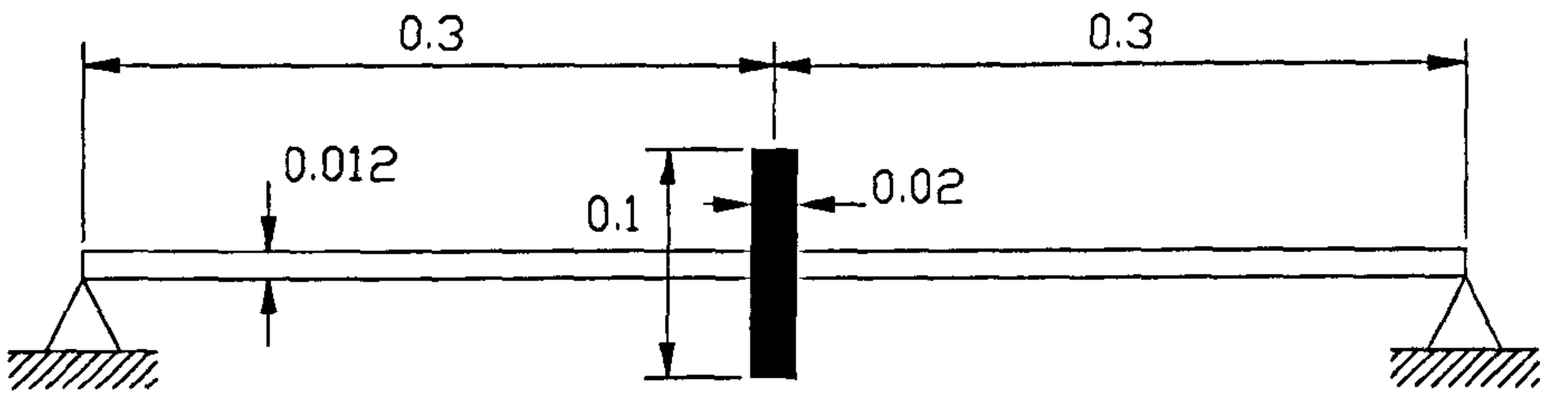


Fig 2.4.1 Simple Rotor Model

Table 2.4.1 Specifications of the Simple Rotor Model

Disk	Diameter	0.1 [m]
	Thickness	0.02 [m]
Shaft	Diameter	0.012 [m]
	Length	0.6 [m]
Damping Factor	ζ	0.05
Density	ρ	7800 [kg/m^3]
Young's Modulus	E	2.07×10^{11}[N/m^2]
1st Nat. Frequency	ω_0	195.5 [rad/s] (= 31.1 [Hz])

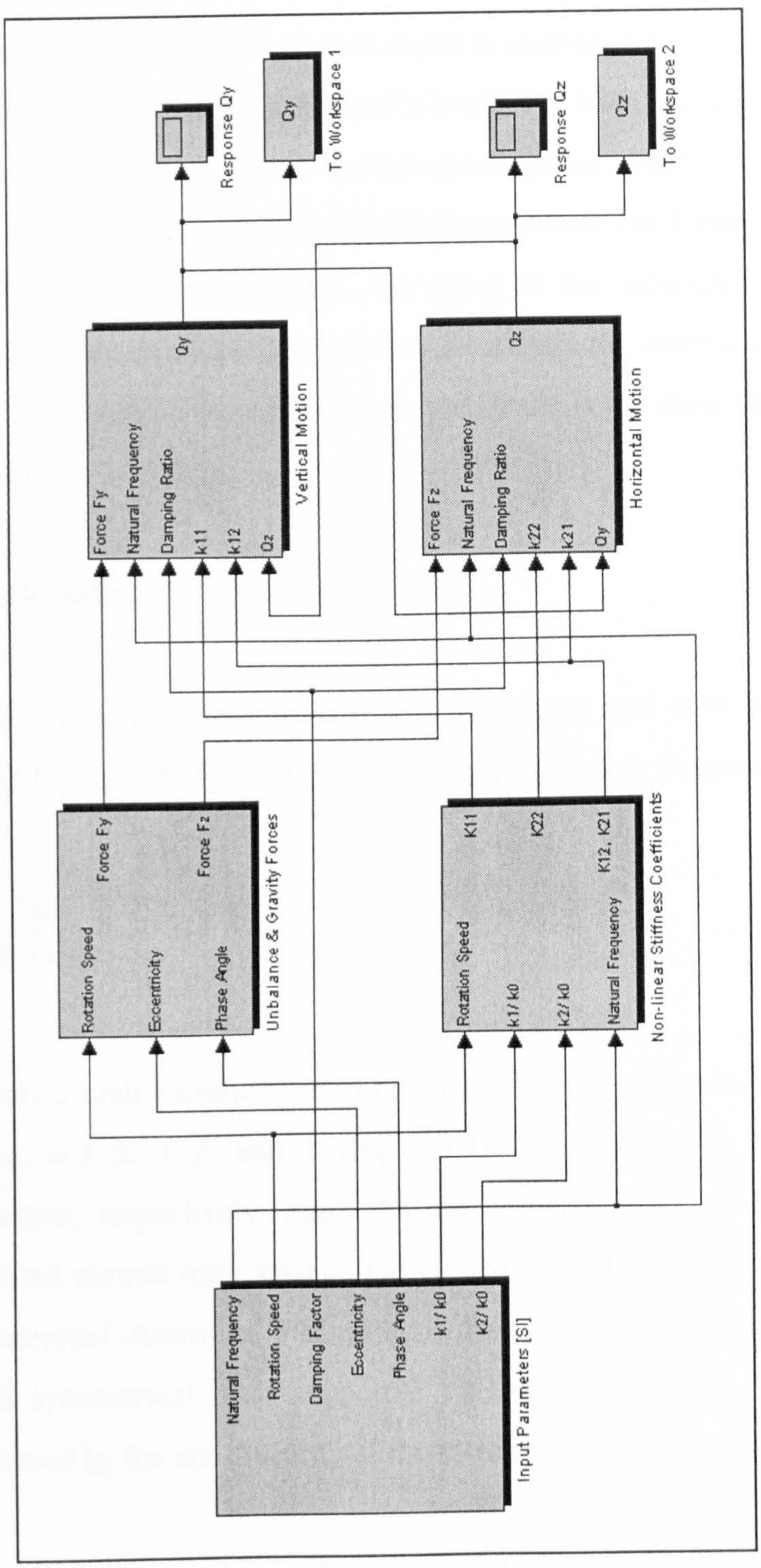


Fig 2.4.2 SIMULINK MODEL for Cracked Simple Rotor System

2.4.1 Transient-State Vibration Response Analysis

The vibration response (obtained in terms of displacement) of the rotor, caused by the self-excitation due to the presence of a crack, has been investigated during the run-up period with a speed ramp rate of 95.5 rpm/s (linear speed-up) for the cases of rotors with unbalance and (i) 10 % & (ii) 20 % transverse crack depths relative to diameter of the rotor cross-section. Also, the effect of the unbalance on the cracked rotor system has been considered in order to investigate the vibration response of a cracked rotor in the presence of unbalance, as unbalance is the most common fault occurring in service.

- **Time Domain**

Generally, a normal rotor system with unbalance will have a resonance at rotation speed of $\Omega/\omega_n = 1$ (Fig 2.4.3), where ω_n is a natural frequency of the normal rotor system:

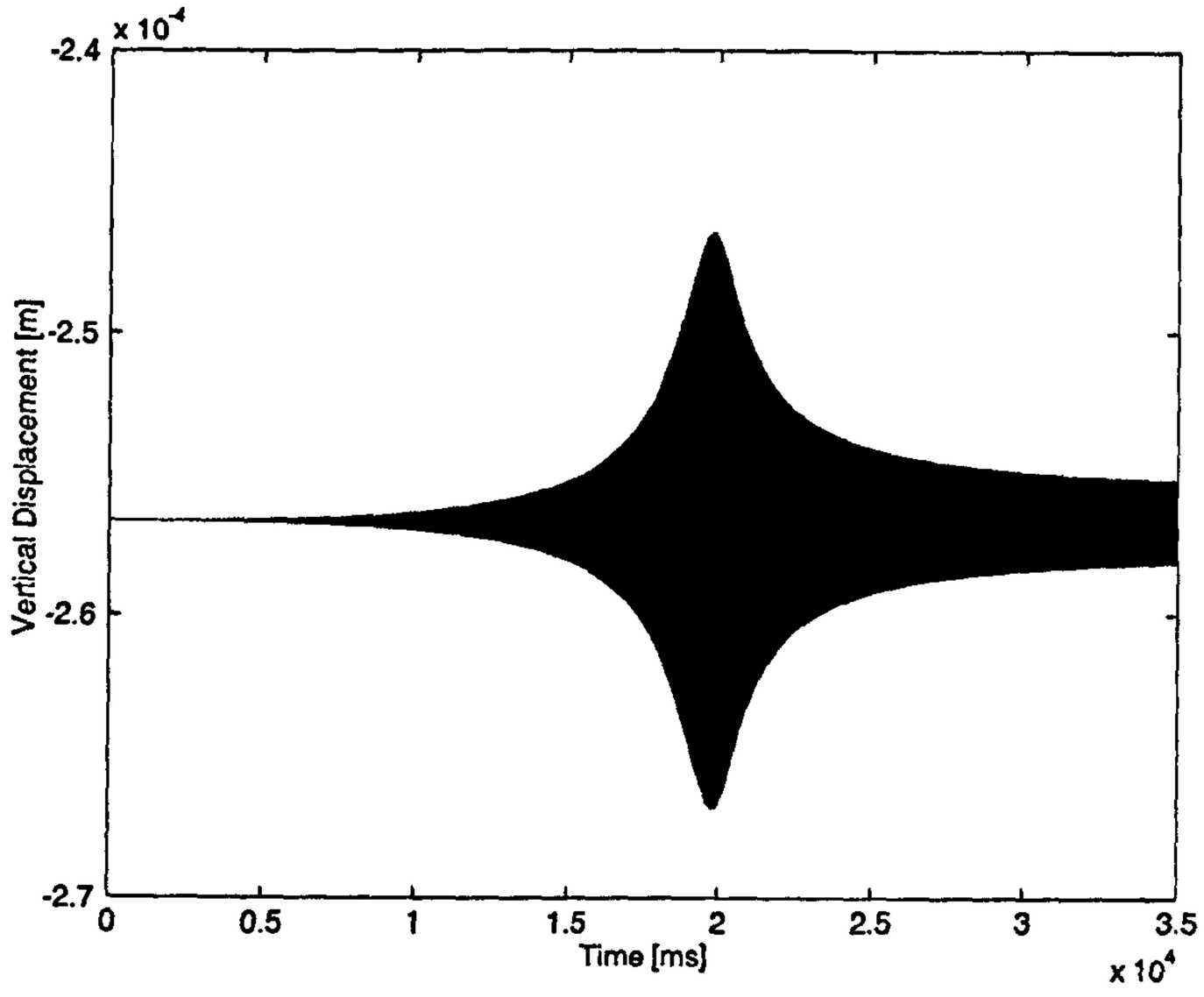
$$\omega_n = \sqrt{\frac{k_0}{m}}$$

However, overall vibrations from the cracked rotor system have resonances at speeds of $\Omega/\omega_n = 1/3,\ 1/2$, and 1 (Fig 2.4.4) due to the 3Ω, 2Ω, and 1Ω vibration components, respectively. Also, for the cracked rotor system, as opposed to the unbalanced normal rotor system, the vibration amplitudes are different in the vertical and horizontal directions. Hence, considering the fact that the analysed model is a cracked symmetrical rotor supported by isotropic bearings, these differences have been caused by the non-linearity of the rotor stiffnesses due to existence of a crack.

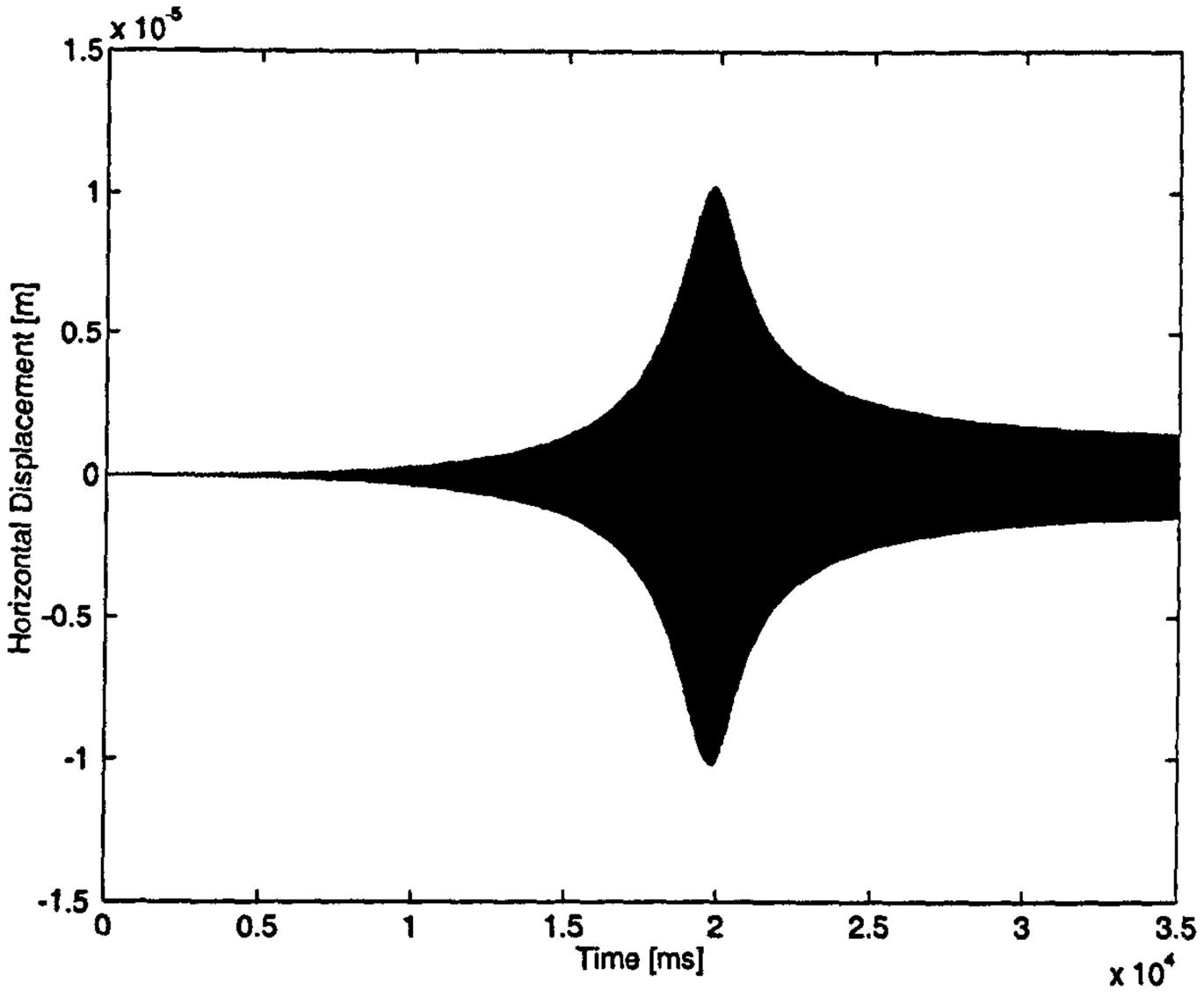
When unbalance coexists with cracks in the rotor system, the angular position (or phase angle) of the unbalance will influence the peak vibration level (Fig 2.4.5).

Under the condition of unbalance which is out-of-phase (180°) with the crack, the 1Ω resonance will be smaller than under the condition of unbalance in-phase (0°) with the crack. As the unbalance only affects the 1Ω resonance, sub-resonances are not affected by the phase angle of the unbalance.

The orbit of cracked rotor has been investigated as presented in Fig 2.4.6. When the rotor speed passes the resonance peak at $\Omega/\omega_n = 1/3$, the whirl orbit exhibits 3Ω vibrations with triple rotational frequency. At $\Omega/\omega_n = 1/2$, the whirl orbit exhibits 2Ω vibrations with double rotational frequency, and at $\Omega/\omega_n = 1$, the orbit forms a narrow ellipse due to the relatively strong backward whirl component. Also, as shown in Fig 2.4.7, the variations in phase angle of cracked rotor caused by harmonic components can be identified at speeds of $\Omega/\omega_n = 1/3$, $1/2$, and 1 while the normal rotor system with unbalance has 180° phase-shift only at speed of $\Omega/\omega_n = 1$ as can be normally expected.

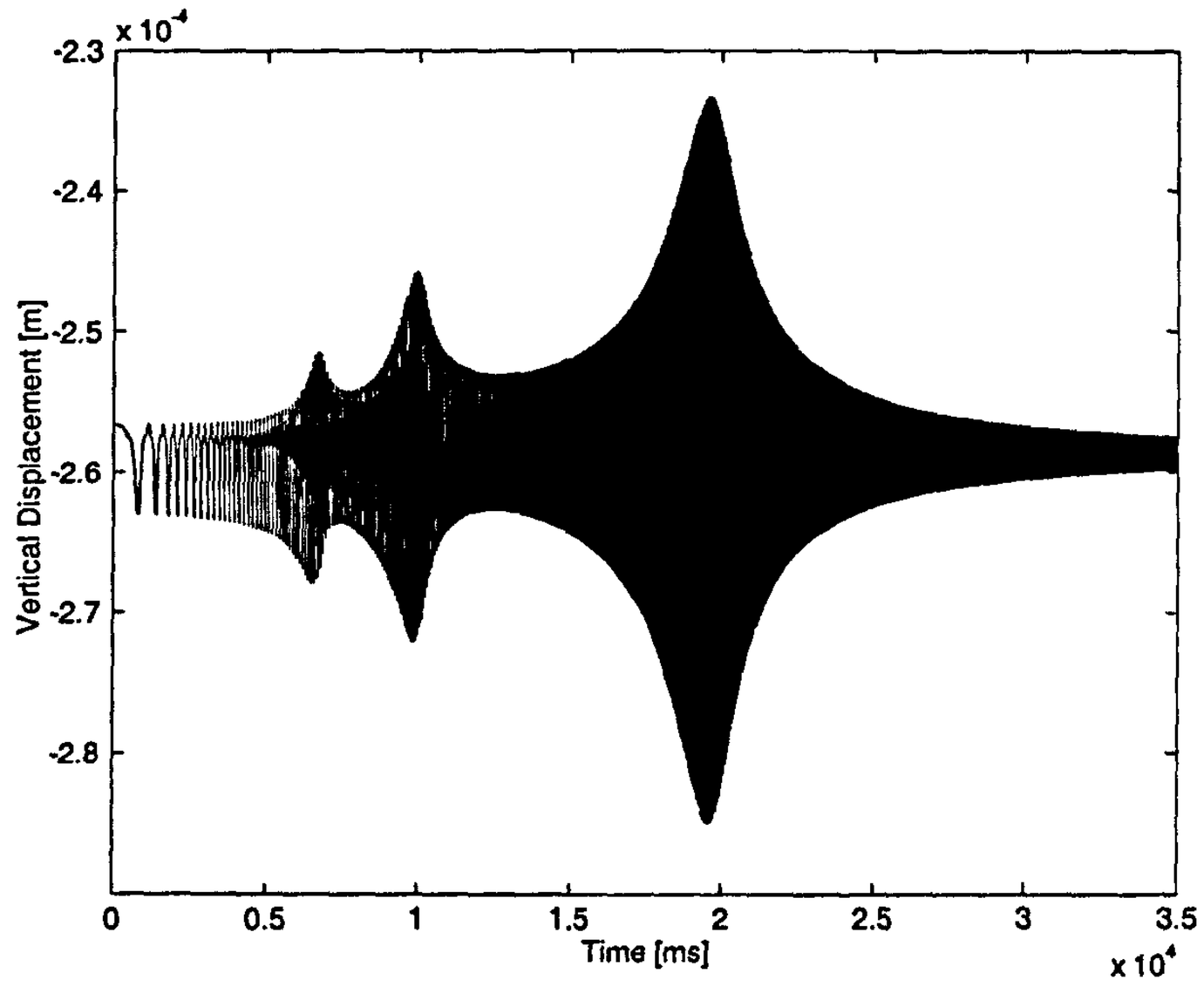


(a) Vertical Displacement

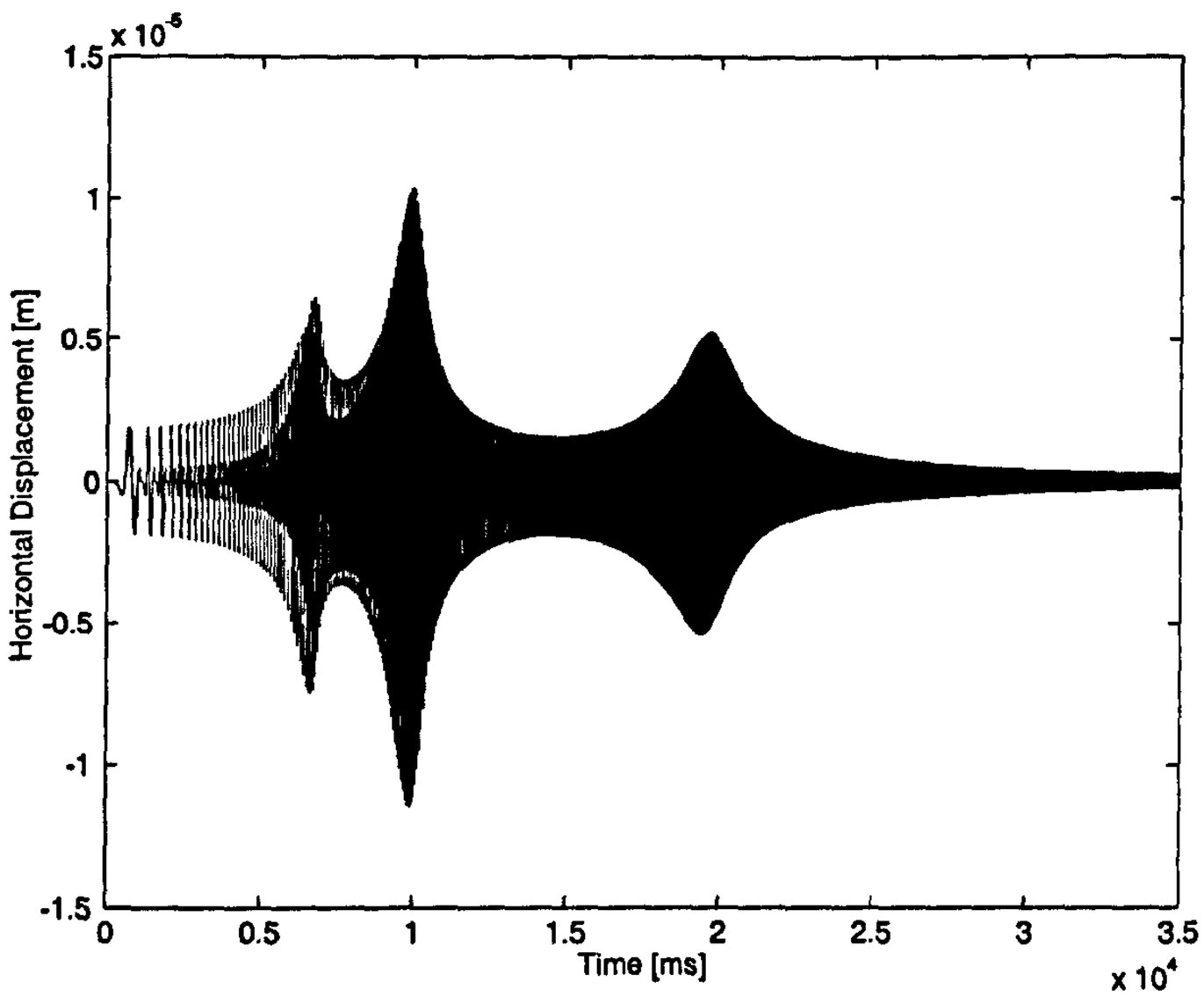


(b) Horizontal Displacement

Fig 2.4.3 Normal Rotor under Unbalance Excitation

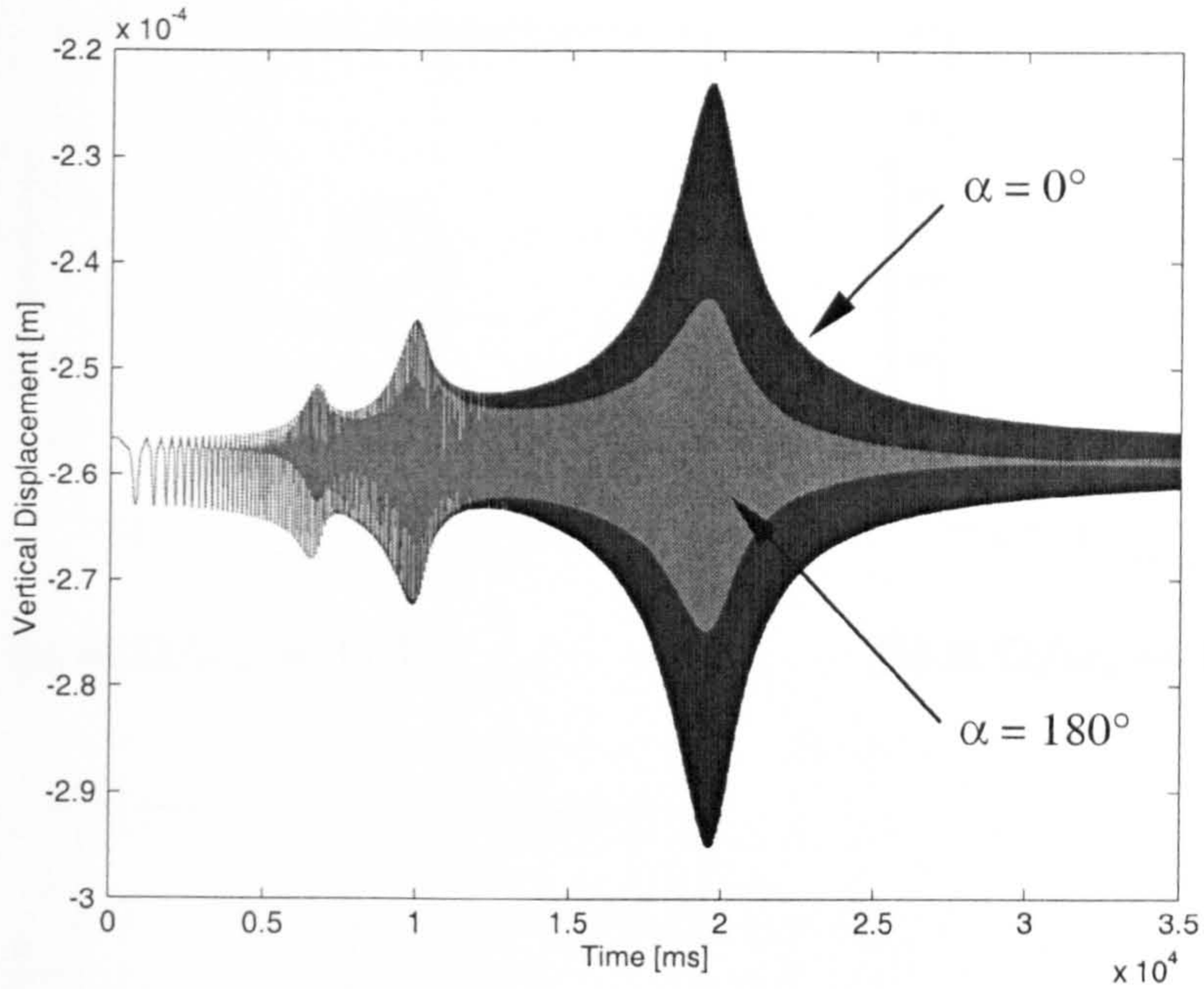


(a) Vertical Displacement

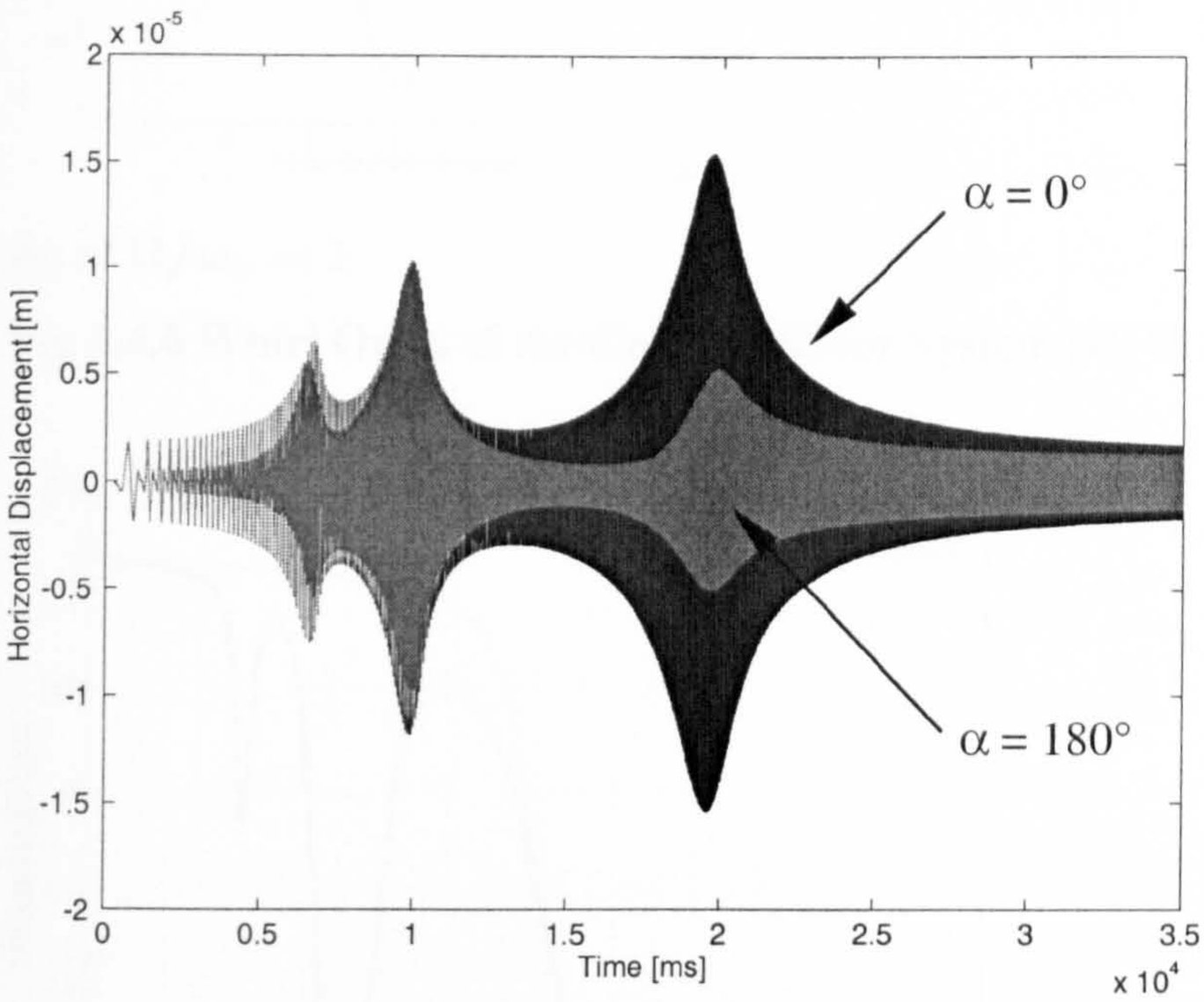


(b) Horizontal Displacement

Fig 2.4.4 Cracked Rotor (10 %) under Gravity Excitation

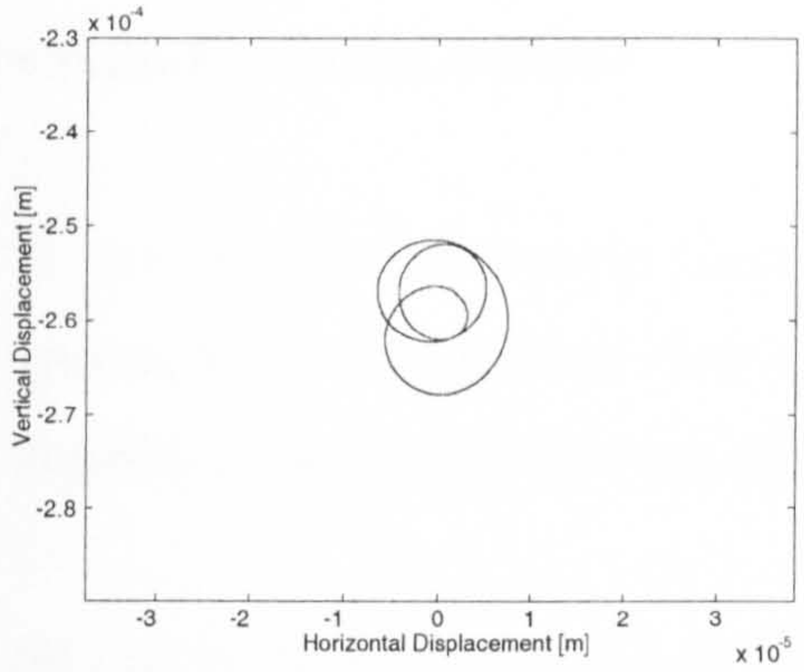


(a) Vertical Displacement

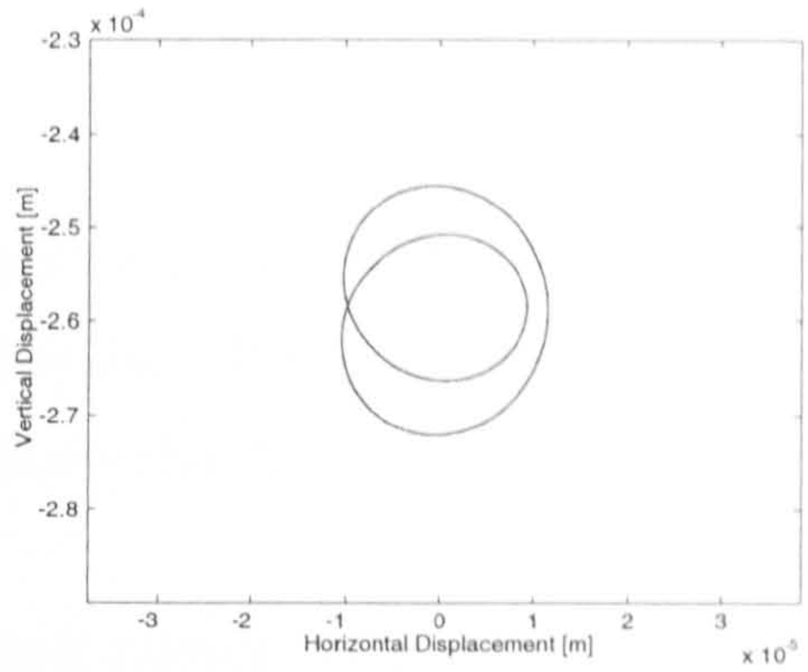


(b) Horizontal Displacement

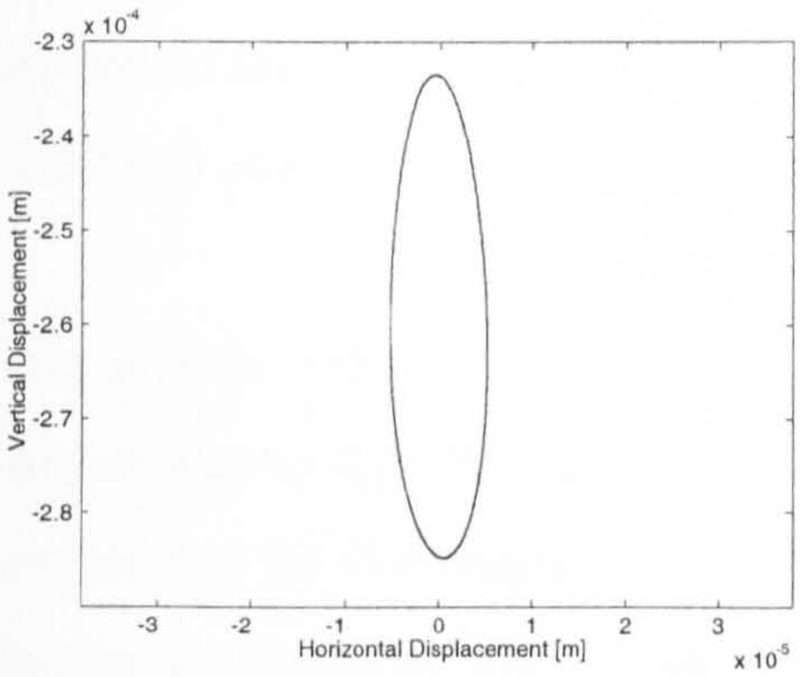
Fig 2.4.5 Effect of Unbalance Phase Angles on the Cracked Rotor (10 % Crack)



(a) at $\Omega/\omega_n = 1/3$



(b) at $\Omega/\omega_n = 1/2$



(c) at $\Omega/\omega_n = 1$

Fig 2.4.6 Whirl Orbit of the Cracked Rotor System (10 % crack)

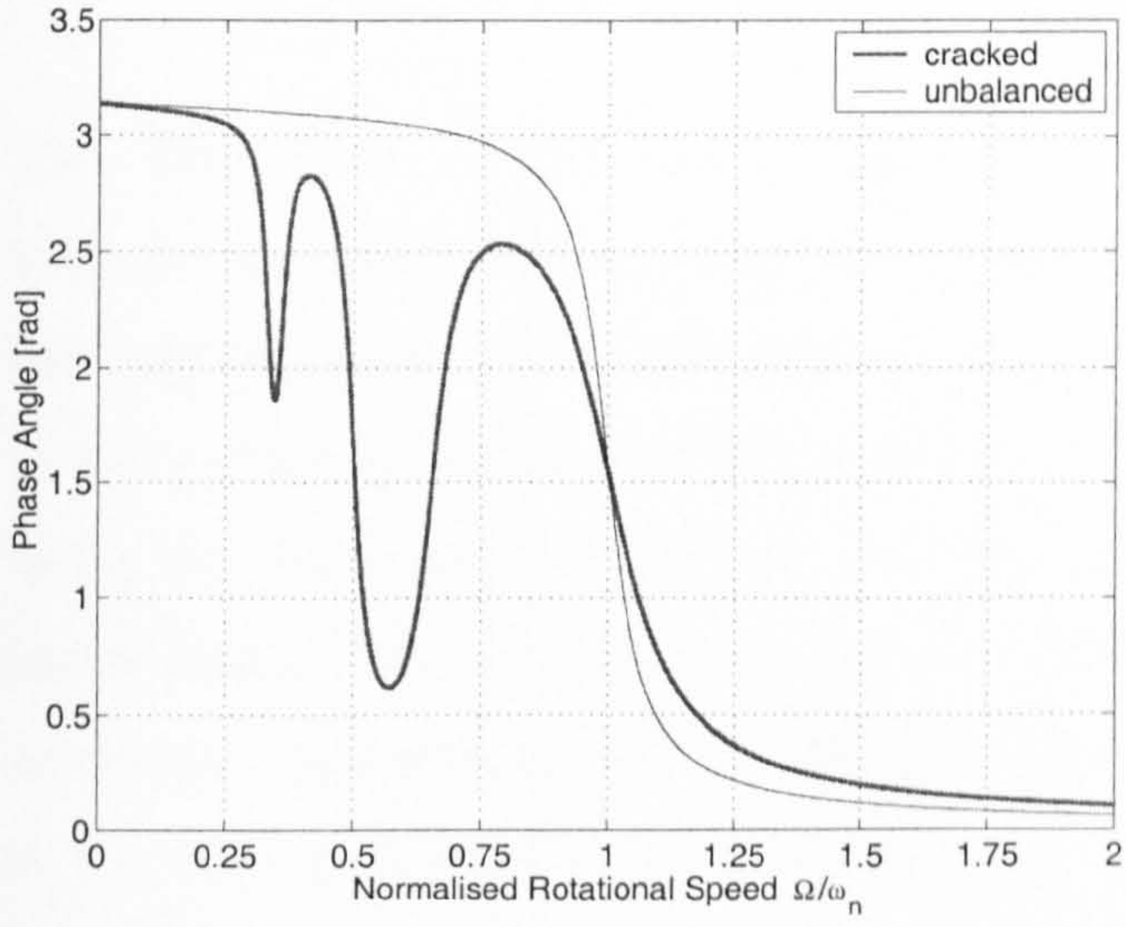


Fig 2.4.7 Phase Angle of the Cracked Rotor System (10 % crack)

• Time-Frequency Domain

To investigate time-varying frequency components occurring in the cracked rotor system, the directional short-time Fourier transform (developed in Dynamics Section, Imperial College [10]) has been applied to the transient vibration data.

As can be seen in Fig 2.4.8 & 2.4.9, for each cracked rotor with a different crack depth, the FW/BW separated spectrogram shows clearly the $\pm 1\Omega$, $+2\Omega$, and $+3\Omega$ vibrations due to the self-excitation associated with gravity on the cracked rotor system. Also, as Gasch [41] first reported with his simplified crack model, the -1Ω vibration can be identified clearly in these diagrams.

For a rotor with only unbalance, as can be expected readily, only $+1\Omega$ vibration occurs due to the unbalance excitation and no backward whirl vibration component exists (Fig 2.4.10) because the model rotor system without a crack can be considered to be a symmetric rotor supported by isotropic bearings (rigid supports). When unbalance coexists with cracks in the rotor system (Fig 2.4.11), the $+1\Omega$ vibration becomes strong relative to other vibrations (-1Ω, $+2\Omega$, and $+3\Omega$) compared with the well-balanced cracked rotor (Fig 2.4.8).

Two other rotor systems, i.e. an asymmetric rotor ($k_\xi/k_\eta = 1.5$) supported by isotropic bearings [ARIB system] and a symmetric rotor supported by anisotropic bearings ($k_y/k_z = 1.5$) [SRAB system] also have been considered to compare the vibration response with that of the cracked rotor system (Fig 2.4.12 & 2.4.13). In both cases, the backward whirl response can also be identified as being present in the spectrograms. The backward whirl in the ARIB system occurs due to the rotor-asymmetry excited by gravity and the backward whirl in the SRAB system occurs due to the bearing-anisotropy excited by unbalance. Hence, during the run-up (or run-down) periods in general, the presence of the backward whirl vibration should be

inspected carefully for the purpose of crack detection. In this regard, accurate system identification of the rotor system, i.e. of the rotor-asymmetry and the bearing-anisotropy, is essential for effective monitoring of rotating systems.

In the spectrograms of the cracked rotor model (Fig 2.4.8 & 2.4.9), it is not easy to identify accurately the resonance regions caused by the presence of a crack due to the inherent overlap property of the short-time Fourier transform (STFT, refer to Chapter 4 for details of this process). Considering the fact that the resonances caused by the presence of cracks are one of major factors for crack detection, a complementary tool is considered necessary in processing the data to overcome the limitation in resolution posed by the STFT technique.

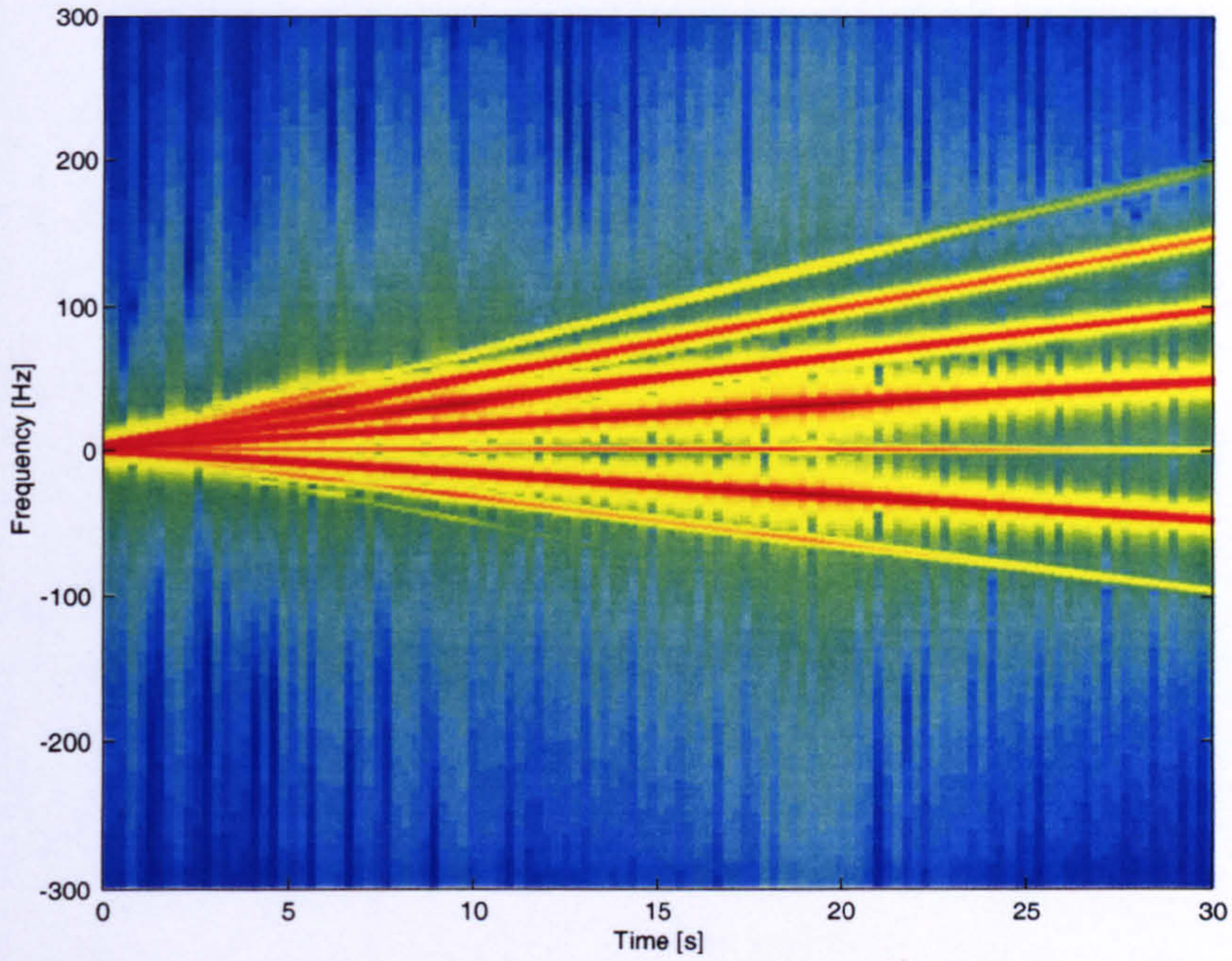


Fig 2.4.8 Spectrogram: 10 % Cracked Rotor

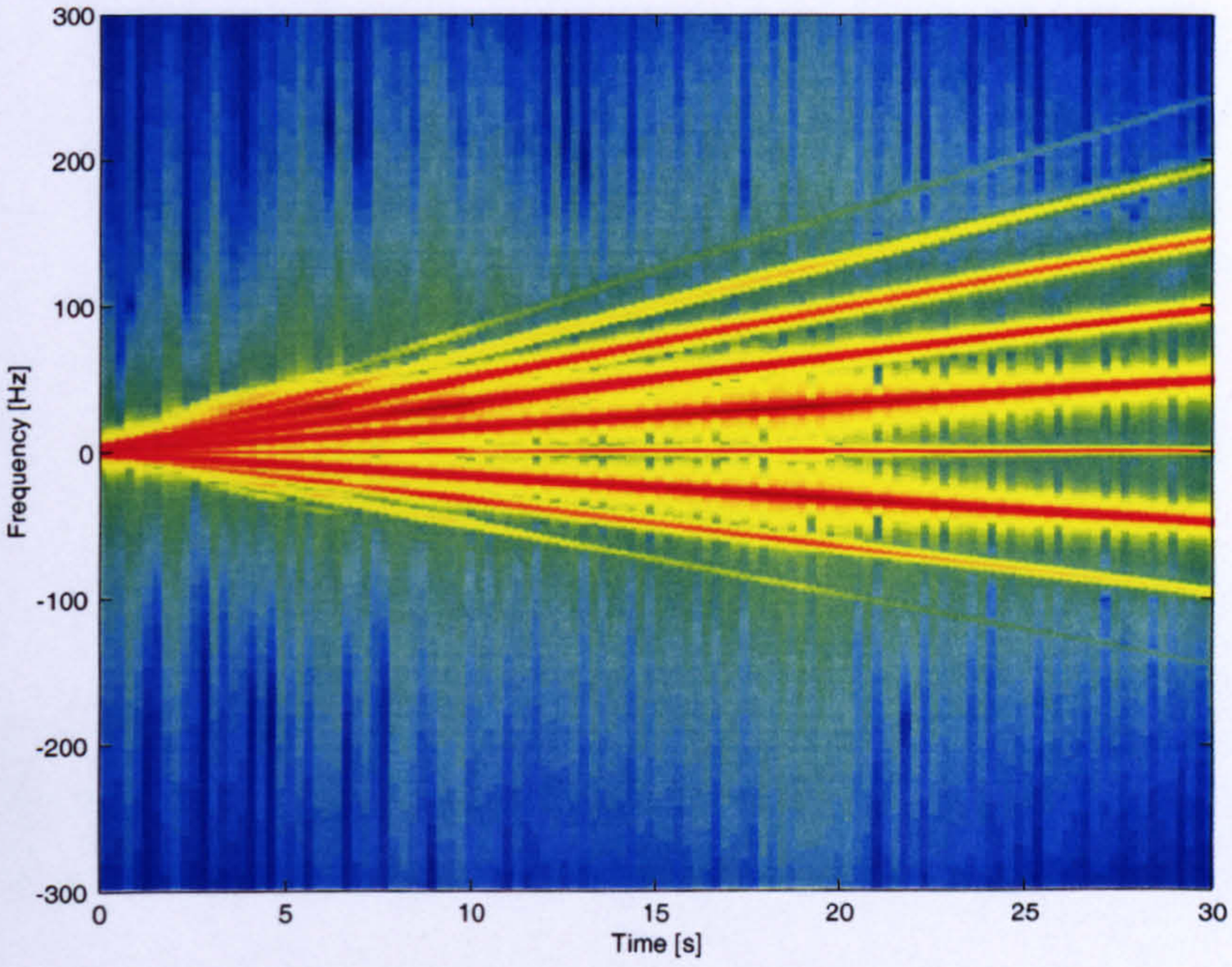


Fig 2.4.9 Spectrogram: 20 % Cracked Rotor

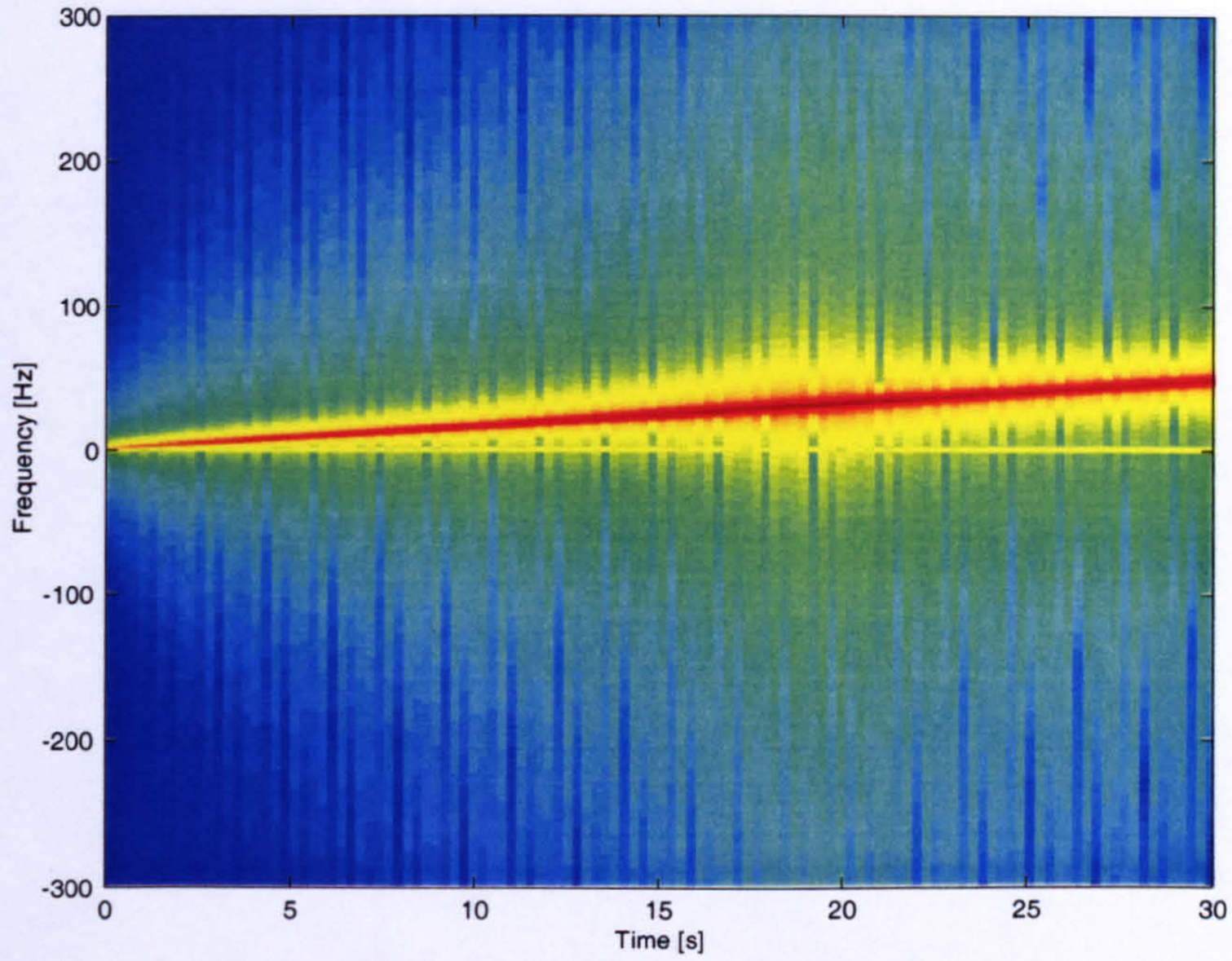


Fig 2.4.10 Spectrogram: Normal Rotor with Unbalance

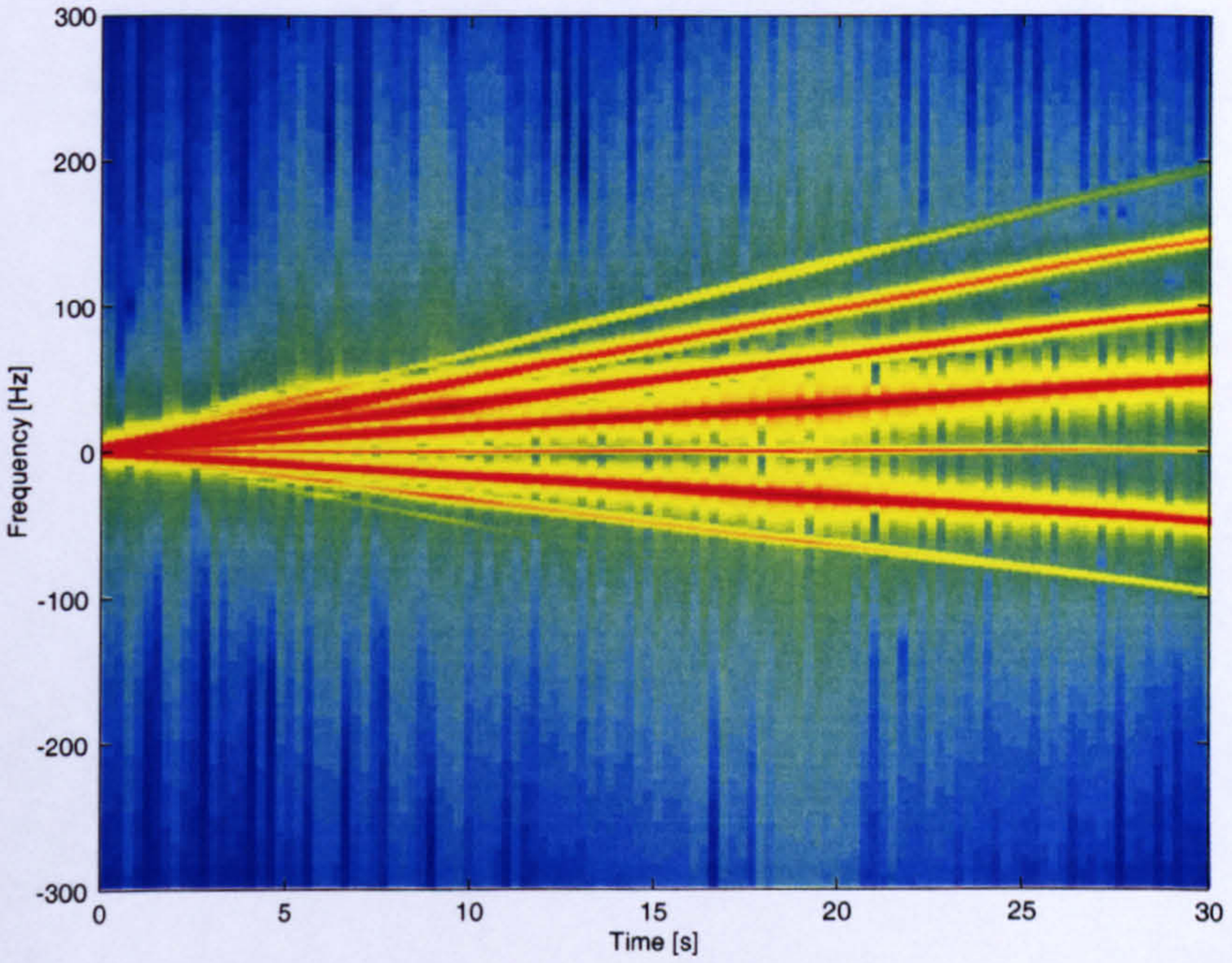


Fig 2.4.11 Spectrogram: 10 % Cracked Rotor with Unbalance

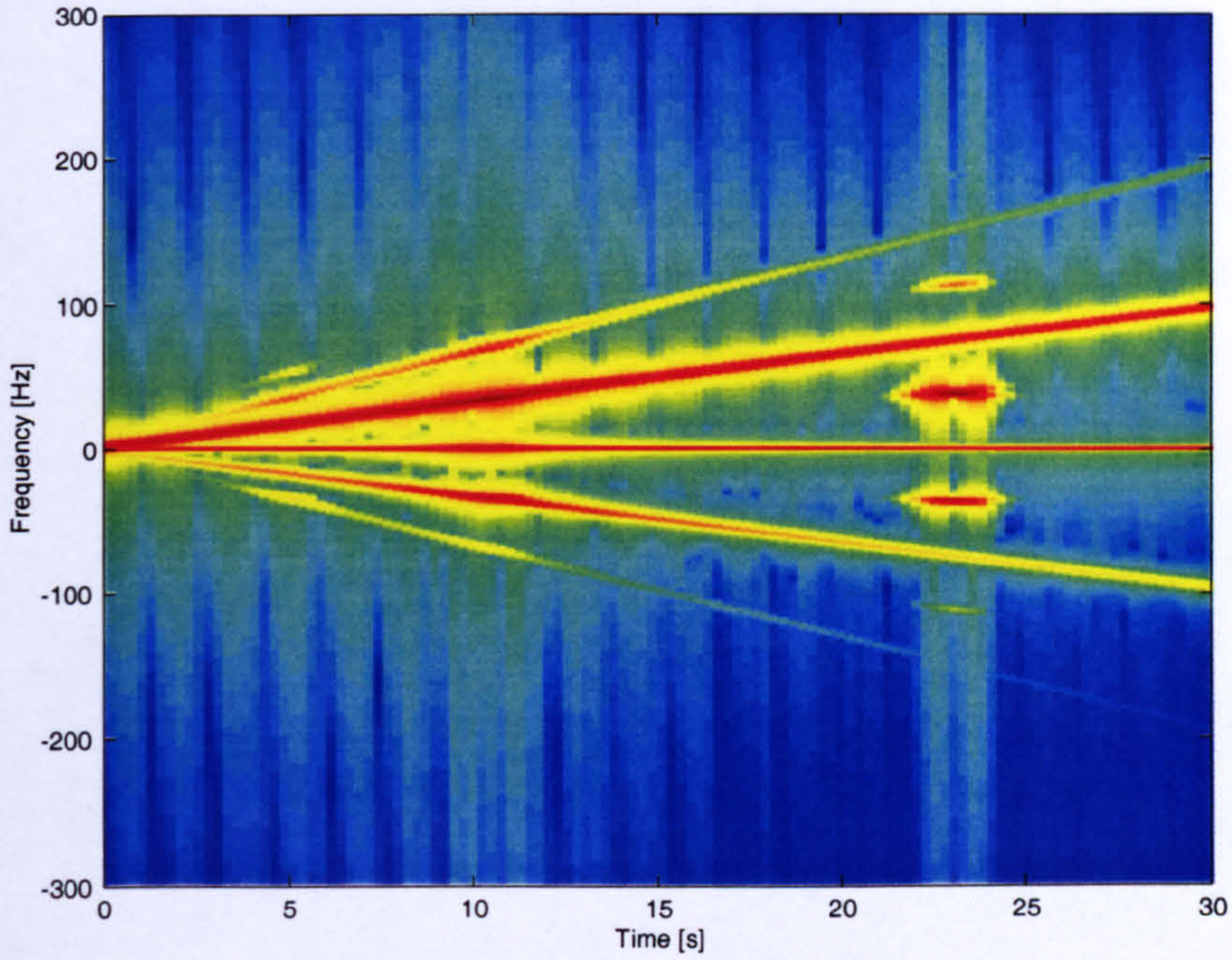


Fig 2.4.12 Asymmetric Rotor, Isotropic Bearings, with Gravity Excitation

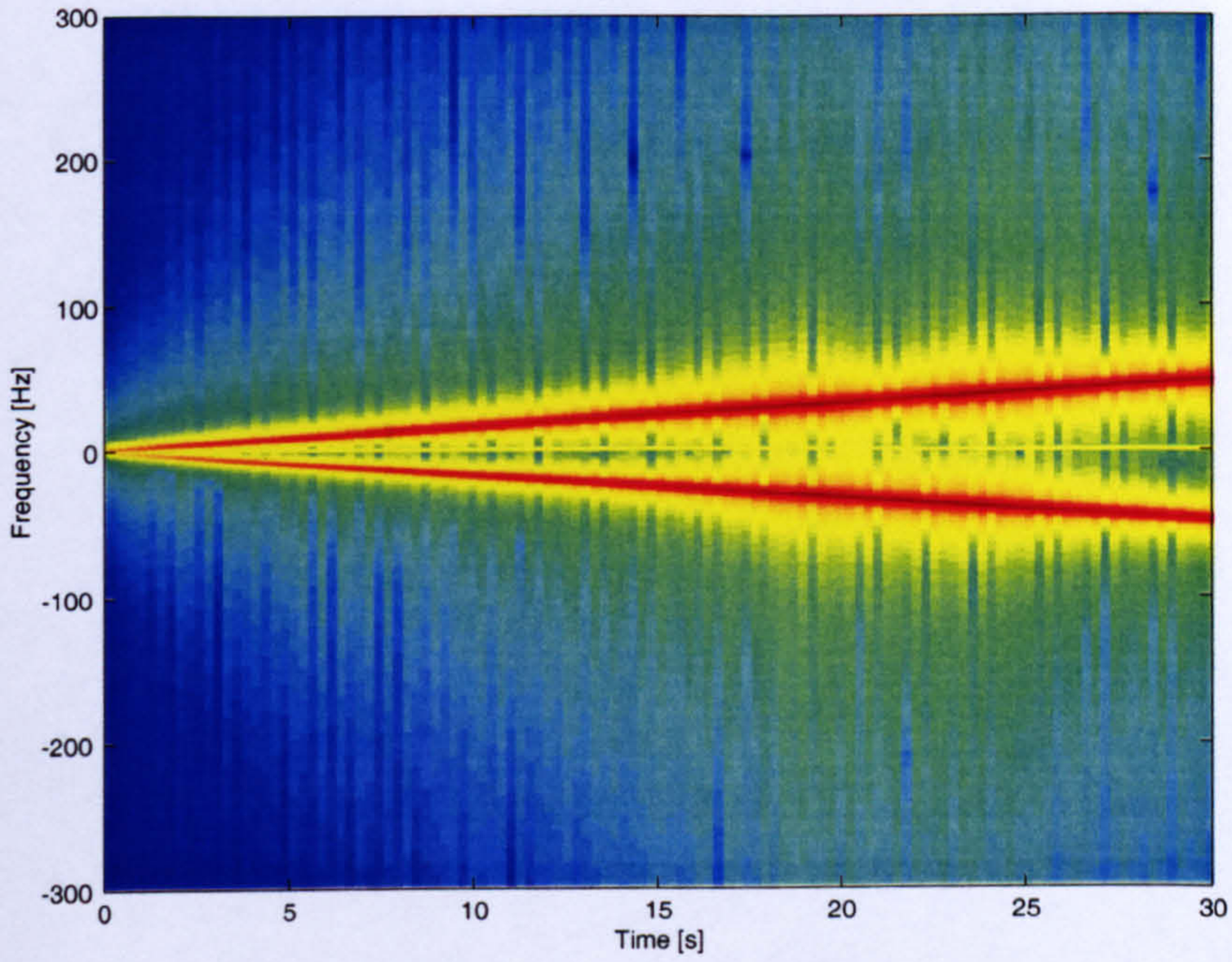


Fig 2.4.13 Symmetric Rotor, Anisotropic Bearings, with Unbalance Excitation

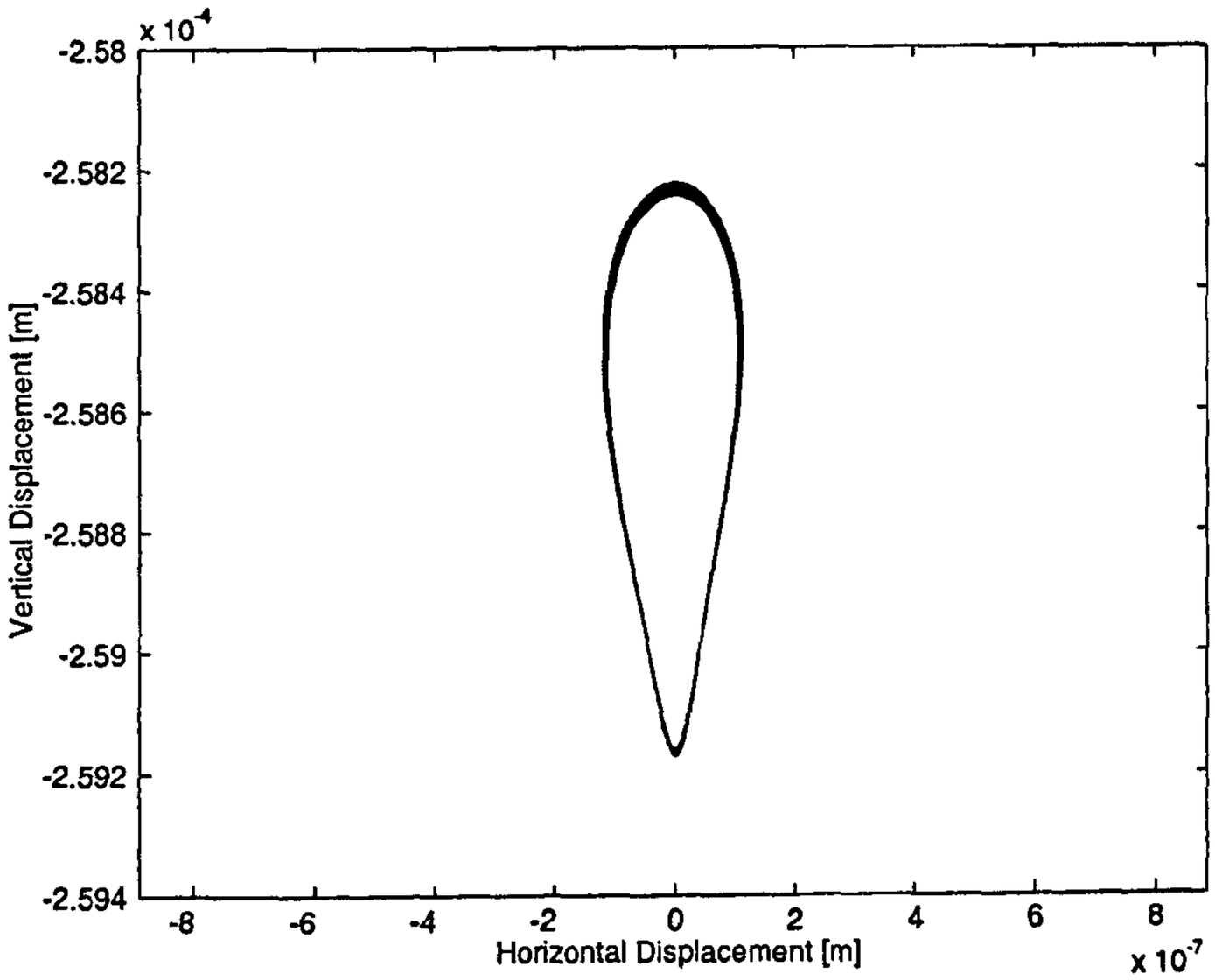
2.4.2 Steady-State Vibration Response Analysis

As with the transient response, the steady-state vibration response of the cracked rotor system operating at a specific speed of rotation (in this case, 500 rad/s) can be compared with other normal rotor systems associated with unbalance excitation.

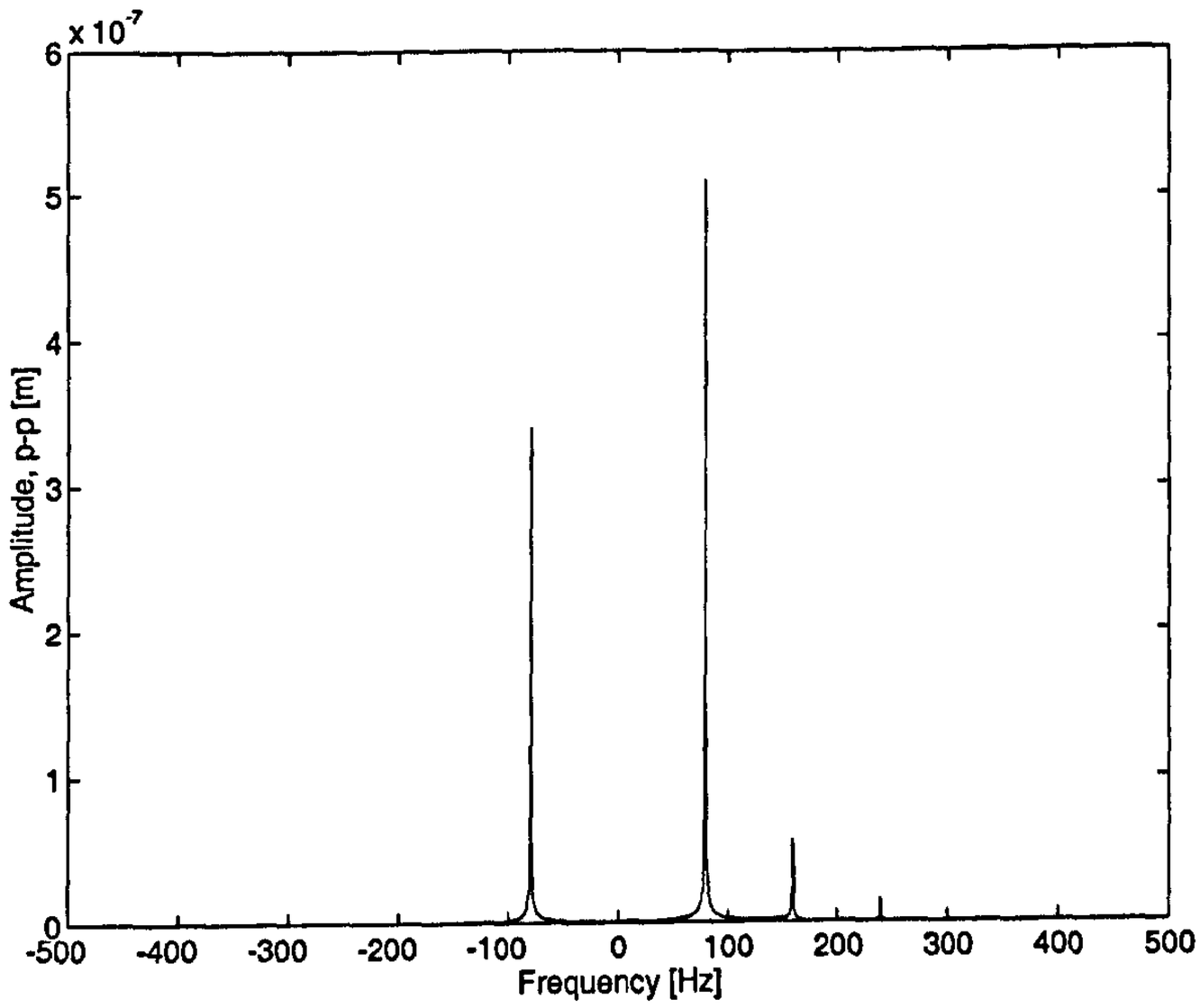
By decomposing the cracked rotor vibration response into forward whirl (FW) and backward whirl (BW) components, the $\pm 1\Omega$, $+2\Omega$, and $+3\Omega$ frequency components can be identified from the cracked rotor system (Fig 2.4.14) as already mentioned in transient response analysis. For 1Ω vibration, it is well-known that the most common fault, i.e. unbalance also excites 1Ω vibration (Fig 2.4.15). Moreover, there are also a large number of other faults besides unbalance which may influence the 1Ω vibration. Due to this fact, it is difficult to use the 1Ω vibration component as a discriminator for any faults - including cracks, which also affect the 1Ω vibration. The problem of determining a fault type in a unique way, based on the 1Ω vibration symptom alone, therefore becomes a non-trivial problem. In the case of 2Ω vibration, however, misalignment is possibly the other common and major fault, besides a crack, which is known to produce the 2Ω vibration. Fortunately, misalignment also generates large axial vibration levels and its lateral 2Ω vibration component remains constant with time. In an asymmetric rotor system such as a 2-pole generator rotor, the 2Ω vibration can also be generated (Fig 2.4.16), this vibration being due to the asymmetry of the rotor but remaining constant with time. Particularly from the cracked rotor vibration response (Fig 2.4.14), a relatively strong -1Ω vibration component can be identified. Due to this backward whirl vibration component, the orbit of the rotor forms a narrow ellipse. The -1Ω vibration component can also be identified in an anisotropic rotor system (Fig 2.4.17) under unbalance excitation. However, in this type of rotor system, backward whirl vibration is mainly excited in regions between two natural frequencies (caused by the two different bearing stiffnesses in orthogonal directions) of the rotor and so, by pre-identifying the modal properties of the bearings (usually provided by

the manufacturers), a certain amount of backward whirl vibration component can be predicted or expected at a given operating speed. For the cracked simple rotor model, when unbalance coexists with a crack, the $+1\Omega$ vibration dominates the response (Fig 2.4.18). However, the -1Ω vibration component remains unaffected by the unbalance excitation because unbalance at the designated operating speed only affects forward whirl synchronous vibration, i.e. the $+1\Omega$ component due to the bearing stiffness isotropy. Hence, in this case, the existence of -1Ω vibration provides an invaluable aid to crack detection.

Generally, it is known to be difficult to detect a crack while the rotor is spinning at a constant speed because most rotors operate in a range away from their critical speeds. In these conditions, the frequency components of multiple harmonics caused by a crack are small and therefore hard to detect. With the existence of unbalance, the 1Ω vibration dominates the vibration response. However, if we consider the physical nature of a crack, i.e. its inevitable growth or propagation, then the $\pm1\Omega$, $+2\Omega$, and $+3\Omega$ vibrations will be expected to increase as the crack grows as shown in Fig 2.4.19 (where the $+3\Omega$ vibration component has not been included due to its smallness). To estimate the growth of the crack-related harmonics only, the harmonics related with other faults have to be properly eliminated. For this purpose, the vibration data of the operating rotor system have to be recorded periodically to serve as baseline data. Based on each rotor model, and by using the pre-calculated growth rate of crack-related harmonics, the possibility and sensitivity of crack detection by analysis of vibration signals can be improved. In engineering situations, the growth rates of the $\pm1\Omega$ and $+2\Omega$ responses are considered to have practical importance, because changes in $+3\Omega$ and higher harmonics are found to be negligible for relatively shallow cracks. Also, it is considered to be essential to investigate the sensitivity of crack-induced harmonics according to the location of the crack along the shaft-line as a crack can be initiated at any location of the rotor.

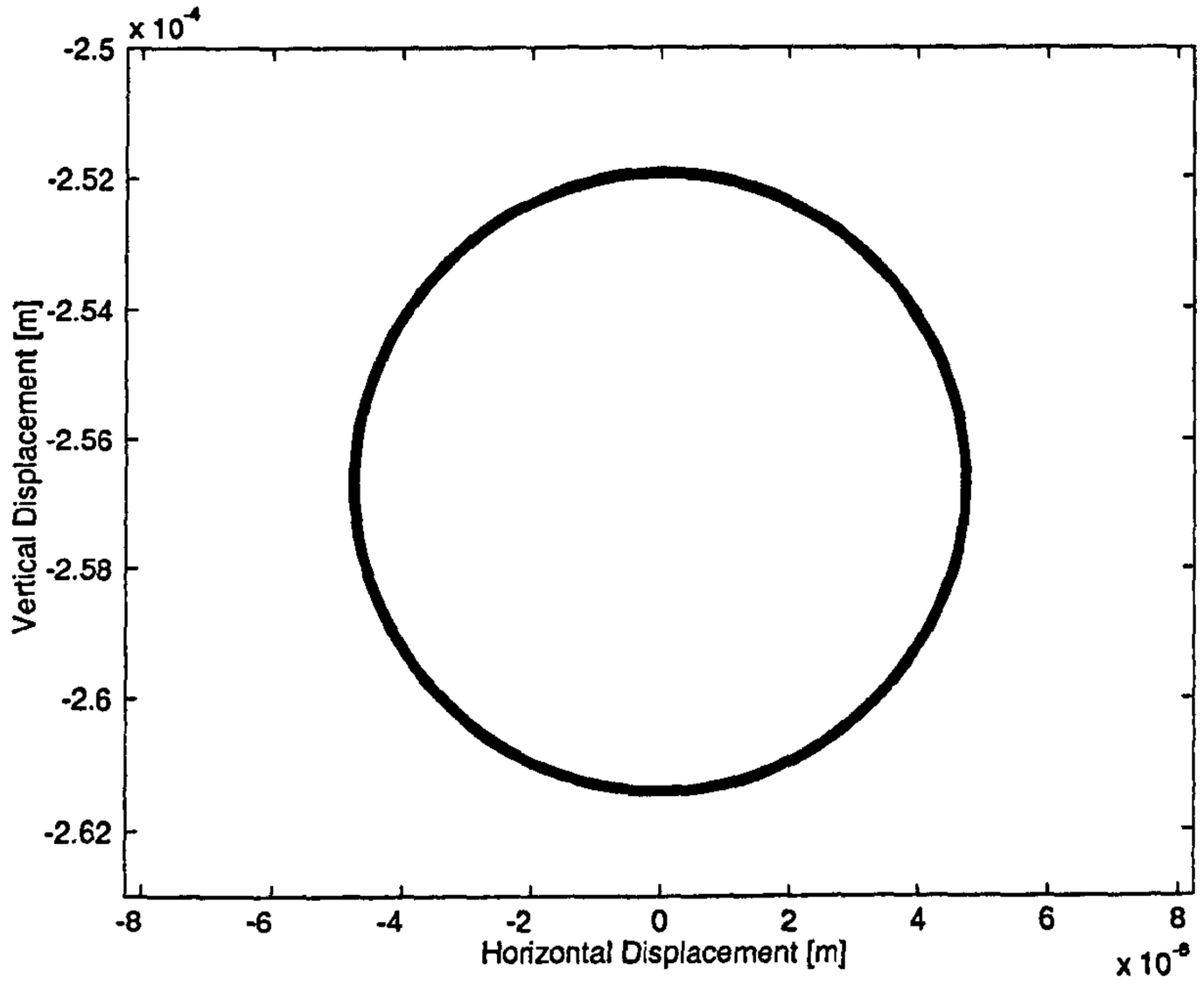


(a) Orbit

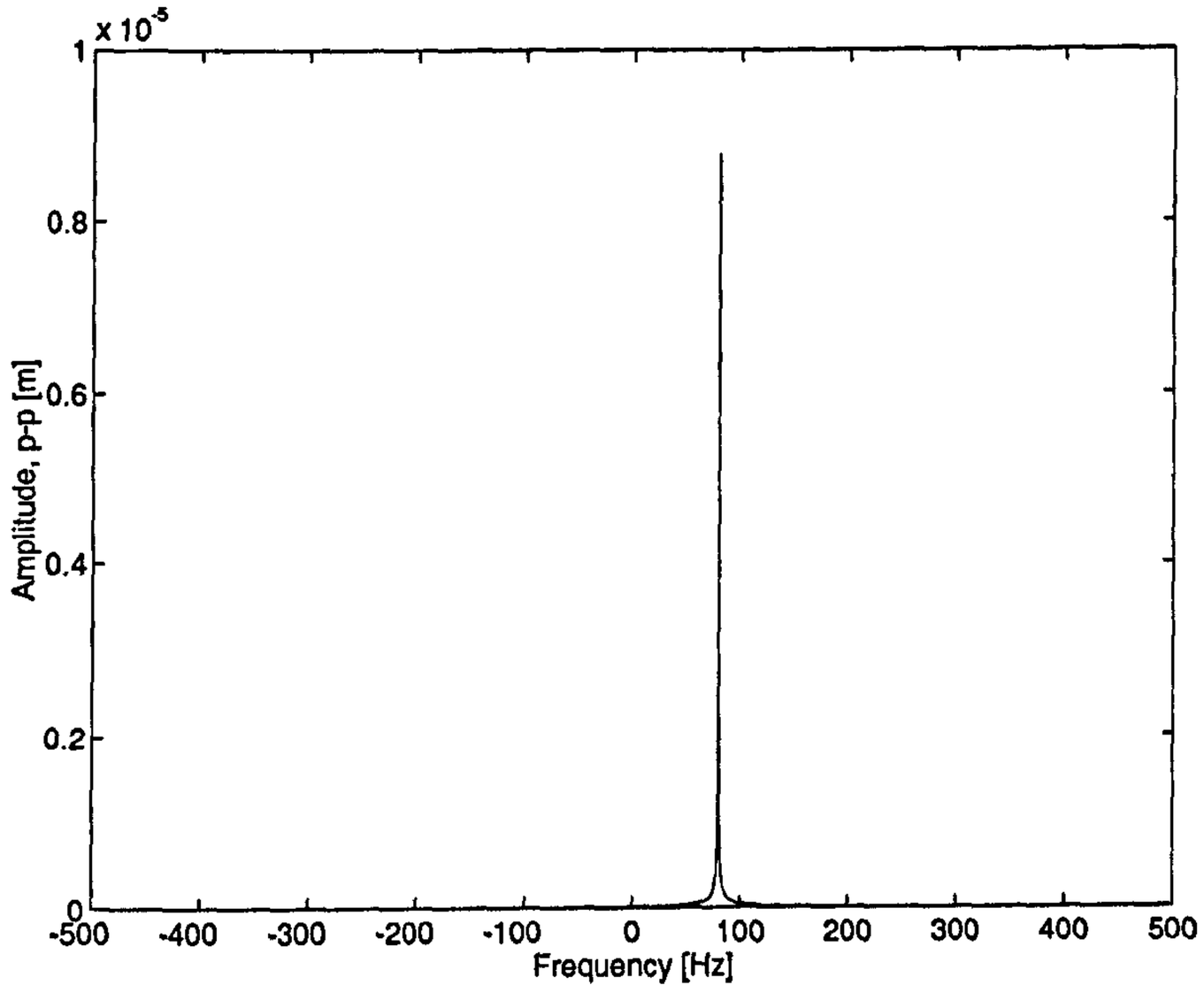


(b) Directional Frequency Spectrum

Fig 2.4.14 10 % Cracked Rotor on Isotropic Bearings

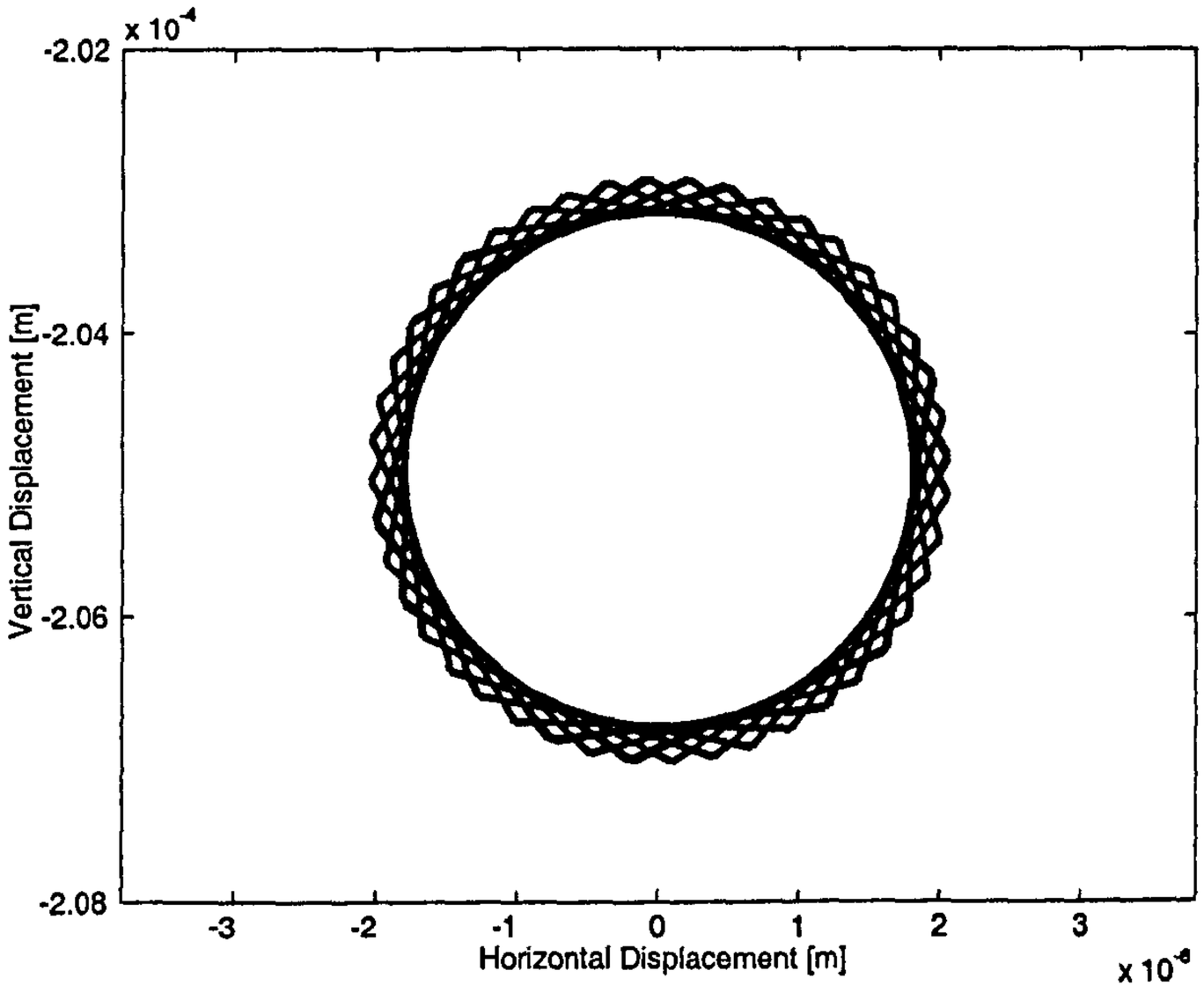


(a) Orbit

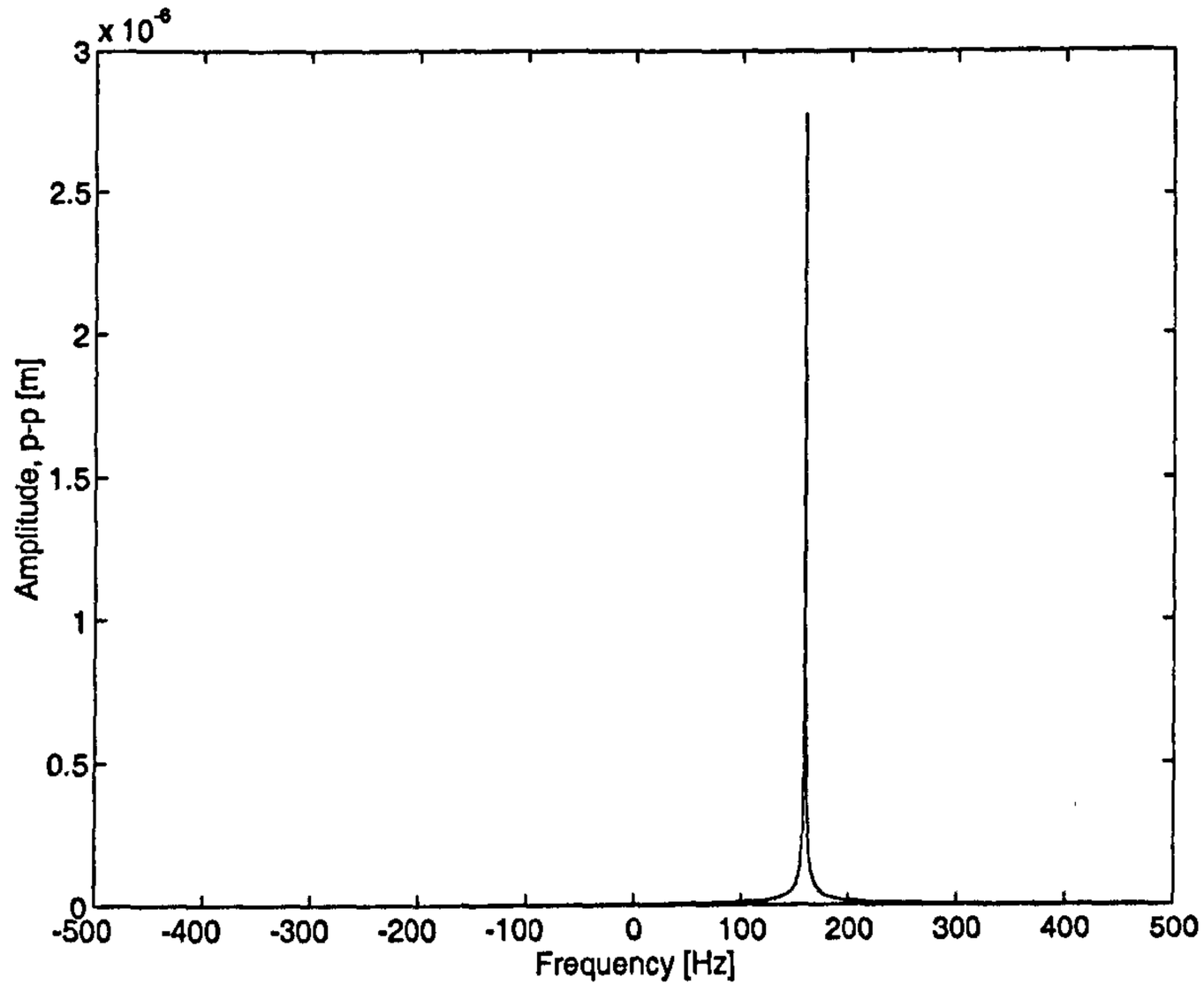


(b) Directional Frequency Spectrum

Fig 2.4.15 Symmetric Rotor with Unbalance on Isotropic Bearings

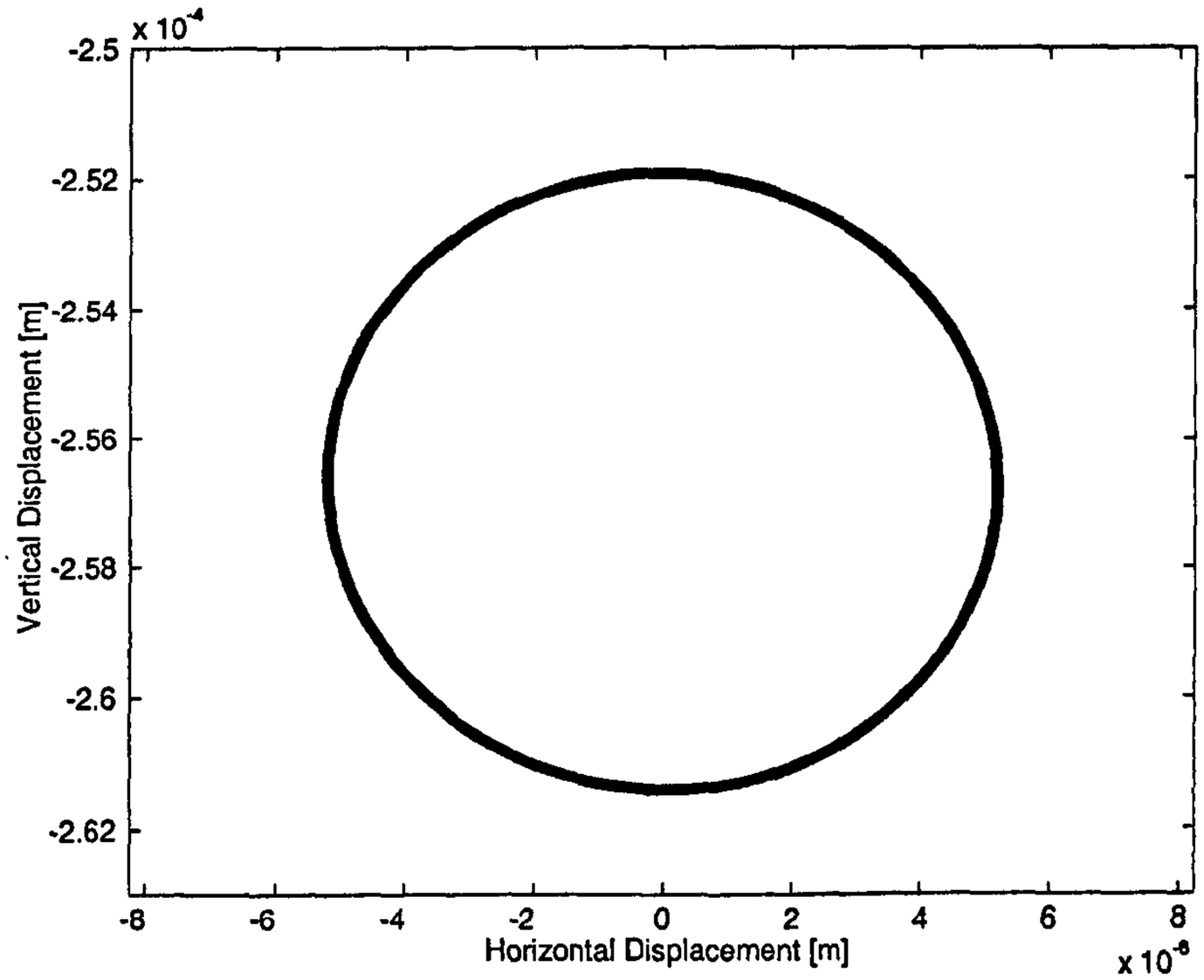


(a) Orbit

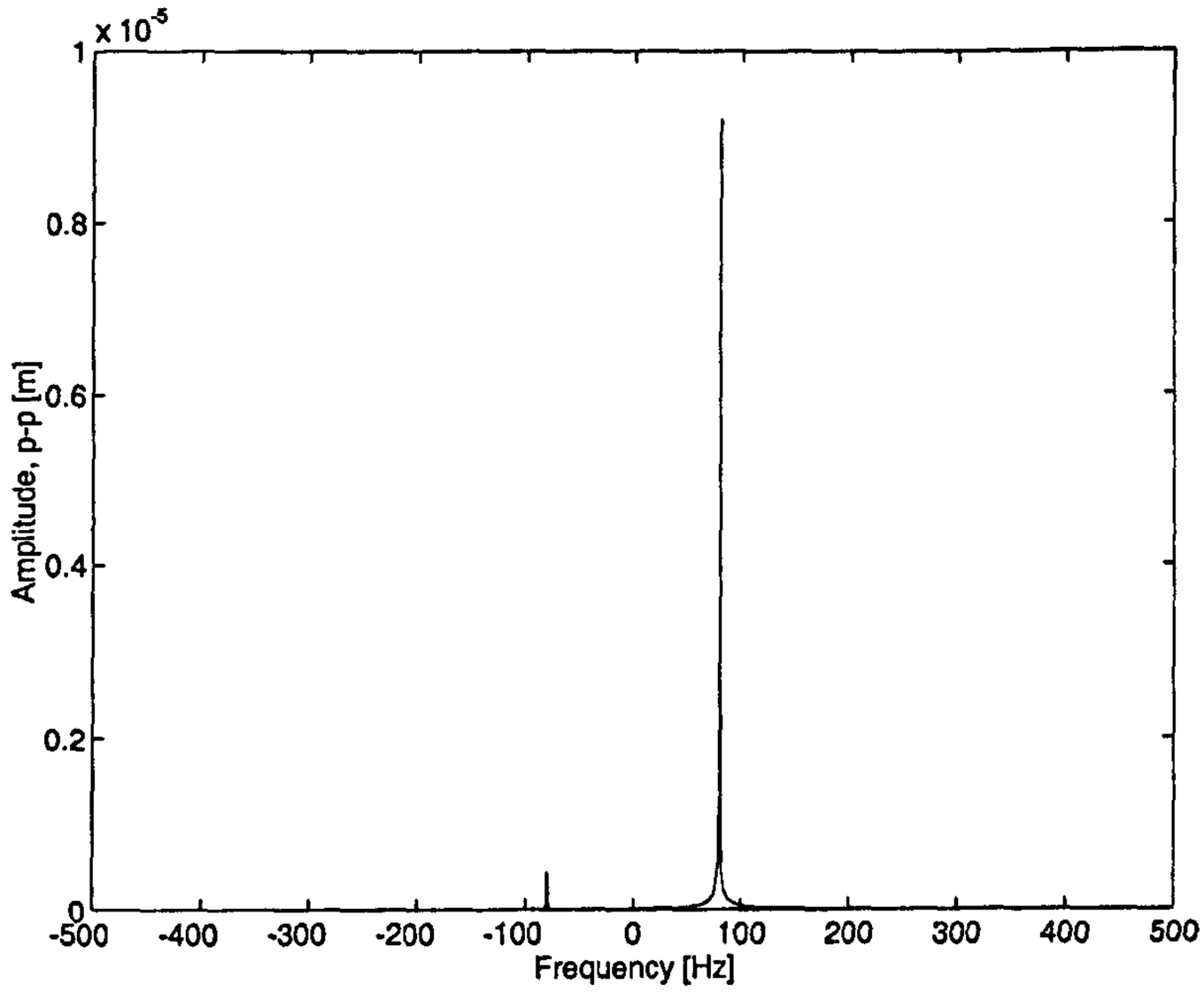


(b) Directional Frequency Spectrum

Fig 2.4.16 Asymmetric Rotor on Isotropic Bearings

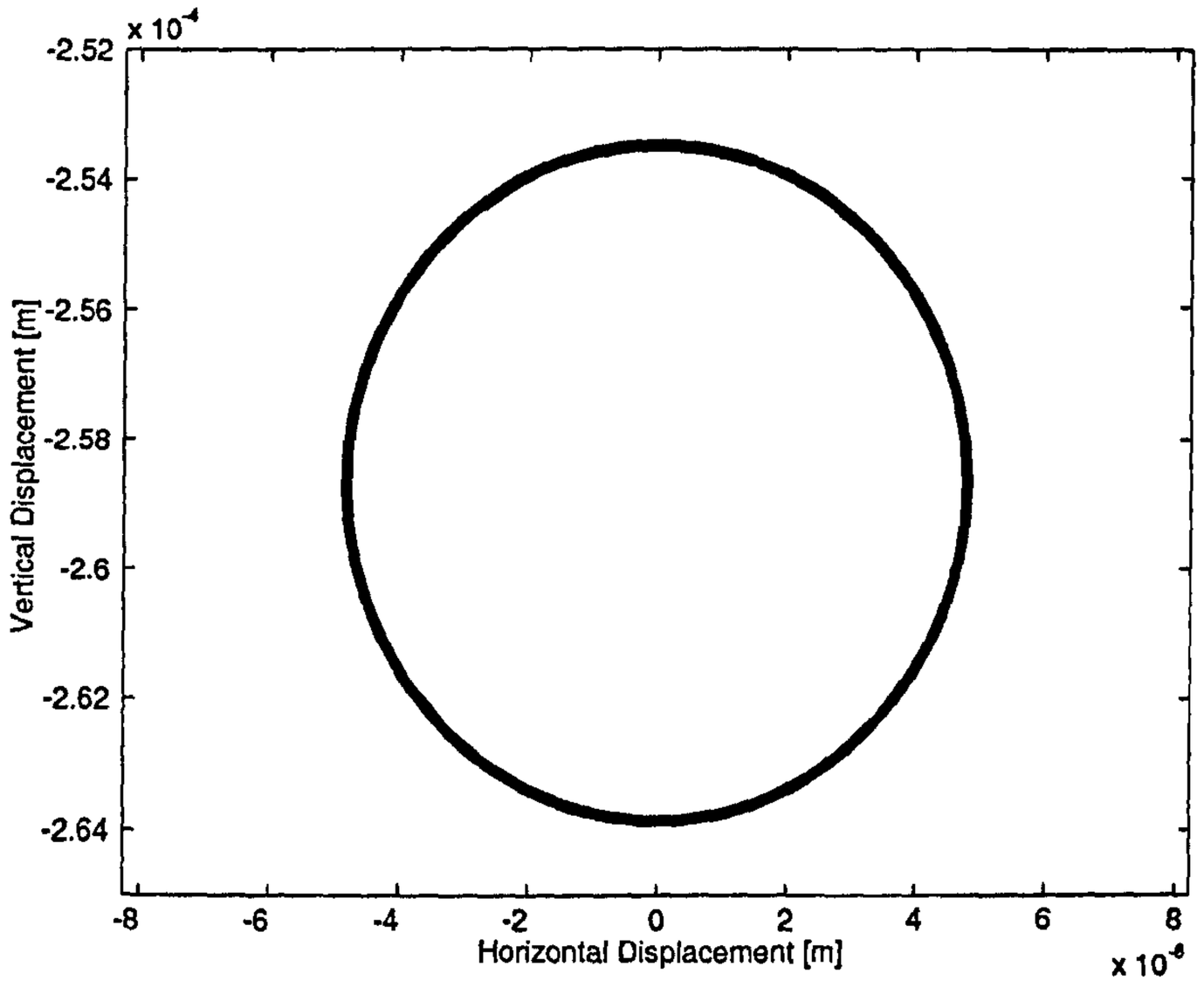


(a) Orbit

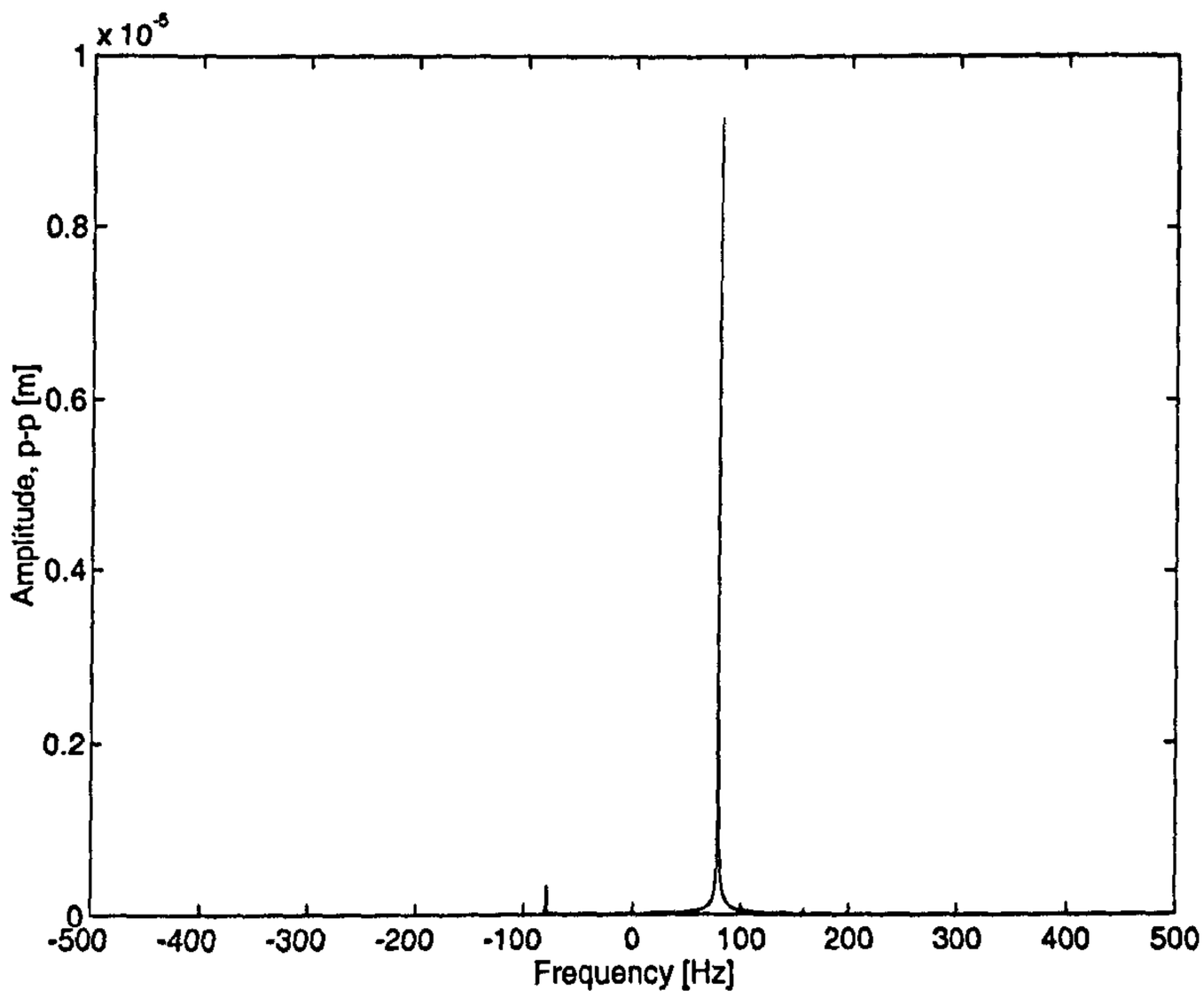


(b) Directional Frequency Spectrum

Fig 2.4.17 Symmetric Rotor with Unbalance on Anisotropic Bearings



(a) Orbit



(b) Directional Frequency Spectrum

Fig 2.4.18 10 % Cracked Rotor with Unbalance on Isotropic Bearings

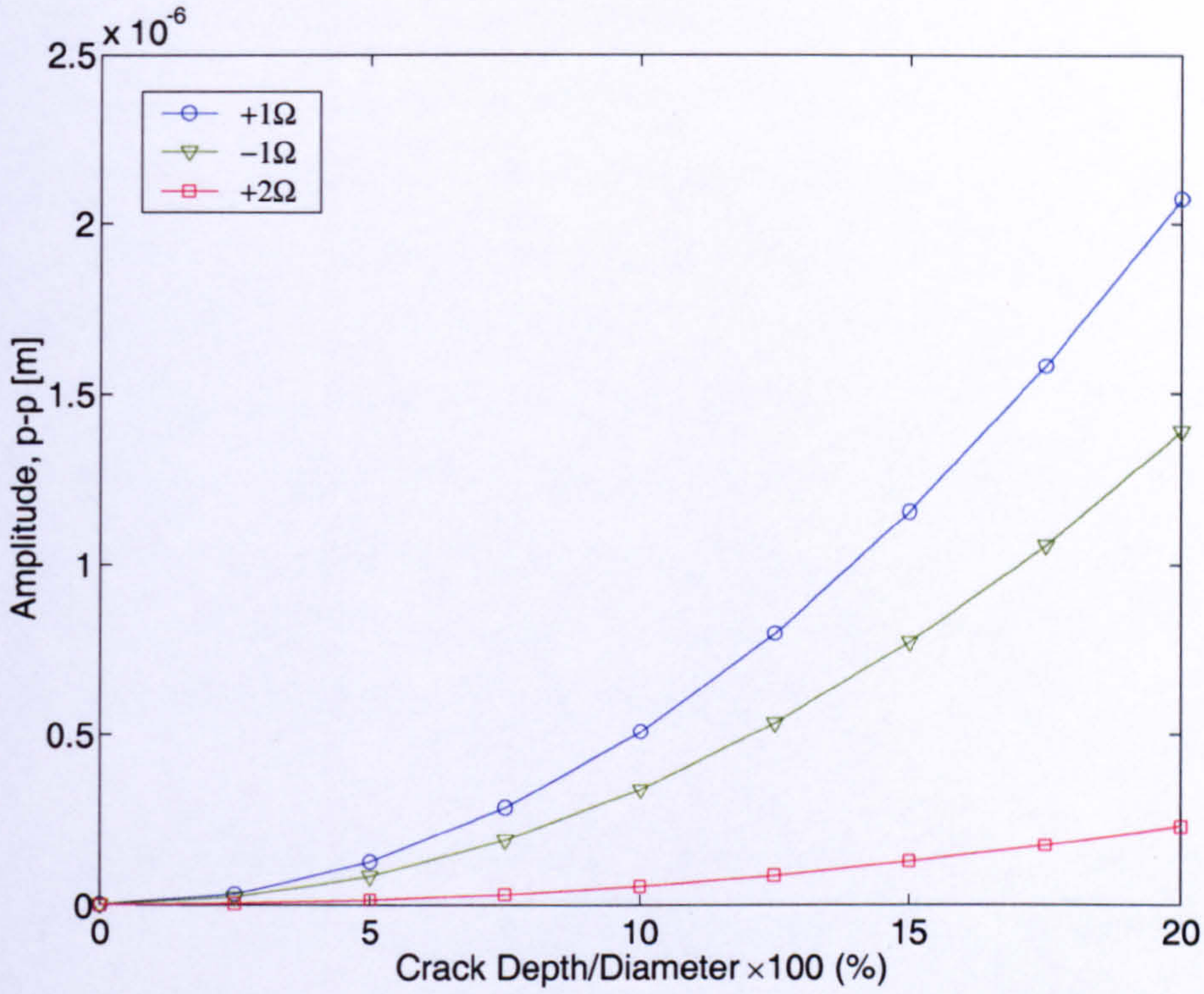


Fig 2.4.19 Directional Harmonics Sensitivity Map (DHSM)

2.5 Conclusions

To provide a basic understanding of the cracked rotor problem, a mathematical model for the simple rotor system with a transverse crack has been established by applying the Mayes & Davies' breathing crack assumption. In the model, due to the existence (open crack) and breathing (breathing crack) of the crack, the rotor stiffness becomes time-varying with the shaft rotation, and this makes the system equations of non-linear motion. Using the model, the cracked rotor's dynamic behaviour has been simulated and analysed both under transient and steady-state conditions. In both conditions, i.e. during a run-up or run-down period, or at constant operating speed, the rotor exhibits relatively strong -1Ω vibration components as well as $+1\Omega$, $+2\Omega$, and $+3\Omega$ components (similar results to those reported in [41] based on Gasch's hinge model where only transient response has been investigated). Stability of the rotor system has not been considered in the analysis according to the fact that the stability is markedly influenced only by a fairly deep crack, [77].

Until the present work, no extensive comparative research on cracked and normal rotor systems with various configurations (rotor asymmetry, bearing anisotropy, etc) has been reported. To develop a practical crack detection method, those rotor systems should be considered together. To this end, comparison of dynamic behaviour (both in transient and steady states) of cracked rotors and equivalent normal rotor systems with various different configurations has been performed here to serve as a basis for an improved crack detection strategy. From a series of calculations, it can be concluded that accurate system identification of the rotor system is essential for effective monitoring of rotating systems as the -1Ω & $+2\Omega$ frequency components can also be generated from anisotropic (bearing-anisotropy) & asymmetric (rotor-asymmetry) rotor systems, respectively.

Chapter 3
MDOF Rotor System with a Transverse Crack

3.1 Introduction

In this chapter, a multi-degree-of-freedom (MDOF) rotor system with a transverse crack has been modelled and analysed to provide a basis for an improved crack detection strategy. Since the 1970s, most previous work on the vibration analysis of cracked rotor systems has been performed with simple rotor models, sometimes represented by the 'Jeffcott rotor model'. Probably, the main reason for this was the fact that, even for the simple rotor system, the dynamic behaviour of the system due to the non-linearity caused by the 'breathing' effect of the crack is very complex. Due to this, the crack was almost always positioned at the disk location (lumped-mass position for the simple rotor system), so the sensitivity of the harmonics according to the various locations of the crack has not yet been investigated properly. To overcome such limitations caused by using simple rotor systems, a multi-degree-of-freedom (MDOF) rotor system with a transverse crack has been modelled based on the Finite Element Method (FEM) and its dynamic characteristics have been investigated for both transient and steady-state rotating conditions.

In particular, various vibration measurement positions and crack locations have been applied to the model by applying the state-space concept from control theory, and the directional harmonics sensitivity map presented in the previous chapter has been extended to a 3-dimensional form.

3.2 Modelling a MDOF Cracked Rotor System via the Finite Element Approach

A typical rotor bearing system is composed of a rotor shaft, disks, and bearings. The mass unbalance is also considered because it cannot be completely avoided in practice. The equations of motion of a general rotor system can be derived by applying Lagrange's equations, [79]:

$$\frac{d}{dt}\left(\frac{\partial T}{\partial \dot{q}_i}\right) - \frac{\partial T}{\partial q_i} + \frac{\partial V}{\partial q_i} = Q_i \tag{3.2.1}$$

where the number of degrees of freedom is N $(1 \leq i \leq N)$, q_i are generalised independent coordinates, and Q_i are generalised forces.

In (3.2.1), the kinetic energy (T) expressions are necessary to characterise the disk, shaft, and mass unbalances. The strain energy (V) expressions are necessary to characterise the shaft. The bearing coefficients can be obtained from the virtual work done by the bearing reaction forces acting on the shaft. Fig 3.2.1 presents the sign convention used for modelling the rotor system.

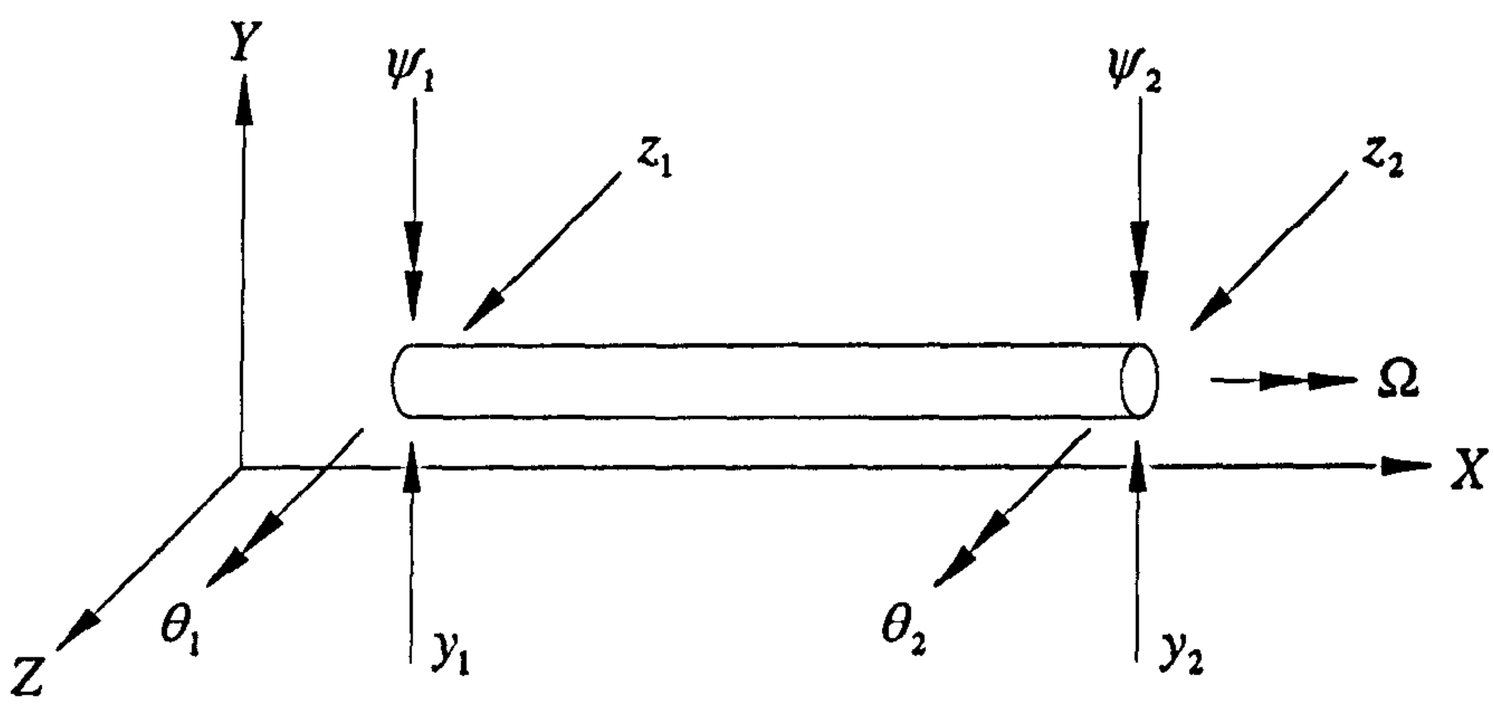


Fig 3.2.1 Sign Convention for Modelling

3.2.1 Shaft

The shaft is modelled as a beam with a constant circular cross-section. The shaft finite element has two nodes, which include 4 translational and 4 angular displacements. In Fig 3.2.1, the relations between translational and angular displacements are:

$$\psi = \frac{\partial z}{\partial x}, \theta = \frac{\partial y}{\partial x} \tag{3.2.2}$$

and the nodal displacement vector is:

$$\boldsymbol{q} = [y_1 \;\; z_1 \;\; \psi_1 \;\; \theta_1 \;\; y_2 \;\; z_2 \;\; \psi_2 \;\; \theta_2]^{\mathrm{T}} \tag{3.2.3}$$

which includes the displacements q_y and q_z corresponding to the motions in the Y and Z directions respectively, i.e.:

$$\boldsymbol{q}_y = [y_1 \;\; \theta_1 \;\; y_2 \;\; \theta_2]^{\mathrm{T}} \tag{3.2.4}$$

$$\boldsymbol{q}_z = [z_1 \;\; \psi_1 \;\; z_2 \;\; \psi_2]^{\mathrm{T}} \tag{3.2.5}$$

The vertical and horizontal displacements can be expressed using the shape (or interpolation) function $\boldsymbol{S}(x)$:

$$\boldsymbol{y} = \boldsymbol{S}(x)\,\boldsymbol{q}_y \tag{3.2.6}$$

$$\boldsymbol{z} = \boldsymbol{S}(x)\,\boldsymbol{q}_z \tag{3.2.7}$$

where $\boldsymbol{S}(x)$ is the typical shape (or interpolation) function of a beam in bending, and it should be noted that the shape functions become the same in both planes due to the choice of coordinates as in Fig 3.2.1.

$$\boldsymbol{S}(x) = [\boldsymbol{S}_1(x)\ \boldsymbol{S}_2(x)\ \boldsymbol{S}_3(x)\ \boldsymbol{S}_4(x)] \tag{3.2.8}$$

where

$$\boldsymbol{S}_1(x) = 1 - 3(x/L)^2 + 2(x/L)^3$$

$$\boldsymbol{S}_2(x) = -x + 2x^2/L - x^3/L^2$$

$$\boldsymbol{S}_3(x) = 3(x/L)^2 - 2(x/L)^3$$

$$\boldsymbol{S}_4(x) = -x^2/L + x^3/L^2$$

The kinetic energy of the shaft can be obtained:

$$T = \frac{\rho A}{2}\int_0^L [\dot{\boldsymbol{q}}_y^{\mathrm{T}}\boldsymbol{S}^{\mathrm{T}}\boldsymbol{S}\dot{\boldsymbol{q}}_y + \dot{\boldsymbol{q}}_z^{\mathrm{T}}\boldsymbol{S}^{\mathrm{T}}\boldsymbol{S}\dot{\boldsymbol{q}}_z]dx + \frac{\rho I}{2}\int_0^L [\dot{\boldsymbol{q}}_y^{\mathrm{T}}\frac{d\boldsymbol{S}^{\mathrm{T}}}{dx}\frac{d\boldsymbol{S}}{dx}\dot{\boldsymbol{q}}_y + \dot{\boldsymbol{q}}_z^{\mathrm{T}}\frac{d\boldsymbol{S}^{\mathrm{T}}}{dx}\frac{d\boldsymbol{S}}{dx}\dot{\boldsymbol{q}}_z]dx$$

$$-2\rho I\Omega\int_0^L \dot{\boldsymbol{q}}_z^{\mathrm{T}}\frac{d\boldsymbol{S}^{\mathrm{T}}}{dx}\frac{d\boldsymbol{S}}{dx}\boldsymbol{q}_y dx + \rho I L\Omega^2 \tag{3.2.9}$$

After integration:

$$T = \tfrac{1}{2}\dot{\boldsymbol{q}}_y^{\mathrm{T}}\boldsymbol{m}\dot{\boldsymbol{q}}_y + \tfrac{1}{2}\dot{\boldsymbol{q}}_z^{\mathrm{T}}\boldsymbol{m}\dot{\boldsymbol{q}}_z + \tfrac{1}{2}\dot{\boldsymbol{q}}_y^{\mathrm{T}}\boldsymbol{m}_R\dot{\boldsymbol{q}}_y + \tfrac{1}{2}\dot{\boldsymbol{q}}_z^{\mathrm{T}}\boldsymbol{m}_R\dot{\boldsymbol{q}}_z - \Omega\dot{\boldsymbol{q}}_z^{\mathrm{T}}\boldsymbol{G}_S\boldsymbol{q}_y + \rho I L\Omega^2 \tag{3.2.10}$$

where the matrix $\boldsymbol{m}$ is the classical mass matrix, $\boldsymbol{m}_R$ gives the effect of rotary inertia, and $\boldsymbol{G}_S$ gives the gyroscopic effect.

Also, the strain energy of the shaft can be obtained:

$$V = \frac{EI}{2}\int_0^L \left[\boldsymbol{q}_y^{\mathrm{T}} \frac{d^2\boldsymbol{S}^{\mathrm{T}}}{dx^2}\frac{d^2\boldsymbol{S}}{dx^2}\boldsymbol{q}_y + \boldsymbol{q}_z^{\mathrm{T}} \frac{d^2\boldsymbol{S}^{\mathrm{T}}}{dx^2}\frac{d^2\boldsymbol{S}}{dx^2}\boldsymbol{q}_z \right] dx \tag{3.2.11}$$

After integration, the strain energy becomes

$$V = \frac{1}{2}\boldsymbol{q}_y^{\mathrm{T}}\boldsymbol{k}_S\boldsymbol{q}_y + \frac{1}{2}\boldsymbol{q}_z^{\mathrm{T}}\boldsymbol{k}_S\boldsymbol{q}_z \tag{3.2.12}$$

where the matrix $\boldsymbol{k}_S$ is the classical stiffness matrix.

Finally, application of Lagrange's equations gives:

$$\frac{d}{dt}\left(\frac{\partial T}{\partial \dot{\boldsymbol{q}}}\right) - \frac{\partial T}{\partial \boldsymbol{q}} + \frac{\partial V}{\partial \boldsymbol{q}} =$$

$$\begin{bmatrix} \boldsymbol{m}+\boldsymbol{m}_R & 0 \\ 0 & \boldsymbol{m}+\boldsymbol{m}_R \end{bmatrix}\begin{bmatrix} \ddot{\boldsymbol{q}}_y \\ \ddot{\boldsymbol{q}}_z \end{bmatrix} + \begin{bmatrix} 0 & \Omega\boldsymbol{G}_S \\ -\Omega\boldsymbol{G}_S & 0 \end{bmatrix}\begin{bmatrix} \dot{\boldsymbol{q}}_y \\ \dot{\boldsymbol{q}}_z \end{bmatrix} + \begin{bmatrix} \boldsymbol{k}_S & 0 \\ 0 & \boldsymbol{k}_S \end{bmatrix}\begin{bmatrix} \boldsymbol{q}_y \\ \boldsymbol{q}_z \end{bmatrix} \tag{3.2.13}$$

where

$$\boldsymbol{m} = \frac{\rho AL}{420}\begin{bmatrix} 156 & 22L & 54 & -13L \\ & 4L^2 & 13L & -3L^2 \\ & & 156 & -22L \\ \mathrm{SYM} & & & 4L^2 \end{bmatrix},\ \boldsymbol{m}_R = \frac{1}{2}\boldsymbol{G}_S$$

$$\boldsymbol{G}_S = \frac{\rho I}{15L}\begin{bmatrix} 36 & 3L & -36 & 3L \\ & 4L^2 & -3L & -L^2 \\ & & 36 & -3L \\ \mathrm{SYM} & & & 4L^2 \end{bmatrix},\ \boldsymbol{k}_S = \frac{EI}{L^3}\begin{bmatrix} 12 & 6L & -12 & 6L \\ & 4L^2 & -6L & 2L^2 \\ & & 12 & -6L \\ \mathrm{SYM} & & & 4L^2 \end{bmatrix}$$

As can be seen in equation (3.2.13), the skew-symmetric gyroscopic matrix changes with the shaft rotation while the mass and stiffness matrices remain constant. Also, due to this skew-symmetry caused by the gyroscopic matrix, there is a coupling in the two planes, i.e. vertical and horizontal planes, which does not appear for non-rotating rotors.

3.2.2 Disk

In most cases, a disk can be considered to be rigid, and this leads the modelling of the disk using the concentrated mass and moment of inertia at a node on the shaft span where the disk is located. At a given node, the rotor has 4 degrees of freedom:

$$\boldsymbol{q} = [\,y \;\; \theta \;\; z \;\; \psi\,]^{\mathrm{T}}\,,\; \boldsymbol{q}_{Dy} = [\,y \;\; \theta\,]^{\mathrm{T}}\,,\; \boldsymbol{q}_{Dz} = [\,z \;\; \psi\,]^{\mathrm{T}} \tag{3.2.14}$$

The kinetic energy of the disk can be obtained:

$$T = \frac{1}{2} m_D(\dot{y}^2 + \dot{z}^2) + \frac{1}{2} I_D(\dot{\theta}^2 + \dot{\psi}^2) + \frac{1}{2} J_D(\Omega^2 - 2\Omega\theta\dot{\psi}) \tag{3.2.15}$$

Hence, by applying Lagrange's equations, the disk has the following form of equations of motion:

$$\frac{d}{dt}\left(\frac{\partial T}{\partial \dot{\boldsymbol{q}}}\right) - \frac{\partial T}{\partial \boldsymbol{q}} + \frac{\partial V}{\partial \boldsymbol{q}} =$$

$$\begin{bmatrix} \boldsymbol{m}_D & 0 \\ 0 & \boldsymbol{m}_D \end{bmatrix} \begin{bmatrix} \ddot{\boldsymbol{q}}_{Dy} \\ \ddot{\boldsymbol{q}}_{Dz} \end{bmatrix} + \begin{bmatrix} 0 & \Omega \boldsymbol{G}_D \\ -\Omega \boldsymbol{G}_D & 0 \end{bmatrix} \begin{bmatrix} \dot{\boldsymbol{q}}_{Dy} \\ \dot{\boldsymbol{q}}_{Dz} \end{bmatrix} \tag{3.2.16}$$

where

$$\boldsymbol{m}_D = \begin{bmatrix} m_D & 0 \\ 0 & I_D \end{bmatrix},\; \boldsymbol{G}_D = \begin{bmatrix} 0 & 0 \\ 0 & J_D \end{bmatrix}$$

As in the case of the shaft, the disk produces a skew-symmetric gyroscopic matrix. It can also be noticed that the gyroscopic effect will be substantial not only with the increase of the rotation speed but also with that of the disk radius as the gyroscopic term is proportional to the 4th-power of the disk radius.

3.2.3 Bearings

The stiffness and viscous damping terms are assumed to be known and, generally, the rotational influences can be neglected. The virtual work, δW, of the forces acting on the shaft can be written as:

$$\delta W = -k_{yy}y\delta y - k_{yz}z\delta y - k_{zy}y\delta z - k_{zz}z\delta z - c_{yy}\dot{y}\delta y - c_{yz}\dot{z}\delta y - c_{zy}\dot{y}\delta z - c_{zz}\dot{z}\delta z \quad (3.2.17)$$

or

$$\delta W = F_{By}\delta y + F_{Bz}\delta z \quad (3.2.18)$$

where F_{By} & F_{Bz} are the components of the bearing reaction forces. In matrix form:

$$\begin{bmatrix} F_{By} \\ F_{Bz} \end{bmatrix} = -\begin{bmatrix} k_{yy} & k_{yz} \\ k_{zy} & k_{zz} \end{bmatrix}\begin{bmatrix} y \\ z \end{bmatrix} - \begin{bmatrix} c_{yy} & c_{yz} \\ c_{zy} & c_{zz} \end{bmatrix}\begin{bmatrix} \dot{y} \\ \dot{z} \end{bmatrix}$$

3.2.4 Mass Unbalance

The unbalance is defined by a mass m_u located at a distance ε from the geometric centre of the shaft. The kinetic energy of the mass unbalance can be expressed:

$$T \approx m_u[-\dot{y}\varepsilon\Omega\sin(\Omega t + \alpha) + \dot{z}\varepsilon\Omega\cos(\Omega t + \alpha)] \quad (3.2.19)$$

Application of Lagrange's equations will give the so-called centrifugal force vector, i.e.:

$$\frac{d}{dt}\left(\frac{\partial T}{\partial \dot{q}_u}\right) - \frac{\partial T}{\partial q_u} + \frac{\partial V}{\partial q_u} = -m_u \varepsilon \Omega^2 \begin{bmatrix} \cos(\Omega t + \alpha) \\ \sin(\Omega t + \alpha) \end{bmatrix} \tag{3.2.20}$$

where

$q_u = [y \;\; z]^T$

3.2.5 Transverse Crack

For general MDOF rotor systems (without a crack), the equations of motion can be obtained by assembling the element matrices into global matrices:

$$M\,\ddot{q}(t) + [\,C + G(\Omega)\,]\,\dot{q}(t) + K\,q(t) = F_g \tag{3.2.21}$$

where

M : mass matrix

C : damping matrix

$G(\Omega)$: gyroscopic matrix

K : stiffness matrix

$q(t)$: displacement matrix

F_g : static force due to gravity

With a transverse crack, the stiffness of the shaft is reduced and becomes time-varying with the shaft rotation. Hence, the equations of motion of a cracked rotor system will have the following form:

$$M\,\ddot{q}(t) + [\,C + G(\Omega)\,]\,\dot{q}(t) + K(t)\,q(t) = F_g \tag{3.2.22}$$

A crack in a rotor usually causes relatively small changes in stiffness, $\Delta \boldsymbol{K}$. Hence the stiffness matrix $\boldsymbol{K}(t)$ of the cracked rotor can be decomposed:

$$\boldsymbol{K}(t) = \boldsymbol{K}_0 + \Delta \boldsymbol{K}(t) \tag{3.2.23}$$

where $\boldsymbol{K}_0$ is the stiffness matrix of the normal rotor system. Further, the vibration response, $\boldsymbol{q}(t)$, can be decomposed from its static deflection, i.e.:

$$\boldsymbol{q}(t) = \boldsymbol{q}_{st} + \Delta \boldsymbol{q}(t) \tag{3.2.24}$$

where $\Delta \boldsymbol{q}(t)$ is the additional vibrational response of the rotor due to the crack. Hence, equation (3.2.22) can be expressed:

$$\begin{aligned} &\boldsymbol{M}\,\Delta\ddot{\boldsymbol{q}}(t) + [\boldsymbol{C} + \boldsymbol{G}(\Omega)]\,\Delta\dot{\boldsymbol{q}}(t) + [\boldsymbol{K}_0 + \Delta \boldsymbol{K}(t)]\,\Delta \boldsymbol{q}(t) \\ &= -[\boldsymbol{K}_0 + \Delta \boldsymbol{K}(t)]\,\boldsymbol{q}_{st} + \boldsymbol{F}_g = -\Delta \boldsymbol{K}(t)\,\boldsymbol{q}_{st} \end{aligned} \tag{3.2.25}$$

If the crack is not very large ($a/r < 0.5$),

$\Delta \boldsymbol{K}(t)\,\Delta \boldsymbol{q}(t) \approx 0$,

so, equation (3.2.25) finally becomes:

$$\boldsymbol{M}\,\Delta\ddot{\boldsymbol{q}}(t) + [\boldsymbol{C} + \boldsymbol{G}(\Omega)]\,\Delta\dot{\boldsymbol{q}}(t) + \boldsymbol{K}_0\,\Delta \boldsymbol{q}(t) = -\Delta \boldsymbol{K}(t)\,\boldsymbol{q}_{st} \tag{3.2.26}$$

The residual term '$-\Delta \boldsymbol{K}(t)\,\boldsymbol{q}_{st}$' due to the crack acts like an external force ('crack-induced self-excitation'), i.e.:

$$\boldsymbol{F}_c = -\Delta \boldsymbol{K}(t)\,\boldsymbol{q}_{st} \tag{3.2.27}$$

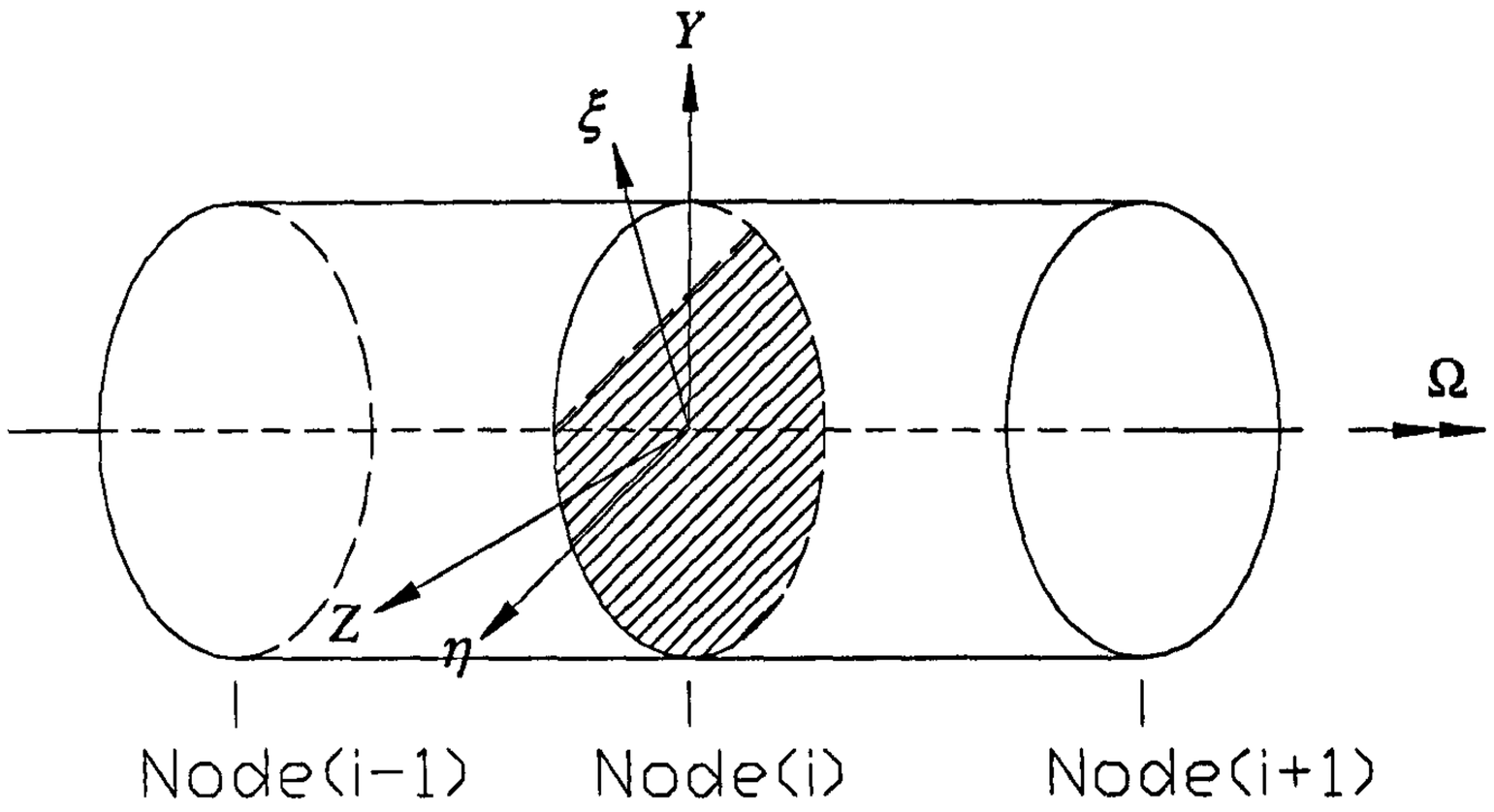


Fig 3.2.2 Transverse Crack located at Node *i*

In deriving the crack excitation force, F_c, the residual stiffness $\Delta K(t)$ must be defined. Assuming that a crack is located at node i along the shaft, as shown in Fig 3.2.2, the residual stiffness can be defined in rotating frame of reference:

$$\Delta K_R = \begin{bmatrix} \Delta k_\xi^i(t) & 0 \\ 0 & \Delta k_\eta^i(t) \end{bmatrix} \tag{3.2.28}$$

At this point, it should be noted that the model complexity has been limited by defining the residual stiffnesses only from translational displacements due to insufficient knowledge of the nature of true stiffness variation of angular displacements due to the crack.

In equation (3.2.28), the residual (or reduced) stiffnesses are:

$$\begin{aligned} \Delta k_\xi^i(t) &= -k_0 \cdot \gamma_\xi \cdot h(t) \\ \Delta k_\eta^i(t) &= -k_0 \cdot \gamma_\eta \cdot h(t) \end{aligned} \tag{3.2.29}$$

The parameters γ_ξ & γ_η represent stiffness reduction ratio, and are usually estimated as ratios of moments of inertia as I_ξ/I_0 & I_η/I_0 due to the crack, respectively. The breathing function, $h(t)$, is a periodic function dependent on the rotation of the shaft. In this work, the following effective moments of inertia, which are based on the geometry of a cracked cross-section [94], have been used:

$$I_\xi = r^4[6(\pi + p) + 8\sin p + \sin 2p]/48,\ p = 2\arcsin(1 - a/r)$$
$$I_\eta = \pi r^4/4 \tag{3.2.30}$$

and Mayes & Davis' crack model [87] has been used for the breathing function which has the following form:

$$h(t) = \frac{1}{2}(1 + \cos\Omega t) \tag{3.2.31}$$

Using the transformation matrix, $\boldsymbol{T}$, relating the rotational and inertial coordinates, the residual stiffness can be described in the inertial frame of reference:

$$\Delta \boldsymbol{K}(t) = \boldsymbol{T}^{\mathrm{T}} \Delta \boldsymbol{K}_R \boldsymbol{T} = \begin{bmatrix} \Delta k^i_{yy}(t) & \Delta k^i_{yz}(t) \\ \Delta k^i_{zy}(t) & \Delta k^i_{zz}(t) \end{bmatrix} \tag{3.2.32}$$

where the transformation matrix

$$\boldsymbol{T} = \begin{bmatrix} \cos\Omega t & \sin\Omega t \\ -\sin\Omega t & \cos\Omega t \end{bmatrix}$$

Finally, an equivalent crack excitation term in equation (3.2.27) can be expressed as:

$$\boldsymbol{F}_c = [F^i_{cy} \quad F^i_{cz}]^{\mathrm{T}} = [-\Delta k^i_{yy}(t)\cdot y^i_{st} \quad -\Delta k^i_{zy}(t)\cdot y^i_{st}]^{\mathrm{T}} \tag{3.2.33}$$

where

$$\Delta k^i_{yy}(t) = -k^i_0 \sin^2(0.5\Omega t) + \frac{k^i_\xi + k^i_\eta}{2}\sin^2(0.5\Omega t) + \frac{k^i_\xi - k^i_\eta}{2}\sin^2(0.5\Omega t)\cdot\cos(2\Omega t)$$

$$\Delta k^i_{zy}(t) = \frac{k^i_\xi - k^i_\eta}{2}\sin^2(0.5\Omega t)\cdot\sin(2\Omega t)$$

With the static deflection information (due to gravity) along the shaft-line, the local transverse crack can be described as an equivalent external excitation term. With this equivalent linearised crack model, the rotor system with a transverse crack located at any node can be simulated. Also, by this way of modelling, i.e. the positioning of a crack at a node, the effect of the crack will be more localised than the conventional way of MDOF cracked rotor modelling where the crack is positioned at an element. Fig 3.2.2 demonstrates the efficiency of the improved modelling technique with the stiffness matrix of a 7-element structure. As can be noticed from the figure, the cracked node concept gives better localisation (1 node) while the existing methods provide an effect spread over effectively 2 nodes. This practical reduction in model complexity also enables faster prediction, and this feature is considered to be particularly useful for industry rotor models where the calculation time often takes lots of time due to its complexity in geometric configurations.

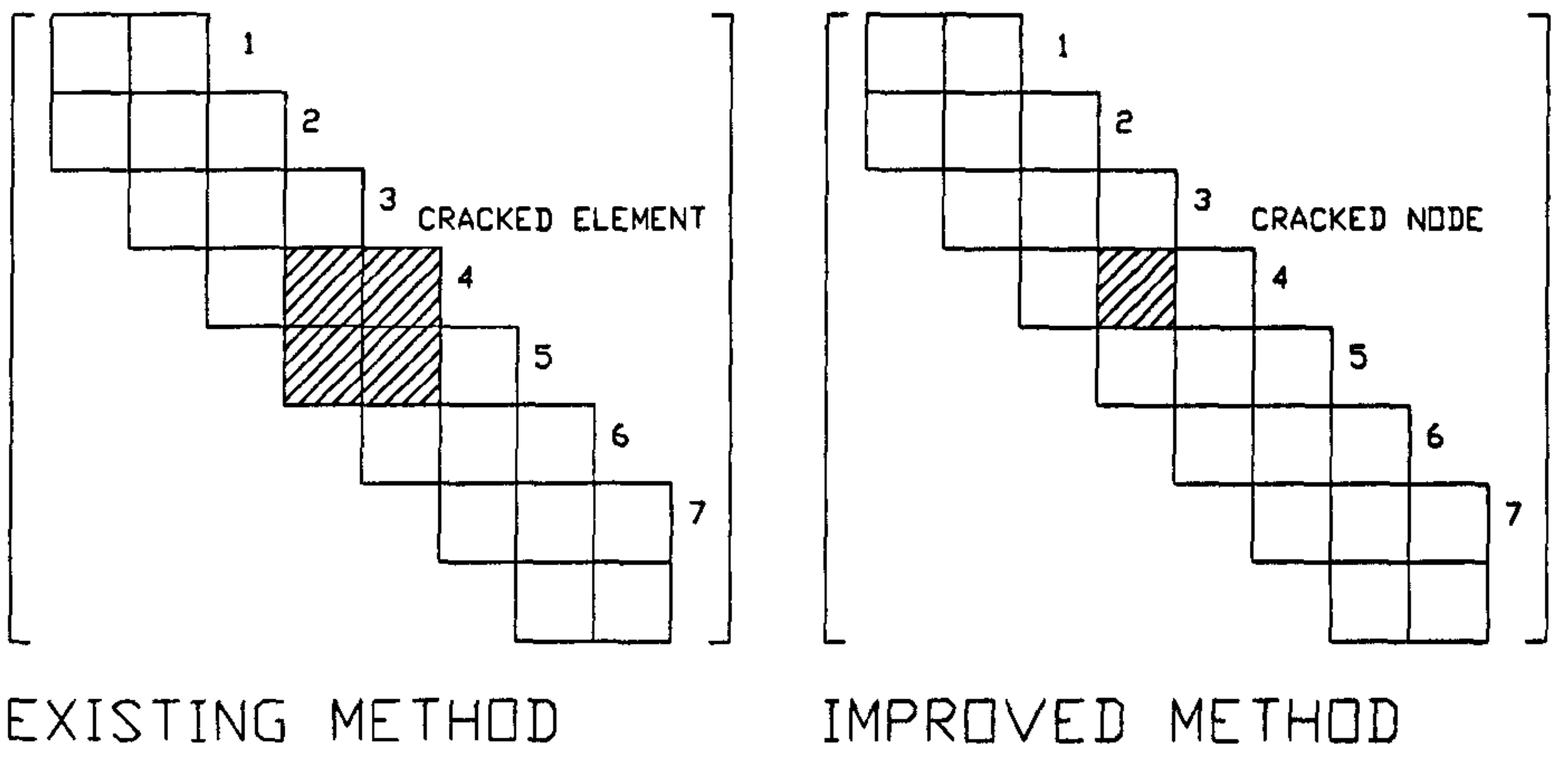


Fig 3.2.2 Concept of Improved Modelling Technique (Stiffness Matrix)

3.2.6 System Equations of Motion

By combining equations (3.2.26) & (3.2.33), the assembled system equations of motion (with unbalance, in case eccentricity exists in the rotor system) can be expressed as:

$$\boldsymbol{M}\,\Delta\ddot{\boldsymbol{q}} + [\boldsymbol{C} + \boldsymbol{G}(\Omega)]\,\Delta\dot{\boldsymbol{q}} + \boldsymbol{K}\,\Delta\boldsymbol{q} = \boldsymbol{F}_u + \boldsymbol{F}_c \tag{3.2.34}$$

Also, in analysing the rotor model, to deal with various fault (or excitation) positions and different response measurement locations, it is necessary to describe the system equations of motion (3.2.34) in state-space format.

Multiplication of the left-hand side of (3.2.34) by $\boldsymbol{M}^{-1}$ leads, with the identity equation $\Delta\dot{\boldsymbol{q}} = \Delta\dot{\boldsymbol{q}}$, to the equations:

$$\Delta\dot{\boldsymbol{q}} = \boldsymbol{0} + \boldsymbol{I}\,\Delta\dot{\boldsymbol{q}} + \boldsymbol{0} \tag{3.2.35}$$

$$\Delta\ddot{\boldsymbol{q}} = -\boldsymbol{M}^{-1}\boldsymbol{K}\,\Delta\boldsymbol{q} - \boldsymbol{M}^{-1}[\boldsymbol{C} + \boldsymbol{G}(\Omega)]\,\Delta\dot{\boldsymbol{q}} + \boldsymbol{M}^{-1}(\boldsymbol{F}_u + \boldsymbol{F}_c) \tag{3.2.36}$$

Hence, for an N-degree-of-freedom multiple-input multiple-output (MIMO) rotor system, with m inputs and l outputs, the state equations for (3.2.34) become:

$$\begin{aligned} \dot{\boldsymbol{x}}_S &= \boldsymbol{A}_S\boldsymbol{x}_S + \boldsymbol{B}_S\boldsymbol{u} \\ \dot{\boldsymbol{y}}_S &= \boldsymbol{C}_S\boldsymbol{x}_S + \boldsymbol{D}_S\boldsymbol{u} \end{aligned} \tag{3.2.37}$$

where

$\boldsymbol{A}_S$: $2n \times 2n$ state coefficient matrix ($= \begin{bmatrix} \boldsymbol{0} & \boldsymbol{I} \\ -\boldsymbol{M}^{-1}\boldsymbol{K} & -\boldsymbol{M}^{-1}[\boldsymbol{C} + \boldsymbol{G}(\Omega)] \end{bmatrix}$)

$\boldsymbol{B}_S$: $2n \times m$ input (or control) matrix ($= \begin{bmatrix} \boldsymbol{0} \\ \boldsymbol{M}^{-1} \end{bmatrix}$)

$\boldsymbol{C}_S$: $l \times 2n$ output matrix

$\boldsymbol{D_S}$: $l \times m$ feed-forward matrix ($= [\mathbf{0}]$)

$\boldsymbol{x_S}$: $2n \times 1$ state vector ($= [\Delta \boldsymbol{q}(t) \quad \Delta \dot{\boldsymbol{q}}(t)]^T$)

$\boldsymbol{y_S}$: l-dimensional output vector

$\boldsymbol{u}$: m-dimensional input (or control) vector ($= \boldsymbol{F_u} + \boldsymbol{F_c}$)

In other words, the original 2nd-order differential equations can be rewritten in a 1st-order form as in (3.2.37) by introducing the state vector, $\boldsymbol{x_S}$. The state vector and associated properties constitute the so-called state-space formulation. By using the state-space format, various fault (or excitation) positions and different response measurement locations can be applied to the MDOF rotor model.

3.3 Vibration Response Analysis

To investigate the dynamic behaviour of a typical rotor system, the specifications presented in Table 3.3.1 have been used for the calculations. Further to accommodate various specifications of the rotor system, a rotordynamic analysis code 'VARS (Vibration Analysis of Rotor Systems)' has been programmed in the MATLAB environment. Also, MATLAB SIMULINK models connected with external code VARS have been established. This connection between SIMULINK model and the external MATLAB code could be realised by using the S-function (or System function), which uses state-space concept (refer to section 3.2.6) to describe the dynamic characteristics of a system.

The system modelled in MATLAB SIMULINK is shown in Fig 3.3.1. The simulation has been performed for both transient and steady-state conditions. The equations of motion have been solved using a 4th-order Runge-Kutta numerical integration algorithm with variable time step option.

Table 3.3.1 Specifications of the Rotor Model

Disk	Diameter	0.075 [m]
	Thickness	0.025 [m]
Shaft	Diameter	0.01 [m]
	Length	0.56 [m]
Damping Factor	ζ	0.05
Density	ρ	7800 [kg/m^3]
Young's Modulus	E	2.07×10^{11}[N/m^2]
1st Nat. Frequency	ω_0	164.8 [rad/s] (= 26.23 [Hz])

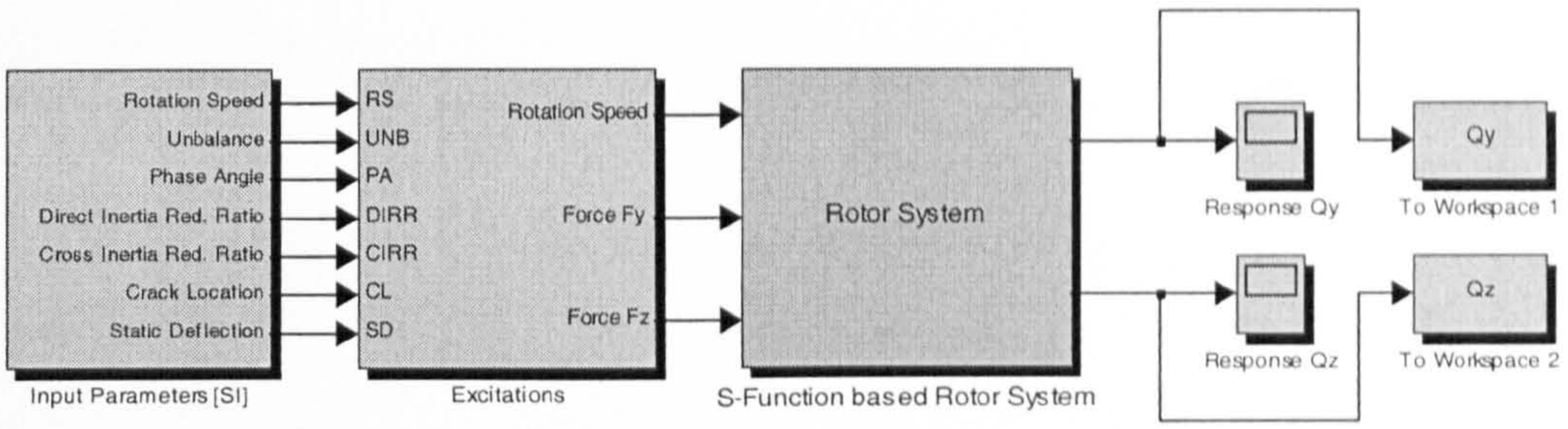


Fig 3.3.1 SIMULINK MODEL for Cracked Rotor System

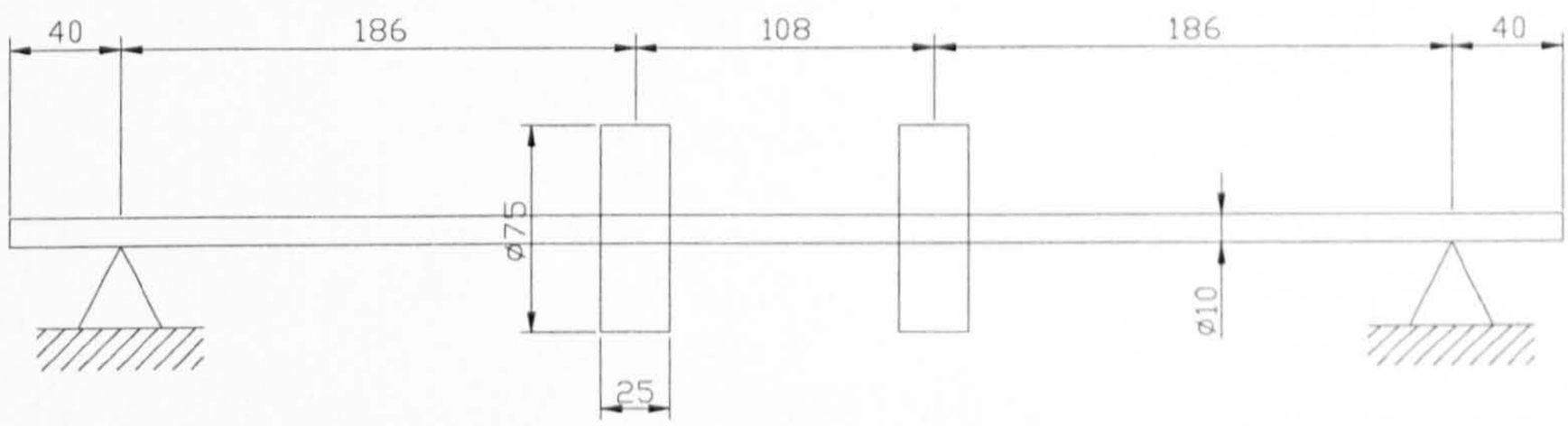


Fig 3.3.2 MDOF Rotor Model

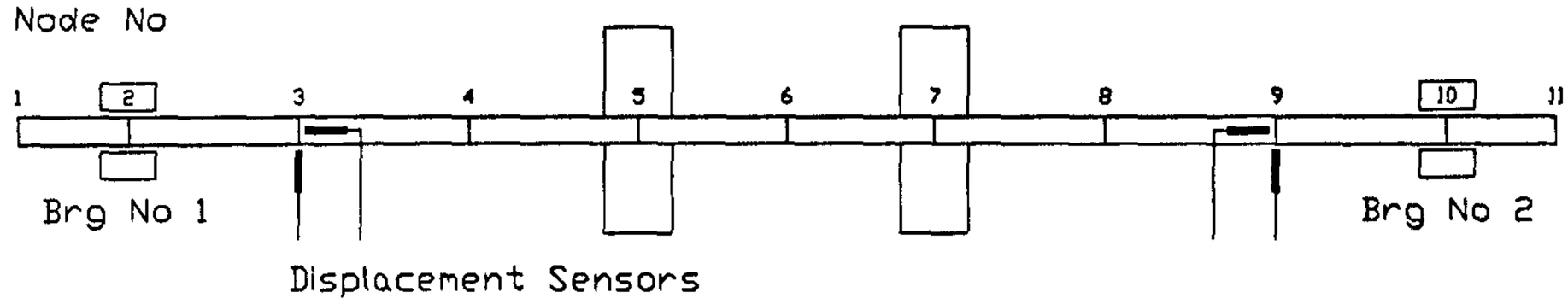


Fig 3.3.3 Discretised Model Rotor System

As shown in Fig 3.3.3, the rotor model supported by isotropic rigid bearings has been discretised into 10 elements, 11 nodes, and the disks at nodes 5 & 7 were treated as added masses and inertias at those nodes. With the discretised model rotor system, various configurations of crack location and measurement locations have been explored.

3.3.1 Transient-State Vibration Response Analysis

The transient vibration response of the MDOF rotor model has been investigated during a run-up period with a speed ramp rate of 6500 rpm/min (linear acceleration) for the case of a rotor with a 10 % crack depth relative to diameter. The location of the crack has been initially assumed to be located at node 6, and the vibration responses have been sampled with a time step of 0.001 s, i.e. at a sampling frequency of 1000 Hz.

The time histories of the sampled data are presented in Fig 3.3.4 and the short-time Fourier transform (STFT) has been applied to these simulated vibration response data. As can be seen in Fig 3.3.5, the FW/BW separated spectrogram clearly shows the fundamental harmonics ($\pm 1\Omega$) and the higher harmonics ($+2\Omega$, $+3\Omega$, $\cdots$) due to the gravity excitation on the cracked rotor system. However, due to the overlap property of the short-time Fourier transform (this will be discussed in detail in the following chapter), it is not so easy to identify the resonances which are caused by the existence of the crack. In the response, there will also be the gyroscopic effect mainly caused by the disks. However, it is considered that the gyroscopic effect will not play an important role at the speed region considered as it is proportional to the speed of rotation.

• Simulated Experimental Noise Model

At this stage, it is considered reasonable to introduce simulated experimental noise into the vibration data of the rotor system. Basically, experimental noise consists of correlated (with the structure) and uncorrelated noise. The correlated noise (or *coloured*-noise) arises mainly from the interaction of the measurement system with the structure, while the uncorrelated noise (or *white*-noise) comes from electrical sources and is constant in nature.

In this work, the following noise model described in equation (3.3.1) has been introduced to the original time histories by adding a correlated (or proportional) noise which is constructed by multiplying to the original time histories a required percentage noise level n and a random number with Gaussian distribution:

$$x_{noise}(t) = x(t)\left[1 + n \times randn\{size(x(t))\}\right] \tag{3.3.1}$$

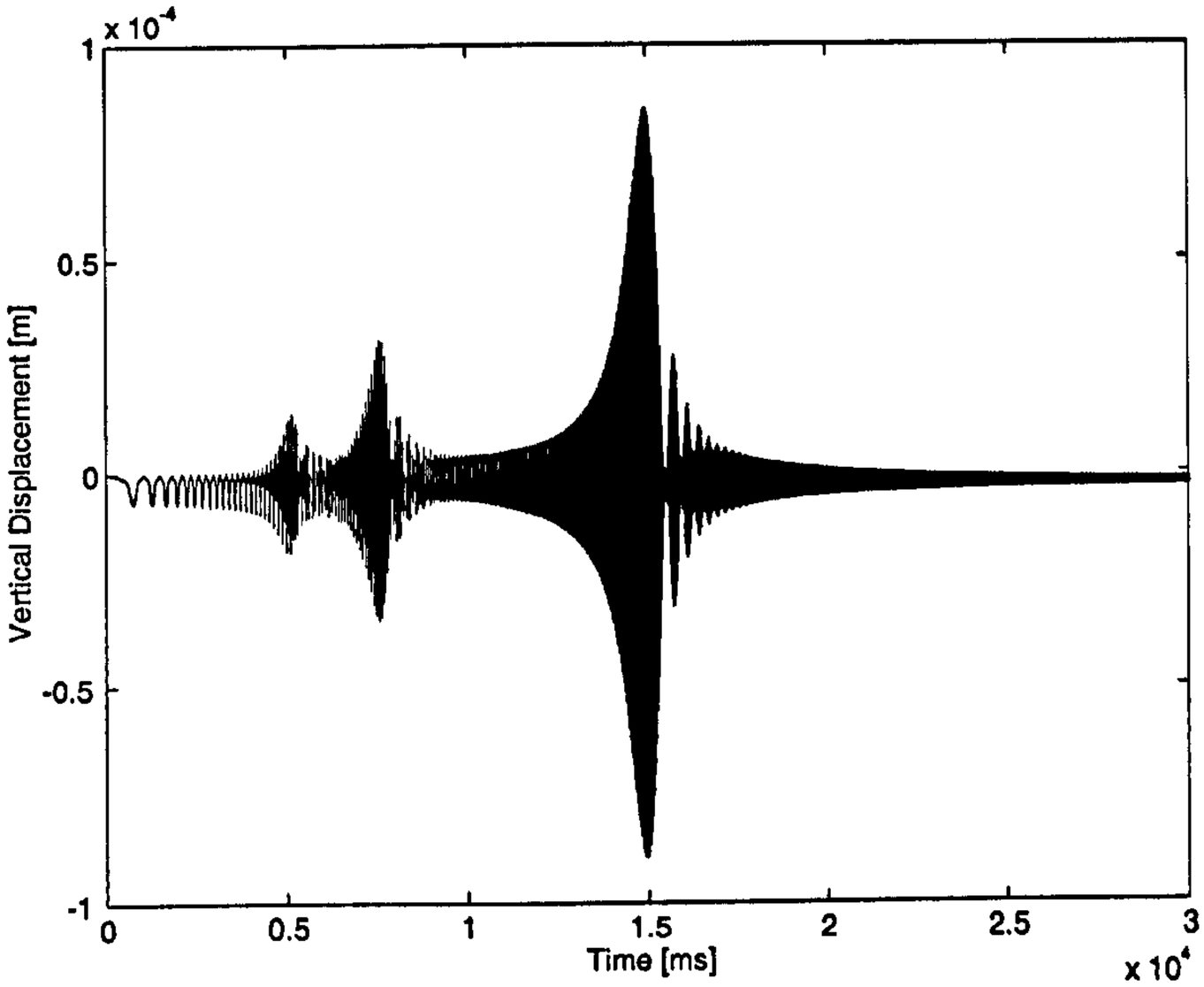
where

n	noise level
$randn\{size(x(t))\}$	random numbers

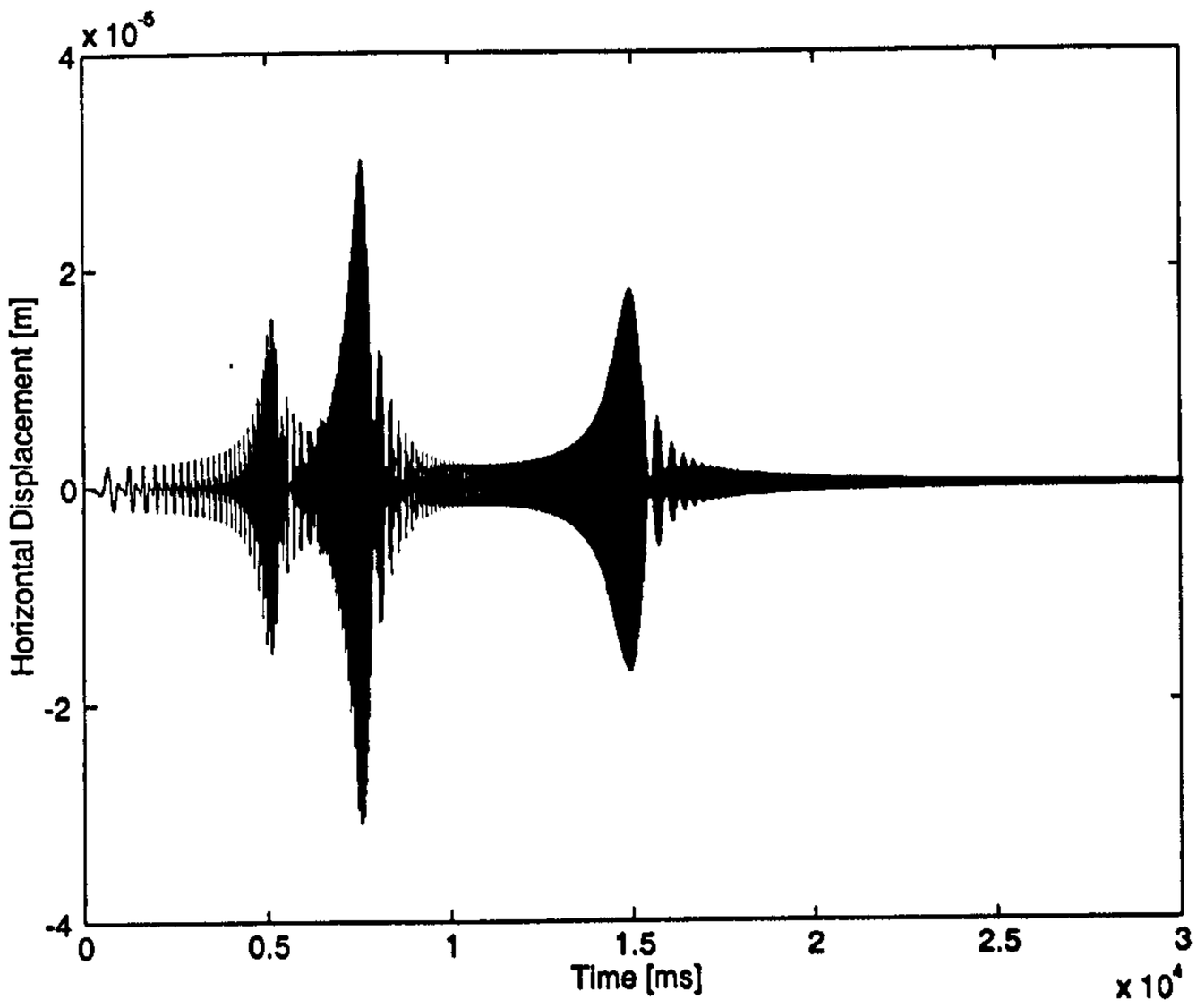
The random numbers have the statistical properties of mean value of 0 and standard deviation value of 1. Hence, every single point in the signal will have a standard deviation which is same with the noise level.

Again, the short-time Fourier transform (STFT) has been applied to the noise-contaminated signals (5 % noise) and the result presented in Fig 3.3.6 shows the noise-sensitive one, especially at the region of resonances due to the property of the noise model which is correlated with the system response.

As a crack can be initiated at any location along the shaft with regard to the geometry of the rotor system and its operating conditions, the crack has been assumed this time to be located at near the support (node 3 in Fig 3.3.3). The directional spectrogram in Fig 3.3.7 reveals the relatively strong higher harmonics ($+2\Omega$, $+3\Omega$) compared to the fundamental harmonics due to the effect (or interaction) of the support to the cracked rotor system. When the noise is associated with the response data, these higher harmonics become more identifiable than the mid-span cracked case as can be seen in Fig 3.3.8.



(a) Vertical displacement



(b) Horizontal displacement

Fig 3.3.4 Time Histories: 10 % Crack at Node 6

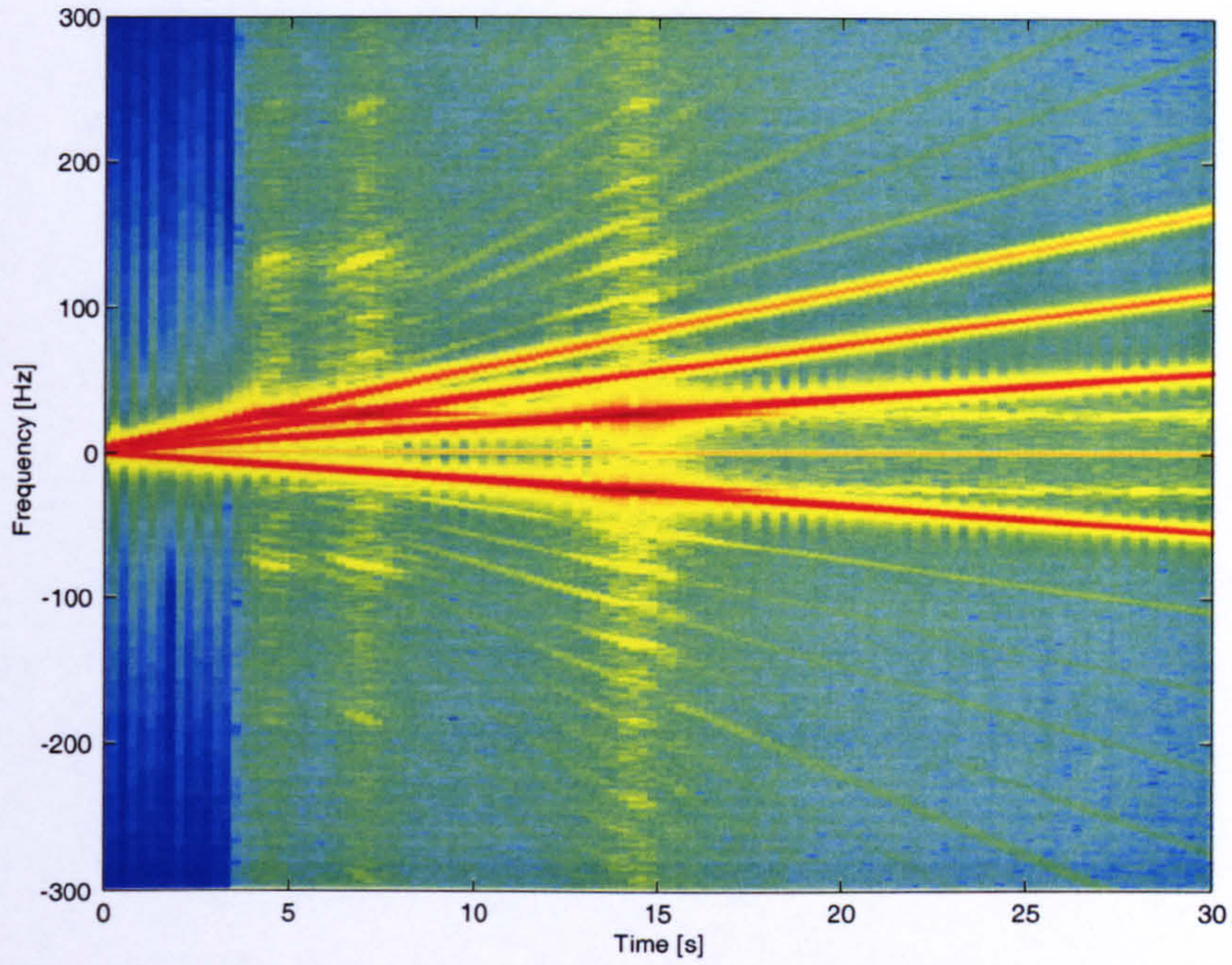


Fig 3.3.5 Spectrogram: 10 % Crack at Node 6

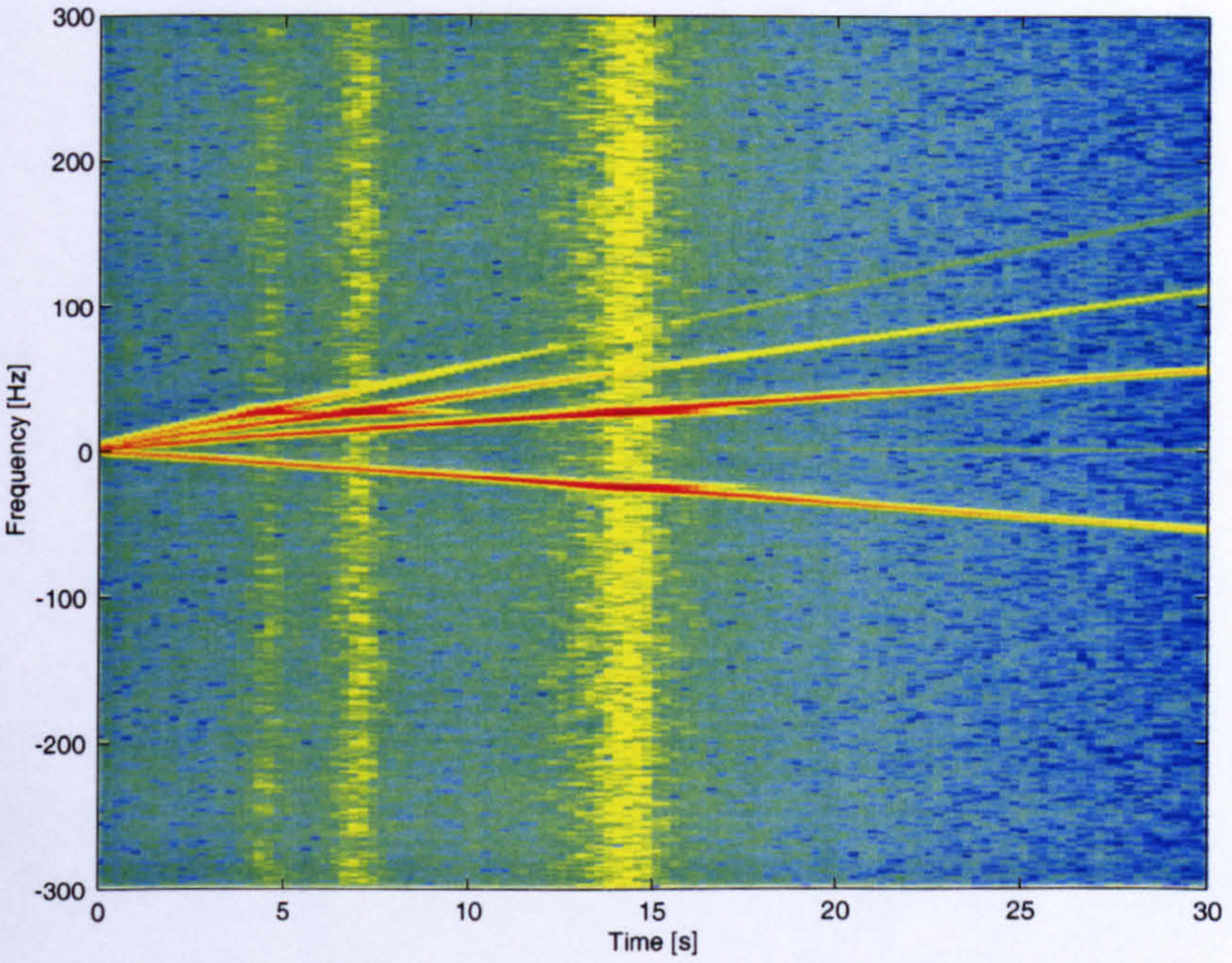


Fig 3.3.6 Spectrogram: 10 % Crack at Node 6 with 5 % Noise

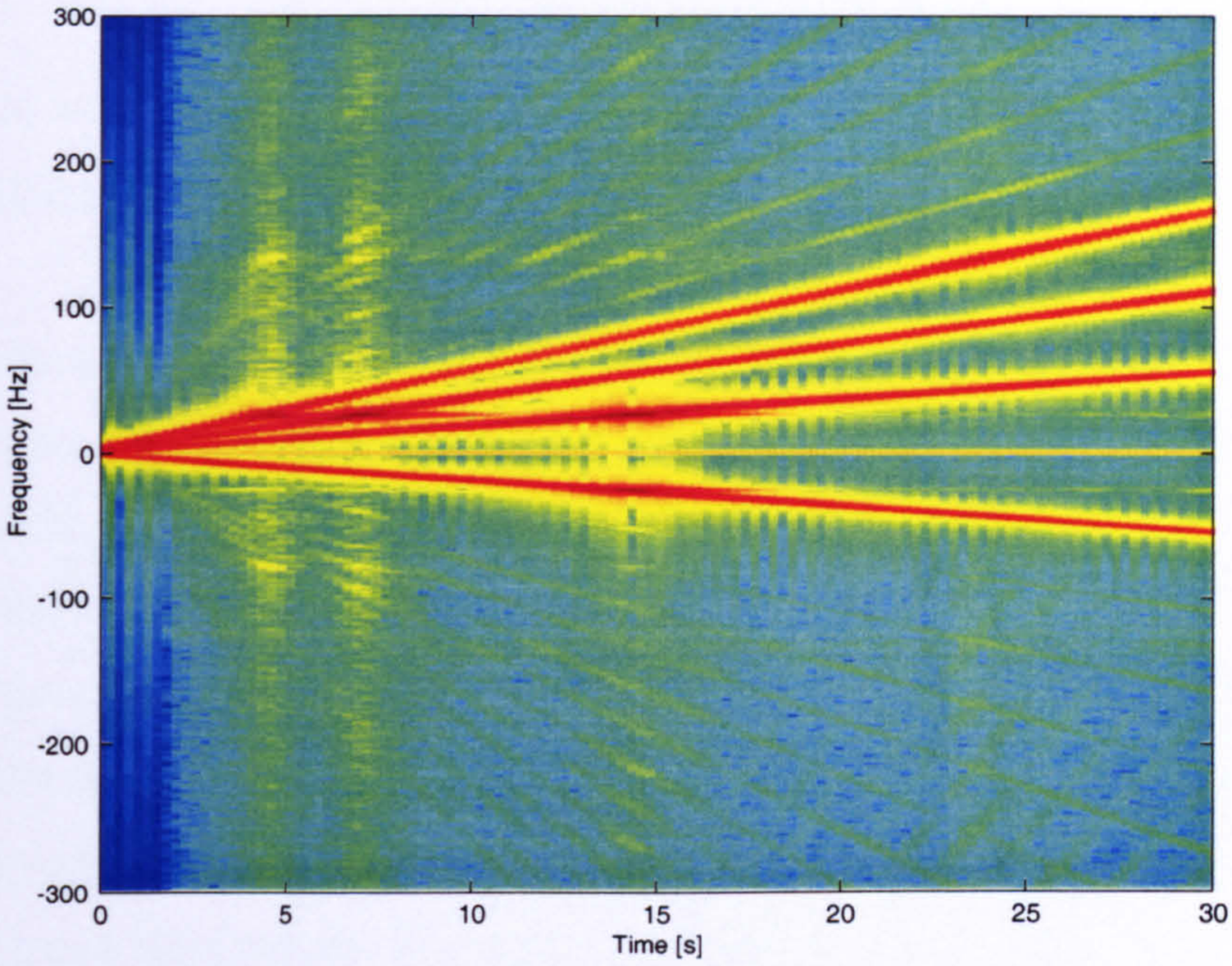


Fig 3.3.7 Spectrogram: 10 % Crack at Node 3

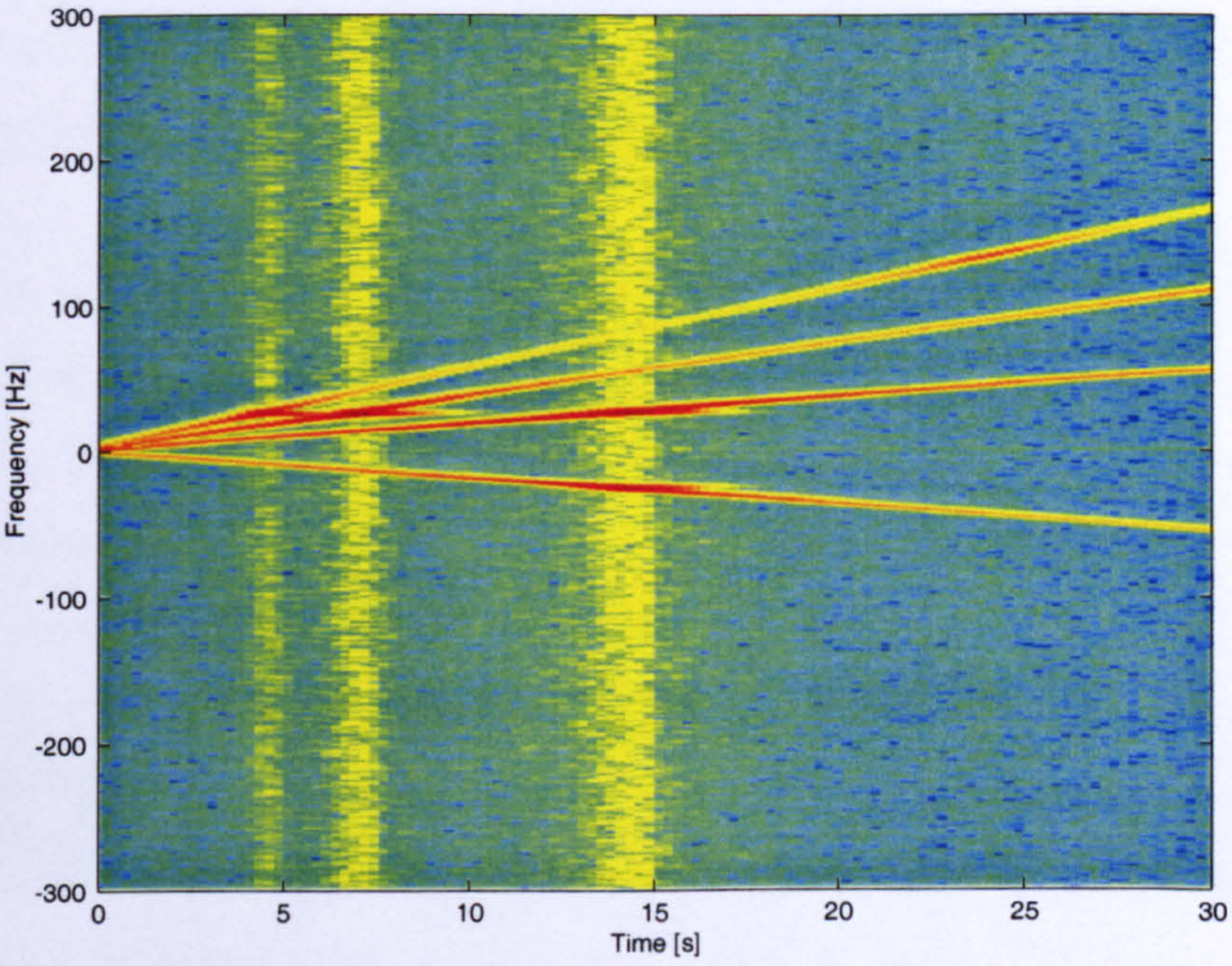


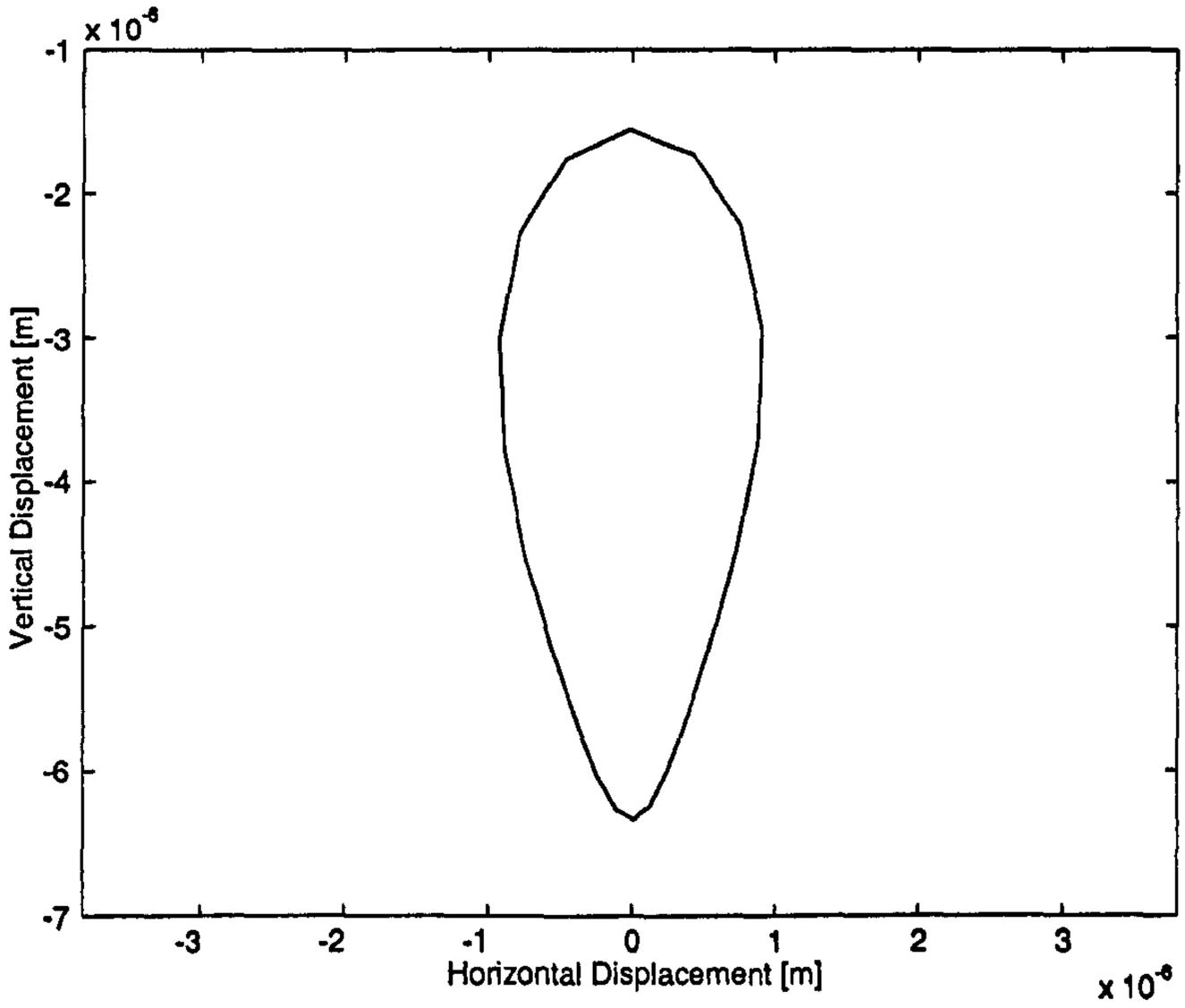
Fig 3.3.8 Spectrogram: 10 % Crack at Node 3 with 5 % Noise

3.3.2 Steady-State Vibration Response Analysis

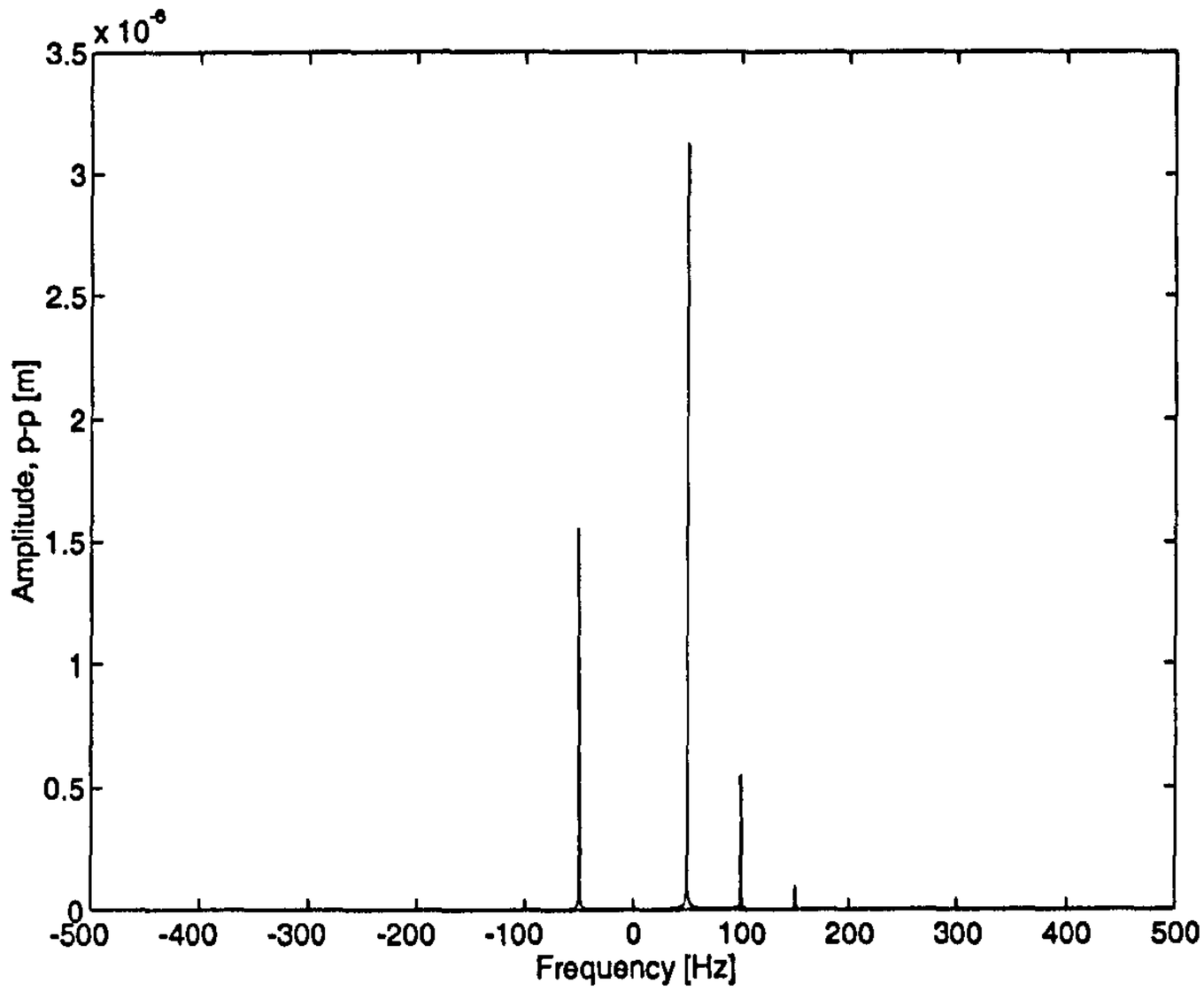
As with the transient case, steady-state vibration response of the cracked rotor system operating at 50 Hz (= 3000 rpm) has been investigated.

Firstly, as with the simple rotor system, a 10 % crack was placed at node 6 of the FE model of the rotor system. Fig 3.3.9 shows the vibration response from the two orthogonally-positioned displacement probes (horizontal and vertical) located at node 6 of the cracked rotor system. The amplitudes of the forward and backward harmonics and the orbit are naturally slightly different with the simple rotor system due to the dissimilar system configuration in geometry. However, the same qualitative spectral properties (caused by a crack) are retained in the MDOF rotor model as in the simple rotor system. In practice, since displacement probes are usually located at the bearing positions and often that makes the crack detection more difficult. To simulate that condition, the response of the cracked rotor has been calculated for varying measurement positions (from node 3 ~ 9) and plotted as shown in Fig 3.3.10. As easily can be expected intuitively, the measured response becomes smaller when the measurement position becomes far away from the crack location.

Secondly, to investigate the sensitivity of the harmonics caused by the crack in the rotor, the vibration response for varying crack position (from node 3 ~ 6, 10 % crack) has been calculated and presented in Fig 3.3.11 ~ 3.3.14. As can be seen in these figures, when the crack is located at the mid-span of the shaft, the $\pm 1\Omega$ vibration components dominate the response due to the strong effect of the self-weight of the rotor. With the change of the crack position from the centre of the span, the $\pm 1\Omega$ vibrations are suppressed and the higher harmonics such as $+2\Omega$ & $+3\Omega$ become relatively more sensitive. Supposing the extreme case to be when the crack is located near the bearings, the $+2\Omega$ & $+3\Omega$ vibrations become dominant in the response due to the strong effect from the supports.



(a) Orbit



(b) Directional Frequency Spectrum

Fig 3.3.9 10 % Crack at Node 6, Displacement Probe at Node 6

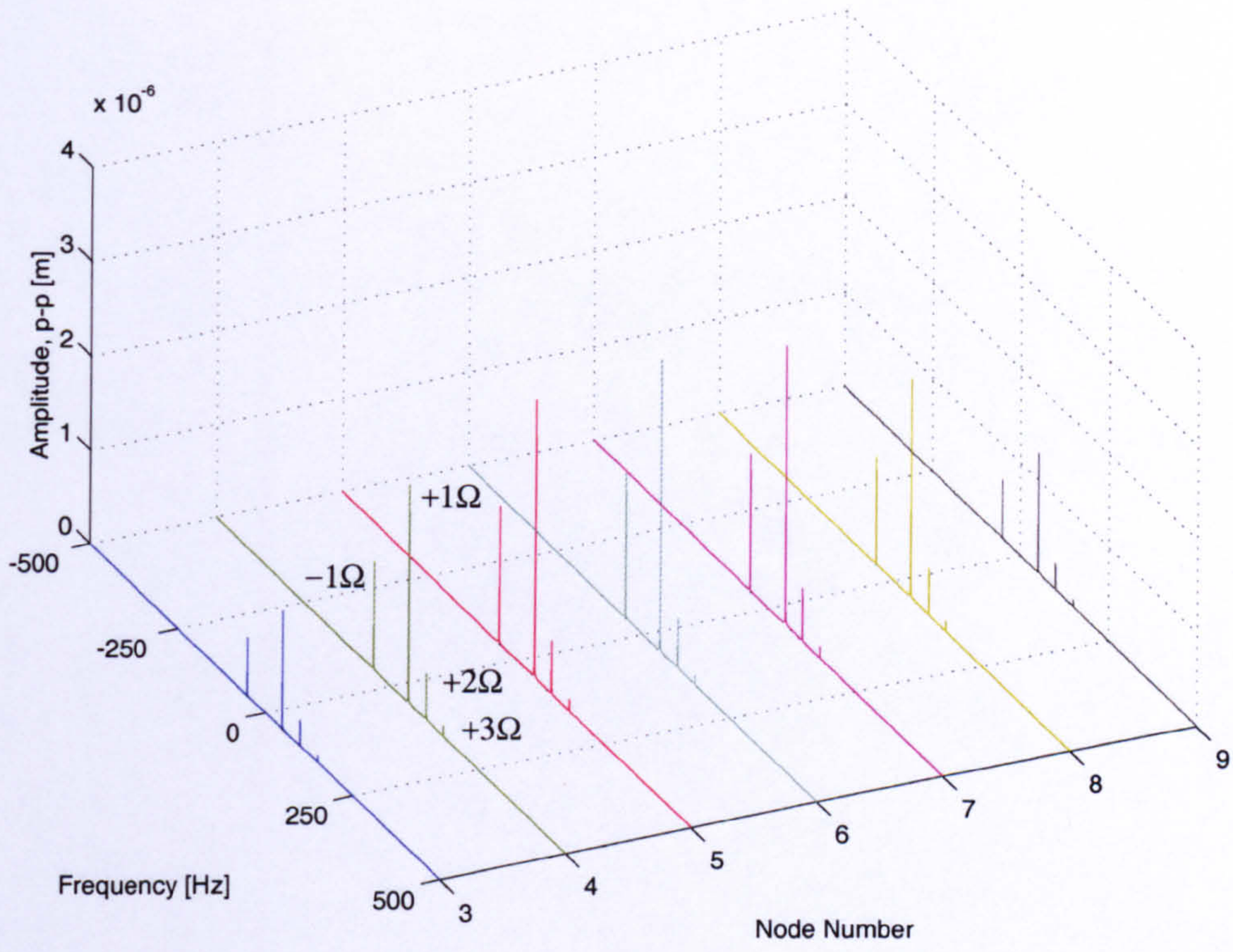
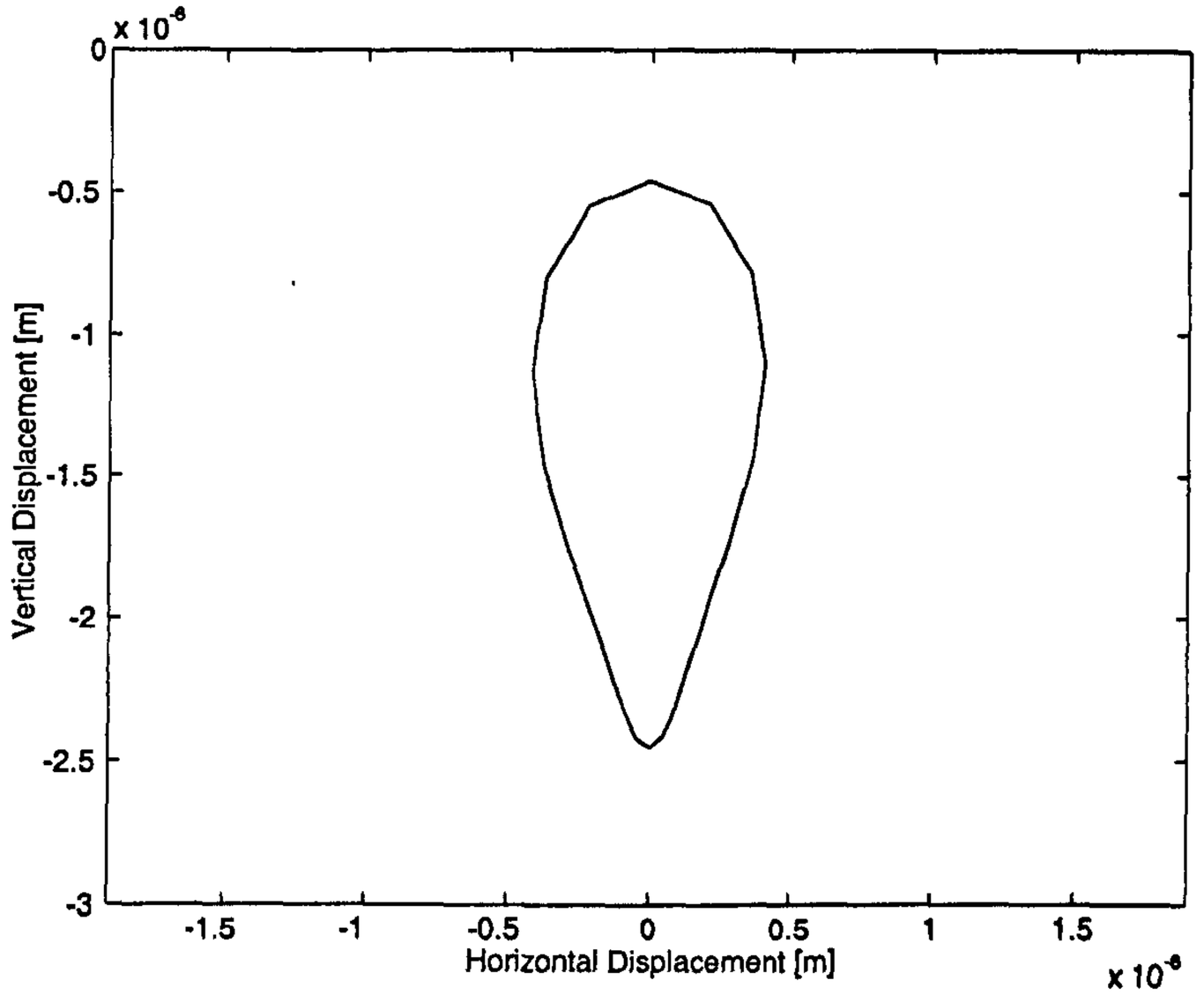
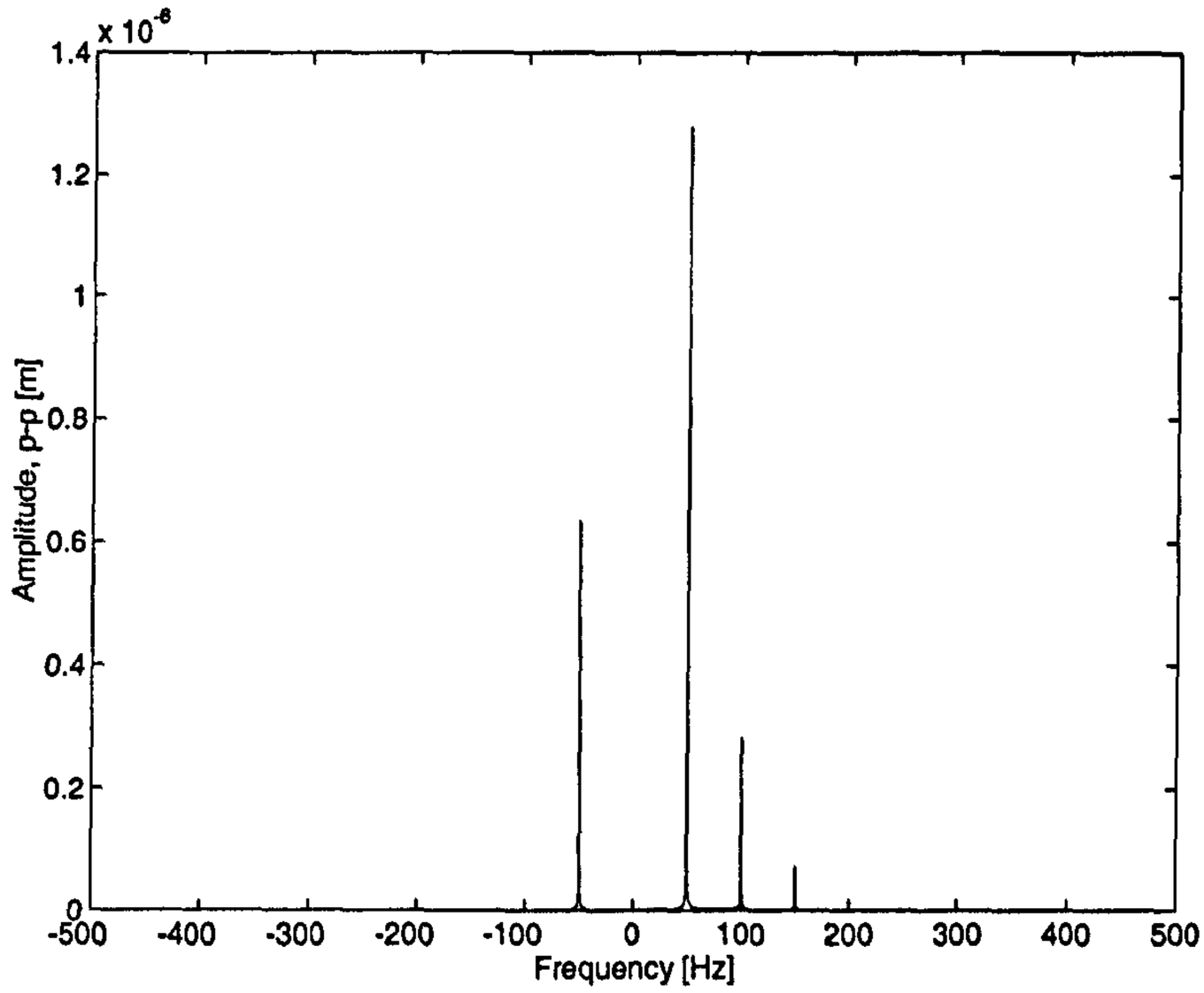


Fig 3.3.10 Directional Frequency Spectra with Various Measurement Positions

(10 % Crack at Node 6, Measurement Positions vary from Node 3 ~ 9)

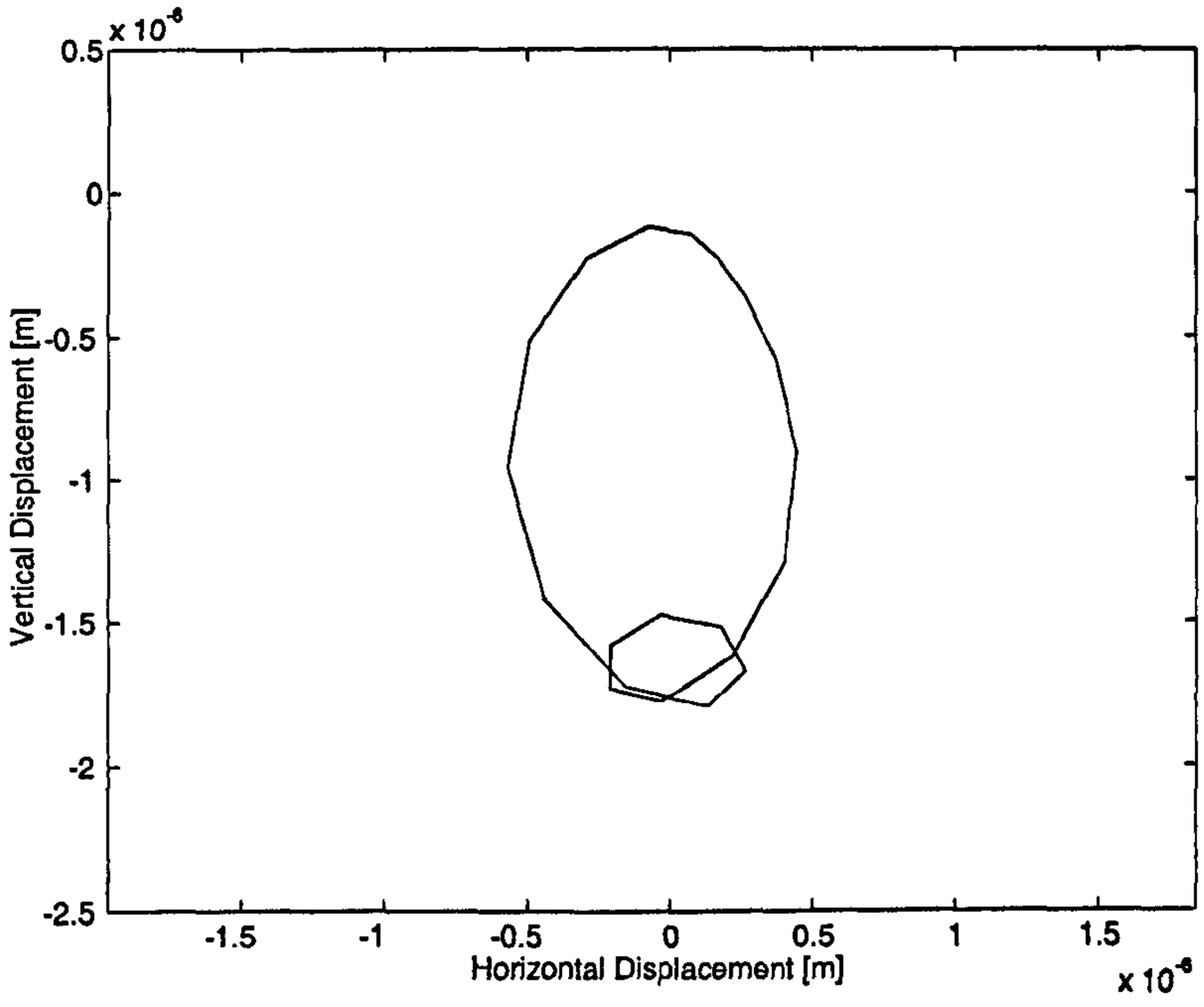


(a) Orbit

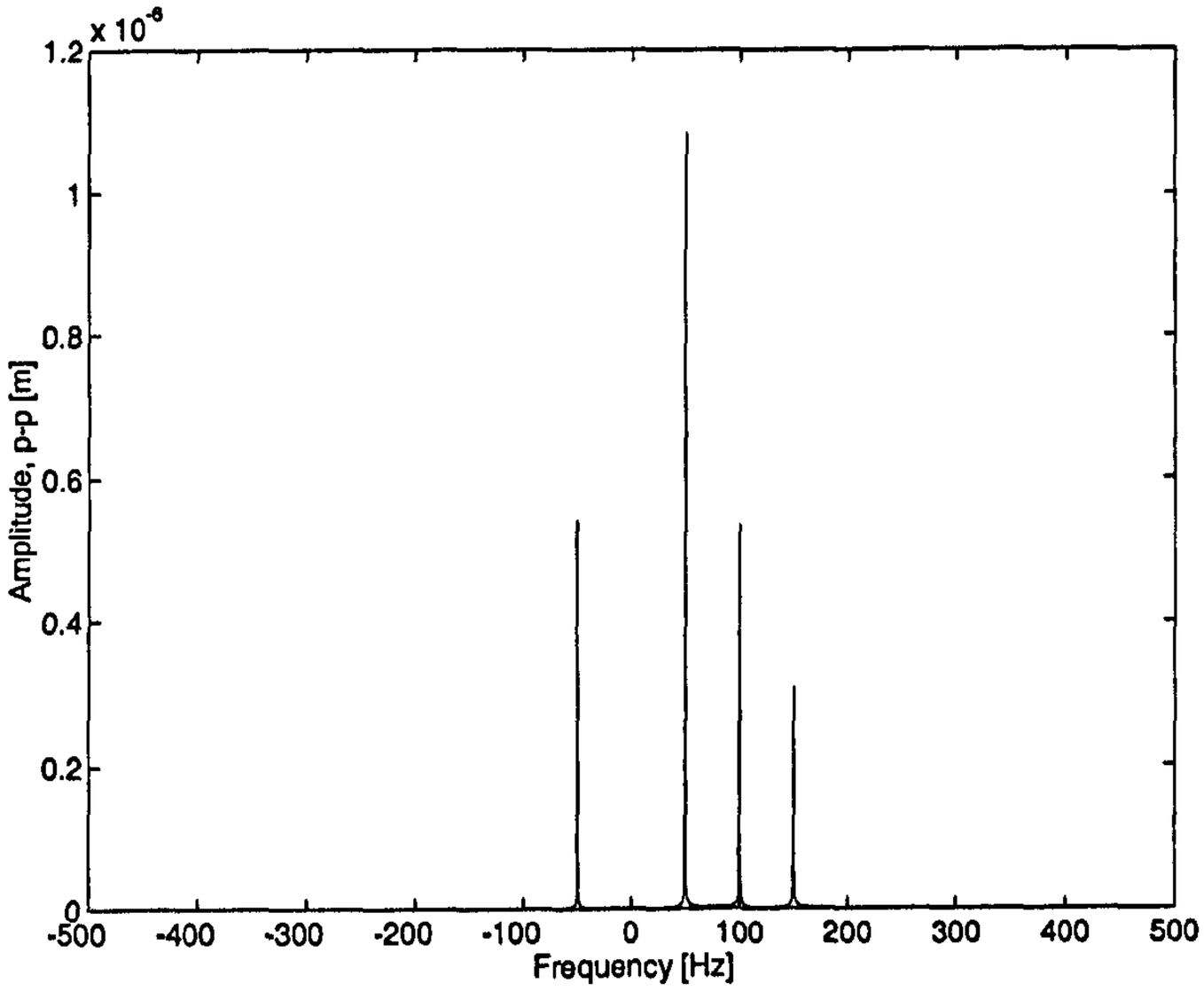


(b) Directional Frequency Spectrum

Fig 3.3.11 10 % Crack at Node 6, Displacement Probe at Node 3

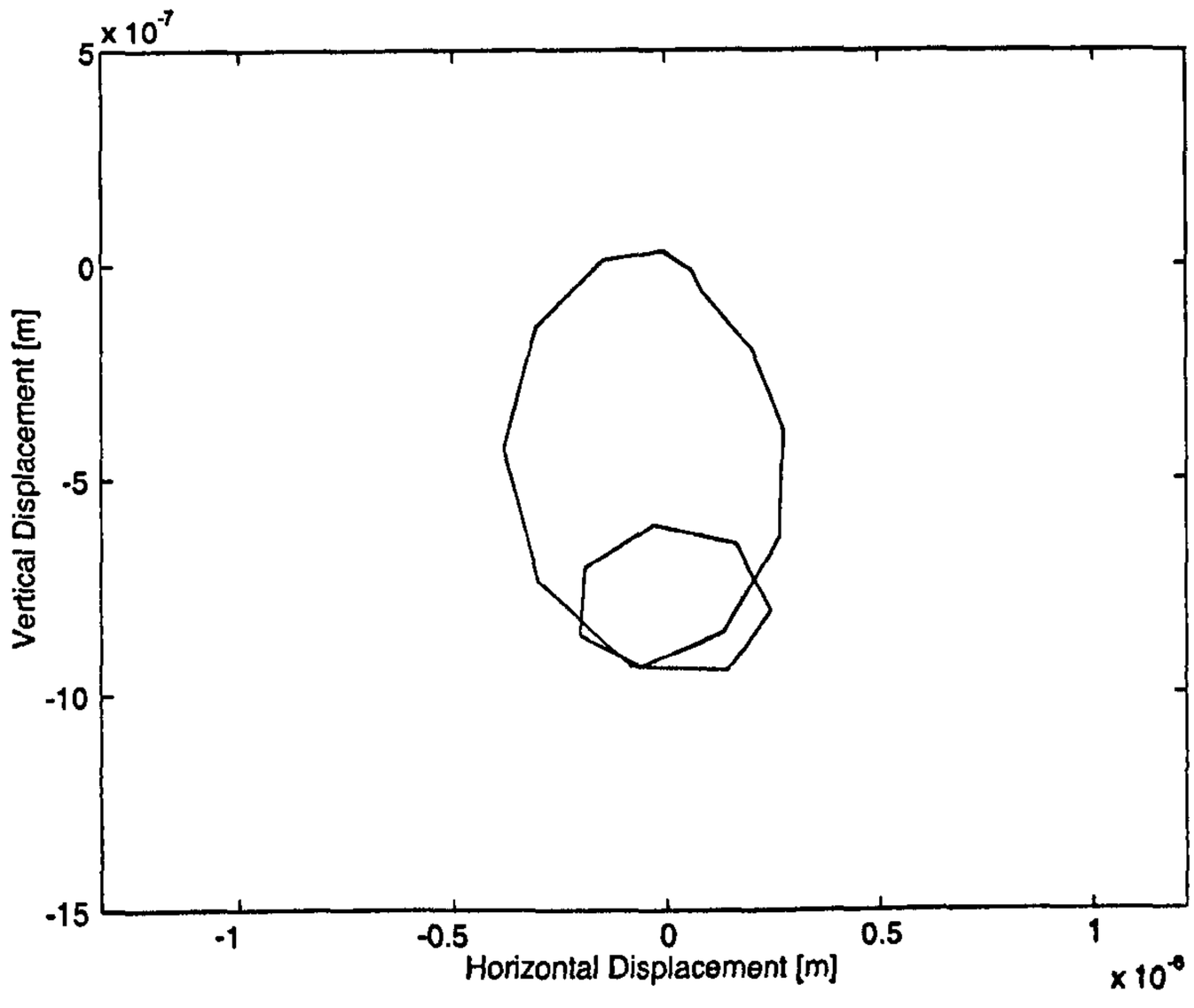


(a) Orbit

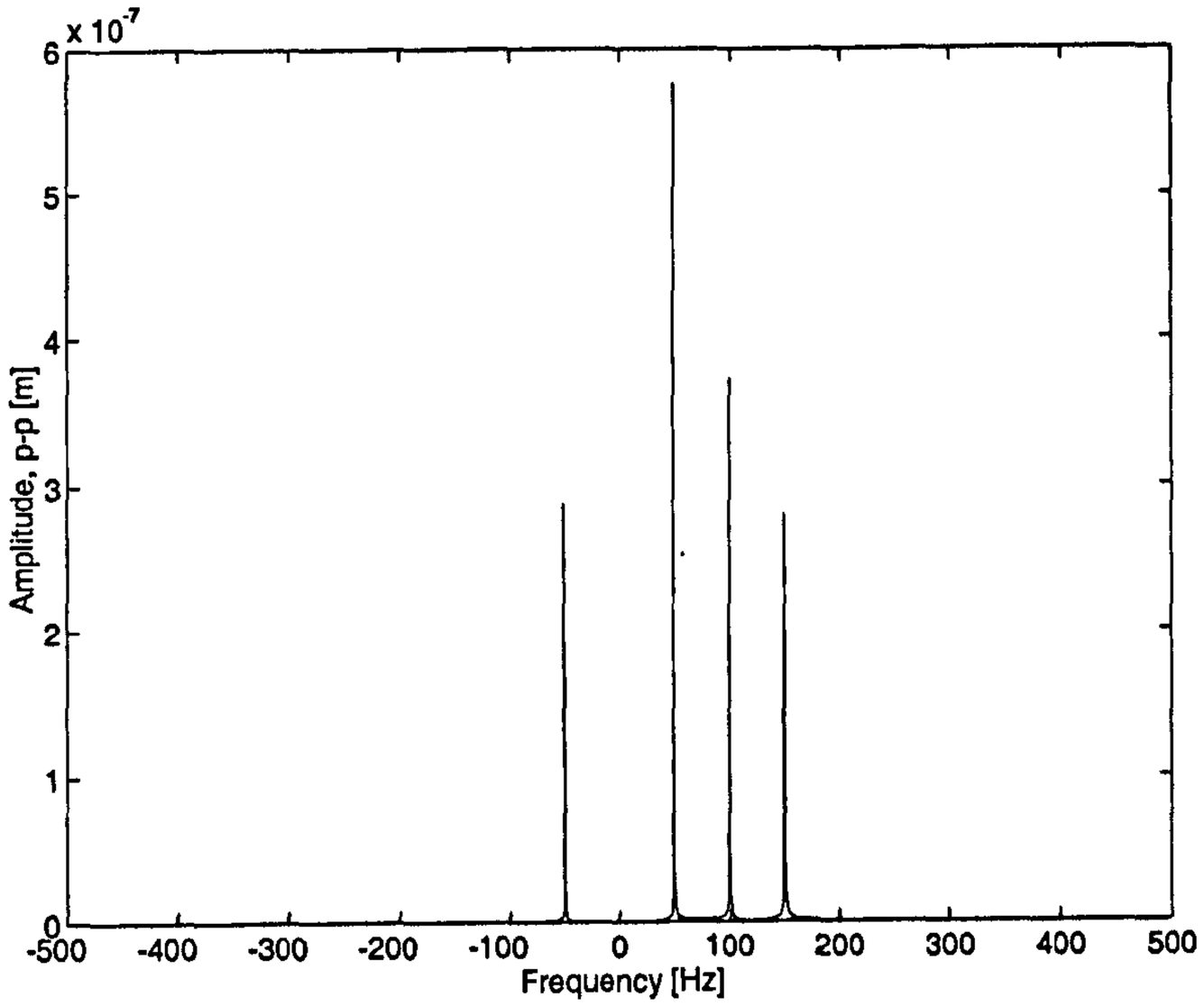


(b) Directional Frequency Spectrum

Fig 3.3.12 10 % Crack at Node 5, Displacement Probe at Node 3

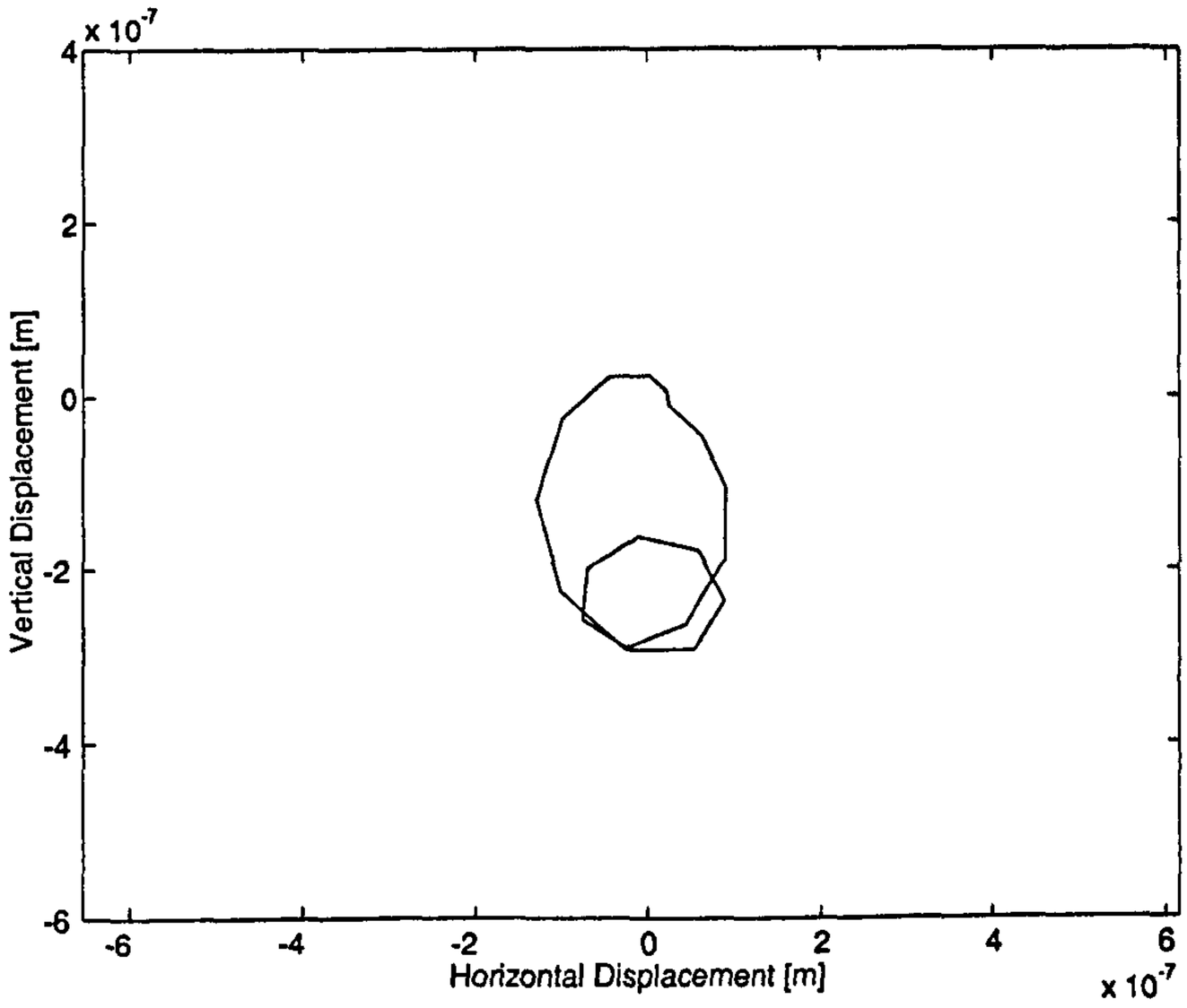


(a) Orbit

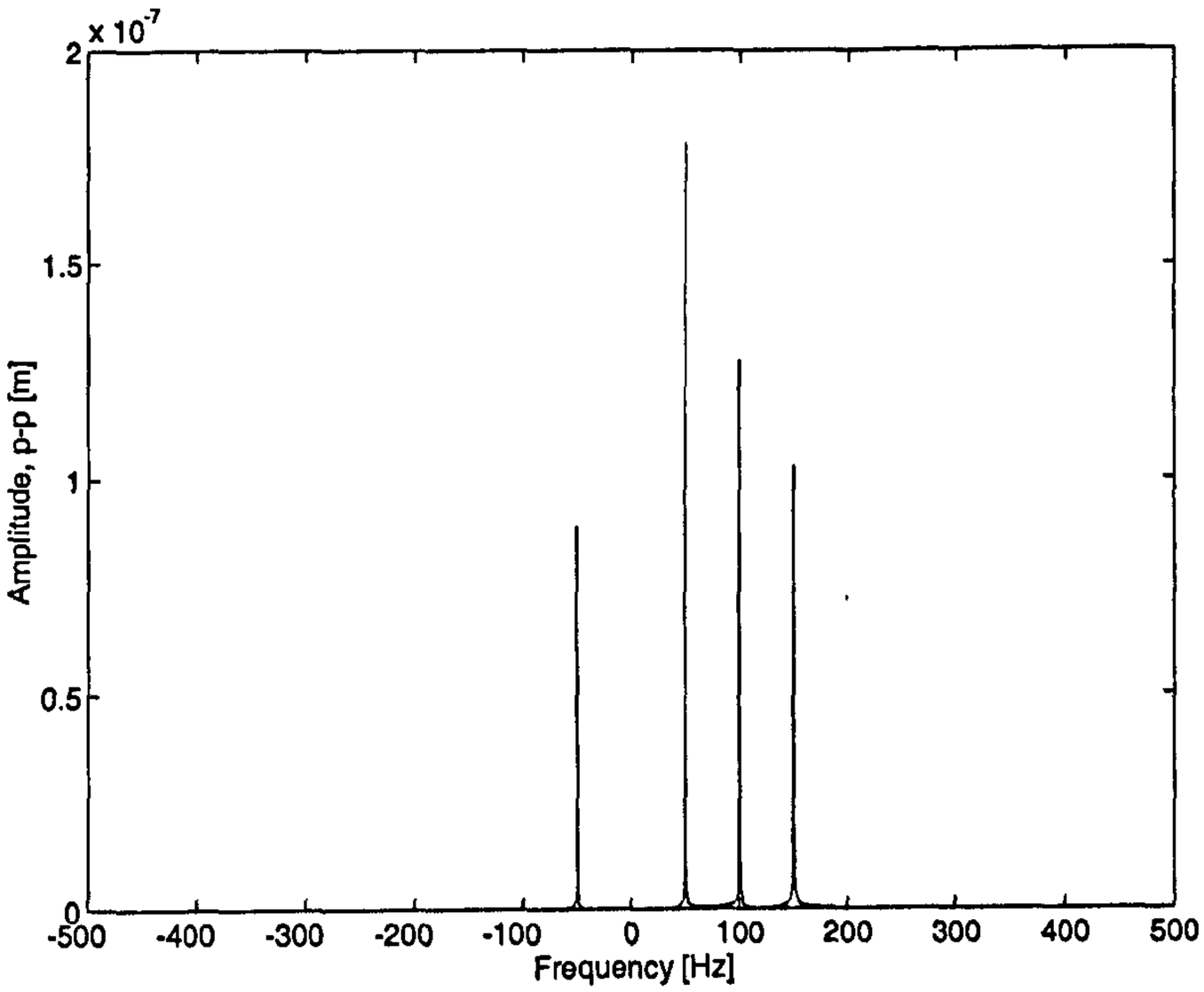


(b) Directional Frequency Spectrum

Fig 3.3.13 10 % Crack at Node 4, Displacement Probe at Node 3



(a) Orbit



(b) Directional Frequency Spectrum

Fig 3.3.14 10 % Crack at Node 3, Displacement Probe at Node 3

Based on the calculated results, the directional harmonics sensitivity map presented in the previous chapter has been extended to 3-dimensional form including the information on the crack location, i.e. 3D-Directional Harmonics Sensitivity Maps (3D-DHSM) as presented in Fig 3.3.15-(a) ~ (d). In establishing each of these maps, the measurement point has been fixed at node 3 (so the map is not symmetric). The sensitivity of each harmonic component, with the varying crack location and increasing crack depth, can be observed with the map. As can be noticed in the map, with the increase of the crack depth, each crack-related harmonics are increasing in magnitude with an exponential form (with each increase rate) as already shown in 2-dimensional harmonics sensitivity map in the case of cracked simple rotor system.

Also, for the MDOF rotor model, the ratios of each harmonic component for different crack extents have been estimated and the following relationship has been obtained:

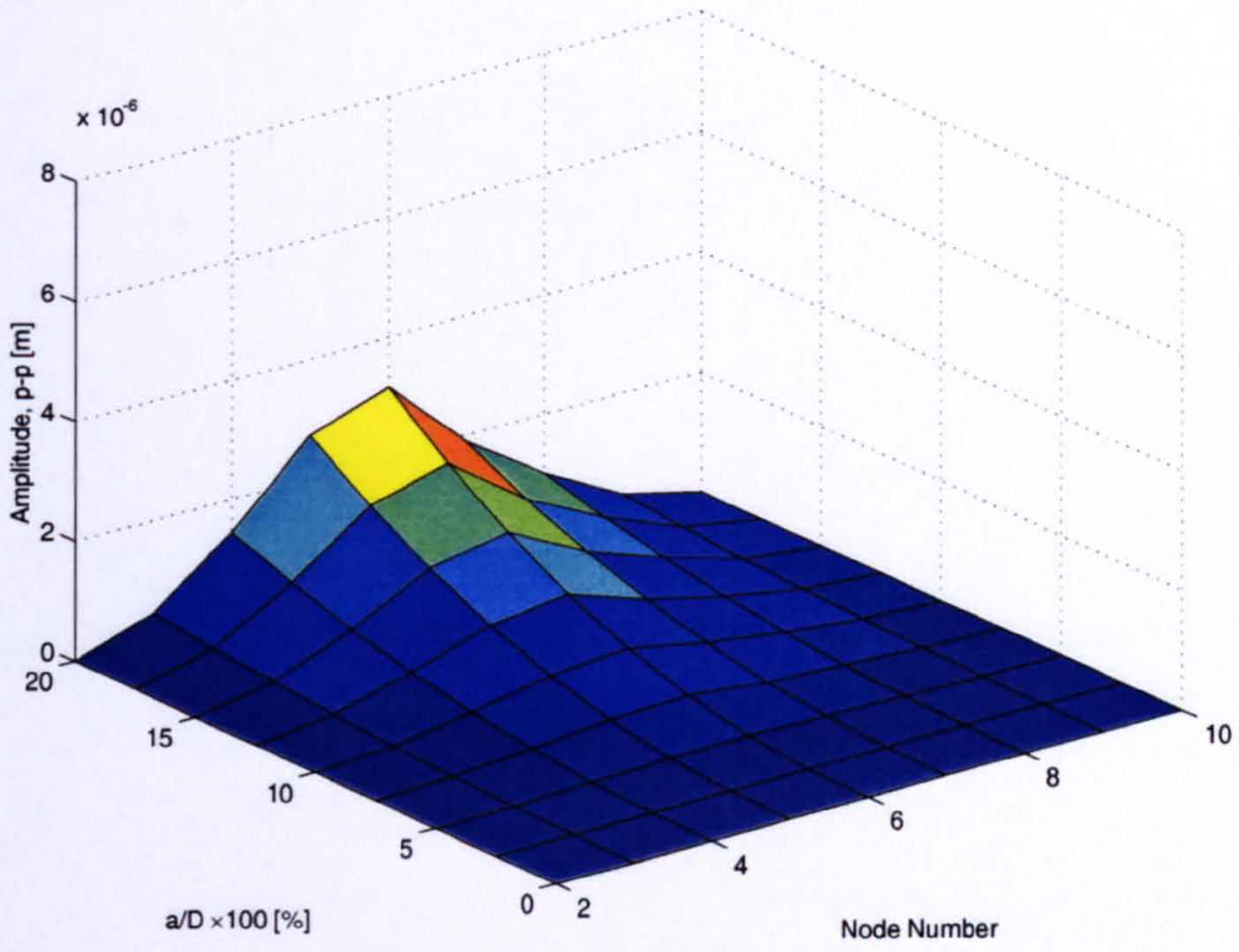
$$\frac{S(-1\Omega)_{\Delta j}}{S(-1\Omega)_{\Delta k}} = \frac{S(+1\Omega)_{\Delta j}}{S(+1\Omega)_{\Delta k}} = \frac{S(+2\Omega)_{\Delta j}}{S(+2\Omega)_{\Delta k}} = \frac{S(+3\Omega)_{\Delta j}}{S(+3\Omega)_{\Delta k}} \tag{3.3.1}$$

where

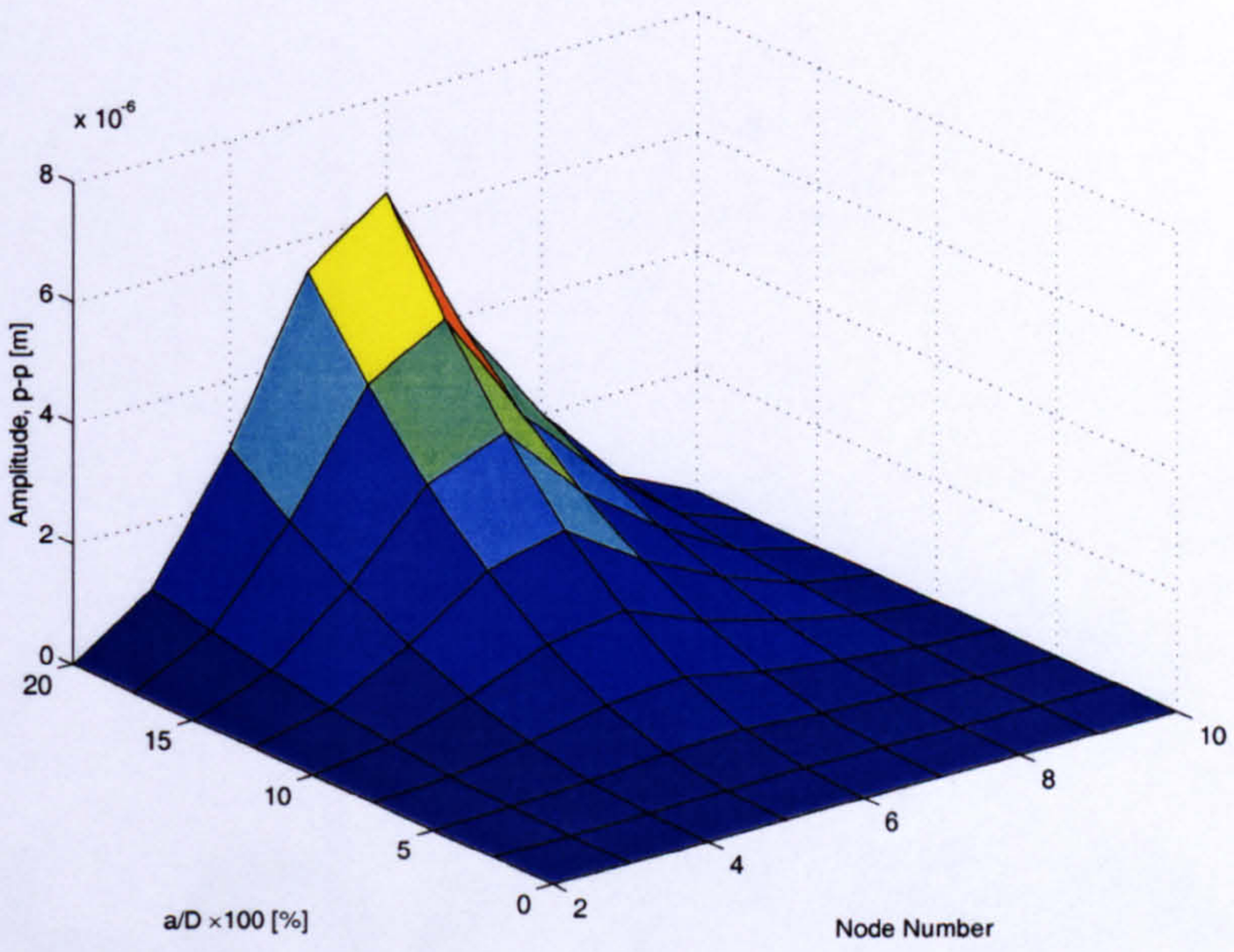
S : magnitude of each harmonic component

$\Delta j, k$: crack extent j and k ($j > k$)

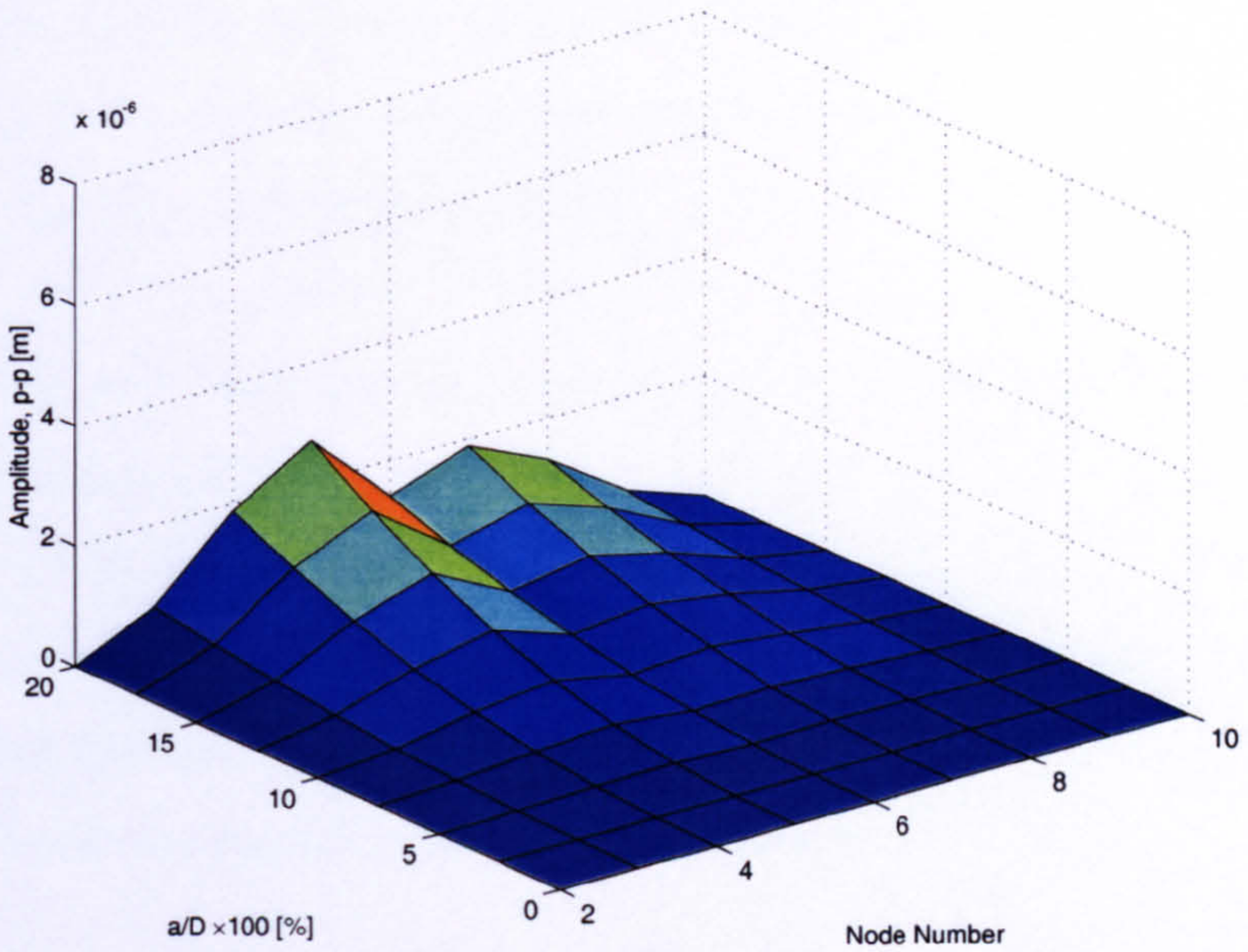
This relationship is also valid in the case of the simple rotor model analysed in the previous chapter where no crack location information was available. Moreover, in the case of the MDOF rotor model, the relationship holds for any crack location. Hence, it is considered that the crack can be detected unambiguously by estimating the ratios of each crack-related harmonic component regardless of its location along the shaft-line. However, it must be reminded that only the crack-related harmonics have to be used in estimating the relationship. Practically, this is almost impossible, so a certain technique is required which can isolate the crack-related harmonics from many other fault-related harmonic components.



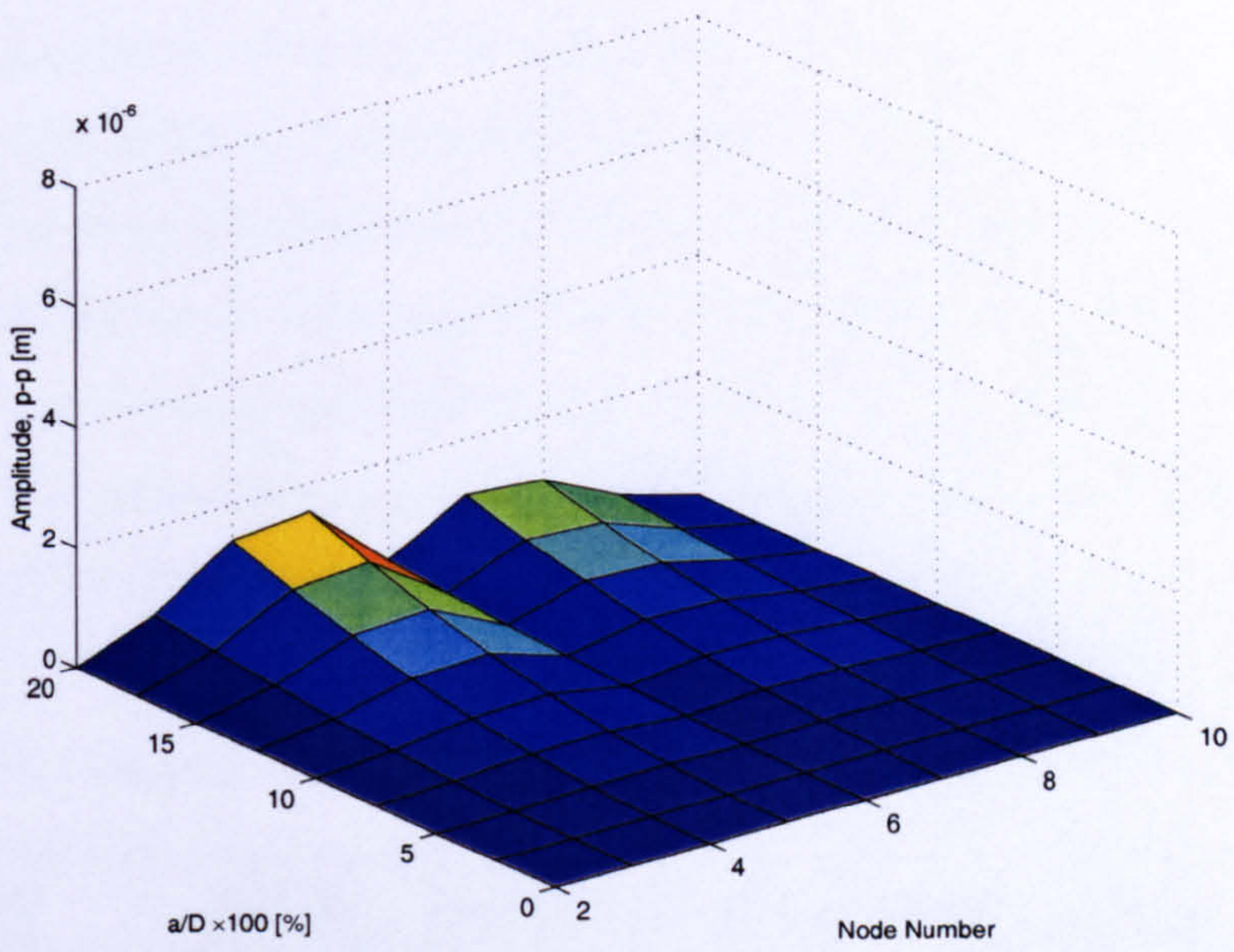
(a) -1Ω Harmonic Sensitivity Map



(b) $+1\Omega$ Harmonic Sensitivity Map



(c) +2Ω Harmonic Sensitivity Map



(d) +3Ω Harmonic Sensitivity Map

Fig 3.3.15 3D-Directional Harmonics Sensitivity Maps

3.4 Conclusions

To provide the basis for an improved crack detection strategy, a multi-degree-of-freedom (MDOF) rotor system with a transverse crack has been modelled using the Finite Element Method (FEM).

The non-linear system equations have been equivalently linearised by extracting the residual stiffness (caused by a crack) from the stiffness matrix (of the cracked rotor system) and treating it as an external force (or crack-induced self-excitation term) at a node where the crack is located. In particular, by locating the crack at a node, a better localisation has been achieved than the existing conventional crack locating ways where the crack is located throughout an element.

With the developed model, both transient and steady-state vibration responses have been investigated numerically as in the case of a simple rotor system. Similar qualitative spectral properties (caused by a crack) have been obtained in the MDOF rotor model as in the simple rotor system. Also, to simulate a practical situation, noise has been introduced to the transient-state vibration data. The spectrograms from the short-time Fourier transform (STFT) showed the noise-sensitive results, and the identification of crack-related resonances was limited in the spectrograms with spectral resolution spread in time domain mainly due to the overlap property of the STFT algorithm.

In analysing the steady-state vibration response, the sensitivity of the crack-induced harmonics to the different crack locations has been investigated, a feature which could not be included in the simple rotor model. The different sensitivities of each harmonic component (i.e., $\pm 1\Omega$, $+2\Omega$, $\cdots$) have been identified and, based on the results, 3-D Directional Harmonics Sensitivity Maps (3D-DHSM) have been devised. Finally, the ratios of the various harmonics related with different crack extent have been estimated

and the relationship on the ratios of directional harmonics (caused by a crack) has been established. With the aid of this relationship, it is considered that the crack can be detected regardless of its location along the shaft.

Chapter 4
Improved Crack Detection Techniques

4.1 Introduction

Rotor crack detection techniques have been developed together with the advances in signal processing techniques. This is mainly because for almost all operating rotor systems, the only available information is the signals (mainly relative displacements between the rotor and the stator) from the probes usually installed at the bearing housings, which are located at both ends of the rotor, mostly with different boundary conditions. Hence, it has been always considered to be difficult to detect a crack at an early stage, reliably. However, in this research, improved crack detection techniques have been developed based on vibration signature analysis for both transient and steady-state situations with a view to enhancing the possibility of reliable early detection of cracks. The development of the methods is based on the predicted results obtained from mathematical models established in the previous chapters. For transient vibration signals, the directional harmonic wavelet transform (DHWT) technique has been introduced together with the existing versatile tool for time-frequency analysis, i.e. short-time Fourier transform (STFT). Likewise, for steady-state conditions, the directional-difference vibration signature analysis (DDVSA) has been introduced as an improved analysis technique which isolates the crack-related harmonics from the overall vibration signature to enhance the reliability of the detection. Also, introductory remarks on spectral analysis are given as those two methods are closely related with the task of signal processing which is based on Fourier analysis.

4.2 Spectral Analysis

It is a fundamental requirement of the signal processing procedure to transform the measured vibration data from presentation in the time domain to an equivalent one in the frequency domain. The reason for this requirement is mainly due to the fact that almost all structures are much more sensitive to the frequency of an excitation signal than they are to its amplitude.

Therefore it is necessary to have the time histories readily classified in terms of their frequency content or, specifically, to have their presentation transformed into a frequency-domain description referred to as a spectrum.

In order to understand better the significance of the spectra which are produced by the transformations, and of how these may be computed in practical situations, it is appropriate to review briefly the basis of Fourier analysis.

4.2.1 Fourier Analysis

The basis of the time-to-frequency transformations is Fourier analysis. There are essentially two basic forms of the Fourier decomposition of time histories into frequency spectra, [31]:

(i) *Fourier Series Transformation*, which applies to periodic signals

(ii) *Fourier Integral Transformation*, which applies to non-periodic signals

• Fourier Series

The Fourier series is the form which states that any periodic signal $x(t)$ with period T can be represented by a series of sinusoidal components:

$$x(t) = \sum_{k=0}^{\infty} X_k \sin(\omega_k t + \alpha_k)\,, \quad \omega_k = 2\pi k/T \tag{4.2.1}$$

where, for each frequency component, ω_k, the amplitude of that component is X_k and its phase angle is α_k. The coefficients, X_k and α_k, can be determined by the following Fourier coefficients, a_k and b_k:

$$a_k = \int_T x(t)\sin\omega_k t\,dt\,, \quad b_k = \int_T x(t)\cos\omega_k t\,dt \tag{4.2.2}$$

Then,

$$X_k = \sqrt{a_k^2 + b_k^2}\,, \quad \alpha_k = \arctan(b_k/a_k) \tag{4.2.3}$$

Hence, the Fourier series transformation of a periodic signal will take the form of a series of sinusoidal or harmonic components with frequencies which are integer multiples of the fundamental frequency of the periodic signal.

• Fourier Integral

Fourier integral is an extended form of Fourier series to deal with certain aperiodic signals by treating them as periodic ones with an infinitely long period, i.e. for a non-periodic signal $x(t)$:

$$x(t) = \int_{-\infty}^{\infty} X(\omega) e^{i\omega t} d\omega \tag{4.2.4}$$

And its spectral component is represented by the Fourier transform of $x(t)$:

$$X(\omega) = \frac{1}{2\pi} \int_{-\infty}^{\infty} x(t) e^{-i\omega t} dt \tag{4.2.5}$$

The spectrum represented by $X(\omega)$ is no longer a series of specific sinusoidal components but instead a continuous function of frequency.

The Fourier integral transform has a requirement (the Dirichlet condition) that the 'area under the modulus of the function (or signal) $x(t)$' must be finite. Due to this requirement, the Fourier integral transform cannot be applied to random signals directly. However, the frequency content of a random signal can be estimated indirectly, in the form of spectral density, by applying the Fourier transform to the autocorrelation function of the random signal (as the autocorrelation function will meet the requirement).

• Discrete Fourier Transform (DFT) and Fast Fourier Transform (FFT)

In most engineering situations, the measured data will be in a discretised form for each discrete value of time t. In such cases, the discrete form of Fourier transform (DFT) may be used to obtain an estimate of the spectral coefficients. A frequency spectrum represented by N discrete values, X_1 to X_N, is obtained from a time history $x(t)$ with N discrete data points, x_1 to x_N, via the DFT operation:

$$x_r = \sum_{k=1}^{N} X_k e^{i(2\pi kr/N)} \tag{4.2.6}$$

$$X_k = \frac{1}{N} \sum_{r=1}^{N} x_r e^{-i(2\pi kr/N)} \tag{4.2.7}$$

where the N complex frequency components, X_k, are in the form of $N/2$ complex conjugate pairs.

Although virtually all types of signal can be analysed by using the DFT, the use of the DFT is limited to records containing small numbers of samples due to the large number of arithmetic operations (being proportional to N^2 for the order-N problem) which must be undertaken to process a record. To overcome this limitation, a more efficient algorithm known as the Fast Fourier Transform (FFT) was devised in the late 1960s. The FFT forces one further requirement, that the number of data points is an integer power of 2. This allows symmetries to occur reducing the number of required multiplications being proportional to $N\log_2 N$, compared to the DFT. The FFT is still the most widely available tool for common signal processing applications, however, it should always be reminded that the fast Fourier transform is actually an approximation to the true Fourier series, or Fourier integral.

4.2.2 Considerations on Digital Signal Processing

In the procedures of digital signal processing (DSP), as the discretised form of originally-continuous signals are processed in also discretised procedures such as the DFT, there would be a loss of information, which sometimes introduces erroneous results leading to misinterpretations. To avoid such possible problems, the limitations

of DSP must be fully understood. In this regard, some required considerations prior to applying the DSP techniques are discussed.

4.2.2.1 Sampling

One of the first processes in digital signal processing to which any signal is subjected is sampling. Correct sampling of a signal is essential to obtain a good estimate of its spectral contents. There are two important factors which should be carefully considered in sampling process.

- **Sampling Frequency**

The sampling frequency f_s is simply the reciprocal of the time interval Δt between samples:

$$f_s = \frac{1}{\Delta t} \tag{4.2.9}$$

If a sampled time signal contain components at frequencies above half the sampling frequency, i.e. $f_s/2$ (which is often referred to as the Nyquist frequency), then misinterpretation of high frequency components (above half the sampling frequency) as lower frequencies arises, which is termed as aliasing problem.

To avoid this problem, there are several possible solutions. The most obvious way is to increase the sampling frequency sufficiently large that all frequencies are reliably reproduced within the sampled data. However, problems may be encountered in increasing the sampling frequency if the number of samples within a record is restricted for any reason. In this case, the solution to this problem is filtering the signal

prior to sampling using a low-pass filter with a suitable cut-off frequency to remove any frequency components above the Nyquist frequency.

• Frequency Resolution

The frequency resolution (or the spacing between adjacent digitised spectral lines) is determined primarily by the length of the time record. Clearly, high frequency resolution is necessary if identification around closely spaced frequencies within the signal is required.

The frequency resolution Δf can be determined from the time record length N by the relation:

$$\Delta f = \frac{f_s}{N} \tag{4.2.10}$$

Then, the frequency components observed as separate peaks within the spectrum will be spaced Δf apart in the frequency domain. Hence, the choice of record length should be made on the basis of some prior knowledge of the likely spacing between adjacent components in the signal.

4.2.2.2 Windowing

• Leakage

One of the common problems encountered in spectral analysis is that of 'leakage'. Leakage is a phenomenon whereby the frequency content of a signal may be

incorrectly identified by the DFT. Most of the leakage problem occurs due to the way in which the sample was taken, mostly where some components within the signal do not have an integer number of cycles within the record. This problem can be solved to some extent by applying a 'window' to the data.

• Windows

'Windows' are effectively weighting functions adjusting the signal which can be compared to a time-domain equivalent of the frequency-domain operation of filtering. By applying windows, the data becomes more periodic within the record, and a better estimate of the time spectrum may be obtained on application of the DFT by minimising the severity of the end-effects which are mainly caused by the leakage. Although windowing is an effective tool for the leakage problem, it should always be reminded that windows are just a means of minimising the consequences of a basic limitation of spectral analysis by applying weighting functions which actually modify the true sample. Hence, windows must not be used in situation which does not require them to avoid any incorrect (or altered) result.

There are many different windows in common use in signal processing such as flat-top, Hanning, exponential, or customised ones for special applications. For the problem in this research, Hanning window has been applied for transient-state vibration data in applying the short-time Fourier transform (STFT) due to its desirable characteristics with respect to the overlap operations of the STFT. And for steady-state vibration data, which is stationary and essentially periodic in nature, no window (often referred to as a rectangular window) has been applied to reserve the original properties of the sampled data.

4.3 Transient State

The vibration data from the run-up or run-down period of a rotor system can be considered as a non-stationary signal as the frequency content of the response of the rotor system is a function of the speed of rotation, Ω. In other words, the monitored vibration signal will be expected to change its characteristics with changes in the rotational speed. To describe the evolution of the spectrum with time, the distribution of the response levels for all frequencies in the measured range - the spectrum - should be plotted against time (e.g. spectrogram, time-frequency format) or against speed of rotation (e.g. Campbell diagram, speed-frequency format). Customarily, two approximate methods of digital spectral analysis have been used for analysing the frequency content of non-stationary processes, i.e.:

(i) Short-Time Fourier Transform (STFT)

(ii) Wigner Distribution

4.3.1 Short-Time Fourier Transform

The short-time Fourier transform (STFT) has been adapted from the conventional Fourier transform in order to analyse just a small section of the signal at a time - a technique called *windowing* the signal. The STFT maps a signal into a 2-dimensional function of time and frequency and represents a sort of compromise between the time- and frequency-based views of the signal.

The definition of the spectrogram around the time t using the short-time Fourier transform is given by:

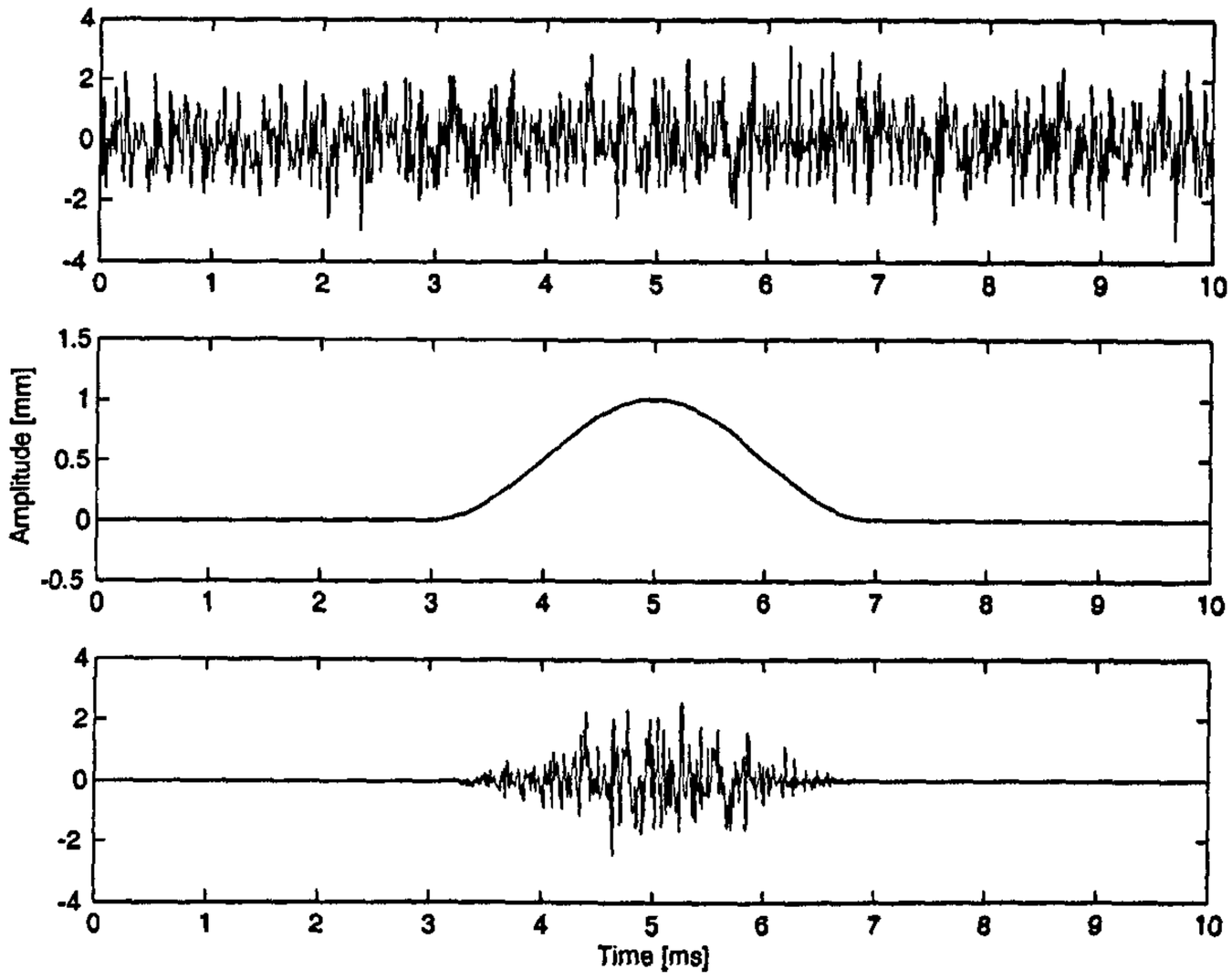


Fig 4.3.1 Localisation of a Time Record in Short-Time Fourier Transform

$$S(\omega, t) = \int_{-\infty}^{\infty} s(\tau)\, window(t-\tau) e^{-i\omega\tau} d\tau \qquad (4.3.1)$$

where $s(\tau)$ is the measured signal at time $t = \tau$.

Fig 4.3.1 illustrates the operation of localisation of a time record using Hanning window and as illustrated, the short-time Fourier transform (STFT) has a short data window centred at local time t, and spectral coefficients are calculated for this short length of data. The idea is that local spectral coefficients are obtained which describe the frequency composition of the record being analysed at time t, the window is then moved to a new position and the calculation is repeated. Considering the fact that the frequency bandwidth is of the order of $1/T$ for the width of the window T, the bandwidth of each spectral coefficient inevitably becomes wide by using a short data

window in order to calculate spectral density coefficients for the length of record that is local to time t. Hence, a high resolution cannot be obtained simultaneously in both the time and the frequency domains due to the fundamental incompatibility of the two requirements of a short data window and a narrow bandwidth. Also, it should be noted that the underlying assumption behind the short-time Fourier transform method is that the measured spectrum does not change too rapidly over the selected time span, i.e. the short-time Fourier transform (STFT) may be used for quasi-stationary processes.

• Directional Short-Time Fourier Transform (DSTFT)

The short-time Fourier transform (STFT) has been extended to form the Directional STFT by Bucher & Ewins [7] for application to rotating machinery vibration analysis. The DSTFT provides enhanced resolution and more information on the non-stationary vibration data from the rotating machinery than the conventional STFT, and for these reasons, it has been widely used in this research as an essential tool for transient vibration analysis.

4.3.2 Wigner Distribution

The Wigner distribution (or Wigner-Ville distribution) is an alternative approach. For a non-stationary process $x(t)$, a measure of the frequency content, $\Phi_{xx}(\omega, t)$ called the Wigner distribution, can be obtained by taking the Fourier transform of instantaneous autocorrelation function (without ensemble-averaging operation) at time t, then $\Phi_{xx}(\omega, t)$ can be expressed:

$$\Phi_{xx}(\omega, t) = \frac{1}{2\pi}\int_{-\infty}^{\infty} x(t-\tau/2)x(t+\tau/2)e^{-i\omega\tau}d\tau \qquad (4.3.2)$$

$\Phi_{xx}(\omega, t)$ is a function of ω and t, and applies for a single sample record. The main difficulty for estimating the frequency content of non-stationary processes with this method comes from the fact that the distribution $\Phi_{xx}(\omega, t)$ is also affected by the characteristics of signal $x(t)$ far away from the local time t because of the integral in (4.3.2) covering an infinite range of τ. Due to the continuing nature of harmonic waves, it is impossible to have a meaningful local spectral density estimation.

To evaluate the performance of the Wigner distribution in handling the non-stationary signals, a signal containing two sine sweeps has been utilised, which has the following form (refer to Fig 4.3.2):

$$x(n) = A_1 \sin(2\pi f_{v1} t + \theta_1) + A_2 \sin(2\pi f_{v2} t + \theta_2) \tag{4.3.3}$$

where

$x(n)$	multi-sine sweep discrete data point (total number of N)
n	data sample number of a discrete time sequence ($0 \leq n \leq N-1$)
A	amplitude, $A_1 = A_2 = 1$
f_v	time-varying frequency ($f_v = f_{initial} + n \frac{f_{final} - f_{initial}}{N}$)
f_{v1}	time-varying frequency from 20 Hz ~ 40 Hz
f_{v2}	time-varying frequency from 30 Hz ~ 90 Hz
t	time
θ	phase angle, $\theta_1 = 0°$, $\theta_2 = 90°$

As the Wigner distribution requires a lot of processing time, only 1000 samples, from a sequence of 1 s digitised with a sampling frequency 1000 Hz, have been processed to estimate a Wigner distribution. As can be clearly seen in the time-frequency distribution presented in Fig 4.3.3, unexpected time-varying frequency components appears between the two time-varying frequencies corresponding to each sine sweep existing in the signal.

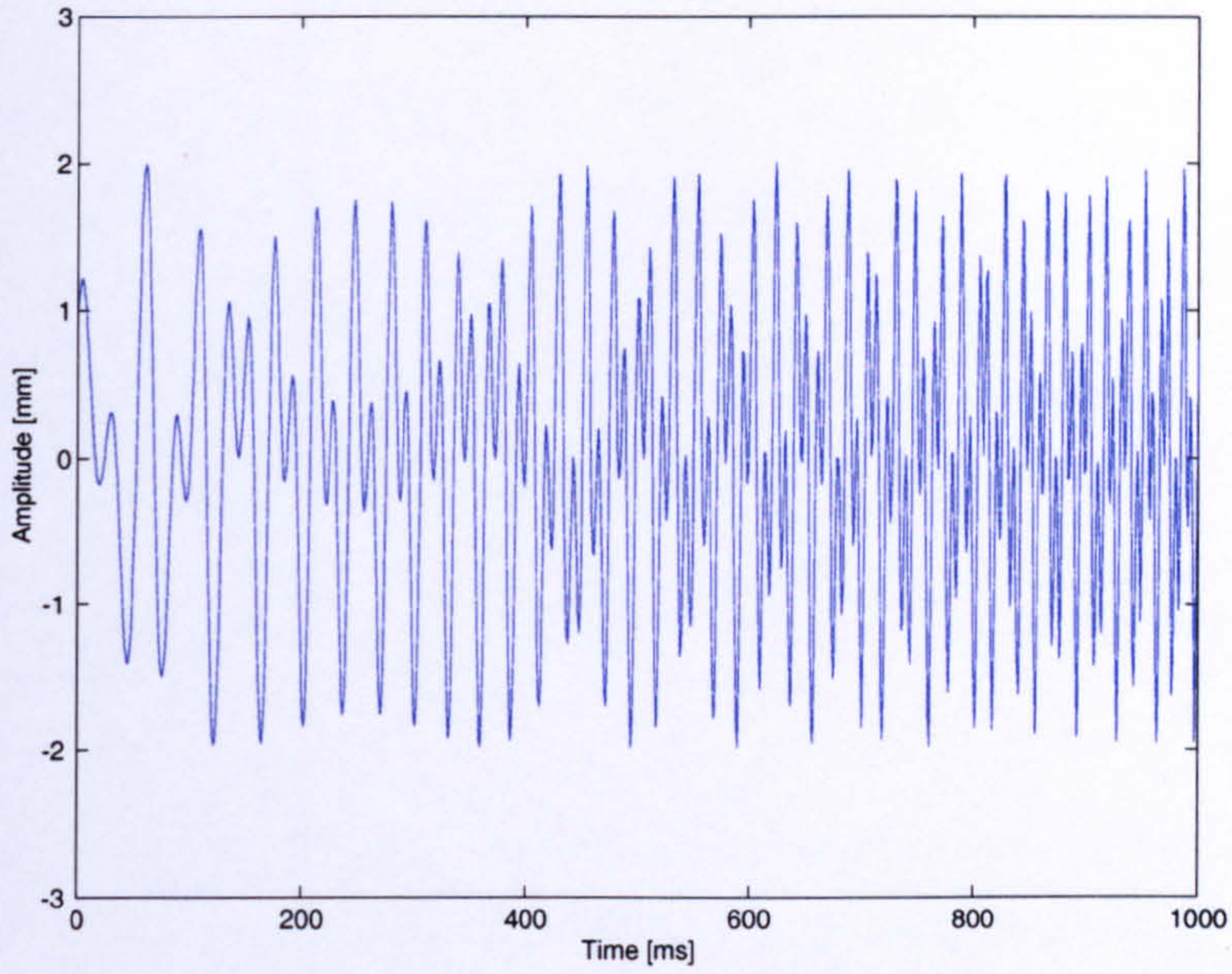


Fig 4.3.2 Time History of a Signal containing Two Sine Sweeps

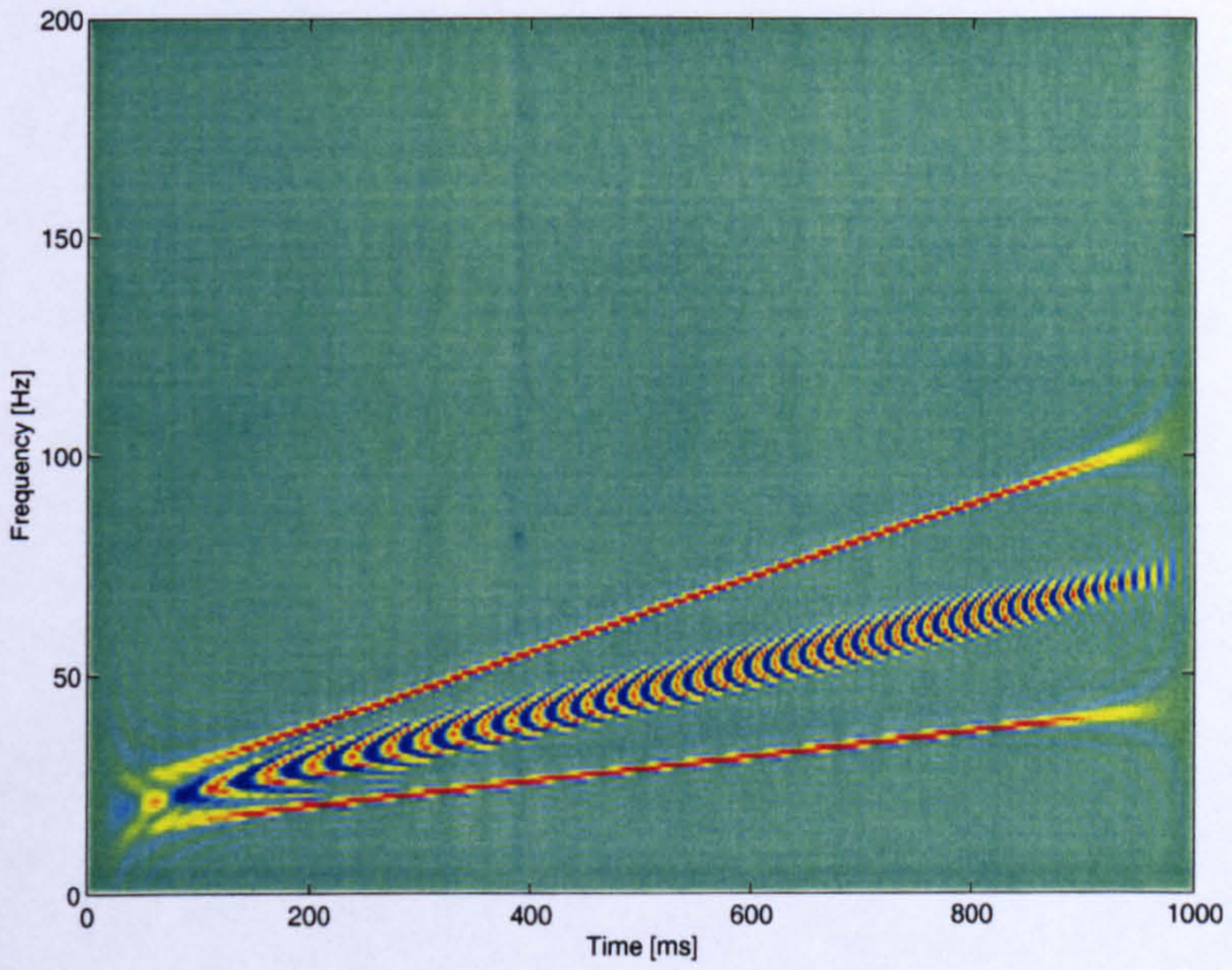


Fig 4.3.3 Wigner-Ville Distribution of the Signal

This phenomenon is caused by the presence of 'cross terms' in implementing the Wigner distribution, particularly to the signals consisting of several frequency components (which is quite common case in practical situations). These cross terms are inherent in all bi-linear time-frequency representations and can never be completely eliminated. Due to this feature, if there is noise present in the signal, the noise will be propagated in the distribution and this is a major drawback of the Wigner distribution, as reported by Cohen [16]. To reduce this problem, a smoothed Wigner distribution, known as pseudo-Wigner-Ville distribution [92] has been introduced.

Although the Wigner distribution provides a relatively better resolution for the original signals than the STFT under the same condition, due to the obvious disadvantage of Wigner distribution aforementioned, it is considered that it is not appropriate to apply the Wigner distribution to the cracked rotor problem, as the vibration data from a cracked rotor system consist of several frequency components as already presented in the previous chapters.

4.3.3 Directional Harmonic Wavelet Transform (DHWT)

As has been mentioned for both methods (STFT & WD), a high resolution cannot be achieved simultaneously in both the time and the frequency domains when estimating the time-dependent spectra. In order to overcome this limitation to the spectral analysis, an alternative method of signal analysis, called wavelet analysis, has been developed. In wavelet analysis, alternative families of orthogonal functions called wavelets are used as the basis functions for decomposing a general signal, instead of using sine and cosine functions. Whereas harmonic functions continue forever by definition, wavelets are local functions. By joining these together and by using

different scales for each wavelet, it is possible to assemble a family of basis functions which is particularly suitable for examining the local characteristics of non-stationary signals. Although wavelet theory is rather new and complex, there are numerical algorithms similar to the FFT for calculating wavelet coefficients. One of those algorithms is the recently-developed Harmonic Wavelet Transform by Newland [98] which has the advantage of computational simplicity. In this research, the Harmonic Wavelet Transform (HWT) algorithm has been extended to the Directional Harmonic Wavelet Transform to accommodate an important characteristic feature of rotating structures; namely, the existence of forward whirl and backward whirl components. With this new method, the local characteristics of non-stationary signals from rotating structures can be better observed by using the further-decomposed wavelets (even though wavelets are already decomposed from the signal), or directional-wavelets (FW Wavelet & BW Wavelet). This modified algorithm, i.e. the directional harmonic wavelet transform (DHWT) is considered to be useful for monitoring rotating machinery transient vibrations. For applications, it has been applied to the transient-state vibration data of the cracked rotor system and the results are presented together with the concepts of the algorithm.

• Directional Harmonic Wavelet Transform (DHWT)

Harmonic wavelet transform can be performed to any function (or signal) by using the scaling function and the harmonic wavelets as a basis for transformation. By definition, the scaling function defined for wavelet level -1 is a special case of the harmonic wavelet, which constitutes the constant part of the signal (because wavelets are defined from level -1, and level -1 has no wavelets and is just a constant level). Harmonic wavelets can be derived by seeking a wavelet $w(x)$ whose spectrum is exactly like a box function so that the magnitude of its Fourier transform, $W(\omega)$, is zero except for an octave band of frequencies, [98].

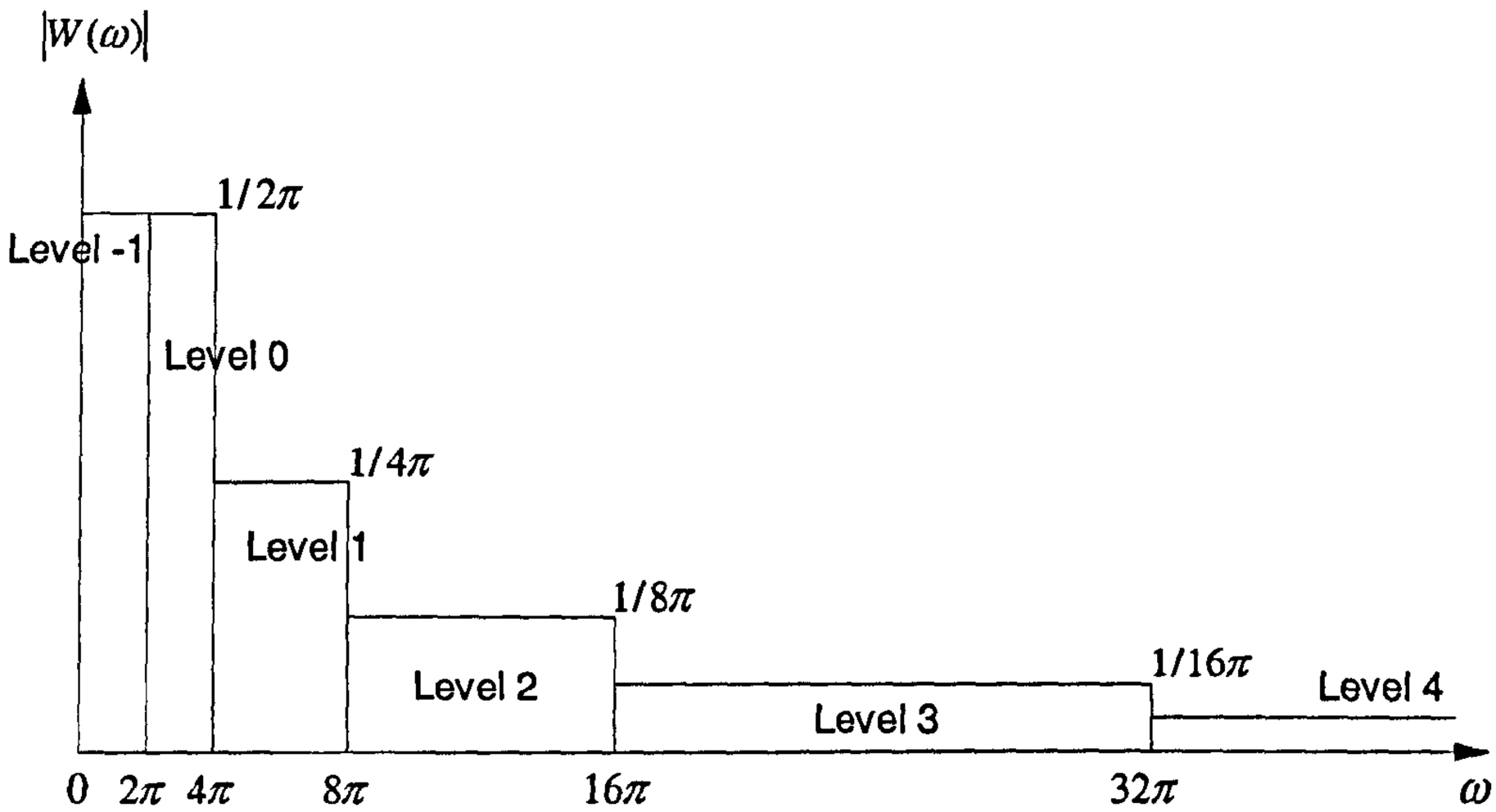


Fig 4.3.4 Magnitudes of the Fourier transforms of Harmonic Wavelets of Different Levels, [98]

To derive the harmonic wavelets according to this concept, the magnitudes of the Fourier transforms of harmonic wavelets, i.e., $|W(\omega)|$, for different levels, can be defined as shown in Fig 4.3.4.

All the Fourier transforms are identically zero for $\omega < 0$, and for level -1, the definition of $W(\omega)$ is:

$$W_{-1}(\omega) = (1/2\pi)e^{-i\omega k} \qquad \text{for } 0 \leq \omega < 2\pi$$
$$= 0 \qquad \text{elsewhere} \tag{4.3.4}$$

The inverse Fourier transform of (4.3.4) gives the scaling function

$$\phi(x-k) = (e^{i2\pi(x-k)} - 1)/i2\pi(x-k), \qquad k = -\infty \text{ to } \infty \tag{4.3.5}$$

Also, for level 0,

$$W_0(\omega) = 1/2\pi \quad \text{for } 2\pi \leq \omega < 4\pi$$
$$= 0 \quad \text{elsewhere} \tag{4.3.6}$$

By calculating the inverse Fourier transform of $W_0(\omega)$, the corresponding complex wavelet is:

$$w(x) = (e^{i4\pi x} - e^{i2\pi x})/i2\pi x \tag{4.3.7}$$

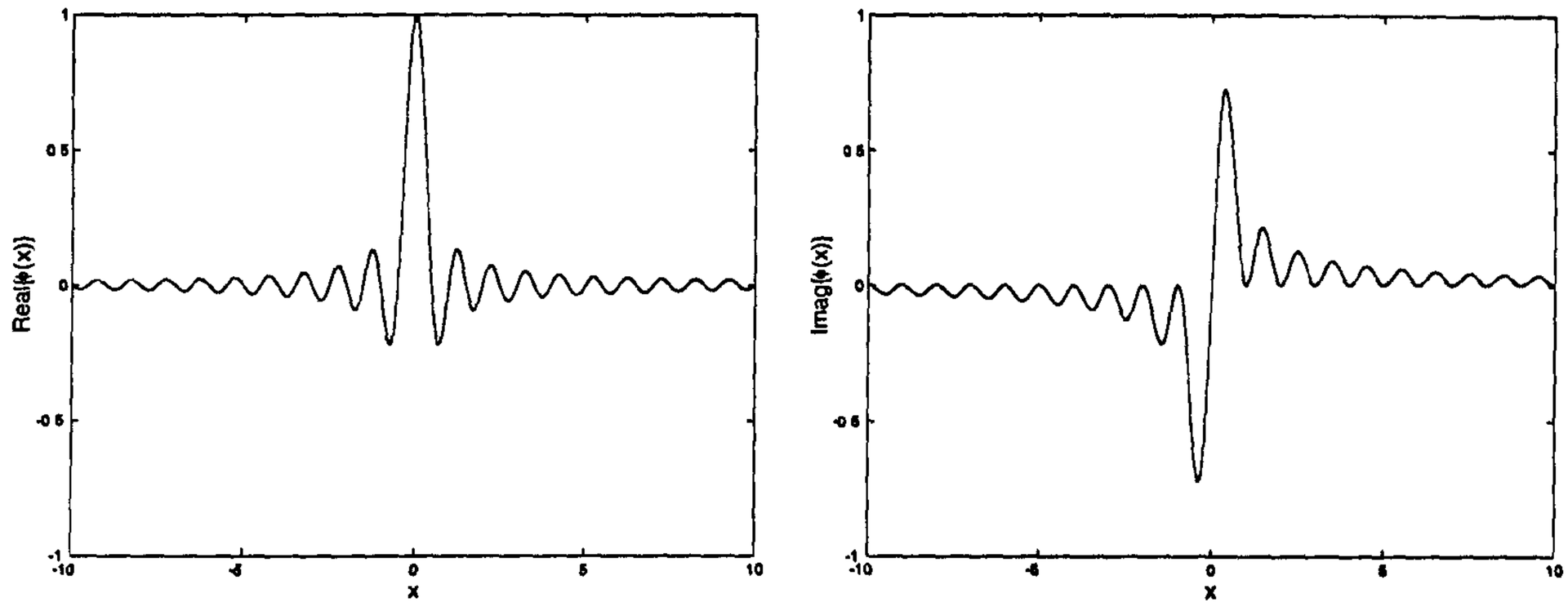
The general complex wavelet at level j, and translated by k steps of size $1/2^j$, can be derived by performing the inverse Fourier transform of (4.3.8):

$$W_j(\omega) = (1/2\pi)2^{-j}e^{-i\omega k/2^j} \quad \text{for } 2\pi \times 2^j \leq \omega < 4\pi \times 2^j$$
$$= 0 \quad \text{elsewhere} \tag{4.3.8}$$

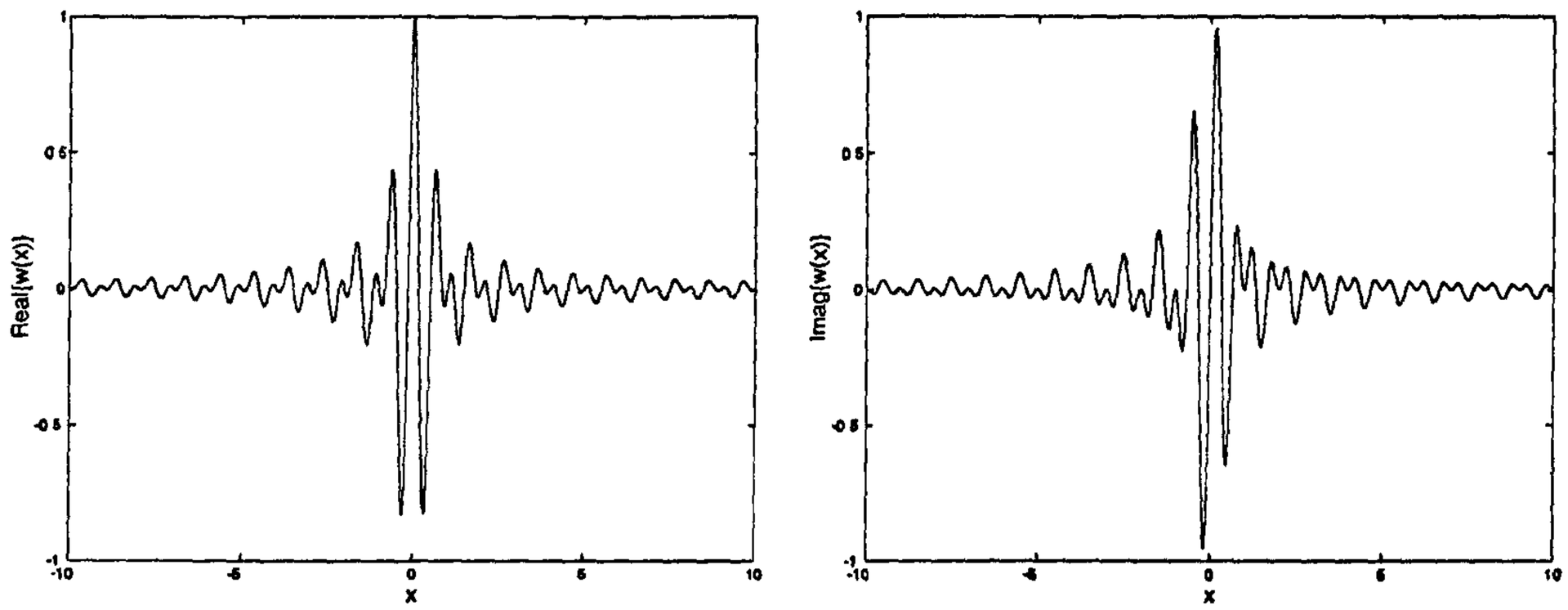
and can be expressed:

$$w(2^j x - k) = [e^{i4\pi(2^j x-k)} - e^{i2\pi(2^j x-k)}]/i2\pi(2^j x - k),$$
$$j = 0 \text{ to } \infty, k = -\infty \text{ to } \infty \tag{4.3.9}$$

The real and imaginary part of the scaling function $\phi(x)$ and harmonic wavelet $w(x)$ are presented in Fig 4.3.5-(a) & (b) respectively. As shown, the wavelets, which are the basis functions for the wavelet transform, are local functions whereas the basis functions for the Fourier transform, i.e. sine and cosine functions, continue forever.



(a) Harmonic Scaling Function



(b) Harmonic Wavelet Function

Fig 4.3.5 Real and Imaginary Part of the Harmonic Wavelets

Hence, by using the scaling function $\phi(x)$ and the complex wavelet $w(x)$ defined in equation (4.3.5) & (4.3.9) respectively, the wavelet expansion of a general function (or signal) $f(x)$ is given by:

$$f(x) = \sum_{k=-\infty}^{\infty} [\, a_{\phi k}\phi(x-k) + \tilde{a}_{\phi k}\phi^*(x-k)] + \sum_{j=0}^{\infty}\sum_{k=-\infty}^{\infty} [\, a_{jk}w(2^j x-k) + \tilde{a}_{jk}w^*(2^j x-k)] \qquad (4.3.10)$$

where the coefficients a_{jk} and $\tilde{a}_{jk}$ for the general complex wavelet $w(2^j x - k)$ are defined as:

$$a_{jk} = 2^j \int_{-\infty}^{\infty} f(x) w^*(2^j x - k) dx \tag{4.3.11}$$

$$\tilde{a}_{jk} = 2^j \int_{-\infty}^{\infty} f(x) w(2^j x - k) dx \tag{4.3.12}$$

If $f(x)$ is real, $\tilde{a}_{jk}$ is the complex conjugate of a_{jk} so that $\tilde{a}_{jk} = a_{jk}^*$ but to allow for the case when $f(x)$ is complex, a_{jk} and $\tilde{a}_{jk}$ should be regarded as two different amplitudes.

Similarly the coefficients $a_{\phi k}$ and $\tilde{a}_{\phi k}$ for the scaling function $\phi(x - k)$ can be defined:

$$a_{\phi k} = \int_{-\infty}^{\infty} f(x) \phi^*(x - k) dx \tag{4.3.13}$$

$$\tilde{a}_{\phi k} = \int_{-\infty}^{\infty} f(x) \phi(x - k) dx \tag{4.3.14}$$

In applying the harmonic wavelet transform technique to vibration problems in rotating machinery, it is essential to decompose the vibration signals into forward-whirl (FW) and backward-whirl (BW) components and for the sake of completeness, the concept will be introduced here again briefly.

Two signals $s_1(t)$ and $s_2(t)$ obtained from a rotating structure by using two orthogonally-spaced displacement probes, can be combined into a single *complex signal*:

$$\boldsymbol{s} = s_1(t) + is_2(t) \tag{4.3.15}$$

This complex-valued signal $\boldsymbol{s}$ describes an orbital motion of the shaft axis away from its equilibrium position, and consists of the forward (co-rotating) and backward (counter-rotating) whirl components.

From the complex notation (4.3.15), the *forward* and *backward* whirl components, $\boldsymbol{r}_f$ and $\boldsymbol{r}_b$, can be decomposed:

$$\boldsymbol{s} = s_1(t) + is_2(t) = \boldsymbol{r}_f e^{i\omega t} + \boldsymbol{r}_b e^{-i\omega t} = \boldsymbol{s}_f + \boldsymbol{s}_b \tag{4.3.16}$$

This well-known complex-notation based FW/BW separation concept [44] has now been incorporated into the harmonic wavelet transform algorithm to form the **directional harmonic wavelet transform technique** (DHWT) to obtain the directional harmonic wavelet coefficients. This new (or improved) algorithm has been coded in MATLAB and the newly-defined directional harmonic wavelet coefficients can be expressed as follows.

The directional coefficients $\{a_{jk}\}_{f,b}$ and $\{\tilde{a}_{jk}\}_{f,b}$ for the general complex wavelet $w(2^j x - k)$ are defined, respectively:

$$\{a_{jk}\}_{f,b} = 2^j \int_{-\infty}^{\infty} \boldsymbol{s}_{f,b}\, w^*(2^j x - k)dx \tag{4.3.17}$$

$$\{\tilde{a}_{jk}\}_{f,b} = 2^j \int_{-\infty}^{\infty} \boldsymbol{s}_{f,b}\, w(2^j x - k)dx \tag{4.3.18}$$

Similarly, the directional coefficients $\{a_{\phi k}\}_{f,b}$ and $\{\tilde{a}_{\phi k}\}_{f,b}$ for the scaling function $\phi(x-k)$ can be defined as:

$$\{a_{\phi k}\}_{f,b} = \int_{-\infty}^{\infty} s_{f,b}\, \phi^*(x-k)dx \tag{4.3.19}$$

$$\{\tilde{a}_{\phi k}\}_{f,b} = \int_{-\infty}^{\infty} s_{f,b}\, \phi(x-k)dx \tag{4.3.20}$$

As shown in equations (4.3.17) ~ (4.3.20), the directional harmonic wavelets can be described by simple analytical formulae; they are compact in the frequency domain, and are described by a complex function so that there are four wavelets for each j, k pair, i.e. two each for forward and backward components, respectively (while the standard harmonic wavelet transform produces two wavelets for each j, k pair so the directional property is not available). Relative to other wavelet transform algorithms, the main advantage of Directional Harmonic Wavelet Transform (DHWT) is its computational simplicity and efficiency in dealing with rotating machinery vibrations. The processing sequence of DHWT algorithm is briefly illustrated in Fig 4.3.6 in discrete form.

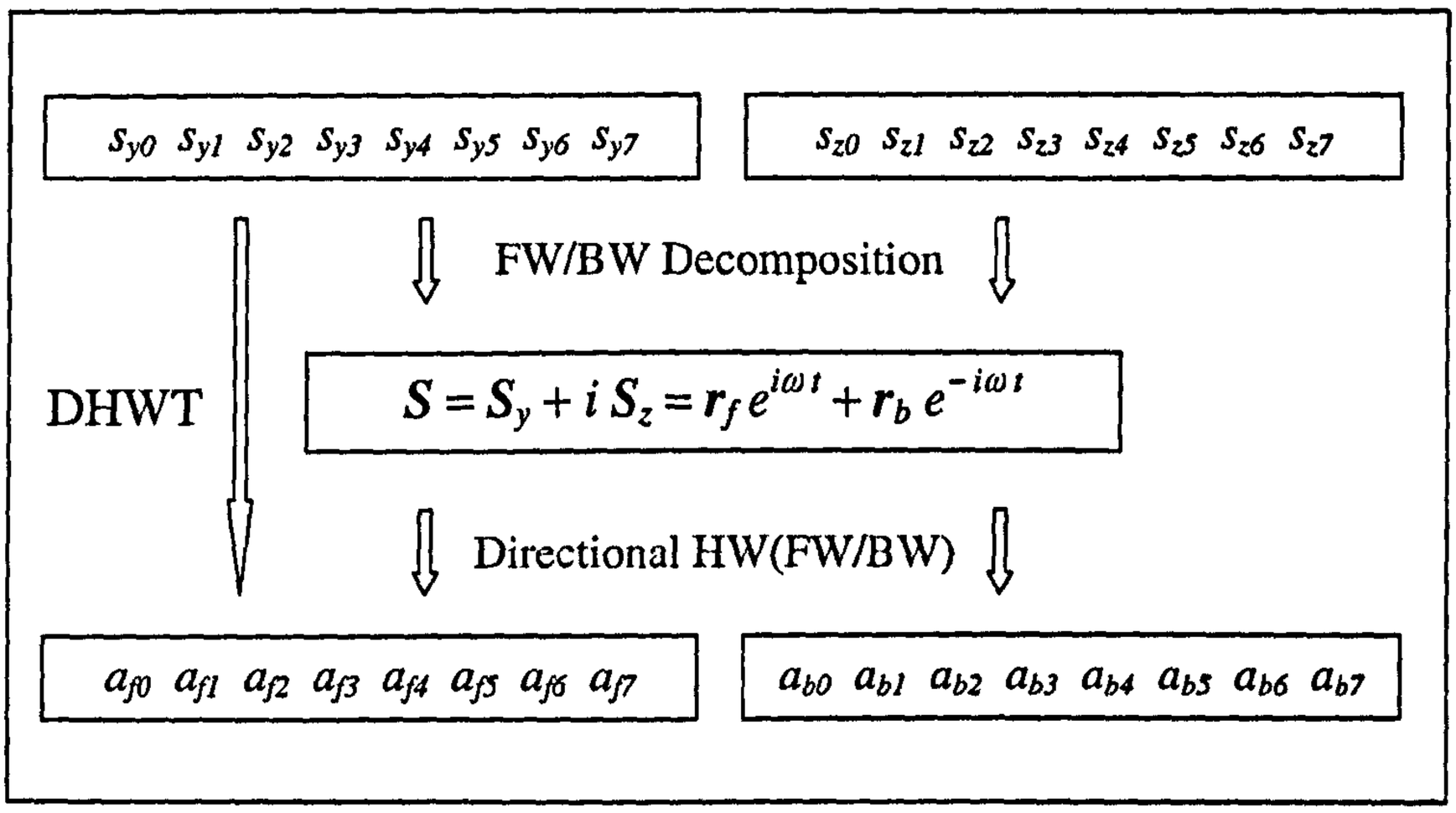


Fig 4.3.6 Schematic Diagram of Directional Harmonic Wavelet Transform

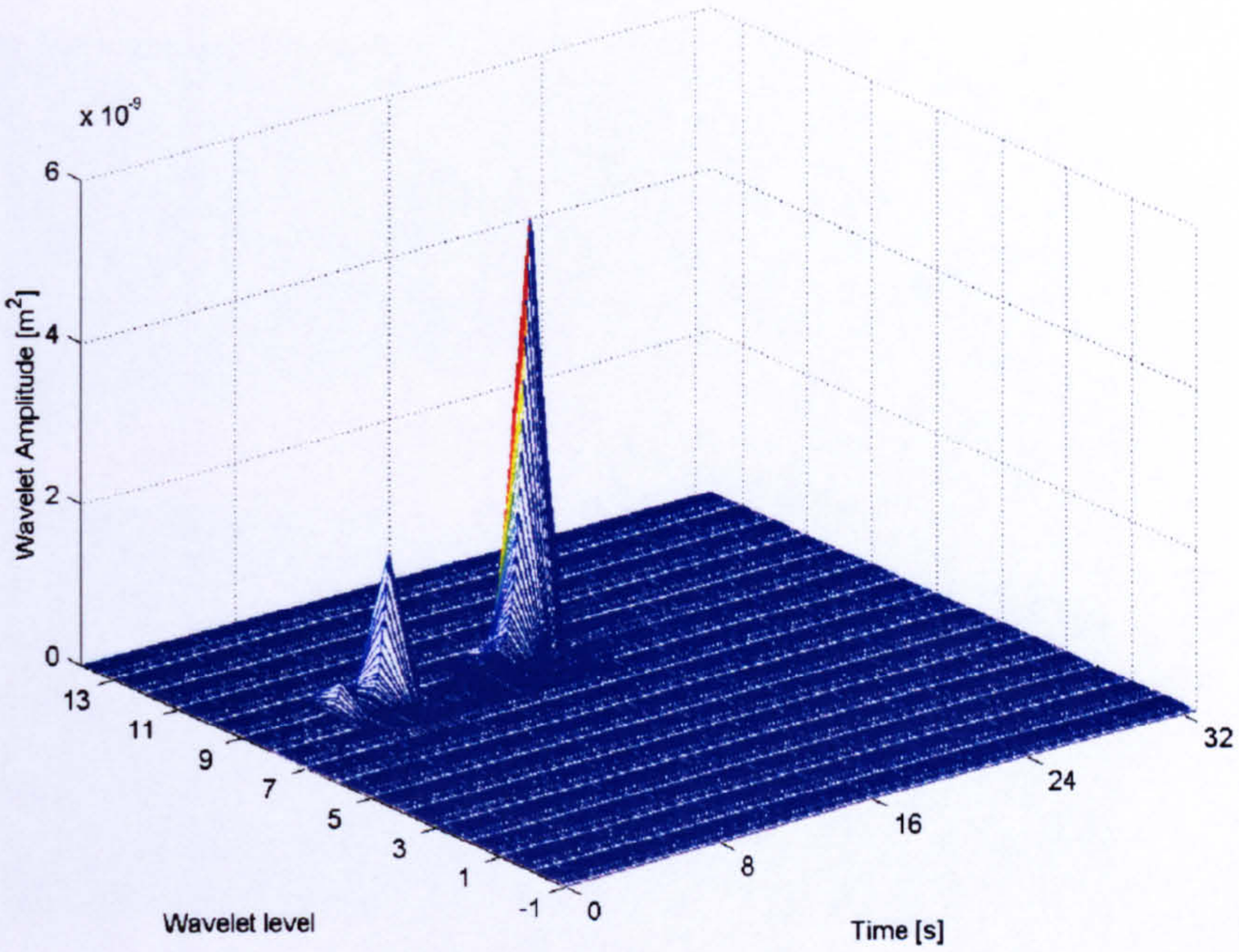
• Application of the Directional Harmonic Wavelet Transform (DHWT)

To study the effectiveness of the DHWT, the method has been applied to the same set of vibration data computed from the MDOF cracked rotor model and analysed using STFT in the previous chapter.

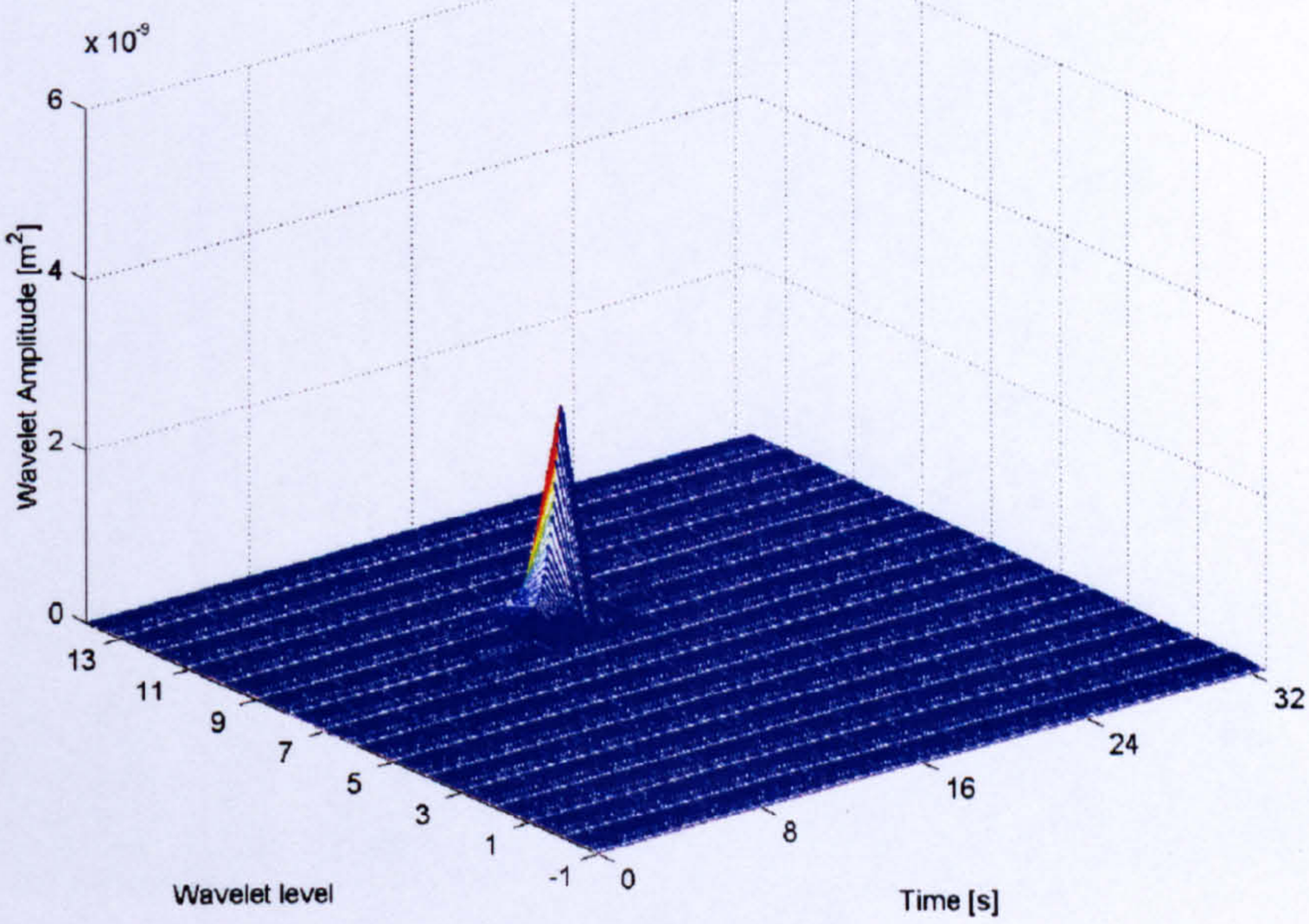
Generally, wavelet analysis provides spectral information in a *time-level* region in contrast to the *time-frequency* format of the STFT. As presented in Fig 4.3.7, the spectral density of the run-up vibration data can be provided in the form of *FW/BW directional mean-square wavelet map* proposed by Kim & Ewins [73]. Instead of a signal's mean-square being given by the area under its spectral density curve, the mean-square is given by the volume under a 2-dimensional wavelet surface with time as one axis and wavelet level (provides a measure of frequency) as the other axis.

In applying the DHWT, a sequence length of 32768 ($= 2^{15}$) corresponding to a sampling interval of 10^{-3} s has been used. As the sampling frequency is 1000 Hz, this sequence covers a time span of $32768/1000 = 32.8$ s, approximately. As can be seen in Fig 4.3.7-(a), the sub-resonance at $t = 9.3$ s ($\Omega/\omega_n = 1/2$), and synchronous resonance at $t = 18.7$ s ($\Omega/\omega_n = 1$), caused by the crack-related 2Ω and 1Ω harmonics respectively, can be clearly identified at wavelet level 9 in the forward directional harmonic wavelet map. Due to the smallness of the crack-related 3Ω harmonic component, the sub-resonance at $t = 6.2$ s ($\Omega/\omega_n = 1/3$) can only just be identified. Also, in Fig 4.3.7-(b), the synchronous resonance at $t = 18.7$ s (caused by the crack-related -1Ω harmonic component) can be identified in the backward directional harmonic wavelet map at the same level, i.e., wavelet level 9. For level 9, the frequency range is centred at 512 ($= 2^9$) cycles in 32.8 s ($= 32768/1000$), which is a frequency of $512 \times (1000/32768) = 15.6$ Hz approximately, and this frequency range (covers $15.6 \sim 2 \times 15.6$ Hz) incorporates well the 1st natural frequency of the MDOF cracked rotor system.

As in the case of the STFT, the directional harmonic wavelet transform (DHWT) has been applied to noise-contaminated signals (simulated 10 % random noise with Gaussian distribution added to the original time histories). The results presented in Fig 4.3.10-(a) & (b) reveal the advantage of DHWT over the STFT, because the results from the DHWT are insensitive to the random noise while the STFT provides noise-contaminated one as in Fig 4.3.9. Also, the limitation imposed by the STFT, related with the resolution caused by the overlap property of the algorithm (refer to Fig 4.3.8 & 4.3.9), could be solved with this new method as the localised spectral information of DHWT suggests (refer to Fig 4.3.7 & 4.3.10). Hence, it can be concluded that the transient response of the rotor system can be much better observed by applying the DHWT together with STFT.



(a) Forward Directional Wavelet Map



(b) Backward Directional Wavelet Map

Fig 4.3.7 Directional Wavelet Map: 10 % Crack

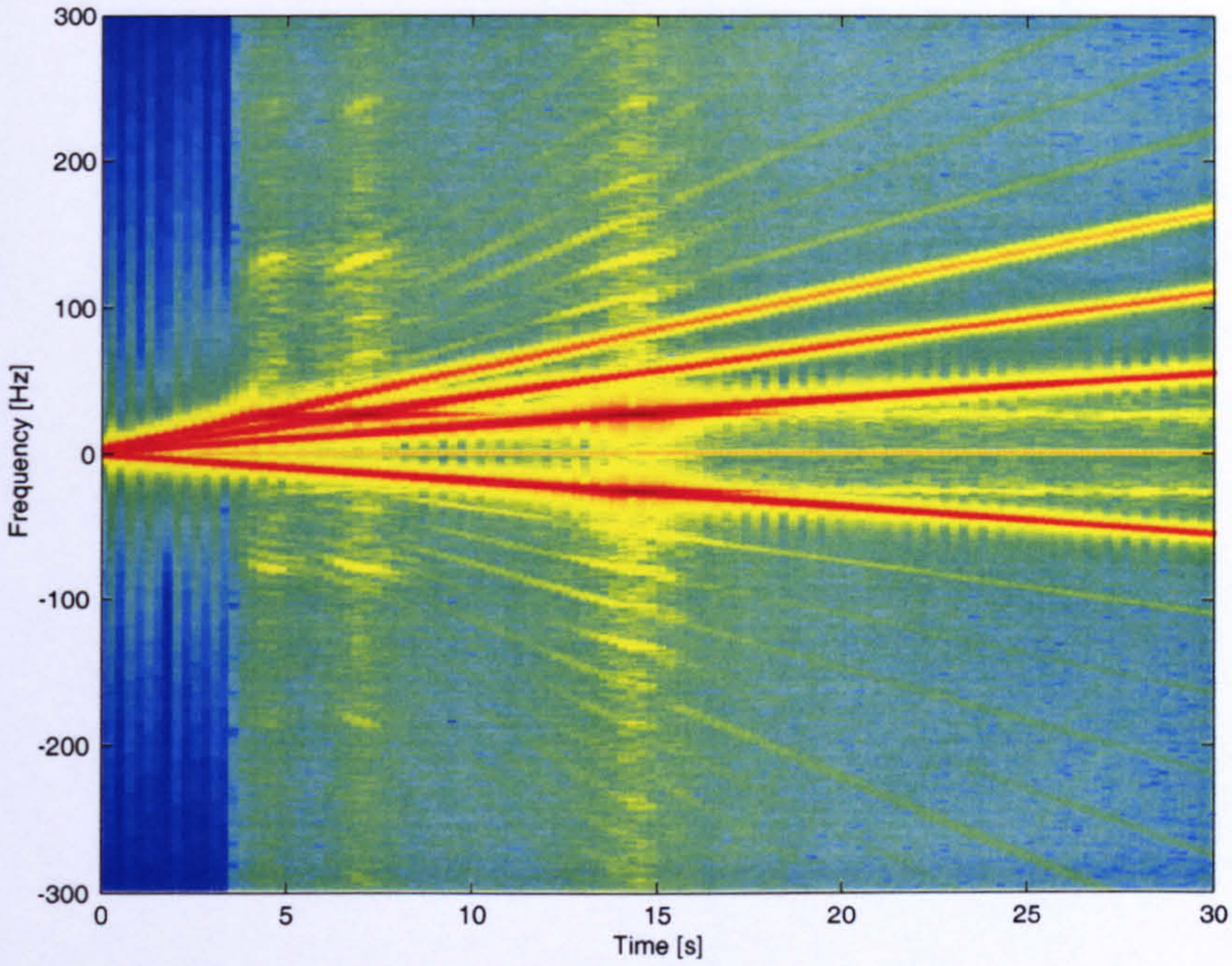


Fig 4.3.8 Spectrogram: 10 % Crack

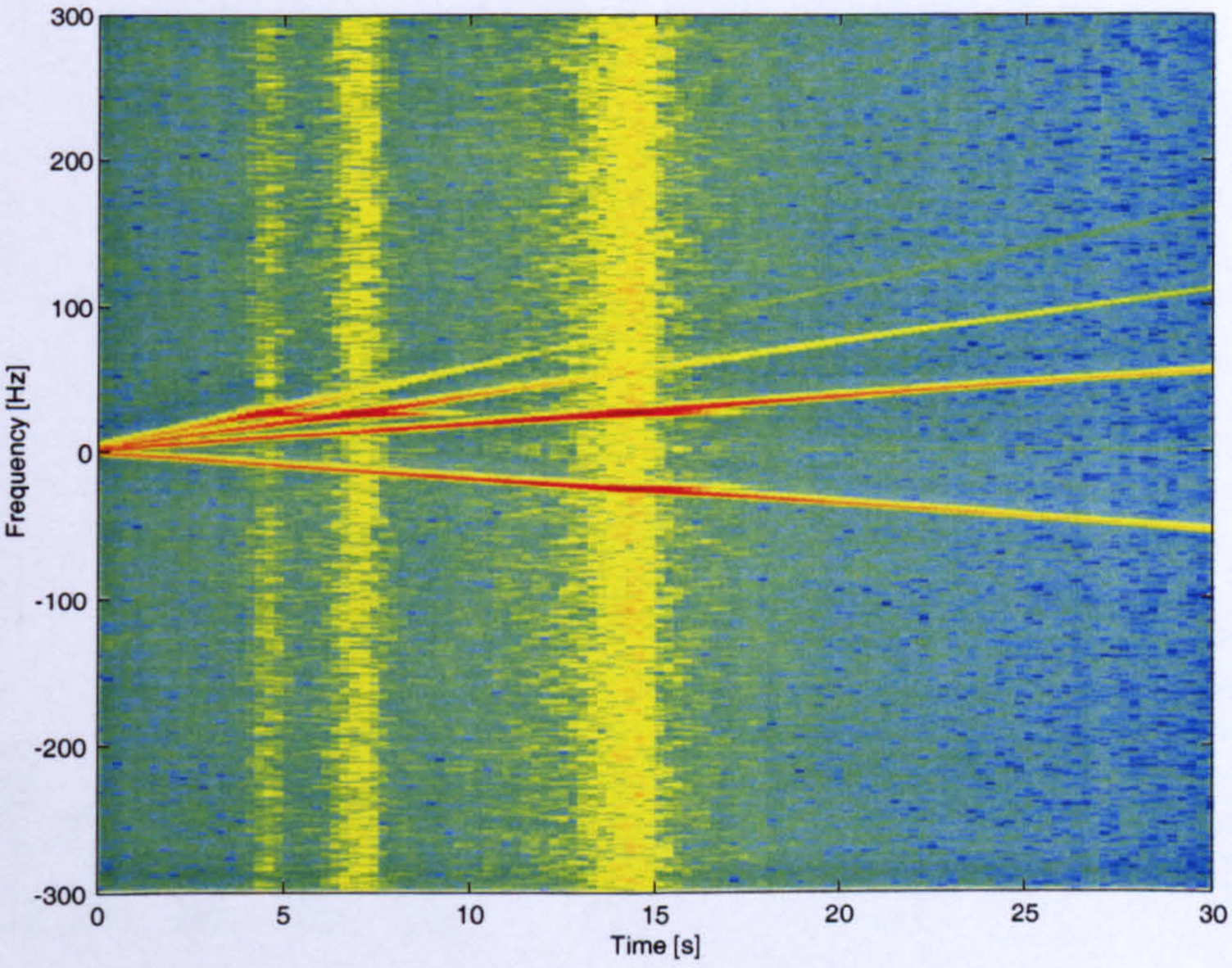
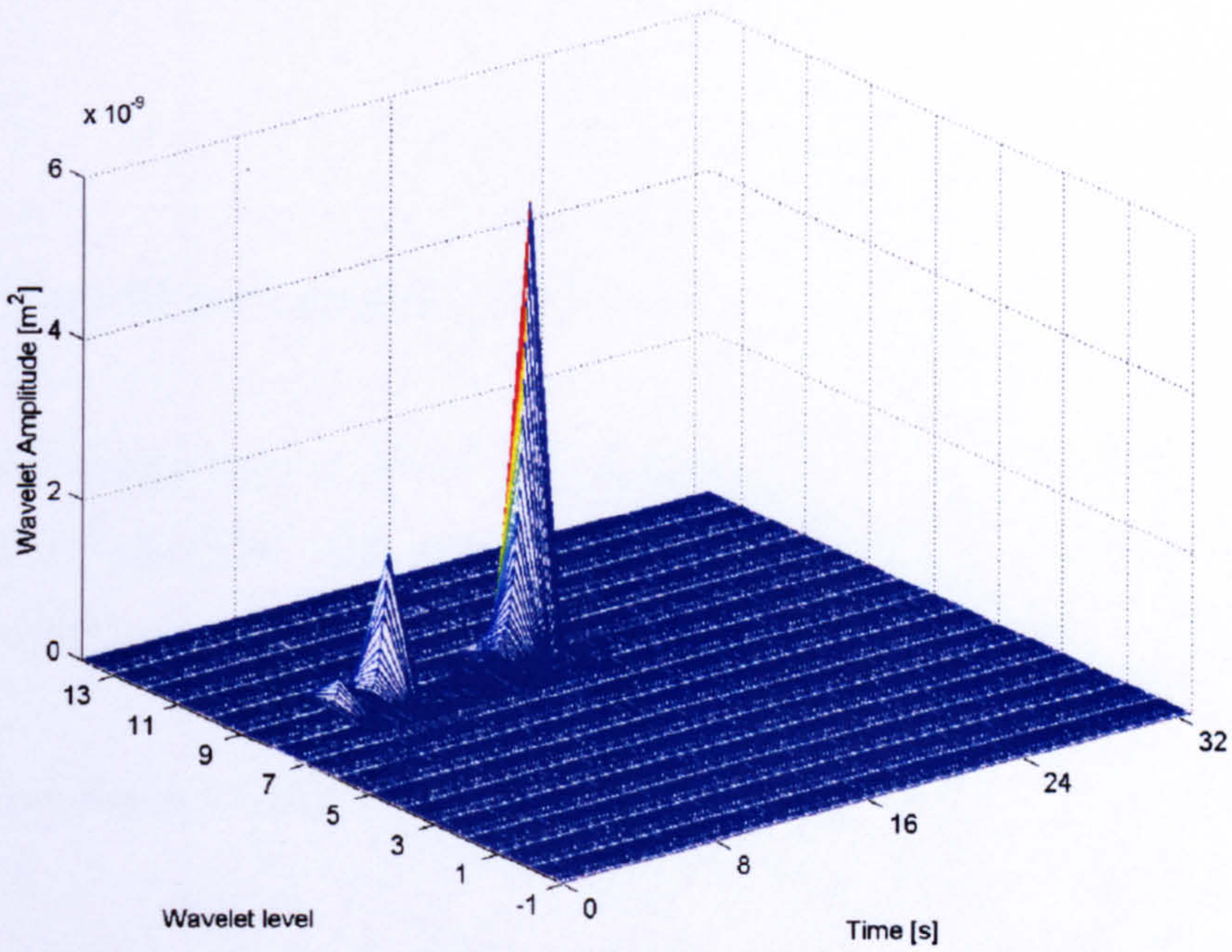
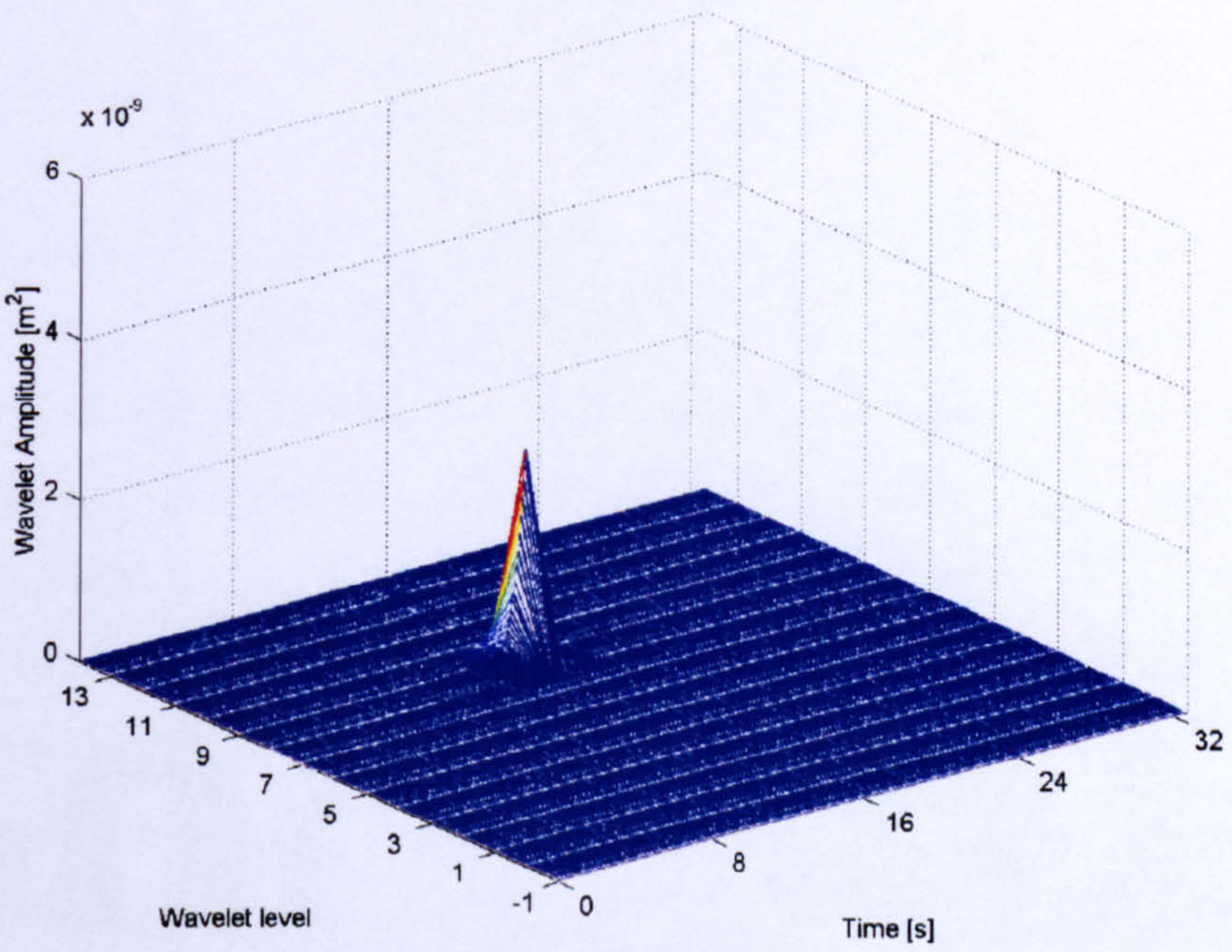


Fig 4.3.9 Spectrogram: 10 % Crack with 10 % Noise



(a) Forward Directional Wavelet Map



(b) Backward Directional Wavelet Map

Fig 4.3.10 Directional Wavelet Map: 10 % Crack with 10 % Noise

4.4 Steady State

4.4.1 The FFT for Complex-valued Data

Among various ways in which the spectral contents of a signal may be presented, the amplitude spectrum will be considered here due to its relative importance in engineering practice.

• Conventional Amplitude Spectrum

An amplitude spectrum is simply a spectrum of the actual amplitudes of the various frequency components present within the signal and may be calculated from the estimated Fourier coefficients by the following formula:

$$A_k = 2[X_k\, X_k^*]^{\frac{1}{2}} \tag{4.4.1}$$

By inspecting the amplitude spectrum, better physical insight into the behaviour of the system can be obtained through direct comparison between the spectrum and the physical dimension such as bearing clearance as the amplitude spectrum will reflect the actual properties of the analysed signal rather than a distorted one caused by the squaring effect as in PSD. In addition, if any small harmonic components are present in the spectrum, those components should still be identifiable. For the problem under consideration, these are quite distinct advantages over the PSD. For these reasons, the amplitude spectrum has been chosen as the basic tool of spectral analysis for steady-state vibration data. Also, as in the case of the transient state, the forward/backward decomposition concept has been applied to the conventional amplitude spectrum.

• Directional Amplitude Spectrum based on FFT for Complex-valued Data

The FFT algorithm is equally valid for real or complex data. If applied to real data, however, there will be two redundancies, [111]:

(i) The imaginary part of each input data value will be zero and thus half the memory will be used for storing zeroes.

(ii) The second half of the resulting spectrum, i.e. the frequencies from f_N to f_s also represent the negative frequencies from $-f_N$ to 0. And the latter are the complex conjugates of the positive frequency values.

The properties of Fourier series can be intuitively understood by using periodic functions. Suppose that $x(t)$ and $y(t)$ are periodic functions of time represented by the Fourier series:

$$x(t) = a_0 + 2\sum_{k=1}^{\infty}(a_k \cos \omega_k t + b_k \sin \omega_k t), \omega_k = \frac{2\pi k}{T} \tag{4.4.2}$$

$$y(t) = c_0 + 2\sum_{k=1}^{\infty}(c_k \cos \omega_k t + d_k \sin \omega_k t), \omega_k = \frac{2\pi k}{T} \tag{4.4.3}$$

Only the k-th harmonic can be considered for the sake of simplicity:

$$x(t) = 2[a_k \cos \omega_k t + b_k \sin \omega_k t], \omega_k = \frac{2\pi k}{T} \tag{4.4.4}$$

$$y(t) = 2[c_k \cos \omega_k t + d_k \sin \omega_k t], \omega_k = \frac{2\pi k}{T} \tag{4.4.5}$$

The Fourier transform of real data $x(t)$ is:

$$X_x(\omega) = (a_k - ib_k)\delta(\omega - \omega_k) + (a_k + ib_k)\delta(\omega + \omega_k) \tag{4.4.6}$$

Hence, in the frequency domain, the magnitude of the Fourier transform of real data $x(t)$ appears always symmetric as the spectrum component X_{-k} $(= a_k + ib_k)$ of negative frequency is the **complex conjugate** of the positive frequency value X_k $(= a_k - ib_k)$. For this reason, the negative frequency spectrum components become **redundant** and are usually ignored.

However, for complex-valued data, e.g. $q(t) = x(t) + iy(t)$:

$$q(t) = 2[\, a_k \cos \omega_k t + b_k \sin \omega_k t \,] + i2[\, c_k \cos \omega_k t + d_k \sin \omega_k t \,] \tag{4.4.7}$$

The Fourier transform of complex data $q(t)$ is:

$$X_q(\omega) = [(a_k + d_k) - i(b_k - c_k)]\, \delta(\omega - \omega_k) + [(a_k - d_k) + i(b_k + c_k)]\, \delta(\omega + \omega_k) \tag{4.4.8}$$

In general, as can be notified from the transformed equation (4.4.8), the spectrum components of negative frequencies are **not** the **complex conjugates** of the positive frequency values and the magnitude plot of the Fourier transform of complex-valued data appears non-symmetric. This feature is similar to the forward/backward whirl decomposition concept already described in Chapter 2, and this direct complex-data based FFT facilitates quicker and more accurate calculation (by reducing the round-off errors accumulated by more multiplications) than the existing way of calculating method [48] proposed by Bently Nevada, which adopts the real-data based FFT.

Fig 4.4.1 shows the aforementioned property of the complex-data based FFT for the following sample signal:

$$q(t) = x(t) + iy(t)$$

where

$x(t) = 2\cos\omega t + \sin\omega t,\ \ y(t) = \cos\omega t + 2\sin\omega t$

together with the real-data based FFT for the signal $x(t)$.

For vibration measurement instruments, ADRE [130] by Bently Nevada is capable of decomposing the vibration signals into forward and backward components relying on the real-data based FFT algorithm. However, in this research, the direct complex-data based FFT has been applied throughout the analytical and experimental work. It is notable to see the connection between rotor dynamics and signal processing concept.

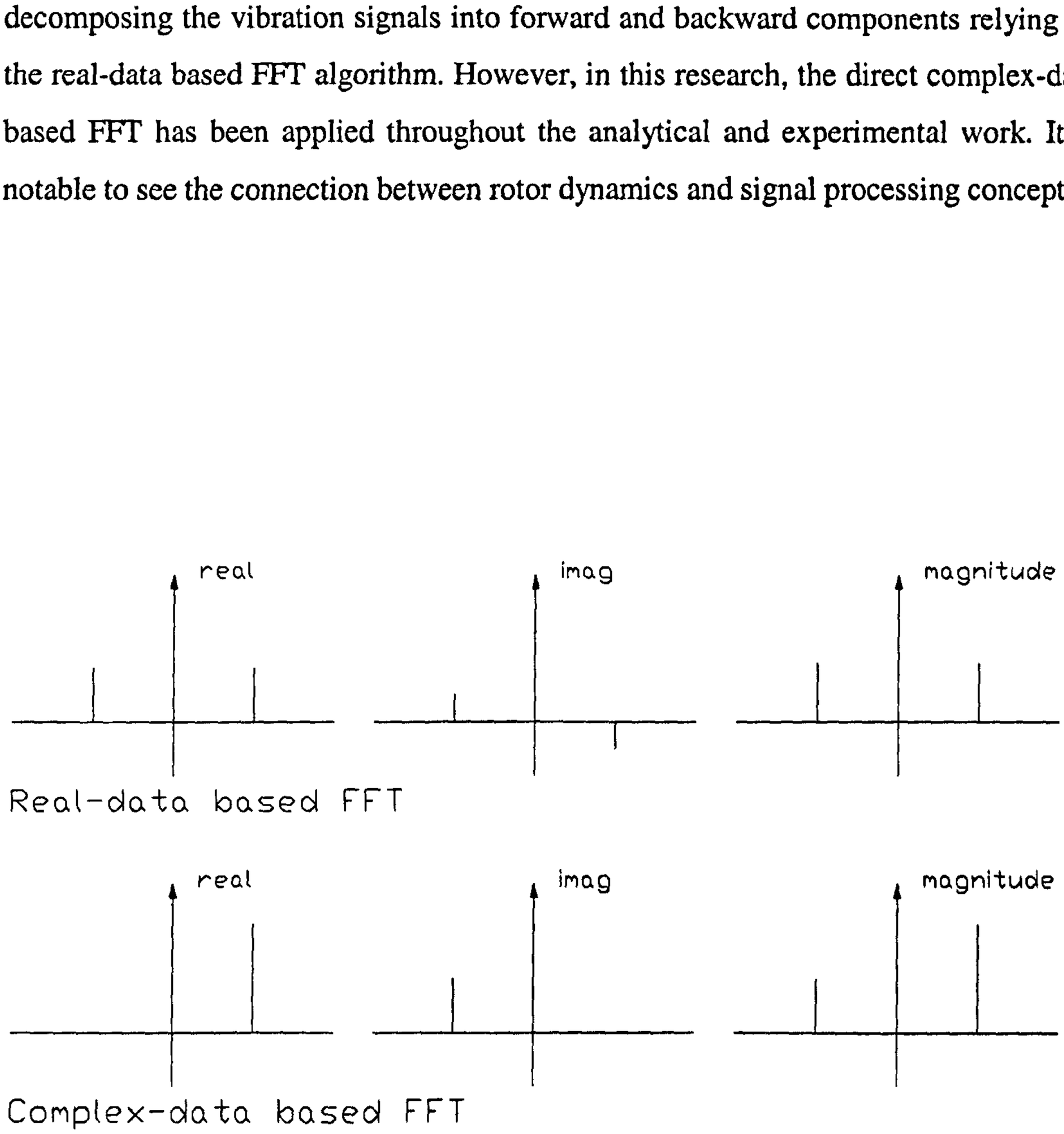


Fig 4.4.1 Real-data based FFT vs Complex-data based FFT

4.4.2 Directional-Difference Vibration Signature Analysis (DDVSA)

One of the main objectives of this research is to develop a method for detection of cracks in rotors by an on-line procedure; that is, while the machine is operating at its designated speed.

In an on-line mode, the most important indication of the presence of a crack is the initial appearance and/or a steady increase over time in $\pm 1\Omega$, 2Ω, 3Ω, and higher harmonics of lateral vibration. The appearance of an increase in $\pm 1\Omega$ and 2Ω harmonics is considered to be especially important because it is the main indication of a transverse crack. When a crack is relatively shallow, the increase in the 2Ω component is small and is likely to be buried in the background noise. Probably, due to this, the main concern in crack detection has been focused on monitoring the crack-induced sub-resonances - caused by higher-harmonic components - during the run-up or run-down periods. Furthermore, in rotating machines, some finite levels of these harmonics are always present, even in a normal condition.

To detect a crack using the crack-related harmonics, the other vibration components have to be eliminated from the overall vibration response. To isolate the crack-related harmonics from the overall vibration signature, an improved technique of vibration signature analysis called 'directional-difference vibration signature analysis (DDVSA)' is proposed here (Fig 4.4.2). This technique enhances the conventional crack detection technique by using directional-difference harmonics (DDH) and also by utilising pre-defined fault-related signatures obtained from an analytical model as a reference. This approach, in addition to reducing the effects of background noise, eliminates the harmonics which already exist in the normal rotor system. In general, harmonics present in the system from sources other than a crack, remain constant and do not change with time. On the other hand, in the case of a cracked rotor, the crack-induced harmonics will change as the crack propagates. For each model, the

relationship such as equation (3.3.1) can be established - based on the Directional Harmonics Sensitivity Map (refer to Fig 3.3.15) - and utilised in crack detection procedures to enhance their reliability. By using 'directional-difference' information from the operating machine, it is possible to use both $\pm 1\Omega$ and 2Ω harmonics together, as opposed to individually, as in the conventional approaches, which mainly rely on 2Ω harmonic component.

Figures from 4.4.3 to 4.4.5 demonstrate the concept of the proposed approach together with the flow diagram in Fig 4.4.2. By using the baseline vibration data (Fig 4.4.3), the cracked rotor vibration signature (Fig 4.4.5) can be isolated from the overall vibration response monitored (Fig 4.4.4). The crack can be detected by estimating the ratio (or growth rate) of each crack-related harmonic component. Based on the concept of DDVSA, an on-line monitoring system has been developed as presented in Fig 4.4.6, where the decision for crack detection can be controlled by pre-setting the standard deviation value of ratios of each crack-related harmonic component.

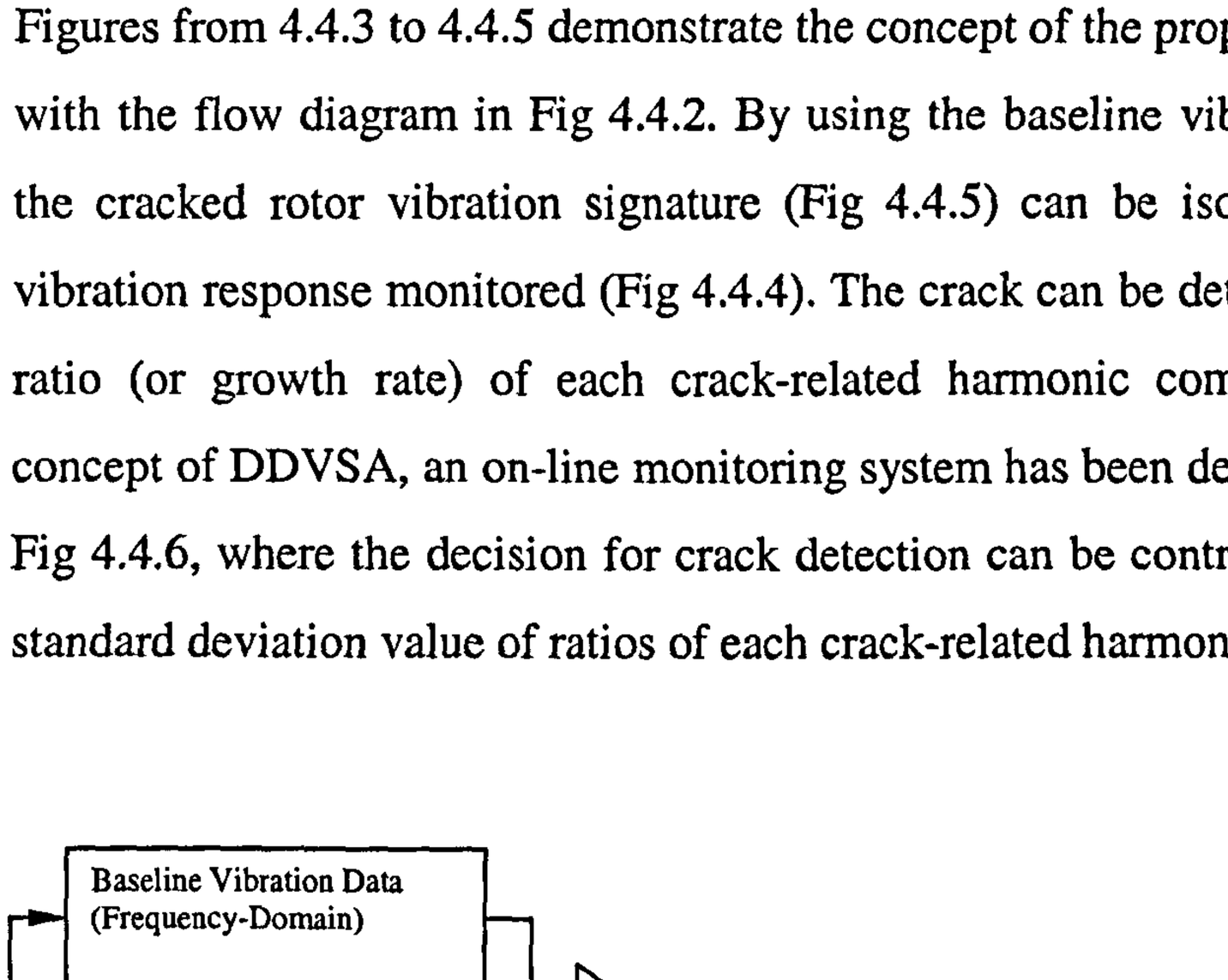


Fig 4.4.2 Directional-Difference Vibration Signature Analysis

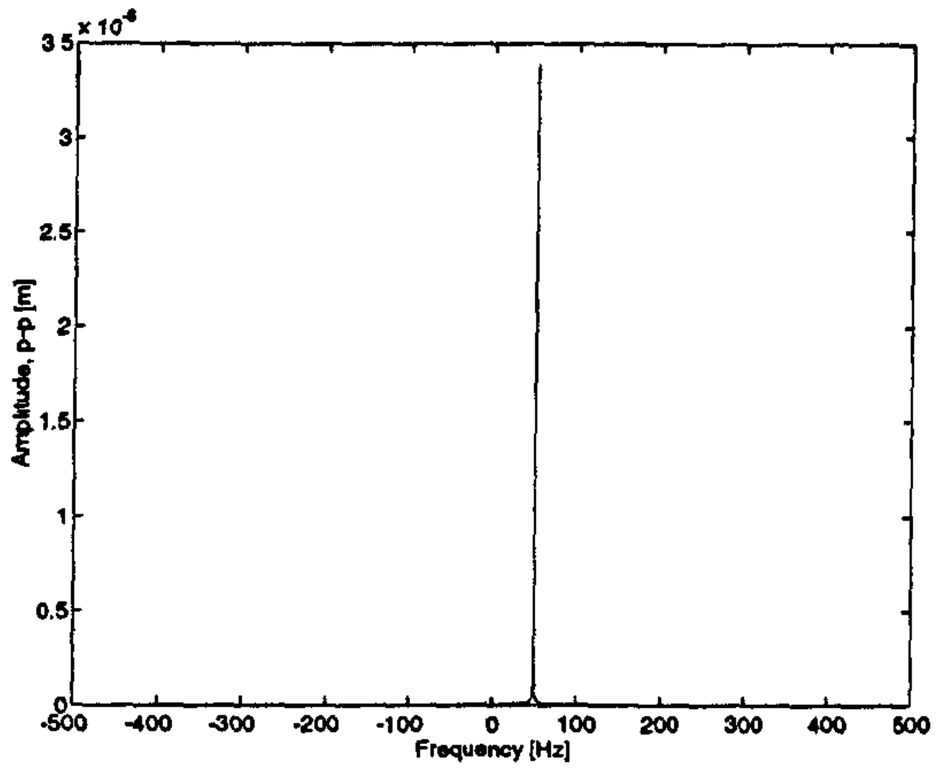


Fig 4.4.3 Unbalanced Rotor

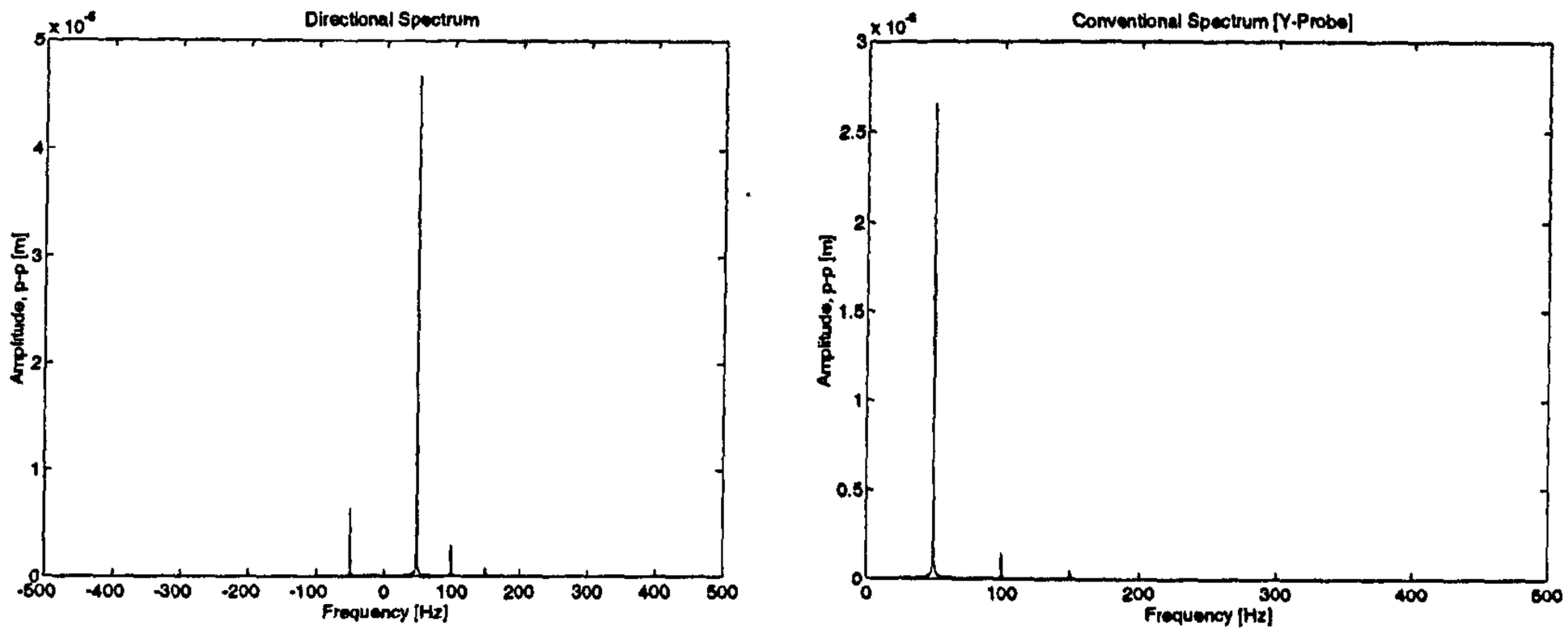


Fig 4.4.4 Unbalanced, Cracked Rotor: Directional vs Conventional FFT

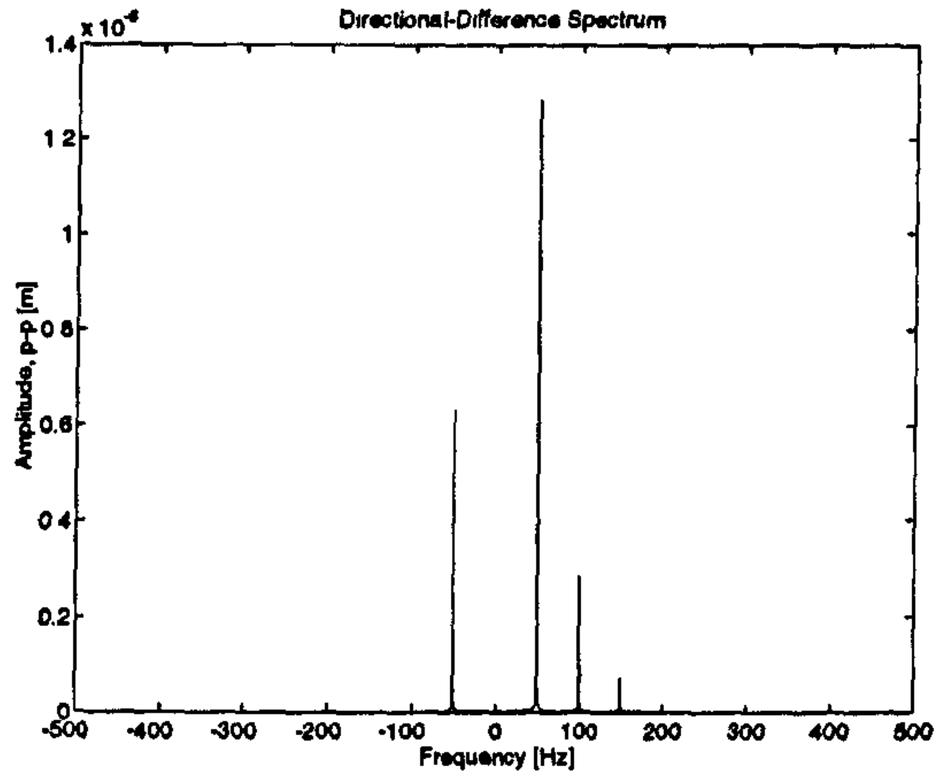


Fig 4.4.5 Unbalanced, Cracked Rotor: DDVSA (Unbalance Effect Removed)

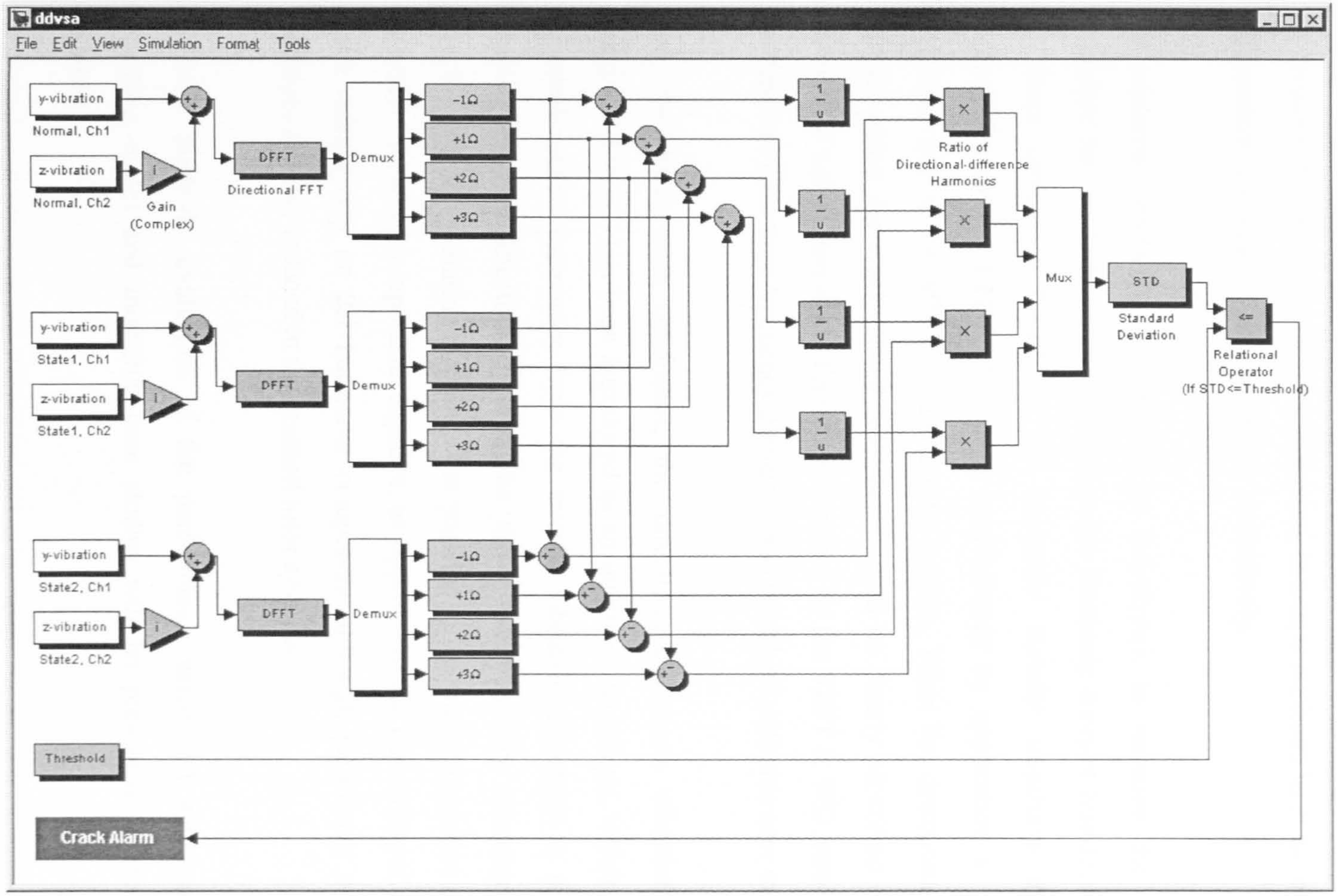


Fig 4.4.6 On-line Crack Detection System based on DDVSA

4.5 Conclusions

To improve the reliability of crack detection, two new methods have been introduced for transient and steady-state conditions, respectively.

For transient conditions (i.e. run-up or run-down), to improve the monitoring procedure for crack detection, the directional harmonic wavelet transform (DHWT) has been developed based on the harmonic wavelet transform theory. The performance of the DHWT has been demonstrated by application to the run-up vibration data of the MDOF cracked rotor system. From the directional harmonic wavelet maps, the crack-related resonances could be clearly identified even in the presence of noise. Hence, the limitation imposed by the STFT & WD, related with the resolution in joint time-frequency domain, could be solved with this new method.

Also, for steady-state conditions, the directional-difference vibration signature analysis (DDVSA) has been introduced as an improved technique, which can isolate the crack-related harmonics from the overall vibration signature to enhance the reliability of crack detection. By using the 'directional-difference' vibration signatures from the operating rotating machine, it is possible to use the synchronous and higher-harmonic vibration components together, as opposed to the conventional approaches which mainly rely on 2Ω harmonic component although significant synchronous vibrations are also induced in the cracked rotor systems.

For both methods, evaluation of the performance associated with experimental (laboratory-scale) and industrial case studies will be presented in the following chapters.

Chapter 5
Experimental Studies

5.1 Introduction

In this chapter, a series of experimental studies has been performed with laboratory-scale rotating structures to evaluate the performances of the developed crack detection techniques for transient and steady-state operating conditions, respectively.

A Bently Nevada Rotor Kit RK4 has been used with modifications made mainly to the shafts (with thin slots to simulate cracks). The same geometric configuration of the rotor analysed in Chapter 3 has been adopted to enable a comparison to be made of the analytical and the experimental results. Different crack depths and locations have been applied to investigate the effects of those variations in the damage styles. To reflect the field situations, measurements have taken at near both bearings under operating conditions for run-up periods (transient state) and for constant designated operating speeds (steady state), respectively. Also, to investigate the effect of unbalance on a cracked rotor system, controlled unbalance masses have been applied at two disk planes in various possible locations (or types) to see the consequences. Prior to the application of unbalance masses, balancing was performed using the influence coefficient method to avoid any possible excessive vibration by reducing the dominant synchronous (1Ω) vibration component.

5.2 Experimental Test Rig

The test rig is based on the RK4 rotor kit from Bently Nevada, which consists of:

- a mechanical base including motor, coupling, shaft with two disks, two journal bearings and bearing blocks, six proximity probes, probe mounts, and safety covers
- a proximitor assembly
- a direct-current motor speed control device

On the mechanical base, the shaft of the motor is connected via a flexible coupling to a main rotor shaft supported at both ends by journal bearings. The basic configuration of a RK4 rotor kit can be seen in Fig 5.2.1.

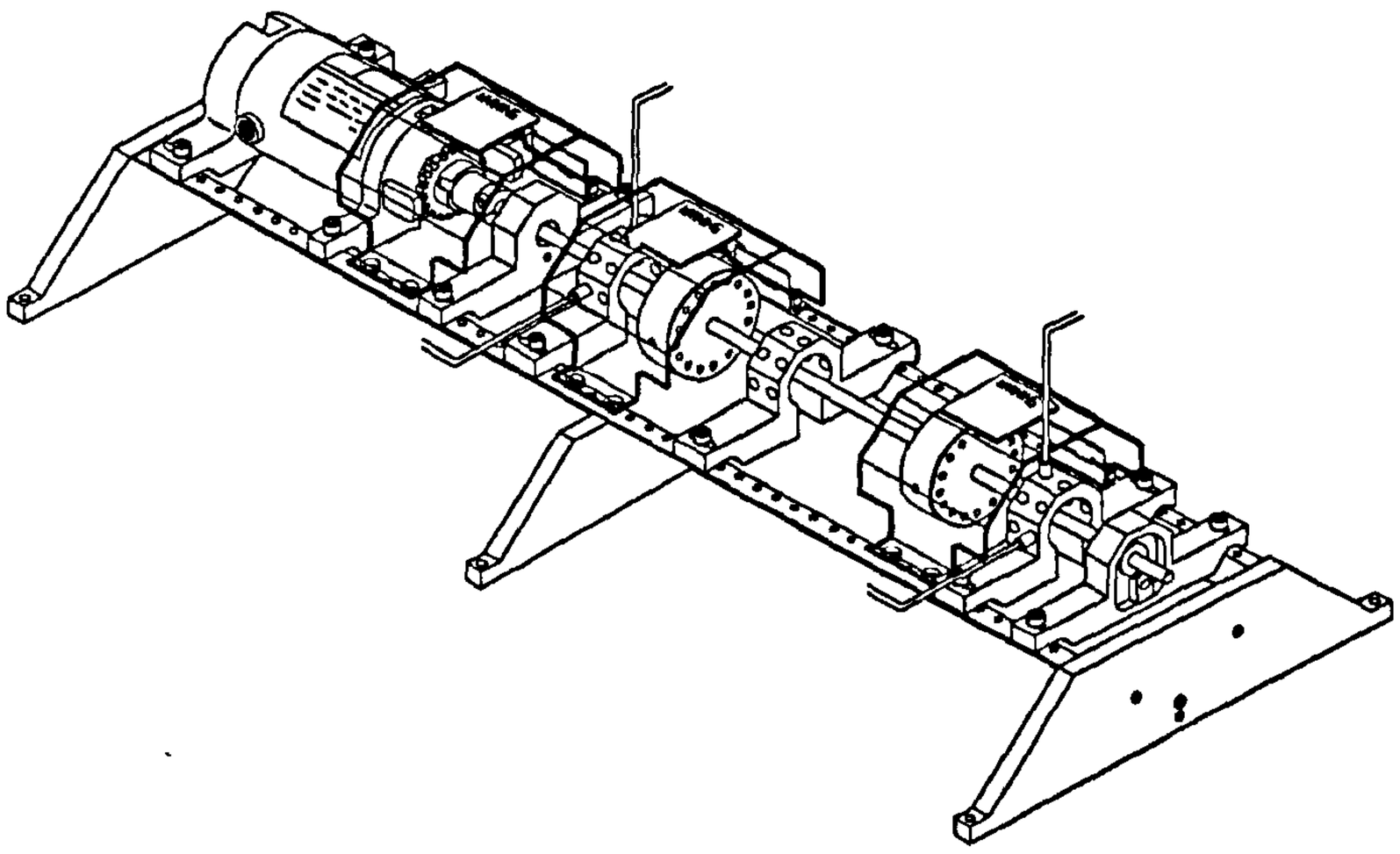


Fig 5.2.1 Rotor Kit RK4

5.2.1 Modified Rotor Assembly

The rotor assembly essentially adopted the same configurations of the rotor analysed in Chapter 3 (refer to Fig 3.3.2, page 75 and Fig 3.3.3, page 76) to compare the experimental results with analytical predictions for validating the new modelling techniques proposed in that chapter. Accordingly, the shaft has two disks and two bearings are supporting the shaft at both ends. Two identical disks having dimensions of a mass of 0.8 kg each have been used. This configuration, combined with bearing stiffnesses has a calculated first critical speed of 26.23 Hz, corresponding to the first bending mode of the rotor, and the second critical speed of 132.6 Hz, corresponding to the second bending mode of the rotor, and a designated operating speed 3000 rpm (50 Hz) of the rotor system is considered sufficiently well separated from the first and second critical speeds as is usually expected in most practical situations.

5.2.2 Slotted Shaft for Simulating Cracked Condition

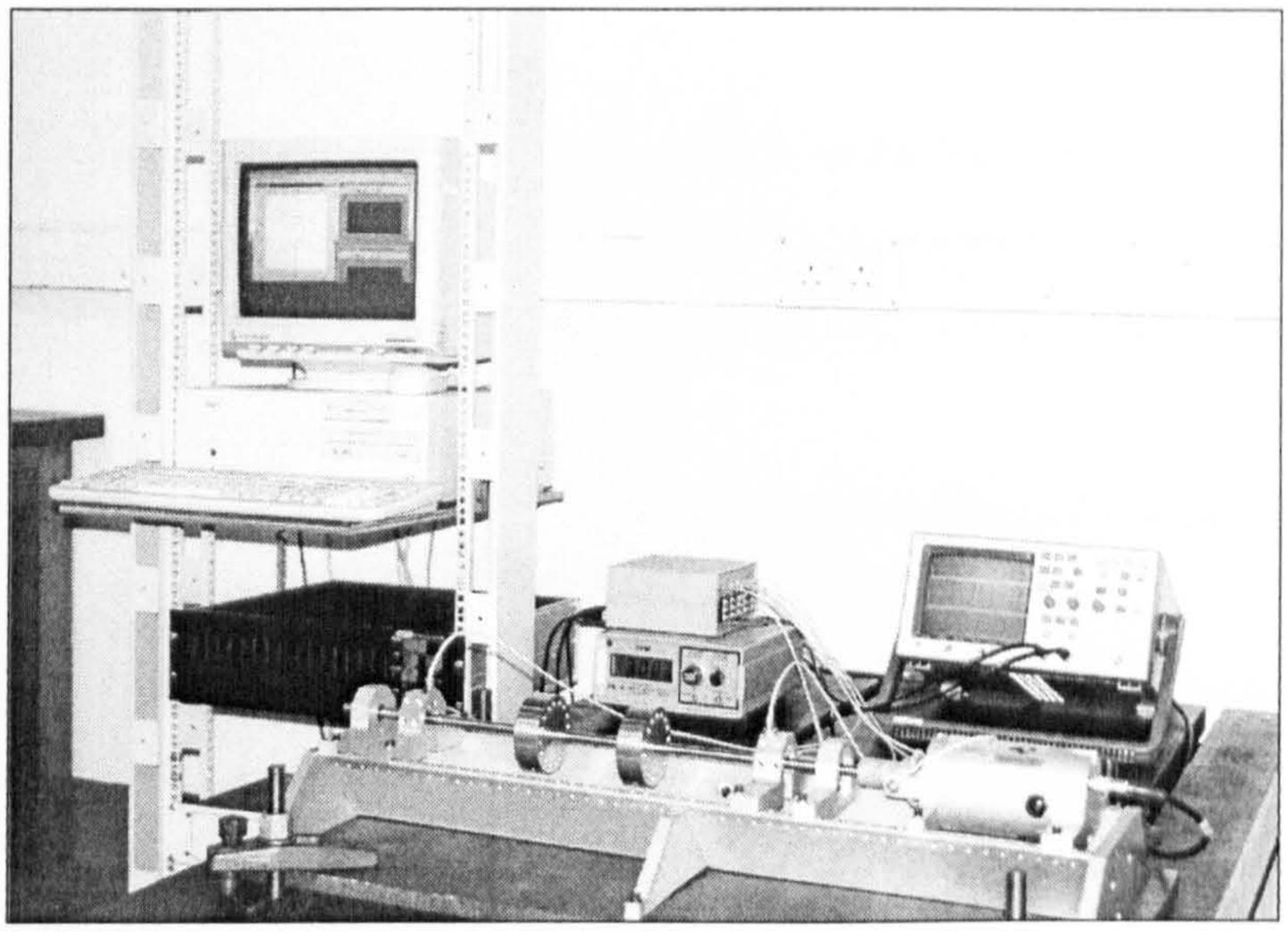
A spark erosion technique was used to make a thin slot (which will be referred to as a 'crack' from now on) with 0.254 mm (0.1 inch) gap to the shaft to simulate a crack. Strictly speaking, this can be classified as an open cracked rotor (or a rotor with local stiffness asymmetry) as the crack will not be completely closed due to its relatively large gap compared to a real fatigue crack. However, due to the self-weight of two rather massive disks on flexible shaft, the non-linearity due to breathing could be excited as the results suggest which will be presented in the following sections. Rather than a real fatigue crack growth test which could lead to an unwanted catastrophic accident, controlled crack depths to the same rotor have been induced to investigate the effect of increasing damage extent. Also, the crack depth has been limited to 20 % of the shaft diameter due to severe vibration in the preliminary tests while the rotor is passing through its 1st resonance speed.

5.3 Instrumentation

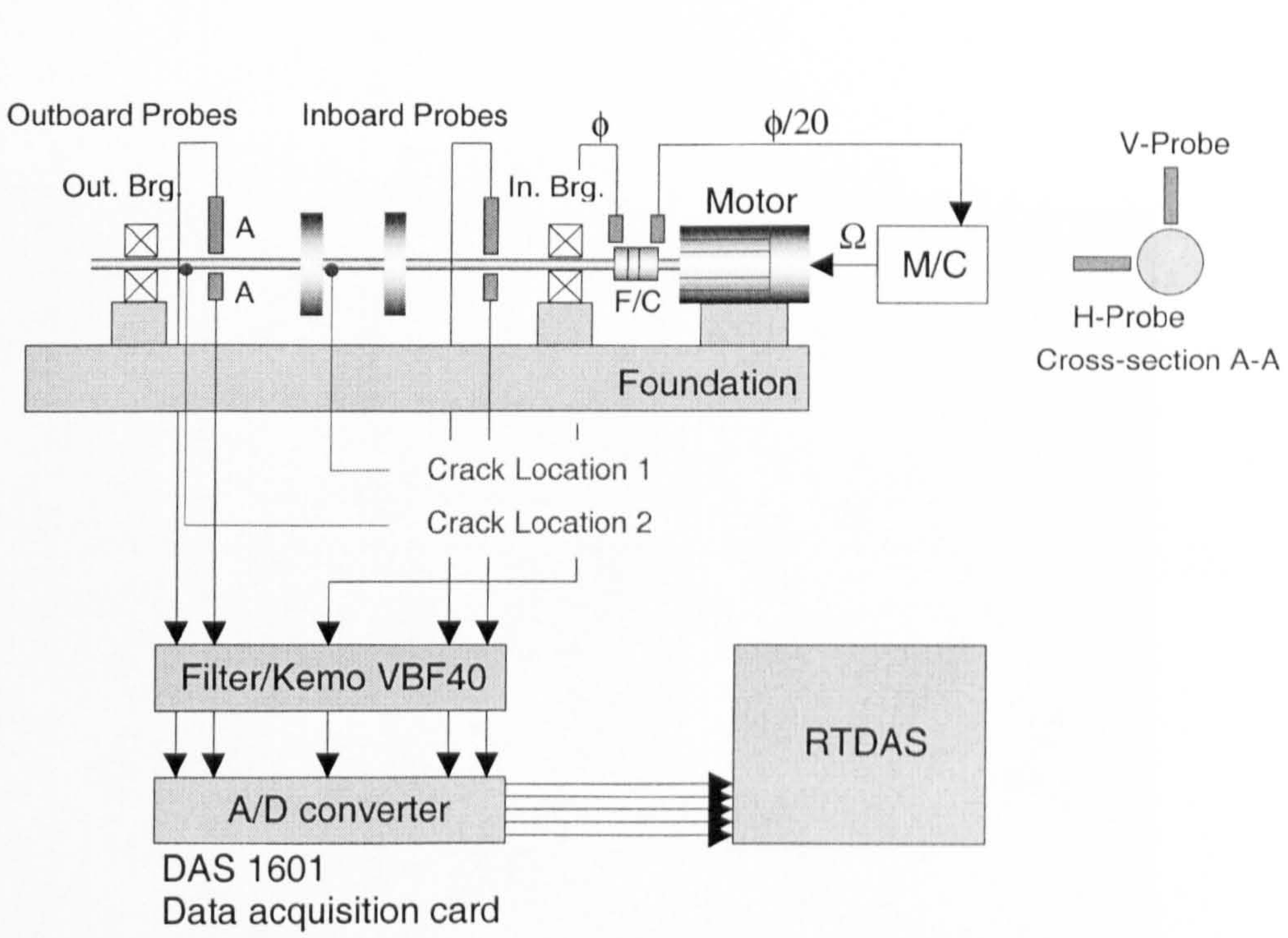
The complete instrumentation set-up for the test rig can be seen in Fig 5.3.1-(a) & (b). The experimental set-up for structures tested consisted of non-contact displacement transducers, signal amplifiers, and an analogue anti-aliasing filter.

A customised data acquisition system has been established for planned experimental work. The subroutines enabling the data acquisition have been written in the MATLAB environment. They can control the data-capture of up to 16 channels at up to 100 kS/s (single-channel sampling rate) simultaneously to the MATLAB work-space. This allows long time records to be stored to analyse rather long transient phenomena at high temporal resolution. The response channels can be low-pass filtered by a programmable, 8-pole, 16-channel analogue filter with variable cut-off frequencies. In addition to the vibration response (or amplitude), an absolute shaft angular position is available as an analogue signal output from a 20-notch wheel mounted on a rotor, from which an instantaneous speed of rotation can also be derived.

By using a PC with a customised software instead of a dedicated commercially available analyser, the tools developed in the analytical work can be seamlessly applied to the experimental data. While the forward and backward whirl components cannot be analysed by using conventional commercial analysers (except ADRE/Bently Nevada, [130]) as they occur in rotating machinery, customised software solutions can accommodate all these effects and will simplify further development of analysis routines.



(a) Picture



(b) Schematic Diagram

Fig 5.3.1 Experimental Set-up

5.3.1 Non-contact Displacement Transducers

The vibration signals have been collected from the calibrated, non-contact displacement transducers (activated by induced eddy-current) as shown in Fig 5.3.2 where the probes are in mounted form. The arrangement of the probes are as follows:

(i) two orthogonal pairs of displacement probes to measure shaft vibration, each pair being positioned close to each bearing, and
(ii) two displacement probes to monitor the shaft running speed (resolution of $\Omega/20$) and to provide a phase reference signal (1Ω), respectively.

These transducers have all been linked, through an appropriate amplifier and anti-aliasing filter, to the A/D converter (Keithley DAS1601 A/D card).

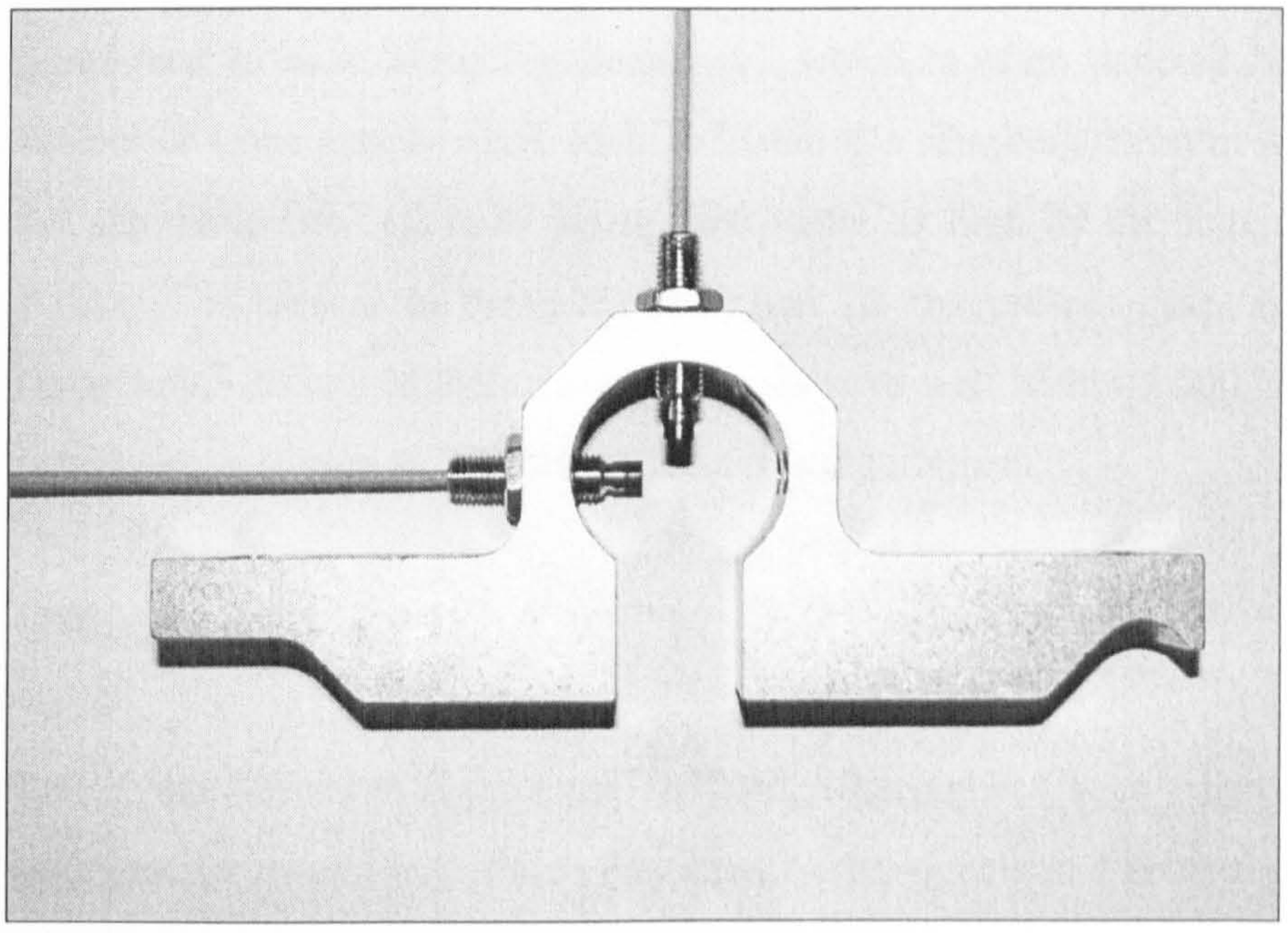


Fig 5.3.2 Non-contact Displacement Probes

• Sampling

Experimental data can be sampled with the specified number of points per channel from the DAS1601 data acquisition card into the MATLAB memory using the *Direct Memory Access* (DMA) technique.

The measured signal should not be higher than the range-limit for the A/D card. A 100 % higher signal might not cause any damage but will cause saturation or clipping. A lower limit does exist in terms of the existing precision, e.g. the acquisition system is currently using a 12-bit A/D converter with ±10 V input, which translates into a resolution of 20/4096 = 0.00488 V. Therefore the minimal input measured should be several times larger than this value, which can be easily accomplished by amplifiers.

The data acquisition card uses a multiplexer device to sample a number of channels simultaneously. And, as a result of the inevitable approximation introduced by sampling, some care must be exercised in the choice of sampling rate. This parameter is referred to as a 'sampling frequency', which is often denoted by f_s and is the subject of some simple rules, such as Shannon's sampling theorem which states that the sampling rate, f_s, must be at least twice as high as the maximum frequency expected or present in the analysed signal. In the present case, as the frequency components present in the measured signals were well within ±500 Hz, the sampling rate has been chosen to 1000 Hz to meet this requirement.

• Filtering

Before the measured signals are sampled, filtering has been carried out using an analogue low-pass filter, which can amplify the signals and protect against aliasing. Aliasing is a very common phenomenon which affects the quality and reliability of a spectral analysis performed via the DFT. Aliasing occurs when the sampling rate used

to discretise the original signal is too low. The cure for this problem is to ensure that before an analogue signal is digitised, which is the point at which the aliasing problem is incurred, it is filtered to ascertain that it has no components at frequencies which are above half the sampling frequency. This state can be achieved by using anti-aliasing low-pass filters which cut out most, if not all, the high frequency components, if left in the signal, would be erroneously 'read' by the spectral analysis as equivalent to lower frequency components. Therefore, the use of anti-aliasing filters is very important in every case where the spectral content of the signals to be analysed is not known, and where unwanted high frequency components are likely to occur. In the experiment, as the signals have been sampled with sampling frequency of 1000 Hz, the cut-off frequency has been applied at 400 Hz as it is reasonable to set the cut-off frequency at most 500 Hz to avoid aliasing.

All filters have a gradual transition from pass to reject regions, and tend to have a marked effect on the phase information which is most pronounced in those components which are closest to the transition region. It thus becomes important, when processing two or more signals simultaneously, to use matched filters so that these effects are the same in each channel, and their effects can be minimised when the signals are ratioed. In the present experimental work, linear phase filter has been applied to enable the accurate estimation of phase information. As there is no phase distortion with this type of filter, the original shape of the signals is preserved in the pass band, which enables accurate synchronous time averaging of measured signals and reliable balancing (if it is required) of the rotor system.

- **Averaging**

In order to obtain statistically accurate data which can be used for condition monitoring, averaging should be performed. There are two basic types of averaging; frequency domain averaging and synchronous time averaging. Frequency domain

averaging is the method most commonly used in machinery analysis, and as averaging is performed in frequency domain, it does not require a phase reference input. However, in the case of rotating machinery analysis, even minor speed variations during the frequency domain averaging process can cause smearing and a corresponding loss of amplitude accuracy. To avoid this problem, *synchronous time averaging* has been accomplished by averaging a series (5 samples in this experiment) of phase-referenced time domain signals. As the synchronous time averaging requires a reference trigger (that is synchronous with the shaft being analysed), a signal obtained from the 1Ω displacement probe has been used (refer to Fig 5.3.4). As the synchronous components will be enhanced by performing synchronous time averaging, very low-level synchronous components can also be extracted from a signal containing unwanted noise.

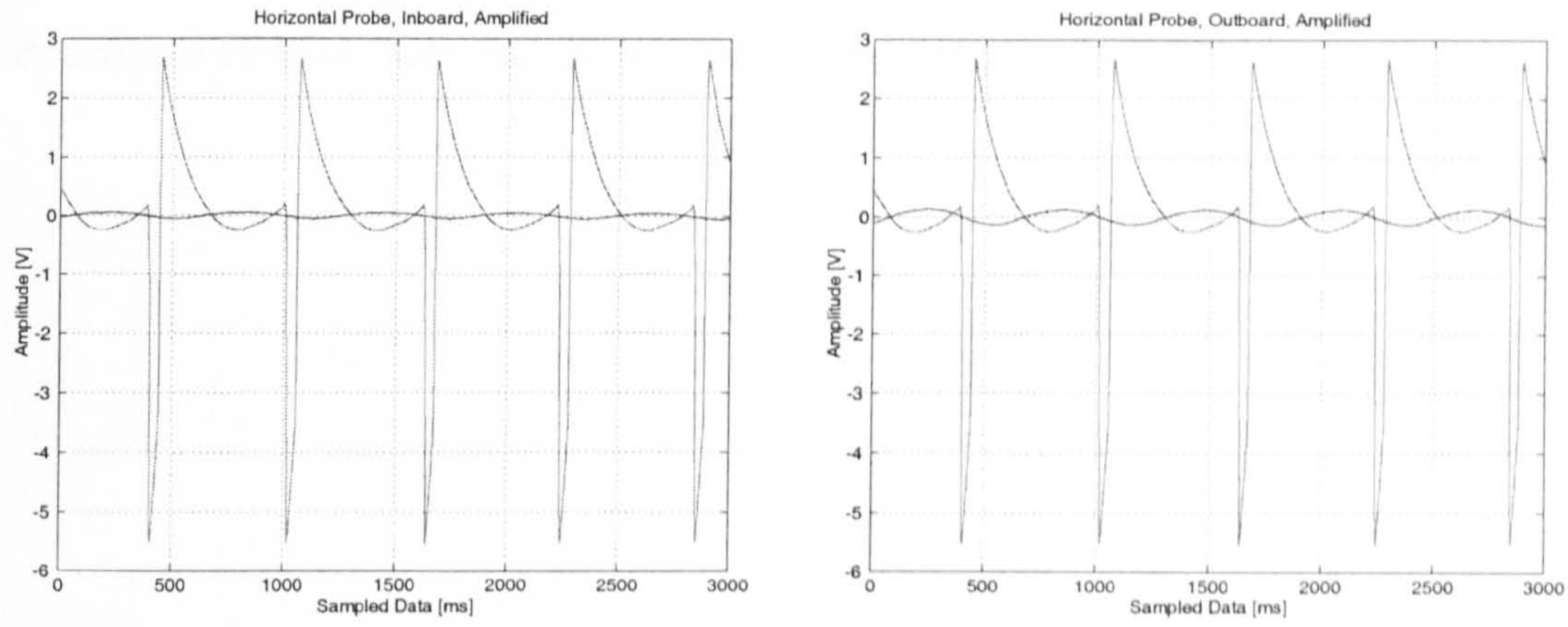


Fig 5.3.4 Main Signal associated with Phase Reference Signal

5.3.2 Data Acquisition and Signal Processing Equipment

For data acquisition, a special code 'RTDAS (Real Time Data Acquisition System)' has been developed as presented in Fig 5.3.5 & 5.3.6 in block diagram form. The RTDAS enables the real-time monitoring of the signals being captured together with data storage for further processing. Also, digital filtering can be applied on- or off-line if required.

For transient data, i.e. for run-up data, the input signals from the rotor system can be monitored on-line from the directional short-time Fourier transform as shown in Fig 5.3.5. Also, all the data from each channel can be stored to the MATLAB memory for post-processing of the vibration data. As has been introduced in Chapter 4, the STFT has been performed on the complex-valued signals to obtain decomposed spectrogram into forward and backward directions.

Steady-state measurement is relatively simple compared with the transient-state measurement as can be seen in Fig 5.3.6 and takes much less memory as the steady-state vibration data does not require a long time record. As in transient state, the directional FFT has been used for on-line monitoring purpose.

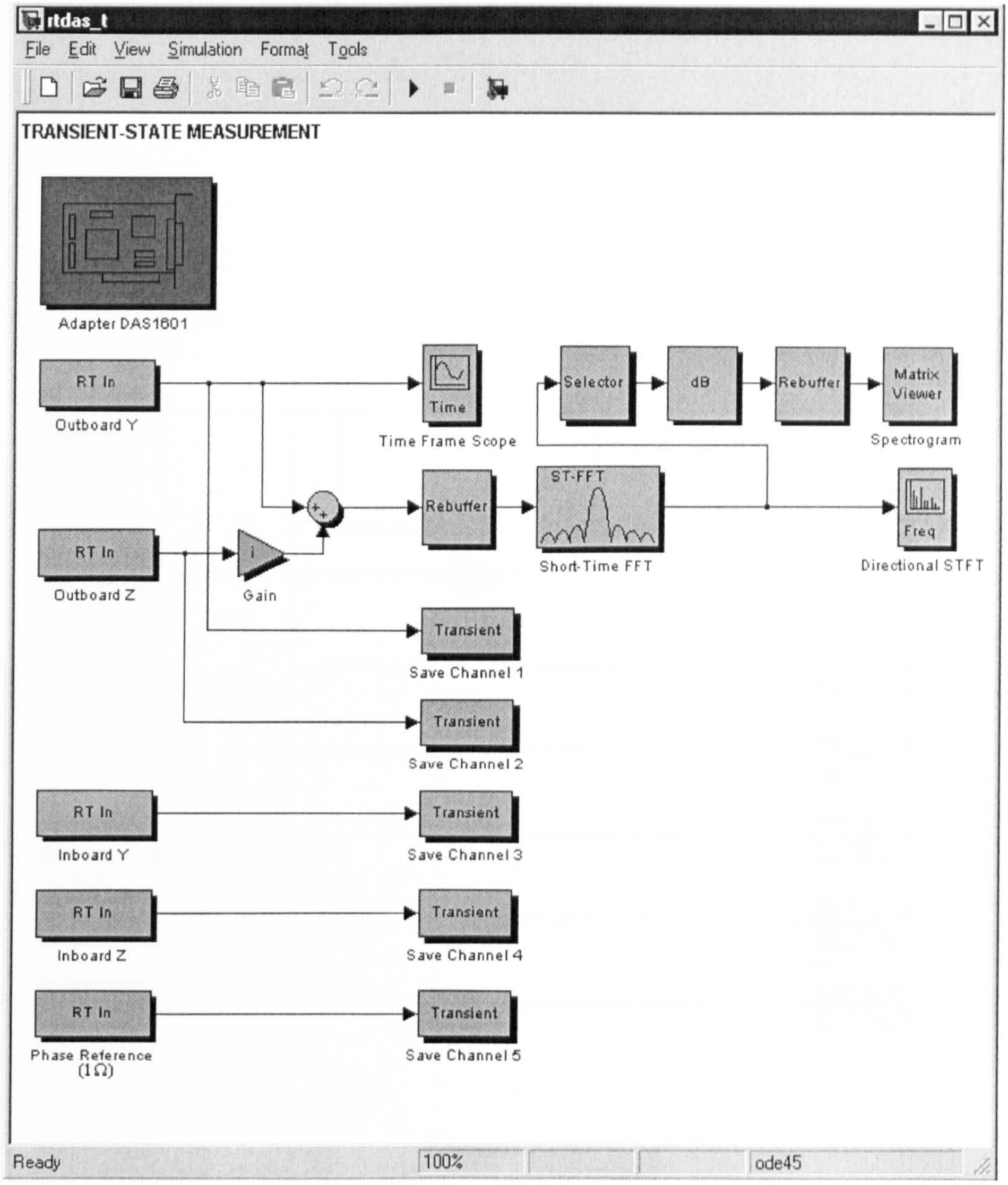


Fig 5.3.5 RTDAS - Transient

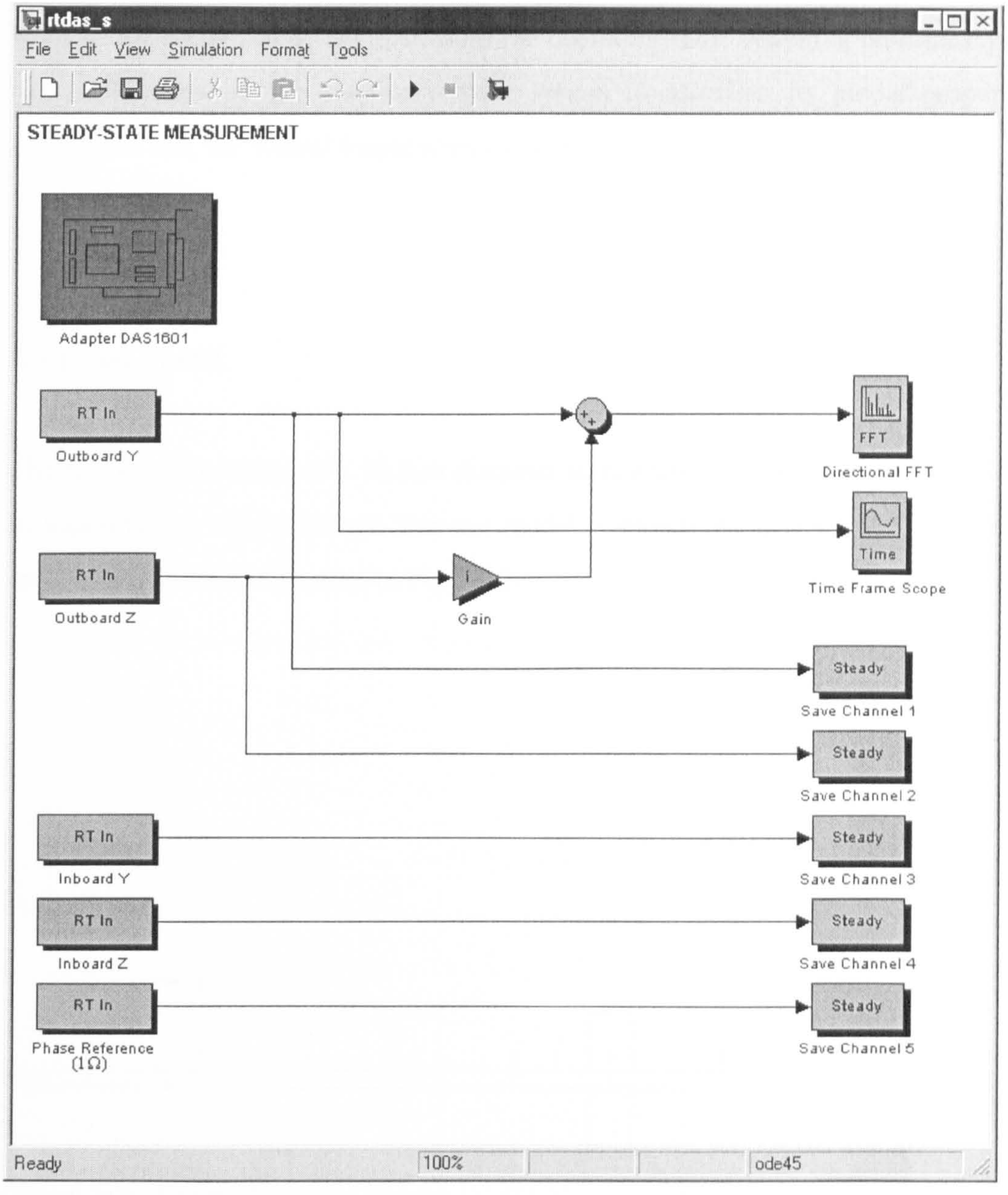


Fig 5.3.6 RTDAS - Steady

5.4 Modal Testing of the Rotor Rig

Prior to the collection of any data from the operating rotor system, a preliminary test was undertaken on the stationary rotor system to ascertain its modal properties. During the test, the natural frequencies and damping levels have been measured.

5.4.1 Test Model

The test model consists of a 10 mm diameter steel shaft and 2 steel disks attached on it, supported by rigid bearings. The test model is shown in Fig 5.4.1 and the bearing and bearing block can be seen in Fig 5.4.2.

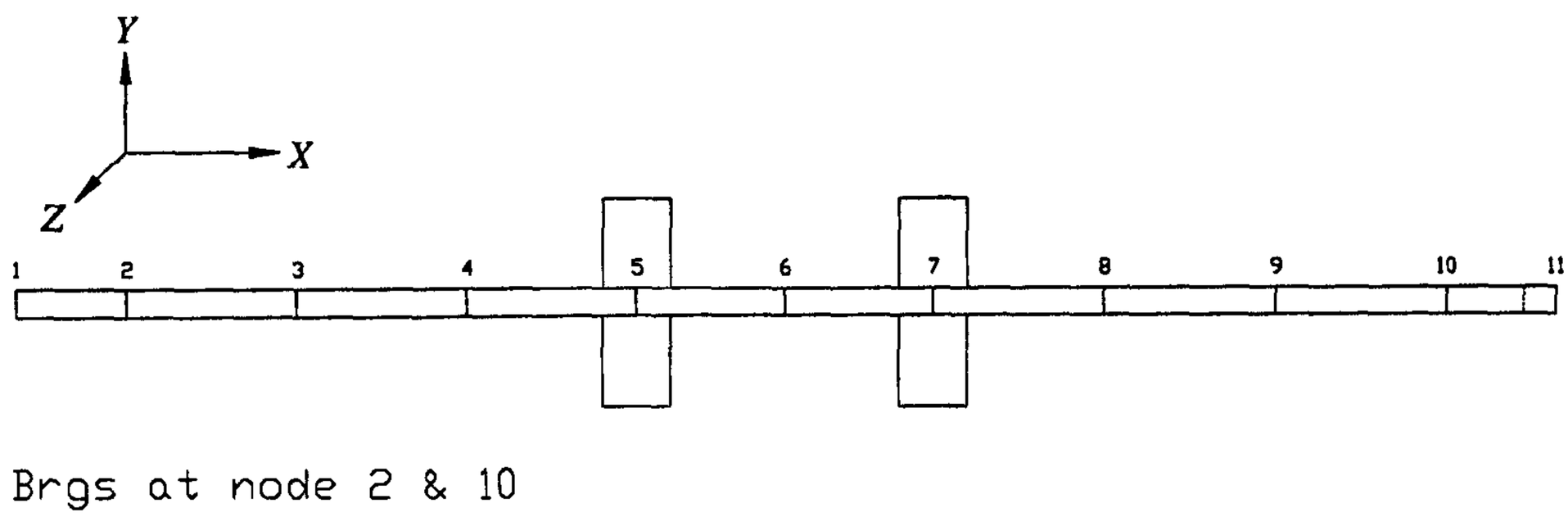


Fig 5.4.1 Test Model: Normal Rotor System

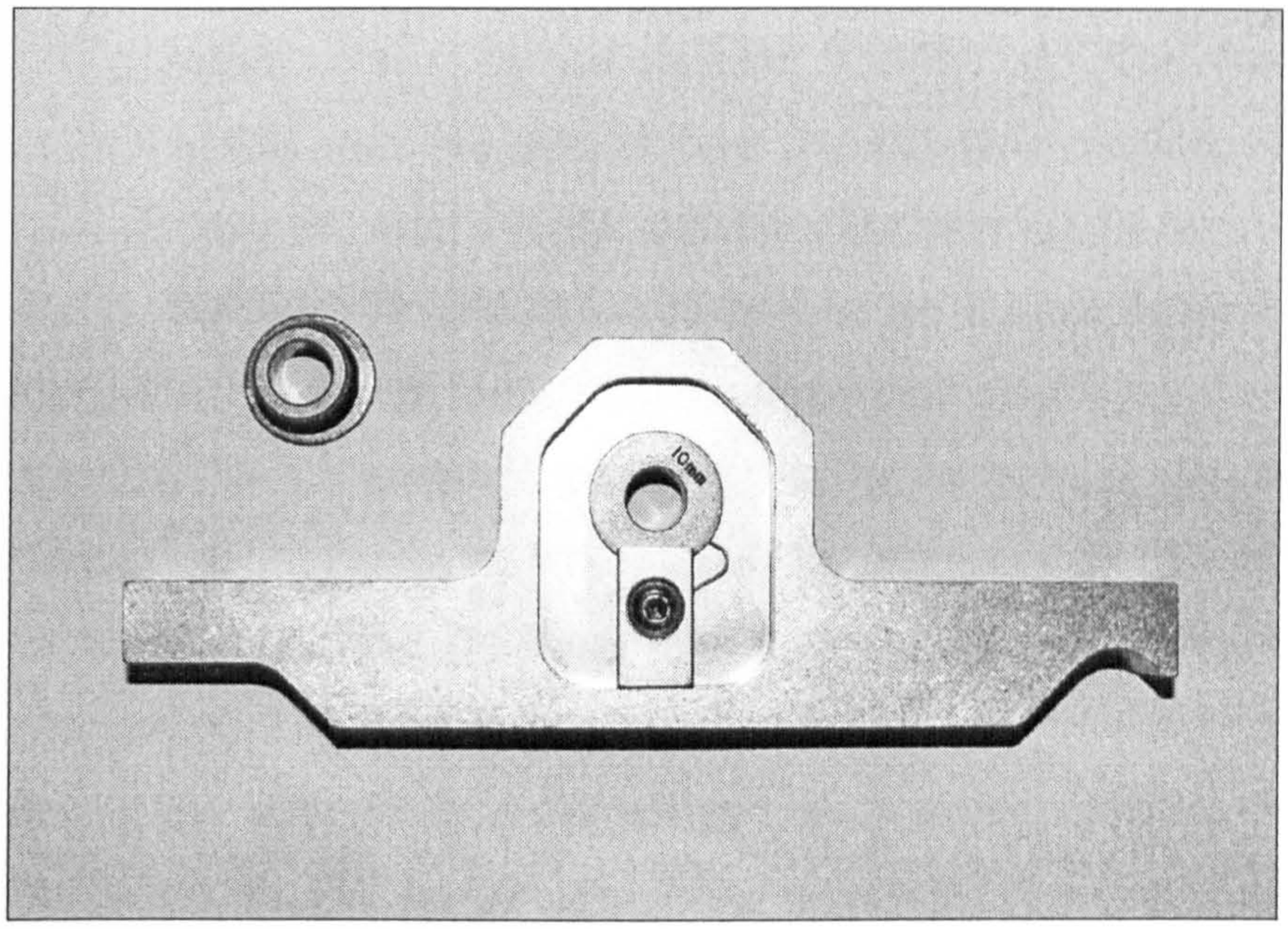


Figure 5.4.2 Bearing & Bearing Block

As can be seen in the Fig 5.4.2, the bearing consists of a relatively rigid oilite bronze bushing and a stiff rubber bush. The bearing is assembled to the bearing block, and the rubber bush acts as a damper between the bearing and the bearing block during operation. The possible axial movement or rotation of the bearing have been constrained, as shown in the picture.

5.4.2 Test Instrumentation and Set-up

The instruments used in the test are listed in Table 5.4.1. The rotor was tested in its static condition with two rigid bearings and a flexible coupling which connects the rotor with the DC motor. In this condition, the rotor can be regarded as constrained and the bearings will have some influence on the flexural modes of the structure. A calibrated, force-gauge fitted, impact hammer with a nylon tip was used to excite the structure. The force applied to the structure by the hammer was measured using the force gauge fitted and then sent to one of the inputs of the FFT analyser (B&K 2032) via a power amplifier (PCB conditioning amplifier). The vibration response of the structure was measured by the accelerometer (3 g) attached at node 4 by wax, and was sent to the other input of the analyser via a power amplifier (PCB conditioning amplifier). The FFT analyser was linked up to a PC to acquire data through the data acquisition code ICATS-MODACQ.

Table 5.4.1 List of Test Instrument

Type	Equipment
Analyser	B&K 2032 FFT Analyser
Excitation	Impact Hammer with a Force Gauge fitted (nylon tip)
Response	Accelerometer (3 g)
Amplifier	2 PCB Conditioning Amplifiers

5.4.3 Test Procedure

As the structure was rather small (shaft axial length: 0.56 m), impact excitation was chosen for modal testing. Impact testing guarantees that the structure does not need to be changed since the accelerometer stays in one position on the structure and the excitation is achieved by use of an impact hammer. Prior to the test, the whole

measurement system was calibrated using a standard 0.2 kg mass. The excitation signal was an impulsive signal produced by a PCB hammer. The test condition and corresponding parameters are summarised in Table 5.4.2. Although, exponential window is a common choice for transient signals, no window (so called rectangular window) has been applied as the response signals had died away quickly due to inherent damping of the rotor system. In this way, it was possible to estimate the damping level more accurately than applying the exponential window which introduces 'additional artificial damping' to the system.

Table 5.4.2 Test Condition and Parameters

Excitation Method	Impact Hammer
Excitation Signal	Impulsive
Excitation Points	Node 1 ~ 11
Window	Rectangular
Frequency Range	0 ~ 600 Hz
Average Number	5

5.4.4 Modal Analysis

All measured FRFs were analysed using modal analysis code ICATS-MODENT. The multi-FRF, MDOF modal parameter extraction technique (based on curve-fitting) has been applied as there are two main advantages in using the technique:

(i) the time for modal analysis is much shorter than single-FRF based identification techniques, and

(ii) the modal parameters obtained are consistent.

From the modal analysis, there were 4 modes identified in the frequency range of 0 ~ 600 Hz, as shown in Table 5.4.3. One of the measured frequency response function (point FRF) is presented in Fig 5.4.3. The analysis has been performed for horizontal

and vertical planes respectively, however the modal properties from both planes were virtually the same as might be expected from the reasonably isotropic support stiffnesses.

Table 5.4.3 Natural Frequencies of the Rotor System

Mode No.	Natural Frequency (Hz)	Damping Factor (%)
1	26.15	2.50 ~ 2.62
2	130.06	1.70 ~ 1.72
3	357.60	2.17 ~ 2.23
4	465.56	1.27 ~ 1.32

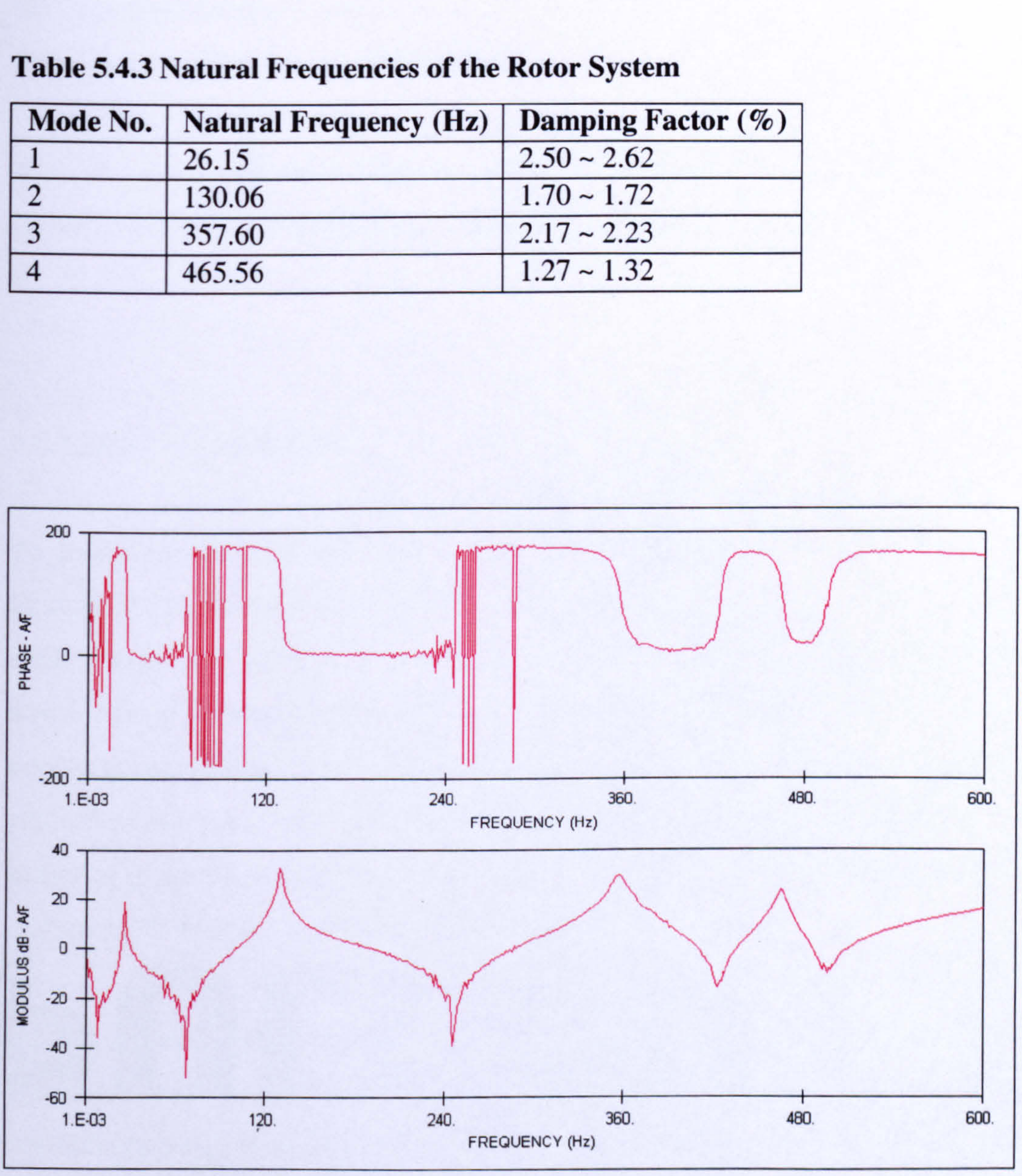


Fig 5.4.3 Frequency Response Function of the Normal Rotor System

5.5 Experimental Procedures and Results

With the cracked rotor rig, the following items have been explored:

(i) effect of crack extent

(ii) effect of crack location

(iii) relationship between crack and unbalance

Also, the developed crack detection techniques have been applied to evaluate the performance when the techniques are used with measured vibration data.

5.5.1 Effect of Crack Extent

To investigate an effect of crack extent, 10 % and 20 % crack depths have been introduced to a normal shaft gradually. Also, two different crack locations have been applied as shown in Fig 5.5.1-(a) & (b) to investigate the effect of crack location, which will be discussed in the following section (Section 5.5.2). The maximum crack depth has been limited to 20 % as the vibration increased to a large amount especially when the rotor passed through its 1st resonance speed. Also, it is considered that the detection of cracks in operating rotor systems must be done no later than a crack depth of at most 20 % to avoid catastrophic failure.

Fig 5.5.2 presents experimentally-obtained time histories of the normal rotor system, and does not reveal any symptom related with crack. Only an unbalance response in the resonance region could be identified due to the inevitable eccentricity of the shaft. Also, mainly due to gravity, it can be seen that the vertical response is a bit larger than

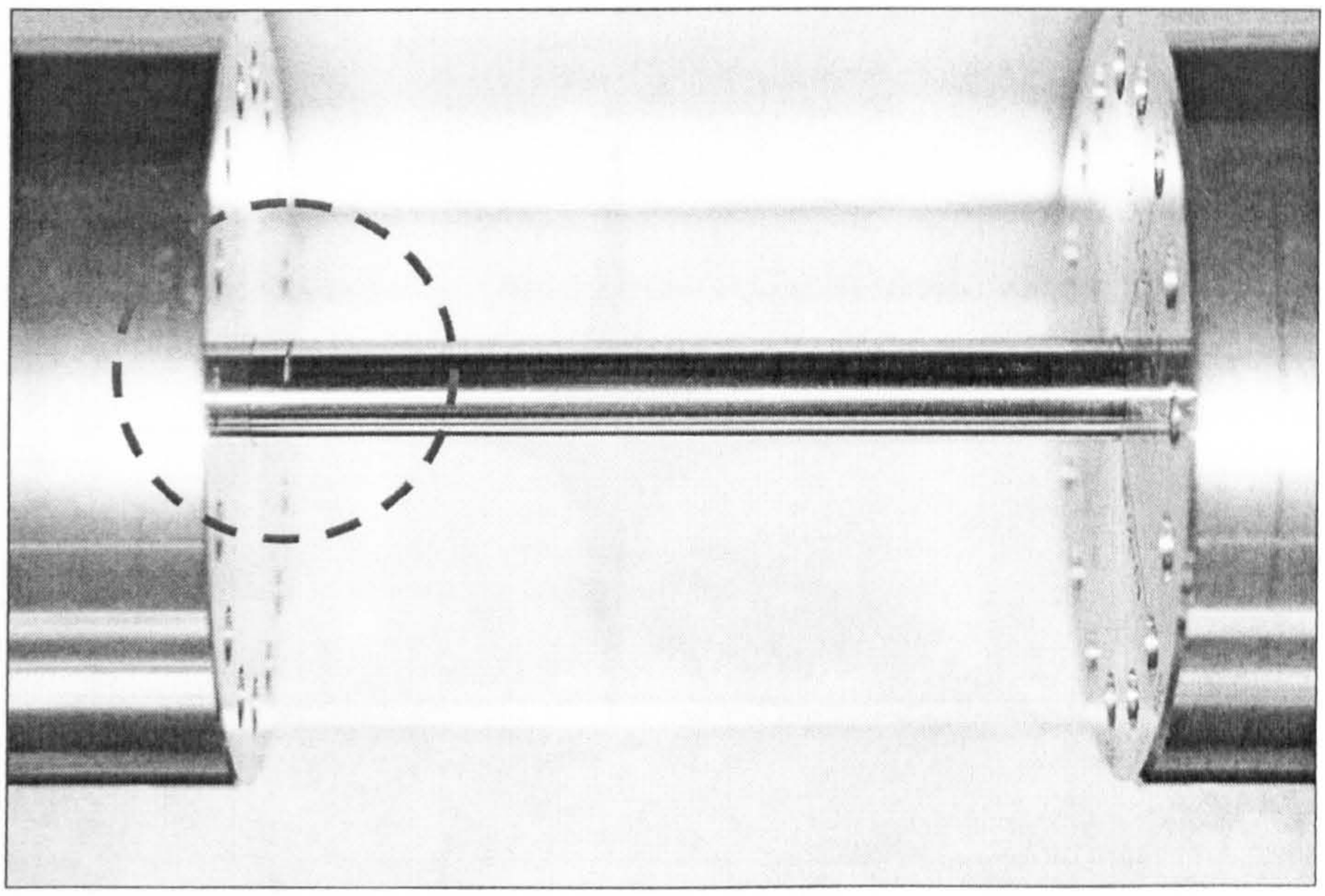
the horizontal response, especially in the resonance region. However, in Fig 5.5.3, i.e. for the 10 % cracked rotor case, it is possible to see the existence of a 2Ω related resonance at $t \approx 7.3$ s ($\Omega/\omega_n = 0.5$) due to a crack. The orbit of the cracked rotor system at the rotation speed of $\Omega/\omega_n = 0.5$ shows dramatically the existence of 2Ω harmonic component in the vibration response.

To investigate the frequency components which exist in the normal and cracked rotor systems, the directional STFT and the directional FFT have been applied to the measured transient and steady-state vibration data, respectively.

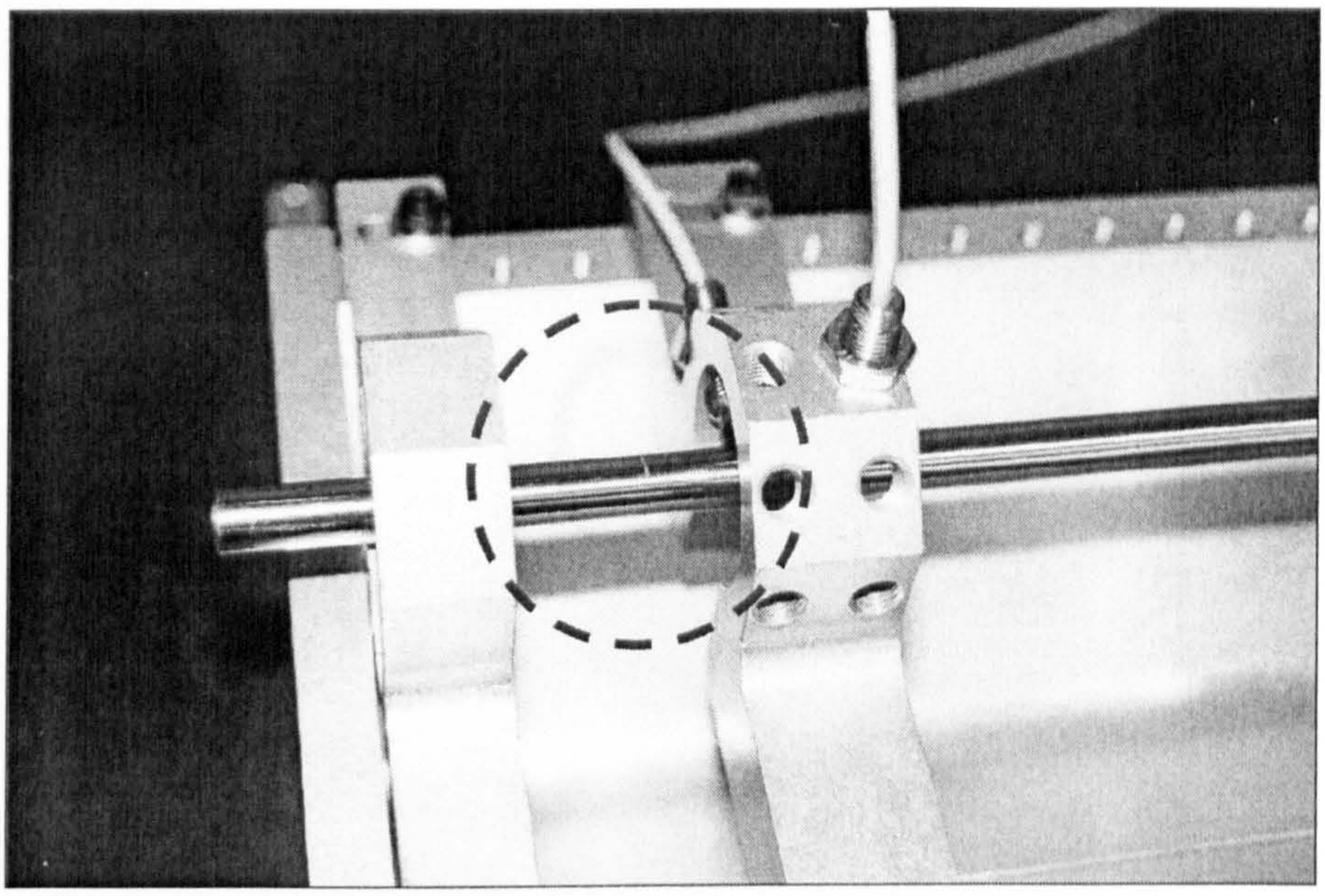
For the normal rotor system, as can be seen in Fig 5.5.4-(a), the directional spectrogram for the run-up period shows the unbalance response due to shaft eccentricity. Also in Fig 5.5.4-(b), the directional FFT frequency spectrum for the designated operating speed (3000 rpm) shows a dominant 1Ω frequency component at 50 Hz which is synchronous with the rotation speed of the rotor. Together with the dominant 1Ω frequency component, higher-harmonic components ($\pm 2\Omega$, $\pm 3\Omega$, $\cdots$) already exist (although they are negligibly small in magnitude) in the spectrum due to structural non-linearity. Also, due to the effect of gravity, there exist small backward vibration components. For reliable fault diagnosis of the rotor system, all this information on each harmonic component must be fully recorded to use them as baseline data for the healthy rotor system.

In Fig 5.5.5-(a), with the introduction of a crack, a 2Ω harmonic component starts to appear and induces a sub-resonance (marked by dotted circle) when the rotor is running up to its designated speed. At constant operating speed, the directional frequency spectrum shows the existence of $\pm 1\Omega$, $\pm 2\Omega$, $\pm 3\Omega, \cdots$ harmonic components as in Fig 5.5.5-(b). If the healthy rotor's baseline vibration data are not available, it will be difficult to identify the existence of a crack due to ambiguity with other common faults such as misalignment or machinery looseness.

When the crack has been increased to 20 %, as Fig 5.5.6-(a) shows, there are strong sub- and fundamental resonances due to the increase of crack extent. From the rotor's steady-state response in Fig 5.5.6-(b), it is possible to identify an increase of the $\pm 1\Omega$ components together with higher harmonics due to increased crack depth, as has been predicted with new crack modelling concept (in Chapter 3). This fact suggests that the $\pm 1\Omega$ vibration components should also be carefully inspected to increase the possibility of crack detection which is unlikely with conventional crack detection methods which usually rely on only 2Ω harmonic component. In particular, at this damage level, due to increased structural non-linearity, relatively (compared to 10 % crack) significant -2Ω and -3Ω harmonic component also begin to grow in the directional spectrum.

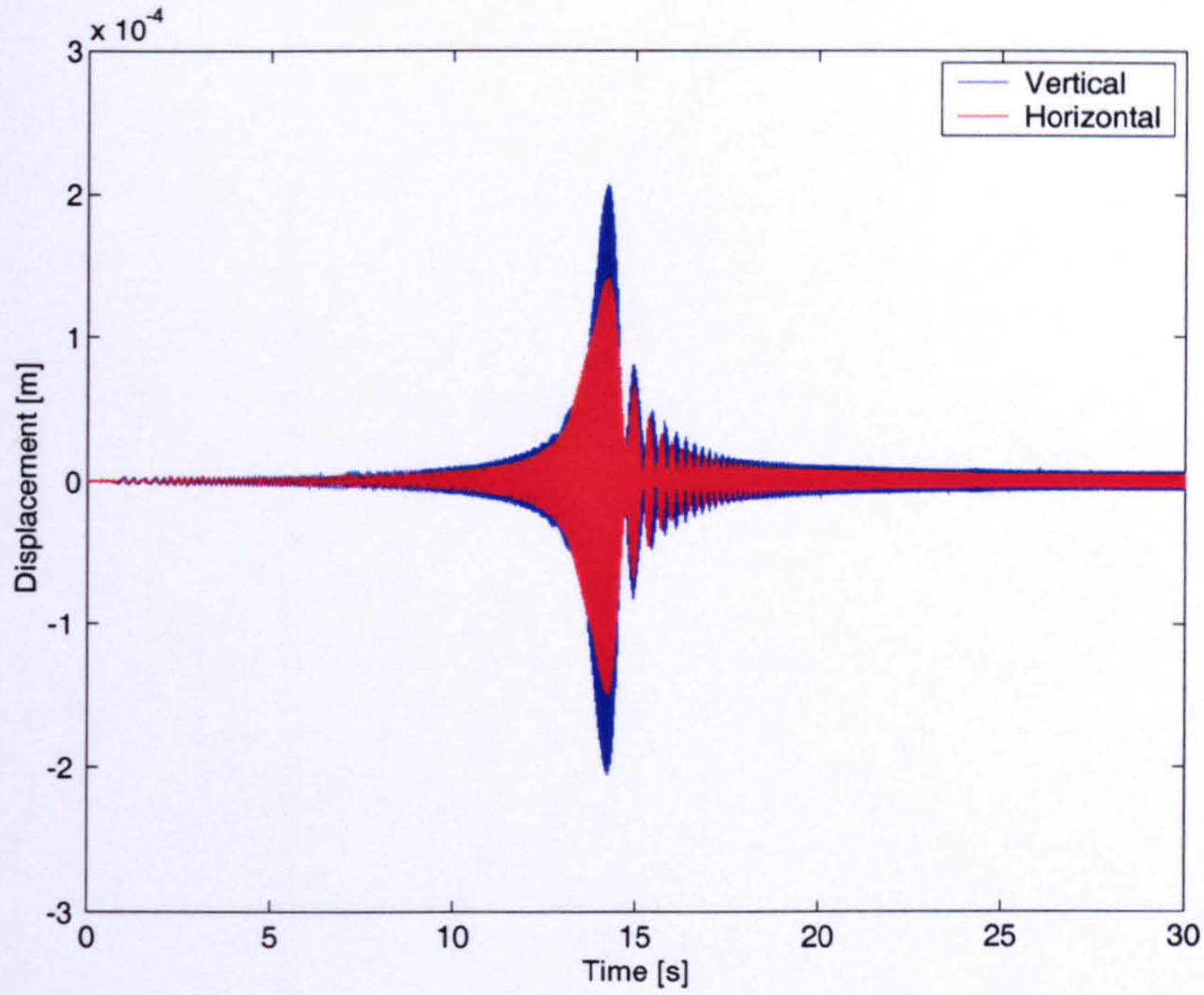


(a) Mid-span Crack

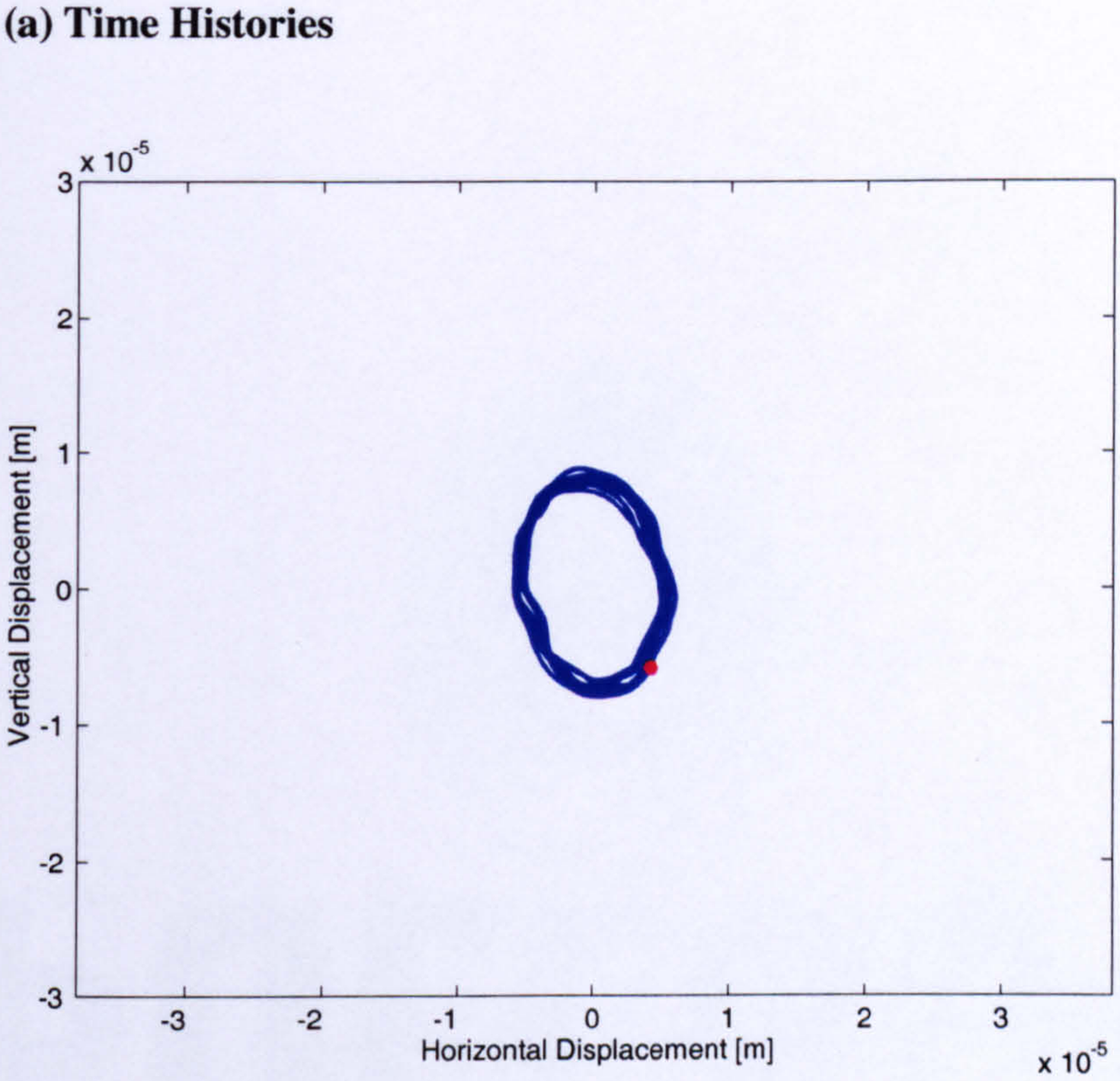


(b) Outboard Crack

Fig 5.5.1 Crack Locations

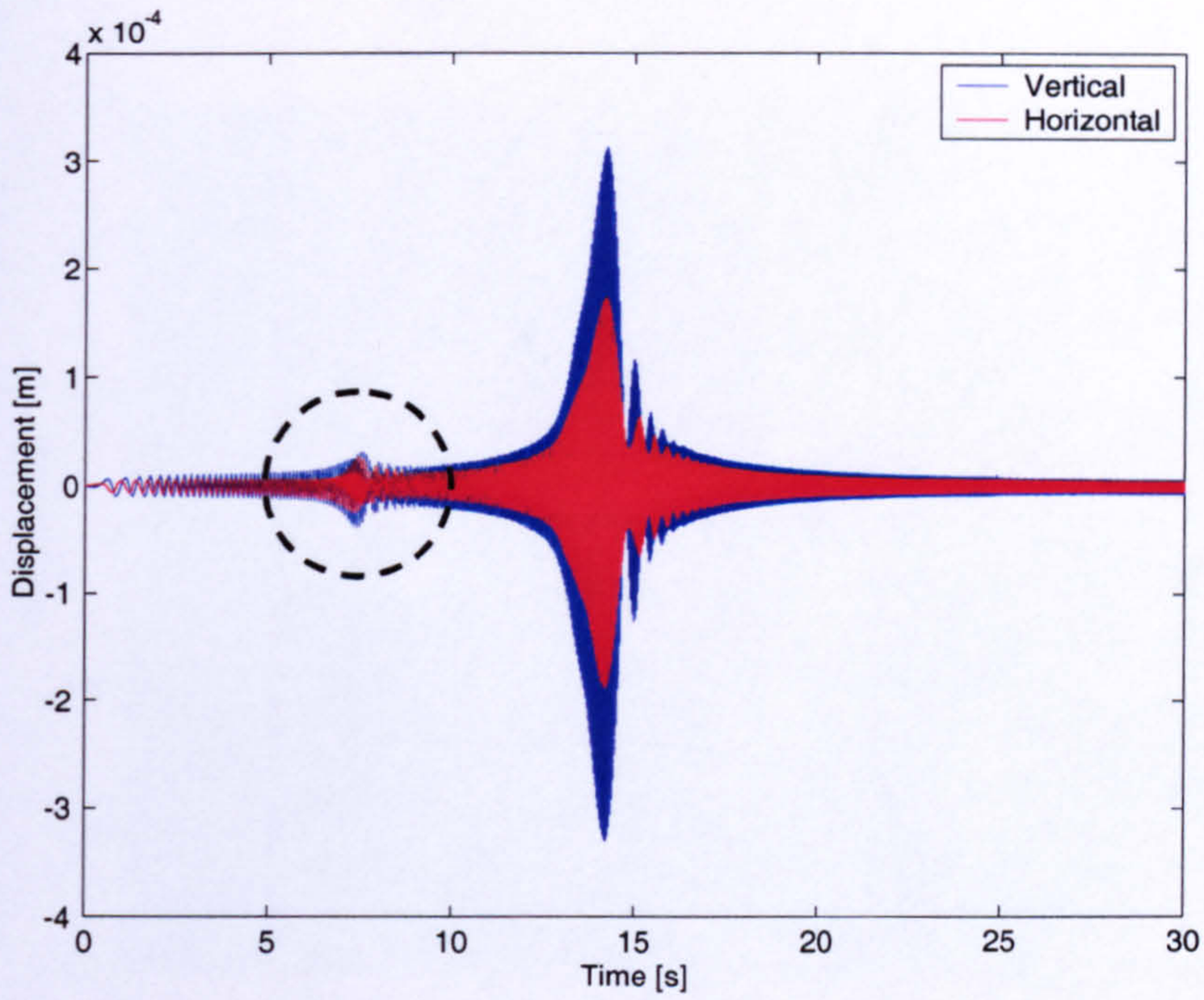


(a) Time Histories

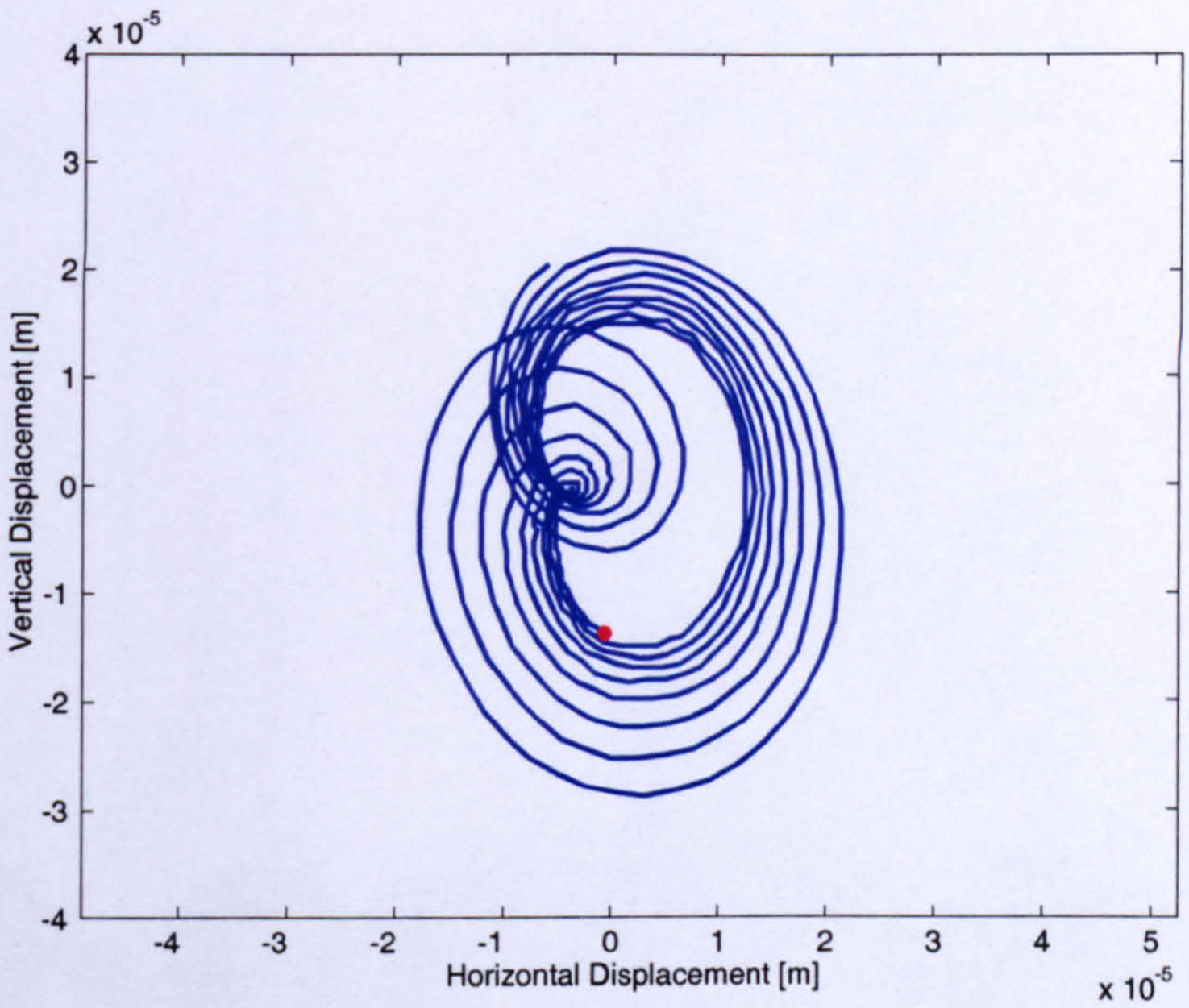


(b) Orbit at $\Omega/\omega_n = 0.5$

Fig 5.5.2 Normal Rotor System

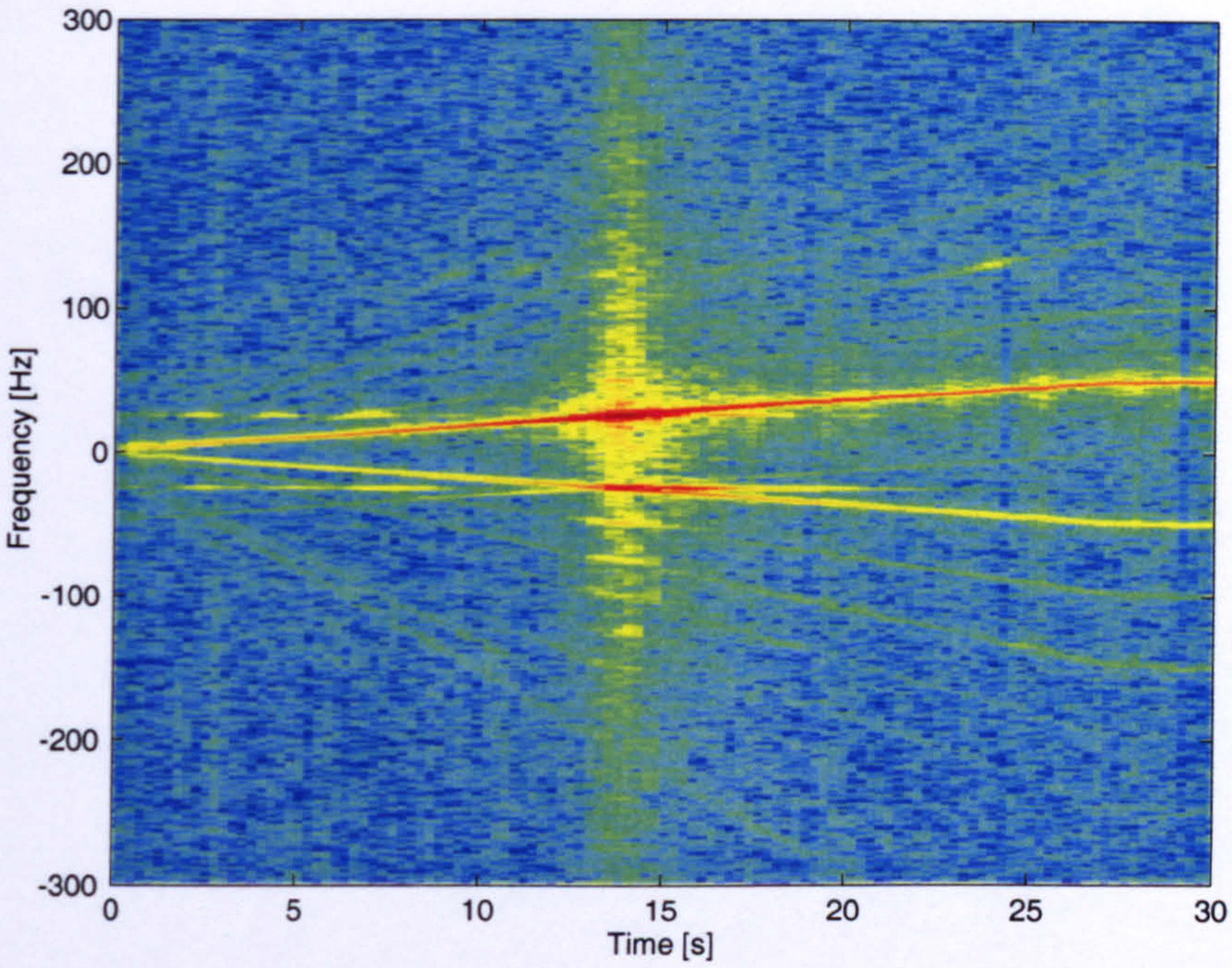


(a) Time Histories

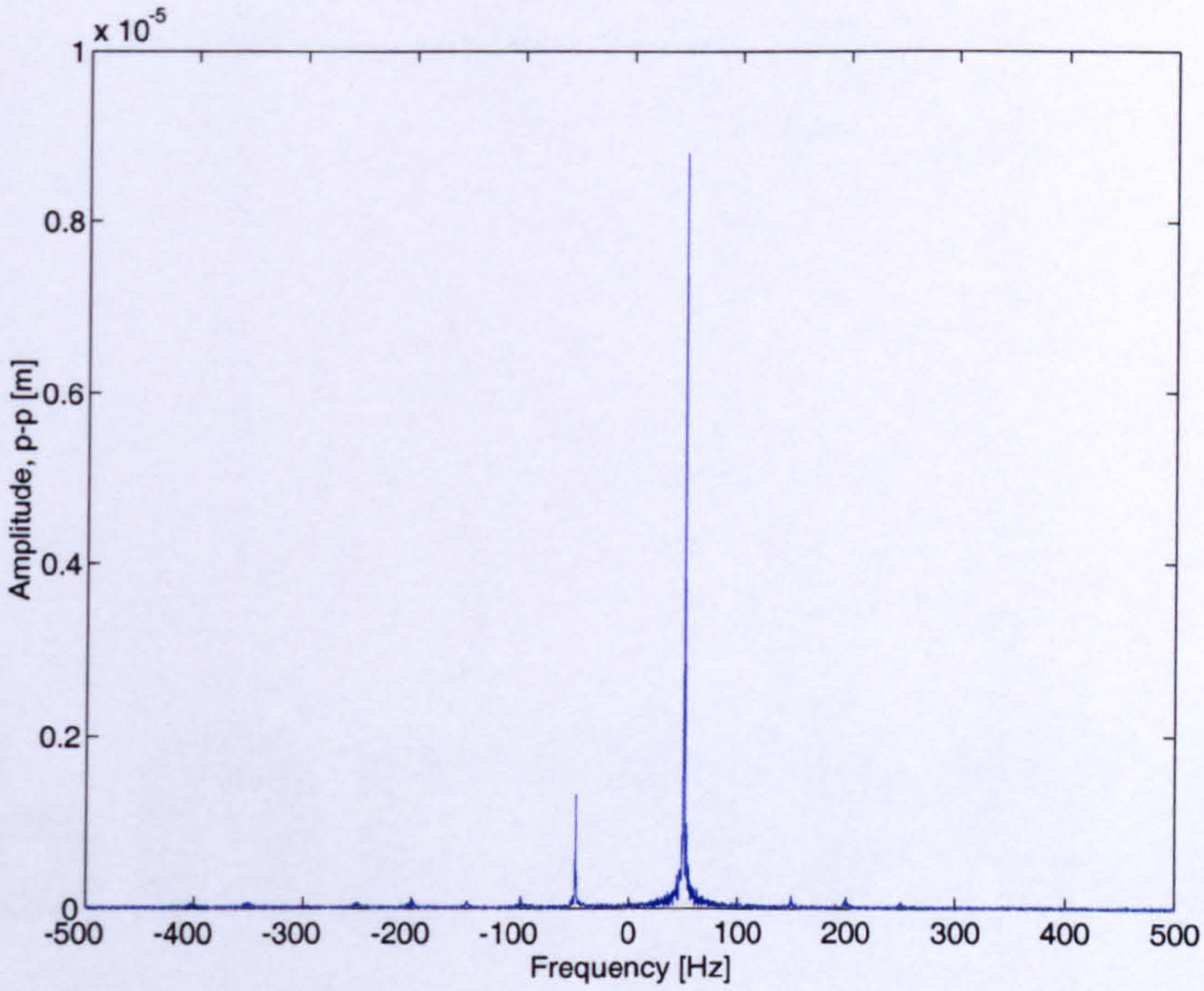


(b) Orbit at $\Omega/\omega_n = 0.5$

Fig 5.5.3 10 % Cracked Rotor System

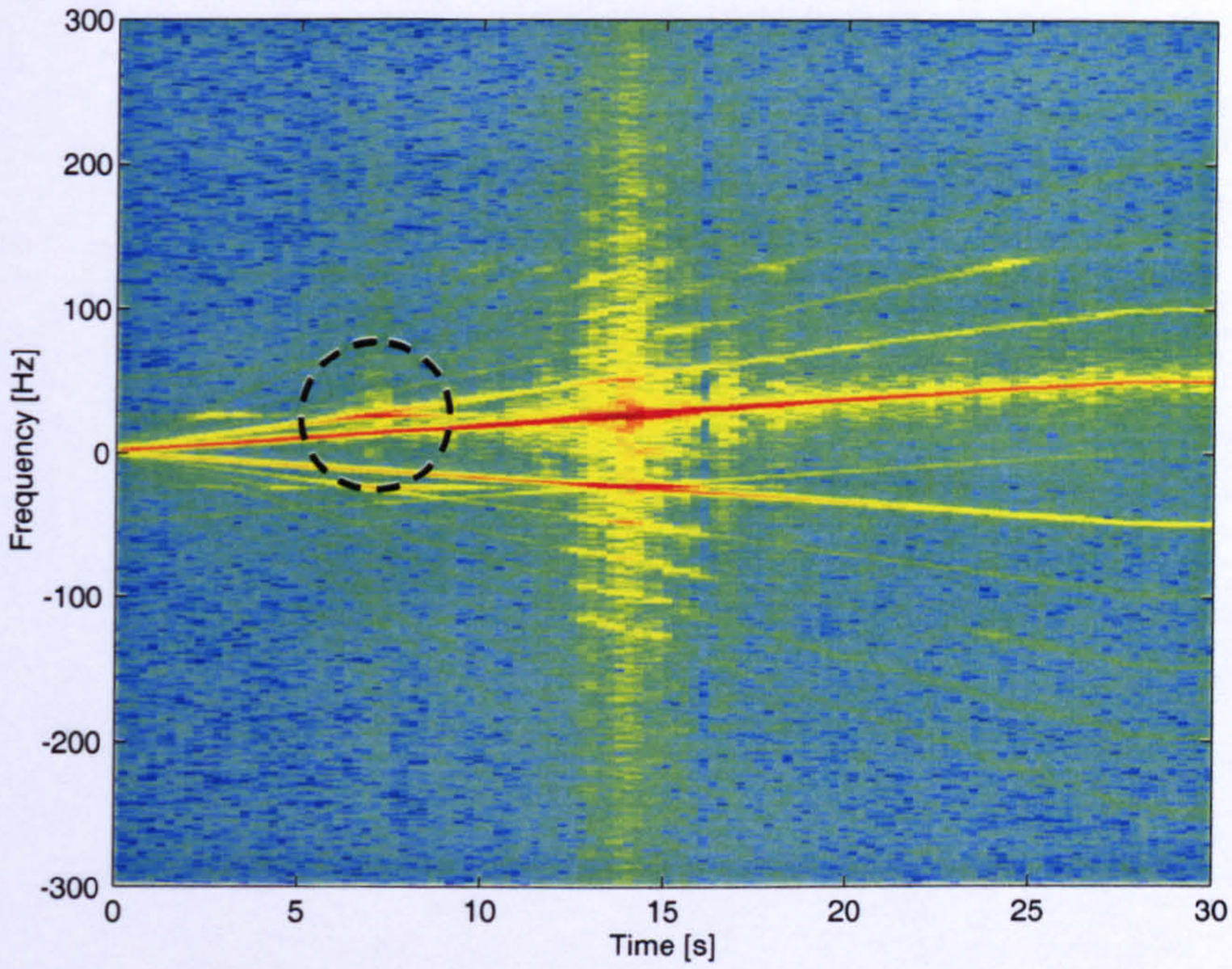


(a) Run-up

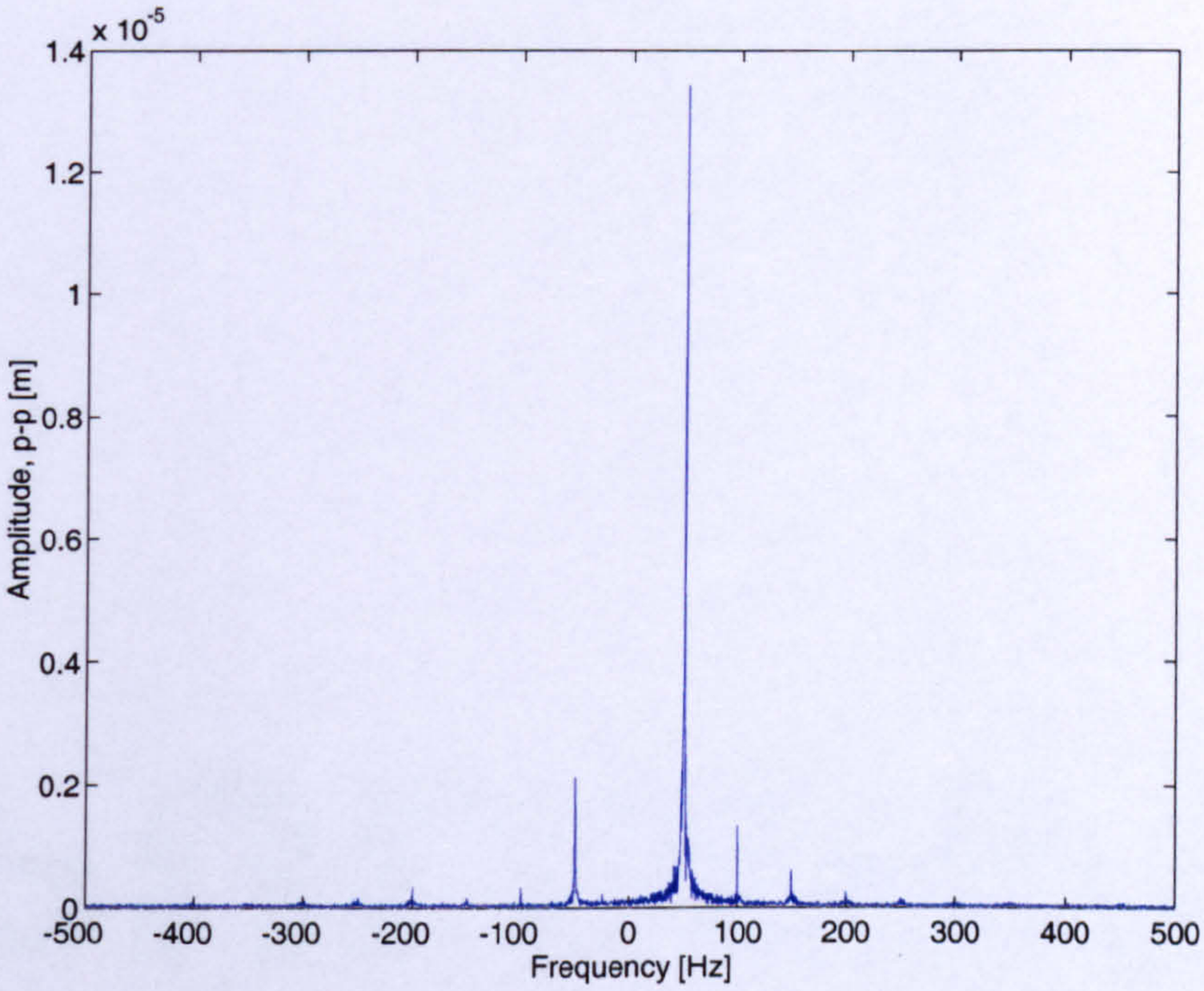


(b) Constant Speed

Fig 5.5.4 Normal Rotor System

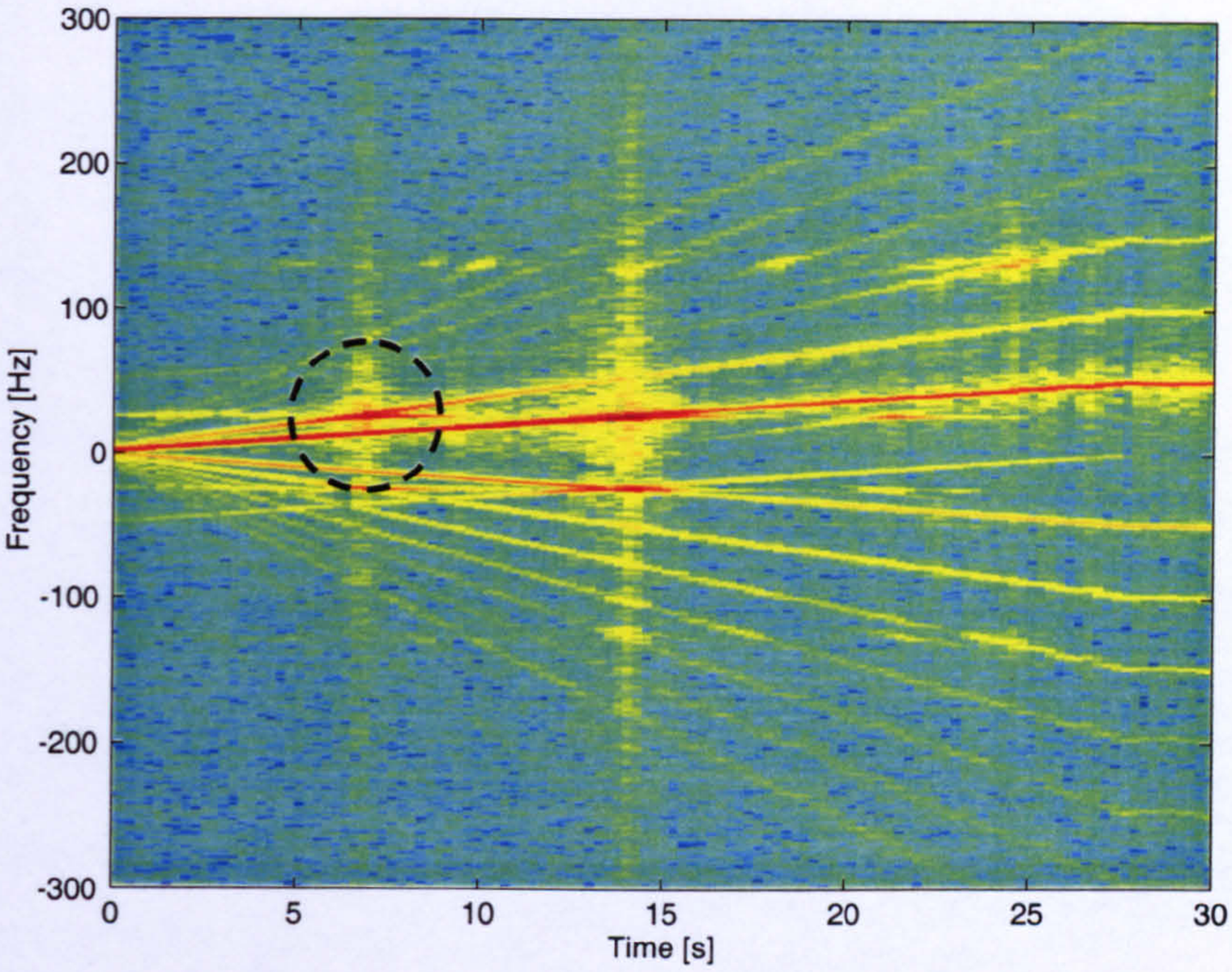


(a) Run-up

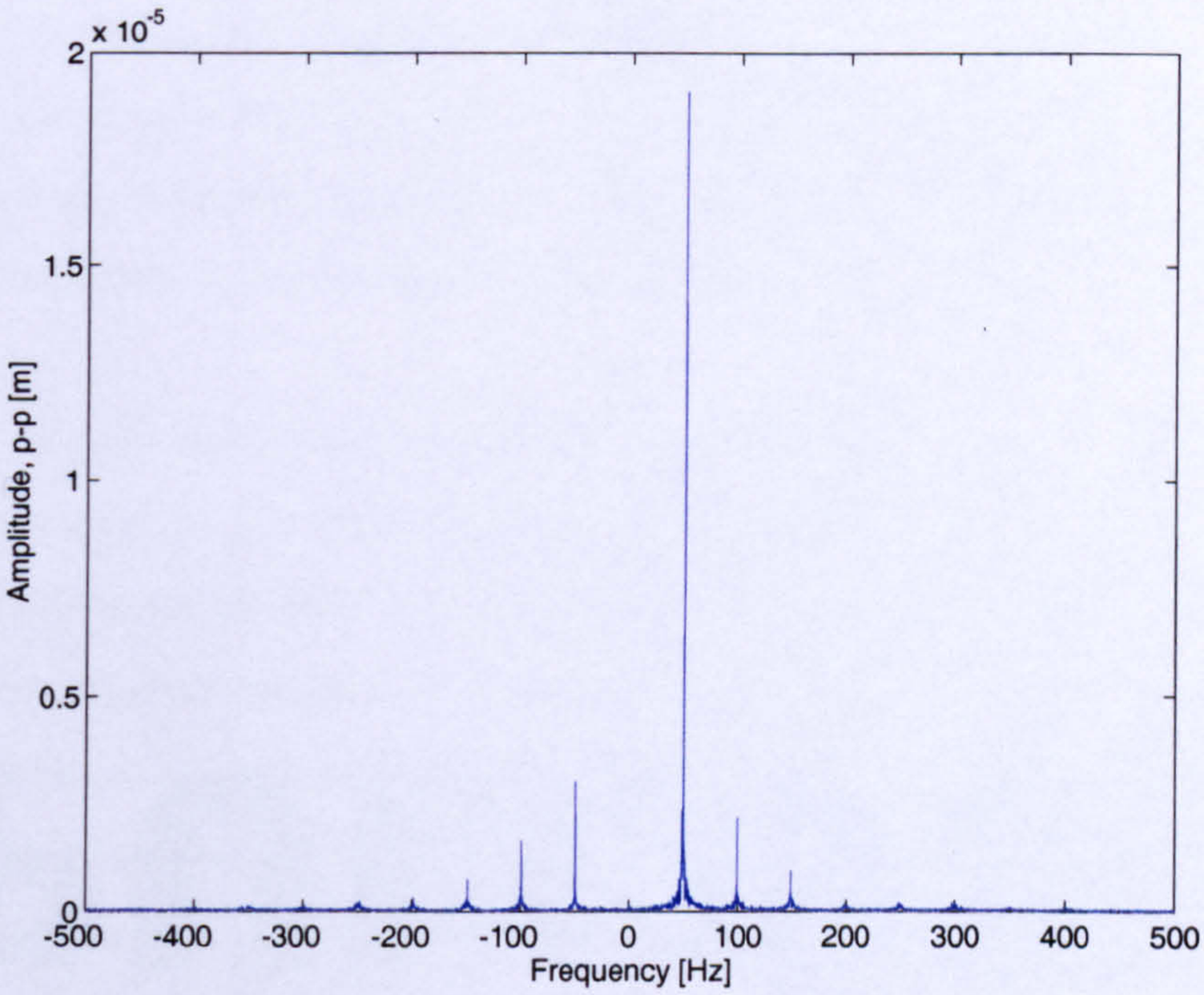


(b) Constant Speed

Fig 5.5.5 Rotor with 10 % Crack at Mid-Span



(a) Run-up



(b) Constant Speed

Fig 5.5.6 Rotor with 20 % Crack at Mid-Span

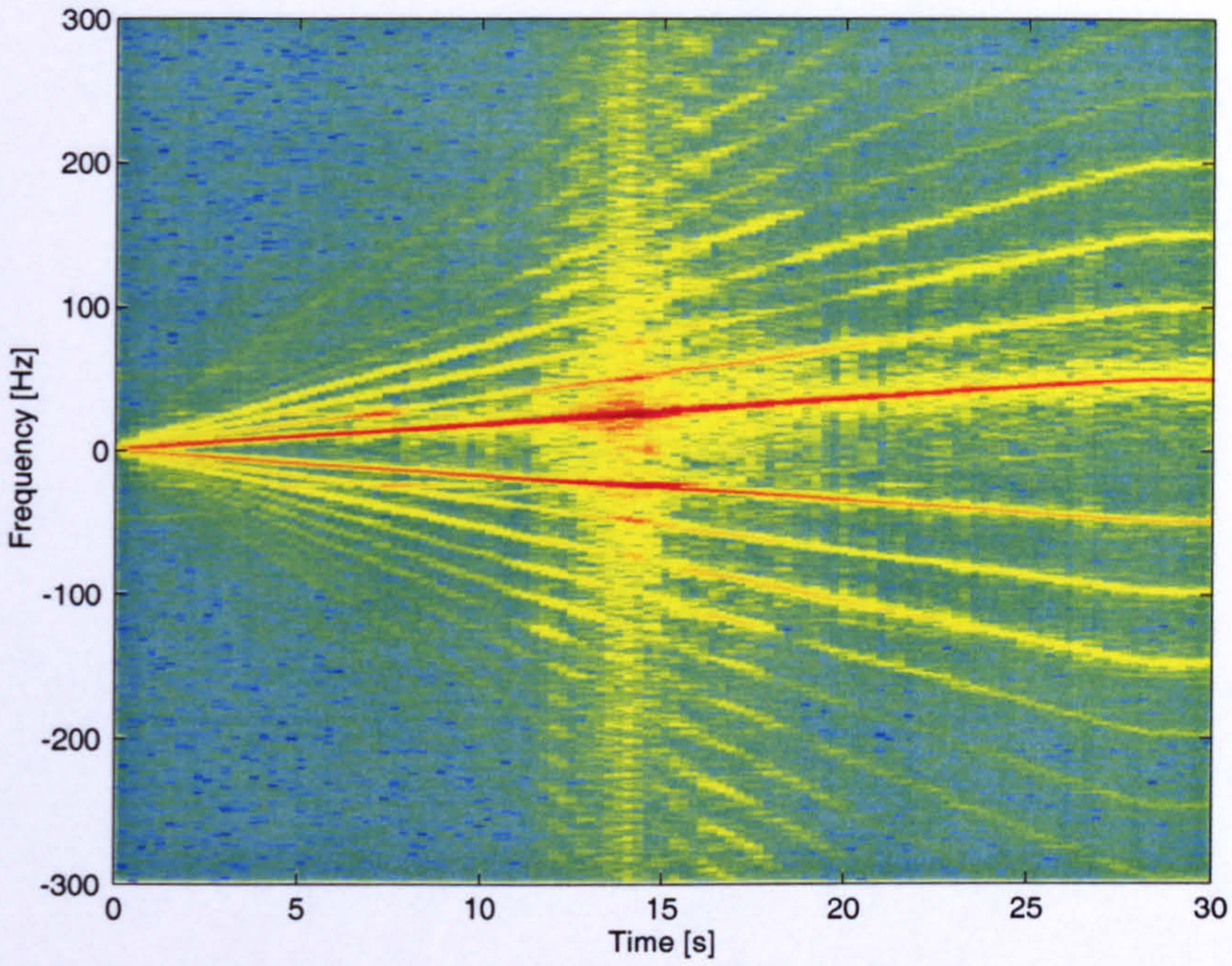
5.5.2 Effect of Crack Location

To investigate the sensitivity of the crack-related harmonics, a crack has been induced at a different position, i.e. near the outboard bearing. As has been predicted and discussed in the analytical research, so also in the experiments have the crack-related harmonics revealed different sensitivities according to the different (more or less extreme) crack positions.

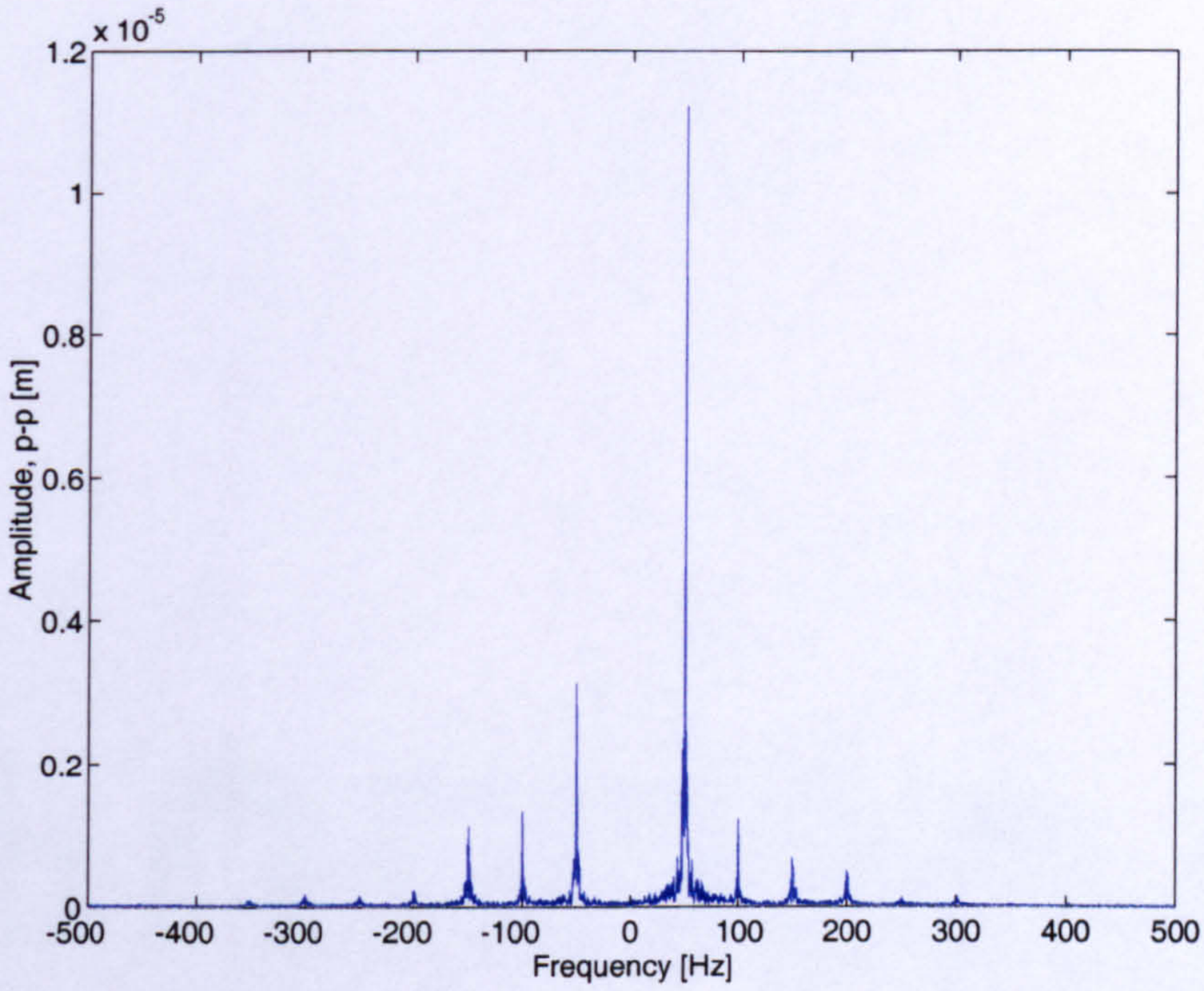
Although measurements have been taken for two positions (inboard and outboard probes), the outboard probe vibration data has mainly been processed and interpreted as it was very difficult to have meaningful interpretation of the data obtained from the inboard probe when the crack was located near to the outboard probes (while the mid-span cracked rotor produced similar vibration data from the two probe positions).

As presented in Fig 5.5.7-(a), the directional spectrogram shows relatively strong higher-harmonic vibration components (2Ω, 3Ω, $\cdots$) compared with the mid-span cracked rotor due to the effect of the support (or bearing) interacted with the rotor system. Moreover, it can be found that the backward higher-harmonic components are also strong due to increased non-linearity of the rotor system.

Although the crack-related harmonic components have different sensitivities according to the crack locations, one important fact that can be noticed in the experiments in both crack locations is the growing property of the crack-related harmonics according to the increase of crack depth. As this feature is considered to be the most obvious discriminating factor between crack and the other faults in the rotating machinery, all these crack-related harmonics must be extracted properly from the vibration data to enable the estimation of growth rate of the crack-related harmonics.

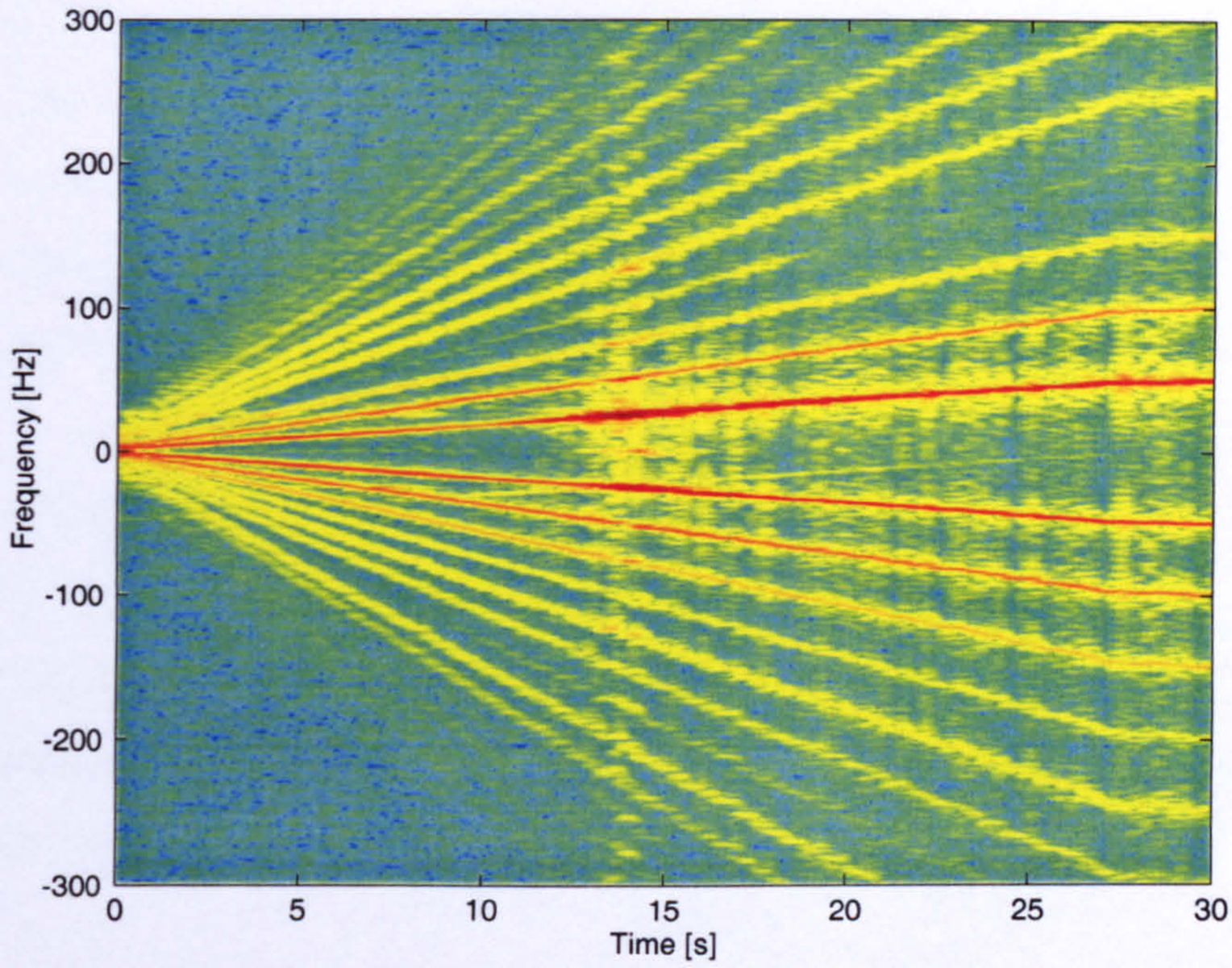


(a) Run-up

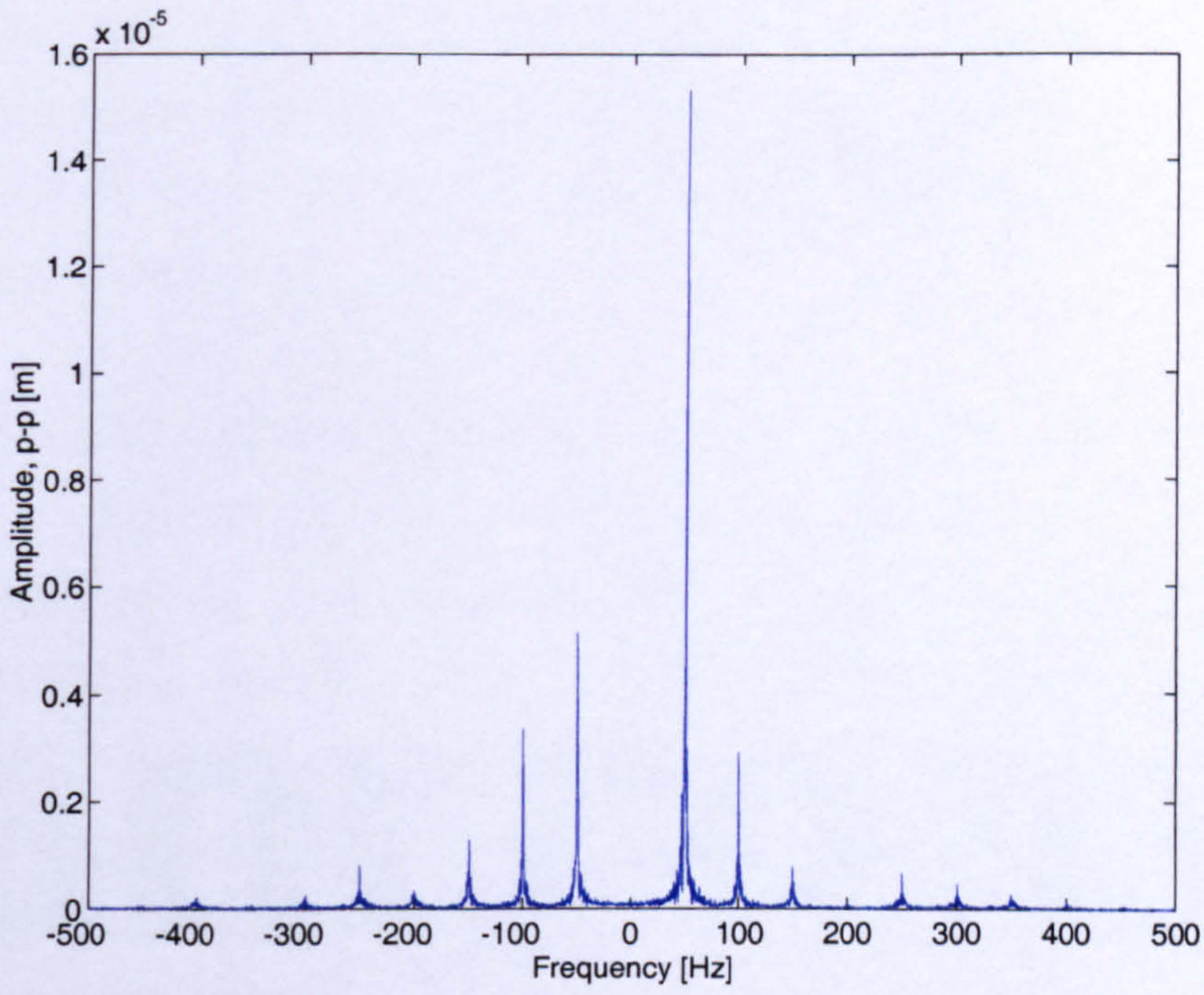


(b) Constant Speed

Fig 5.5.7 Rotor with 10 % Crack at Outboard



(a) Run-up



(b) Constant Speed

Fig 5.5.8 Rotor with 20 % Crack at Outboard

5.5.3 Application of New Methods

The new methods for crack detection developed in Chapter 4 have been applied to evaluate their performance when applied to measured vibration data. For transient vibration data, the DHWT has been applied and for steady-state vibration data, the DDVSA has been applied.

• Application of DHWT

The Directional Harmonic Wavelet Transform (DHWT) has been applied to the measured vibration data from the cracked rotor system to evaluate the performance of the DHWT.

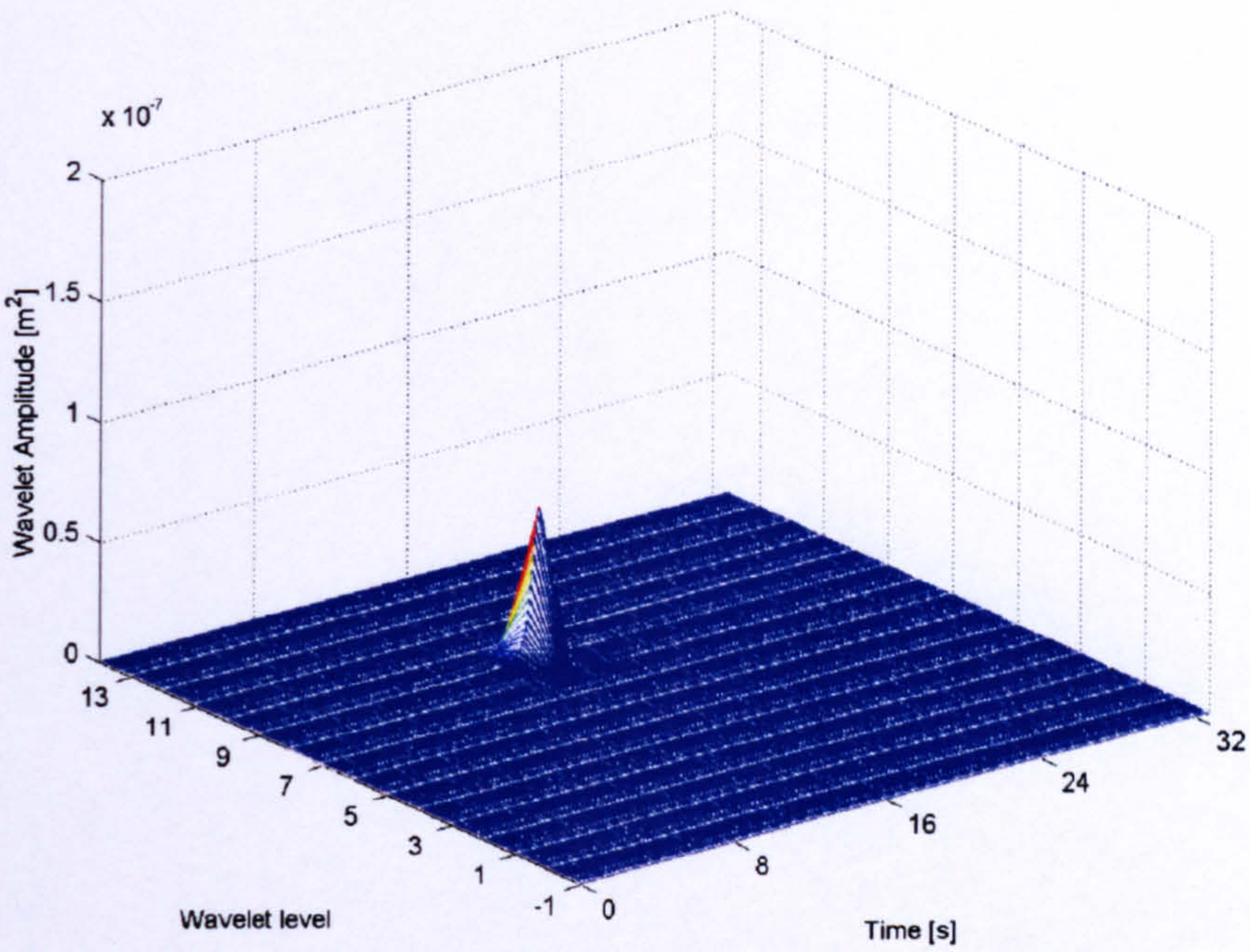
Fig 5.5.9 shows the directional wavelet map for the normal rotor system, and as can be clearly seen in the map, the $+1\Omega$ resonance can be identified in the forward directional wavelet map, i.e. Fig 5.5.9-(a), which has been caused by inherent eccentricity of the rotor system. Also, there exists a small -1Ω resonance as in Fig 5.5.9-(b) due to the effect of gravity which makes the bearing stiffness property slightly anisotropic.

For the 10 % cracked rotor system, as can be seen in Fig 5.5.10-(a), the sub-resonance at $t \approx 7.3$ s ($\Omega/\omega_n = 1/2$), and fundamental resonance at $t \approx 14.6$ s ($\Omega/\omega_n = 1$), caused by the crack-related 2Ω and 1Ω harmonics respectively, can be clearly identified at wavelet level 9 in the forward directional harmonic wavelet map. Due to rather fast run-up rate (6500 rpm/min, which has been selected so as to pass through the resonance region quickly to avoid excessive vibration), another sub-resonance due to crack-related 3Ω harmonic component is not recognisable. Also, in Fig 5.5.10-(b), the fundamental resonance caused by the crack-related -1Ω harmonic component at

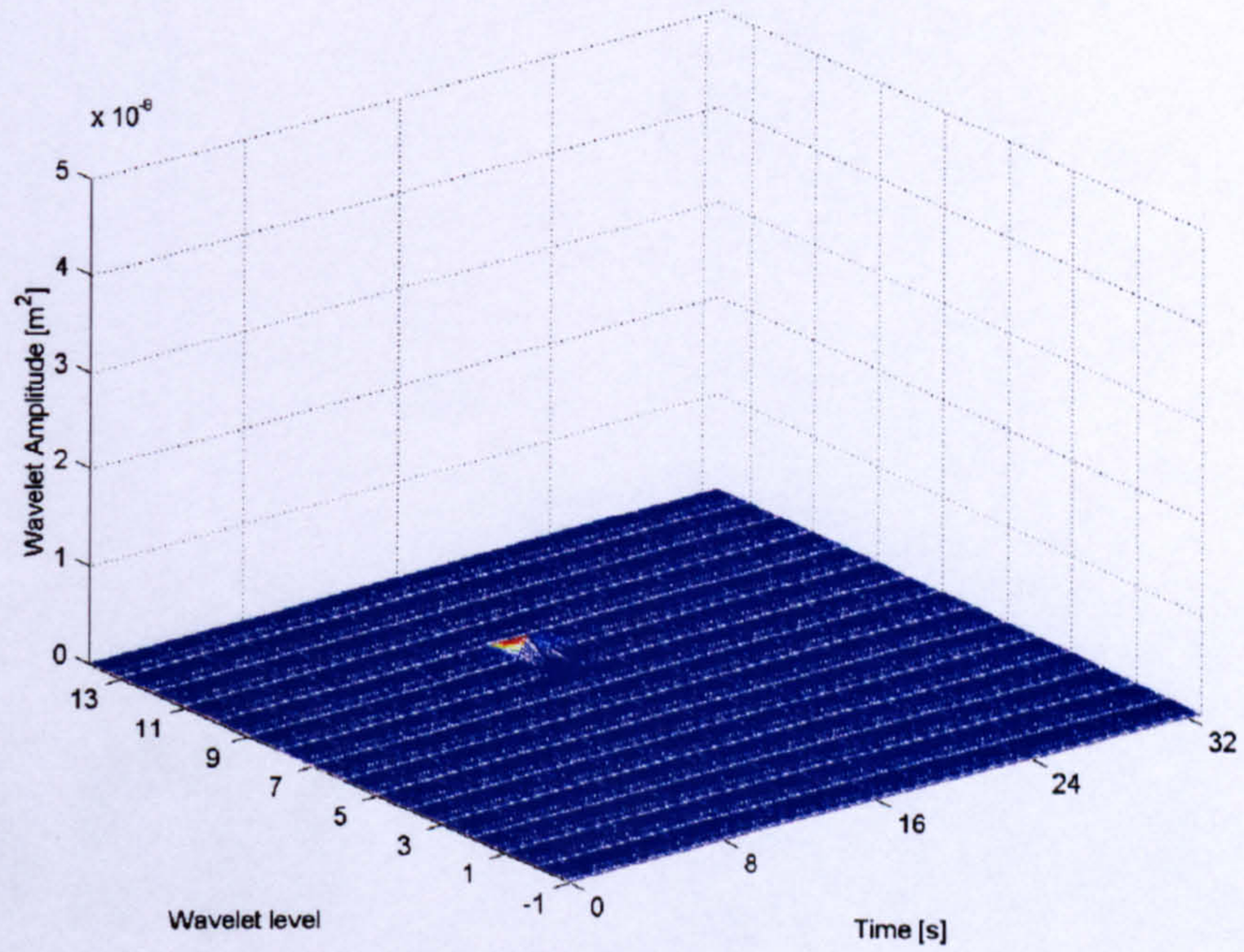
$t \approx 14.6$ s can be identified in the backward directional harmonic wavelet map at the same level, i.e. wavelet level 9.

Fig 5.5.11-(a) & (b) show the directional harmonic wavelet maps for the 20 % cracked rotor system, and it is clearly possible to identify the increase of amplitudes of crack-related resonances relative to a less damaged rotor system. As was already mentioned, the increase of $\pm 1\Omega$ resonance is noticeable together with increase of 2Ω resonance.

As can be seen in the results, the harmonic wavelet transform provides quite a compact information (in the time-*wavelet level* region) which is sensitive to local changes in the vibration response of the rotor system. Considering the fact that the crack-related resonances are the most representative symptoms used to detect cracks in operating rotors for run-up or run-down conditions, the DHWT technique is considered to be an important new tool for crack detection.

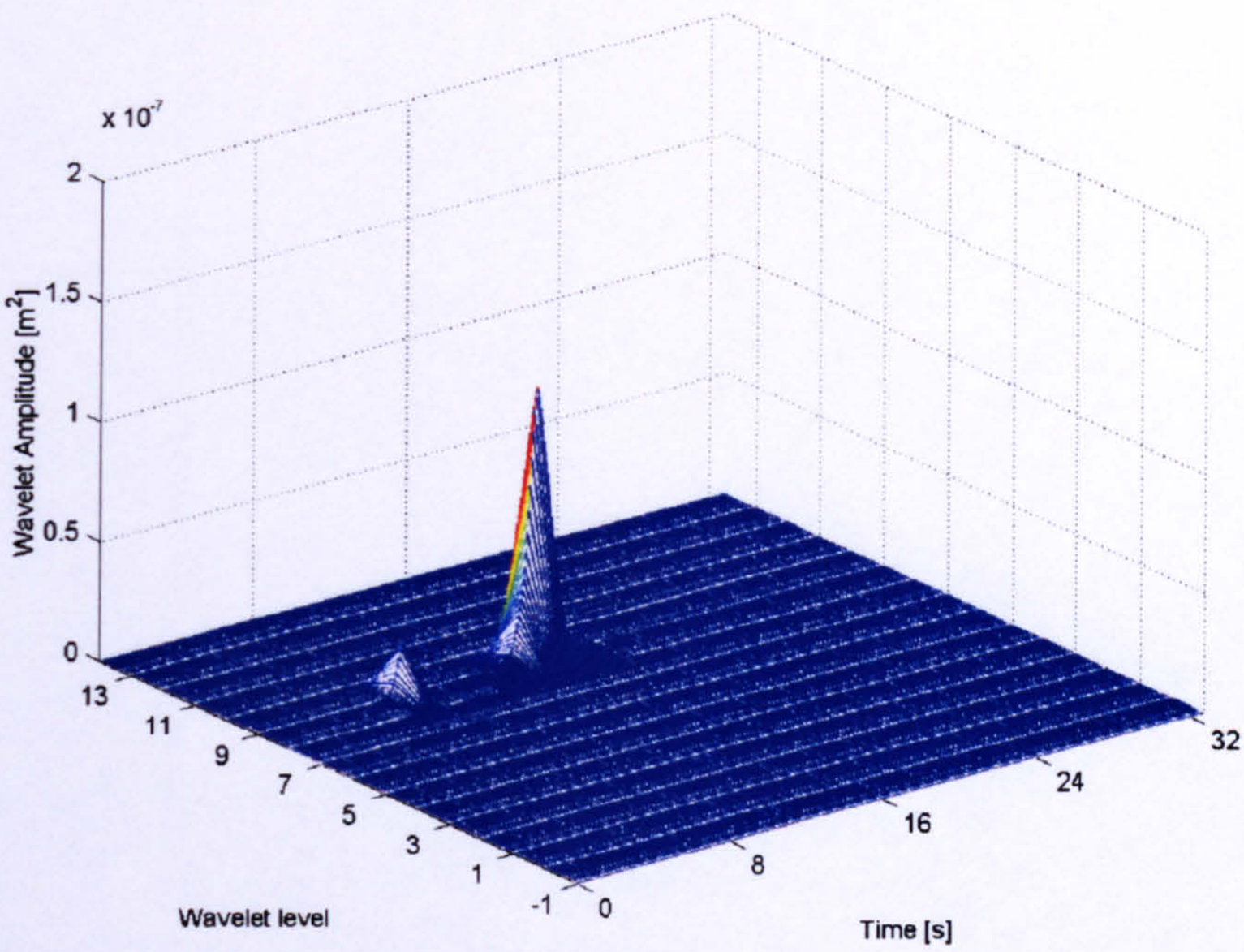


(a) Forward Directional Wavelet Map

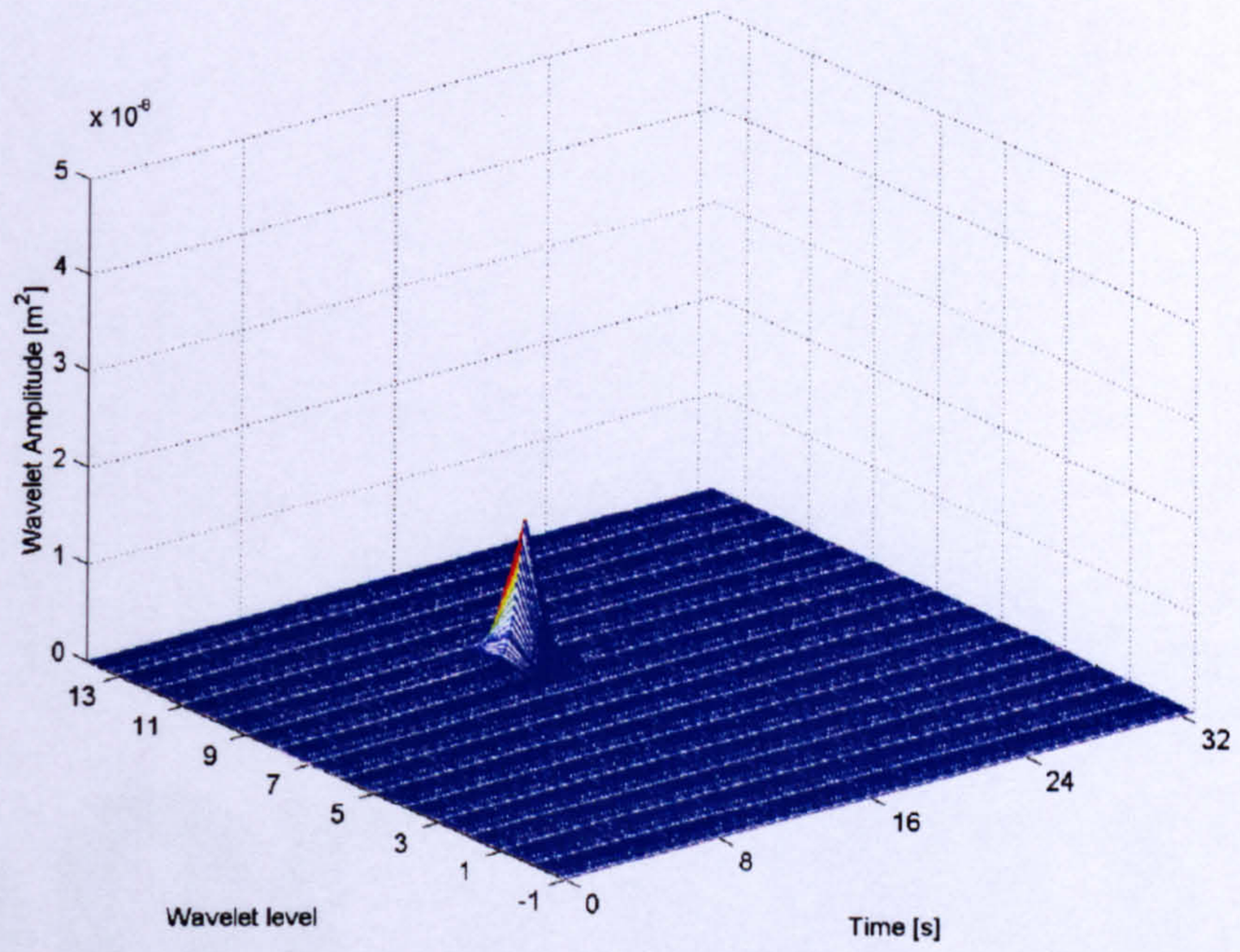


(b) Backward Directional Wavelet Map

Fig 5.5.9 Normal Rotor System

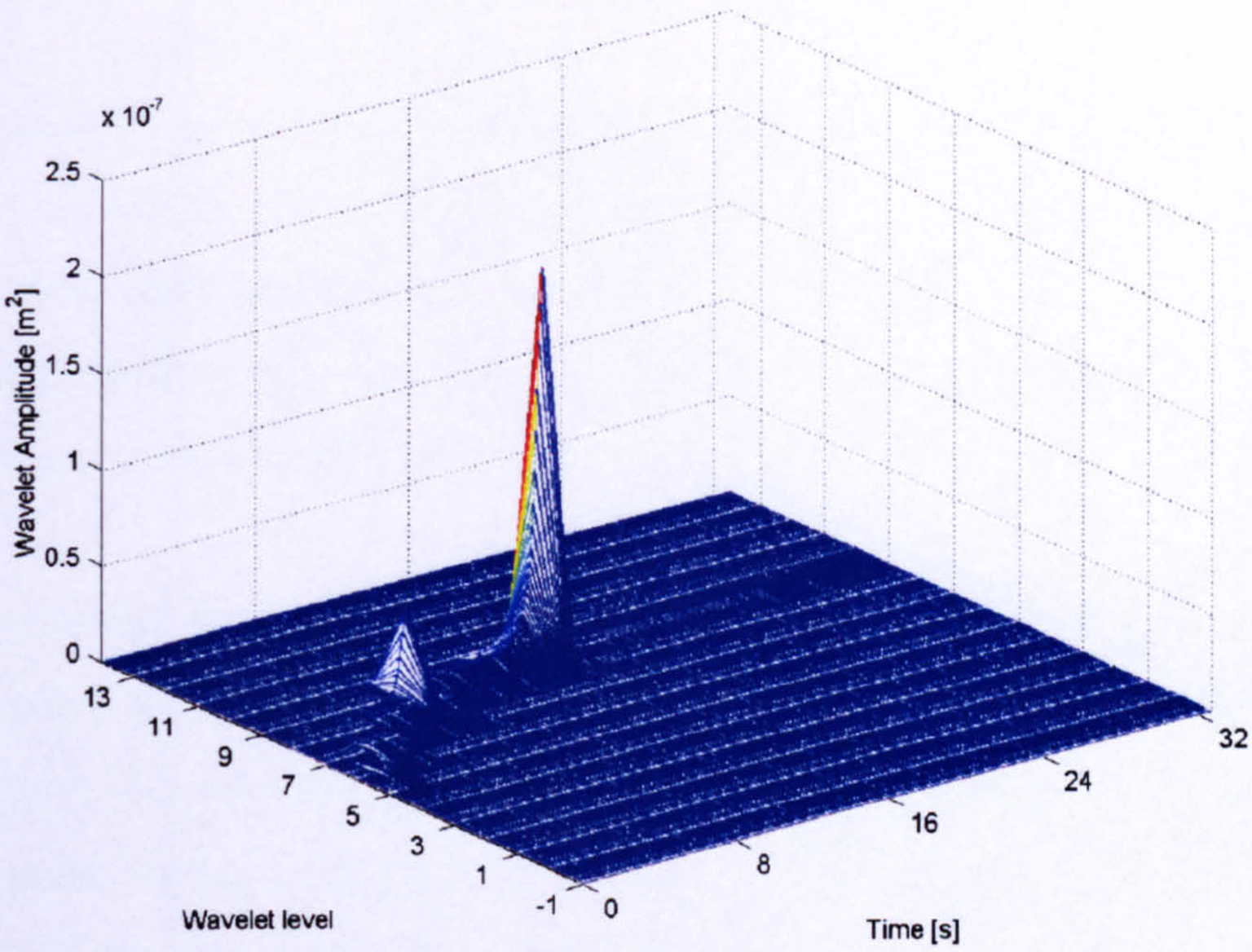


(a) Forward Directional Wavelet Map

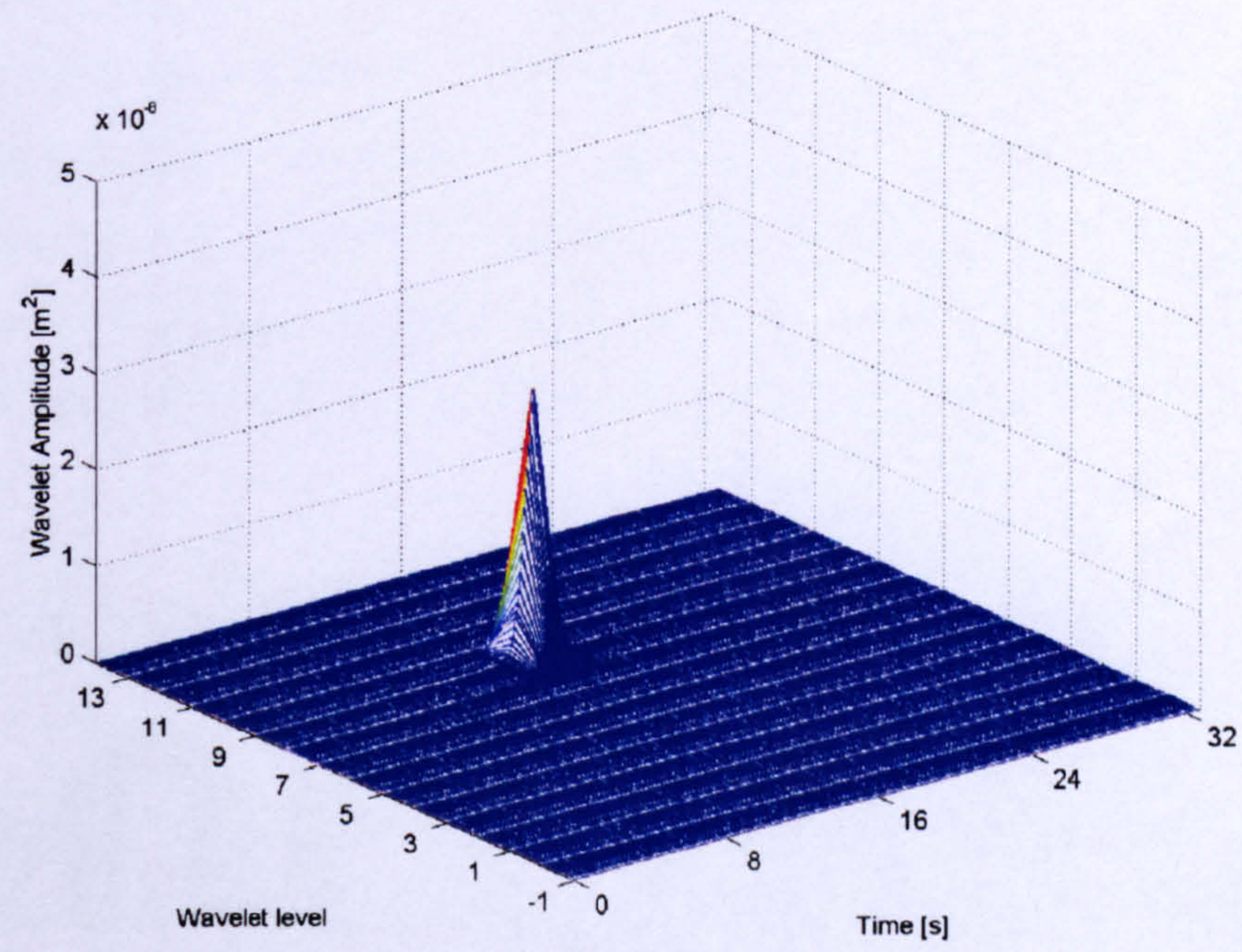


(b) Backward Directional Wavelet Map

Fig 5.5.10 10% Cracked Rotor System



(a) Forward Directional Wavelet Map



(b) Backward Directional Wavelet Map

Fig 5.5.11 20% Cracked Rotor System

• Application of DDVSA

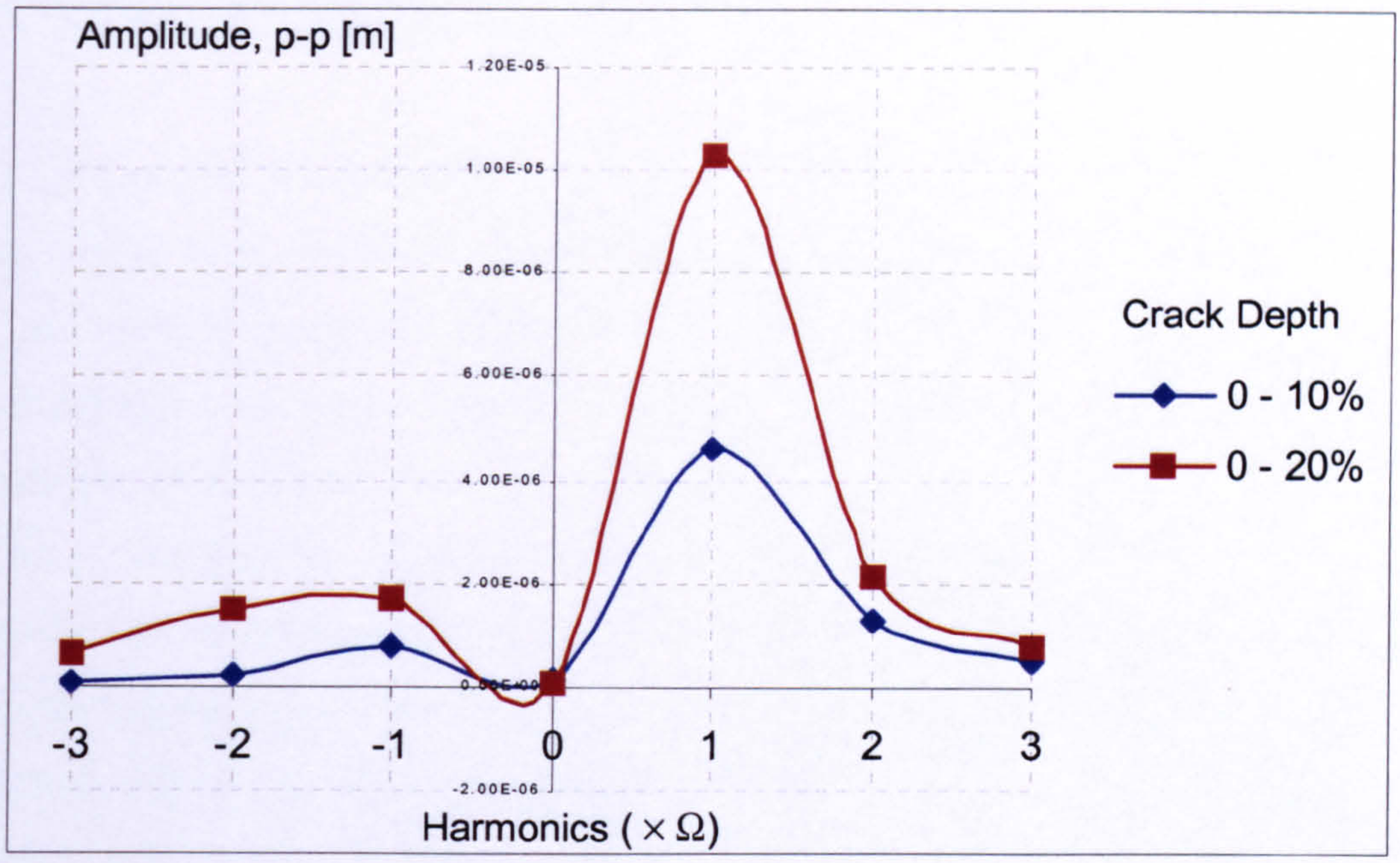
For steady-state vibration data, i.e. the rotor is operating at its designated speed of 3000 rpm (50 Hz), the DDVSA has been applied as shown in Fig 5.5.12-(a) & (b) for mid-span and outboard cracked rotors, respectively. In both cases, to extract the directional-difference vibration components ($\pm 1\Omega$, $\pm 2\Omega$, and $\pm 3\Omega$) for increasing crack depth, the normal rotor's vibration signature has been used as baseline data.

As presented in Fig 5.5.12-(a) & (b), the crack-related harmonics can be clearly identified by applying the DDVSA (directional-difference vibration signature analysis). The domination of the $+1\Omega$ harmonic component (in the directional-difference vibration signature) can easily be noticed in Fig 5.5.12-(a) due to the strong effect of the self-weight of the rotor when the crack is located at mid-span. With the change of crack location far away from the mid-span, as in Fig 5.5.12-(b), the $+1\Omega$ vibration is suppressed and the higher harmonics such as $\pm 2\Omega$ and $\pm 3\Omega$ become relatively large due to mutual interaction between the rotor and the supports. With these directional-difference vibration signatures, it now becomes possible to estimate the growth-rate of crack-related harmonics explicitly as the harmonics are in fully decomposed form into forward and backward vibration components. For the harmonic components obtained from the rotor systems with two different crack locations, the relationship of the crack-related harmonics proposed in Chapter 3 (page 89):

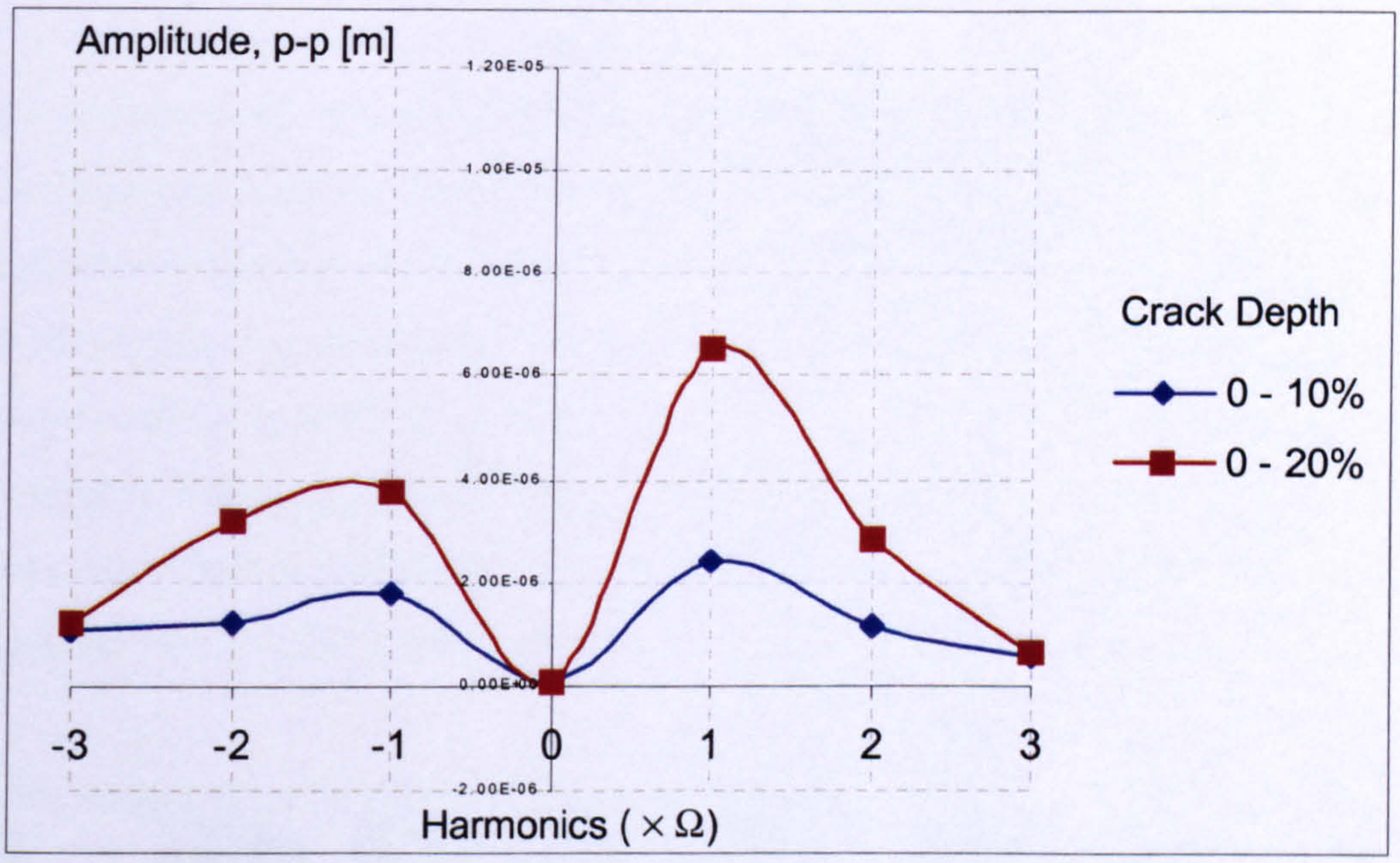
$$\frac{S(-1\Omega)_{\Delta j}}{S(-1\Omega)_{\Delta k}} = \frac{S(+1\Omega)_{\Delta j}}{S(+1\Omega)_{\Delta k}} = \frac{S(+2\Omega)_{\Delta j}}{S(+2\Omega)_{\Delta k}} = \frac{S(+3\Omega)_{\Delta j}}{S(+3\Omega)_{\Delta k}} \qquad (3.3.1)$$

was satisfied with a standard deviation of 0.3, which suggests the existence of a crack in both rotor systems. Considering the possible errors during assembling and reassembling procedures to increase the crack depth to the same rotor system, this result is quite promising for unambiguous crack detection. Also, this method can be

practically implemented to detect cracks for long-term operating rotors at constant speed which is usual in the power generation industry. In field situations, unnecessarily frequent crack alarms could be avoided by narrowing the standard deviation factor to a smaller value to increase the reliability of crack detection.



(a) Mid-Span Crack



(b) Outboard Crack

Fig 5.5.12 Directional-Difference Vibration Signature

5.5.4 Effect of Unbalance on the Cracked Rotor System

To detect a crack reliably, it is necessary to clarify the relationship between crack and unbalance as the unbalance is the most common problem in rotating machinery. In this regard, by using various forms of trial mass as a controlled unbalance, the effect of unbalance on the cracked rotor has been experimentally investigated for a 20 % cracked rotor in its steady-state condition.

Before applying the controlled trial mass, balancing of the cracked rotor has been performed using the influence coefficient method to avoid excessive vibrations mainly caused by large synchronous 1Ω vibration component, especially during the run-up period. For two balancing planes, each horizontal probe has been used in balancing procedures.

• Influence Coefficient Method

There exist many methods to balance a rotor such as *separate single-plane balancing*, *simultaneous single-plane balancing*, the *static/couple derivation method*, and the *influence coefficient method* [91], increasing the sophistication to accommodate for multi-planes, high speeds, and flexible rotors etc. For all these balancing methods, the basic underlying idea is to counteract the existing unbalance U by introducing corrective balancing masses to have an effective vector $U_{bal} = -U$. In the present case, the influence coefficient method has been used for its convenience of application together with reliable performance.

• Balancing Trial Weight

The balancing weight should be sufficient to make a change in the vibration of a rotor system but not so large that it could destroy the machine if placed in a wrong position. Several sources recommend a weight which will exert a force (at operating speed)

equal to 10 % of the rotor's normal weight (at rest) on one bearing. This weight can be calculated as follows, [91]:

$$W = \frac{F}{KRN^2} \tag{5.5.1}$$

where W trial weight [g]

F 10 % of rotor weight on a single bearing [kg]

$0.1 \times$ rotor weight $\div$ number of bearings

R radius at which trial weight will be applied [cm]

N rpm/1000

K constant = 0.011

From the equation, the trial mass has been decided to 400 mg, however the trial mass has been applied gradually from smaller amount mass of 200 mg. Also as the rotor is operating between the 1st and 2nd critical speeds, which accompanies the phase shift of 180°, the trial mass has been placed on the high spot during the balancing procedures.

• Balancing Procedures

The initial step is to record the shaft static runout from the inboard and outboard planes:

$$\begin{bmatrix} x_{in} \\ x_{out} \end{bmatrix}_{runout} = \begin{bmatrix} 2.6873 \times 10^{-6} m \angle 4.2371 \text{ rad} \\ 6.7037 \times 10^{-6} m \angle 4.5596 \text{ rad} \end{bmatrix} \tag{5.5.2}$$

This runout measurement has been done at 100 rpm, well below any resonance and at a speed where the unbalance response is negligible due to slow shaft rotation. The

second step is to record the unbalance response at the desired speed, chosen to 3000 rpm:

$$\begin{bmatrix} x_{in} \\ x_{out} \end{bmatrix}_{bf-bal} = \begin{bmatrix} 1.9114 \times 10^{-5} m \angle 3.9567 \text{ rad} \\ 2.1066 \times 10^{-5} m \angle 4.8946 \text{ rad} \end{bmatrix} \tag{5.5.3}$$

To find balancing masses and their phase angles, two trial-runs have been conducted; in the first the trial mass has been applied to the inboard plane and in the second the same trial mass has been attached to the outboard plane:

$$\begin{bmatrix} x_{in} \\ x_{out} \end{bmatrix}_{tw-in} = \begin{bmatrix} 1.7186 \times 10^{-5} m \angle 3.8880 \text{ rad} \\ 1.8960 \times 10^{-5} m \angle 4.9357 \text{ rad} \end{bmatrix} \tag{5.5.4}$$

$$\begin{bmatrix} x_{in} \\ x_{out} \end{bmatrix}_{tw-out} = \begin{bmatrix} 1.7522 \times 10^{-5} m \angle 3.7176 \text{ rad} \\ 1.9507 \times 10^{-5} m \angle 4.7486 \text{ rad} \end{bmatrix} \tag{5.5.5}$$

By applying the influence coefficient method with runout-compensated vibration data, corrective balancing masses for inboard and outboard planes can be estimated as follows:

$$\begin{bmatrix} m_{in} \\ m_{out} \end{bmatrix} = \begin{bmatrix} 1.18\, g \angle 0.1632 \text{ rad} \\ 1.96\, g \angle 3.9507 \text{ rad} \end{bmatrix} \tag{5.5.6}$$

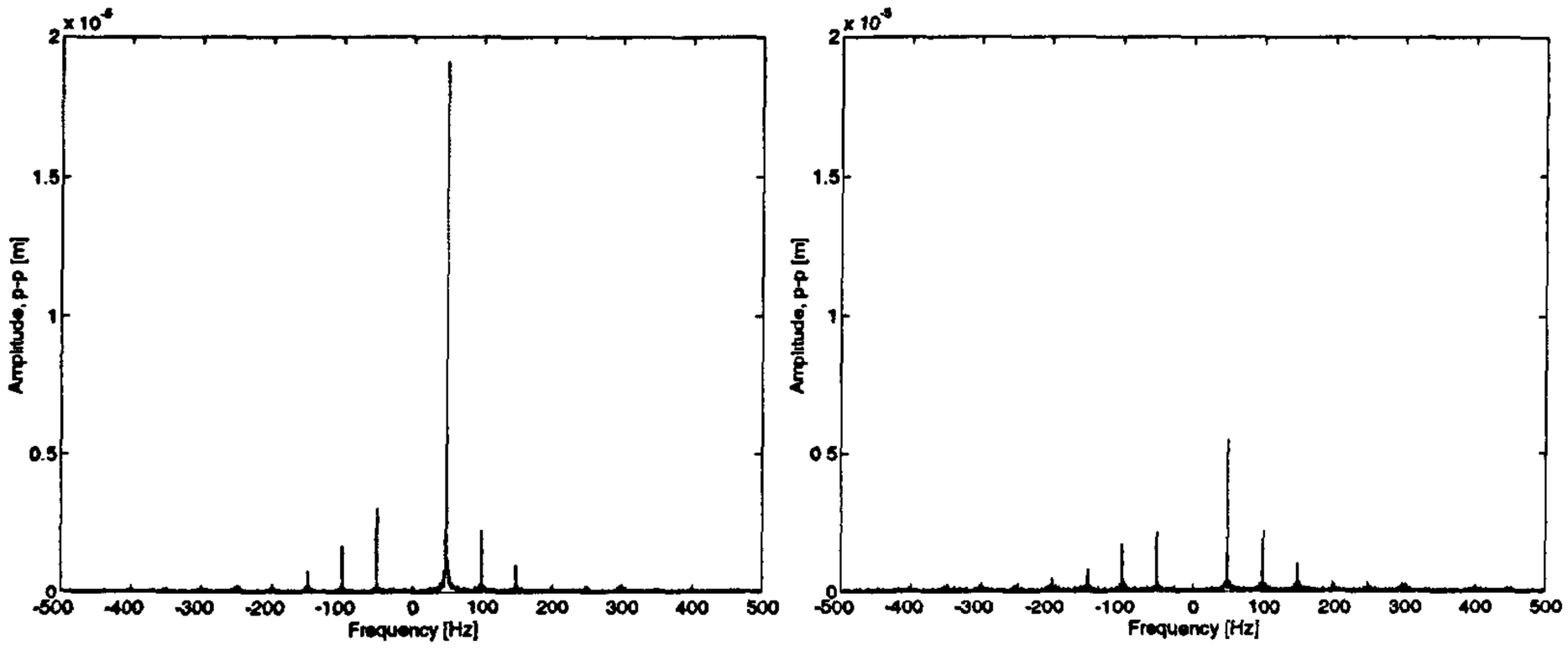
As the balancing masses cannot be attached at arbitrary locations for the given rotor design, where the balancing holes are placed 15° apart on each plane, the balancing masses obtained have been split vectorially and then applied to each balancing plane.

By performing the balancing, the 1Ω vibration component has been greatly reduced as can be seen in Fig 5.5.7 although the rotor system has non-linearity due to a crack. As a result, the rotor could pass through the resonance region (or speed) with reduced vibration level to its designated operating speed. Also from the comparison of the

directional spectra before and after the balancing, it can be seen that the higher-harmonic vibration components have not been affected throughout the balancing procedures.

As presented in Fig 5.5.8, various configurations of unbalance have been applied to accommodate every possible occasions regarding the unbalances. In all cases, the 1Ω vibration component increased with the increase of the unbalance masses, i.e. from 200 mg to 400 mg with virtually no influence to higher-harmonic vibration components as shown in Fig 5.5.9-(a) ~ (l). Particularly, in the case of unbalance type 'couple 0°', small 1Ω vibration component can be found (also no change in higher-harmonic components) as the unbalance mass ironically acted as a balancing mass to the rotor system, however, again, the vibration increased a bit with unbalance level increased to 400 mg.

As the experimental result shows clearly, the independence of crack-related higher harmonics and the unbalance-related 1Ω vibration component can be identified. Hence, for unbalanced rotor, which is the most common problem in rotating machinery, the crack can be identified (even without performing the balancing of the rotor, considering the balancing is the most common first remedial action for large vibration problems in rotating machinery) by estimating the growth-rate of harmonics after removing the unbalance-related harmonic component by using DDVSA as the DDVSA can isolate the crack-related harmonics and the crack-related harmonics are not affected by unbalance.



(a) Before Balancing **(b) After Balancing**

Fig 5.5.7 Balancing

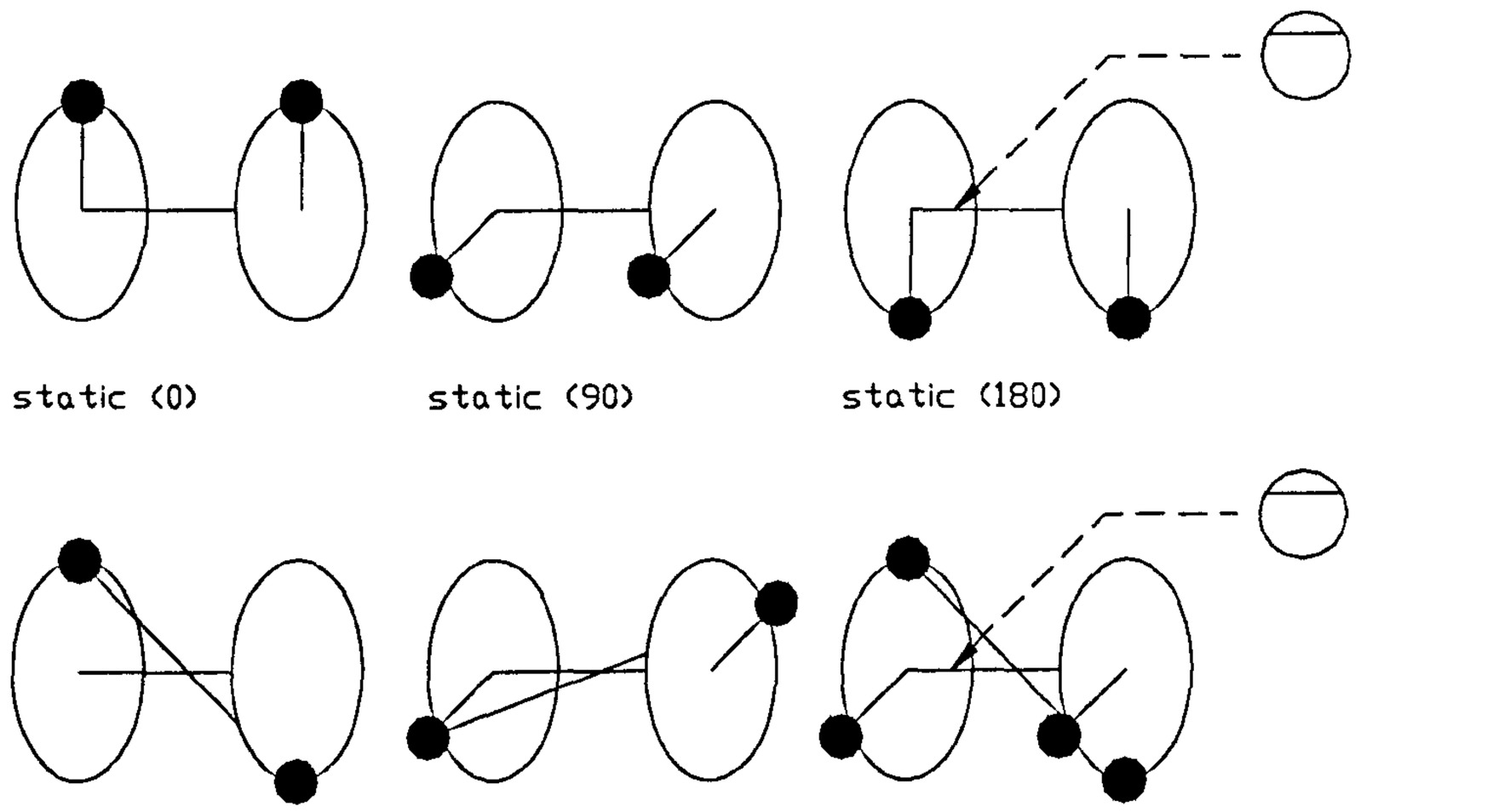
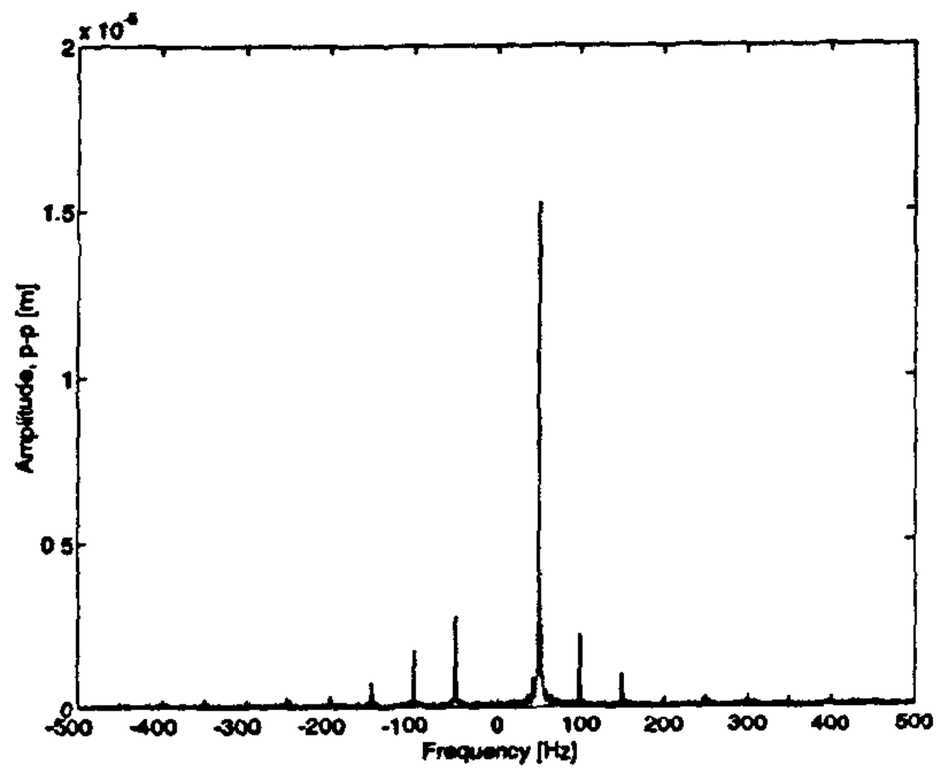
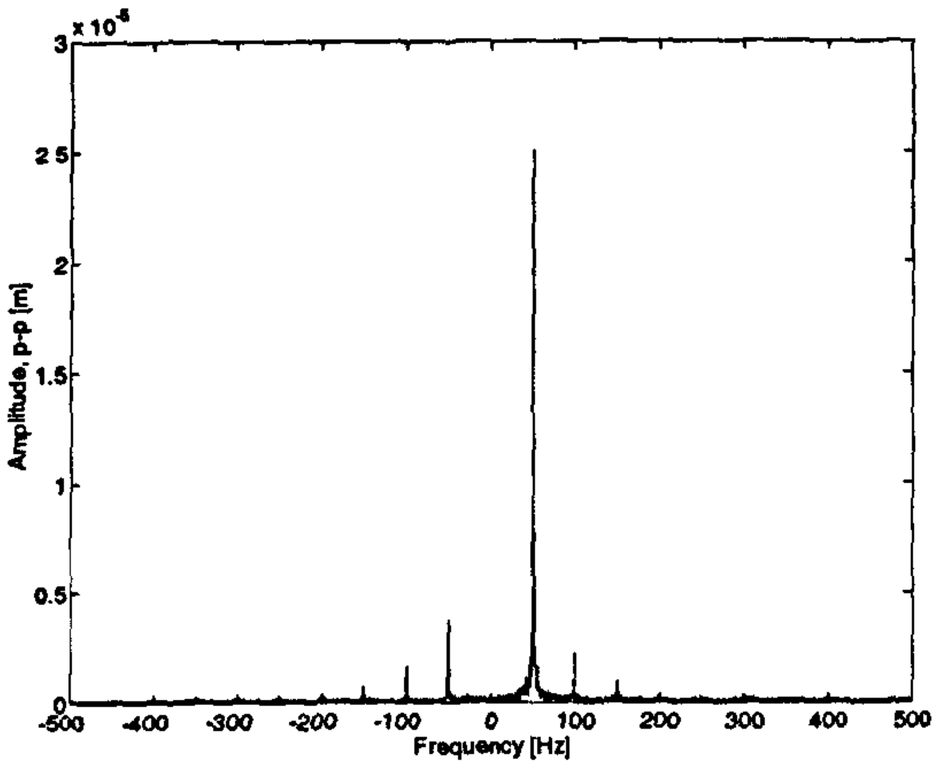


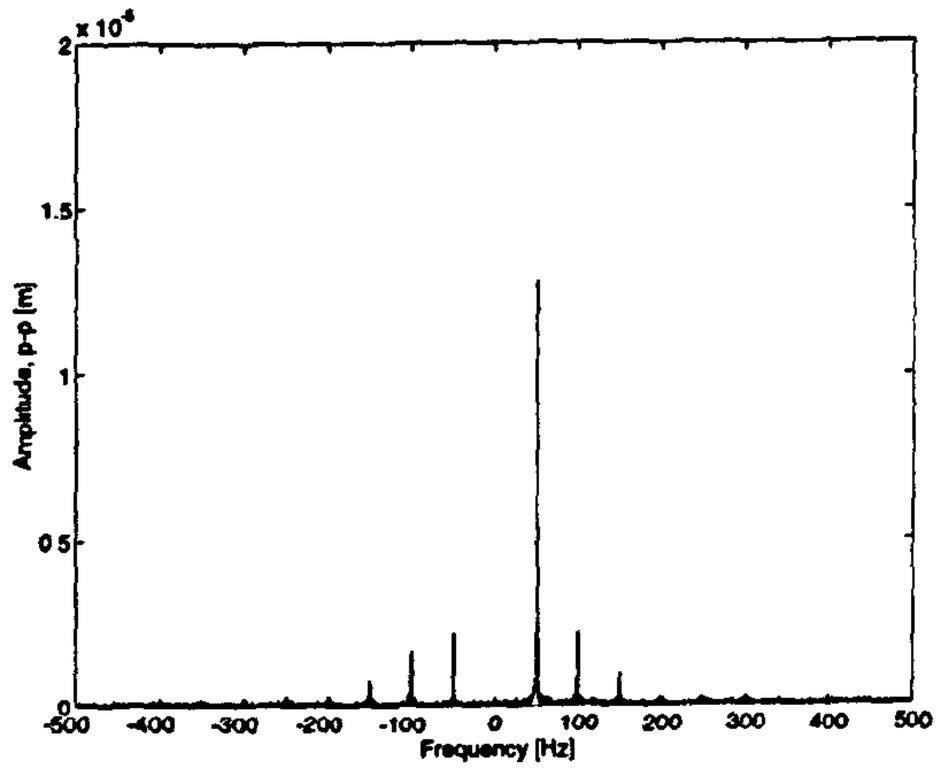
Fig 5.5.8 Types of Unbalance applied in the Test



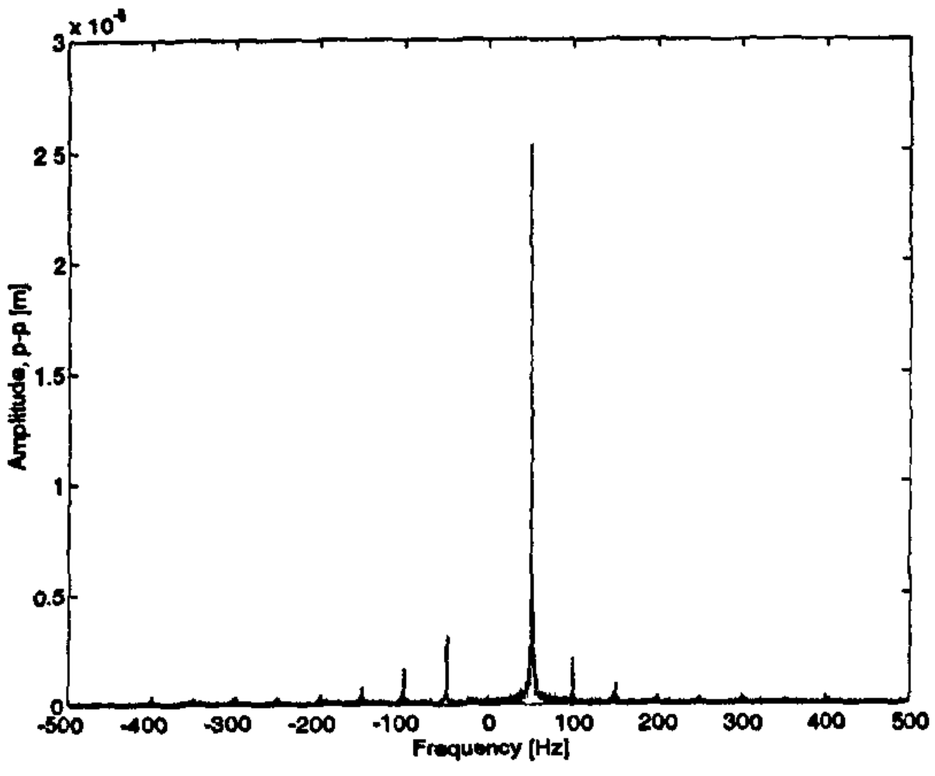
(a) 200 mg, Static 0°



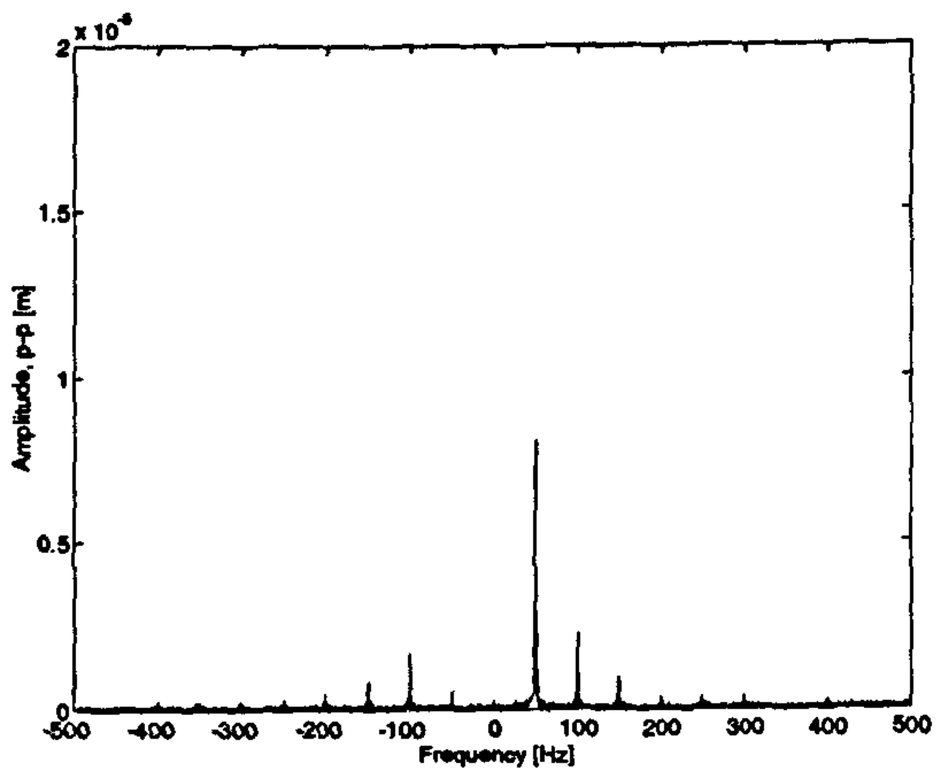
(b) 400 mg, Static 0°



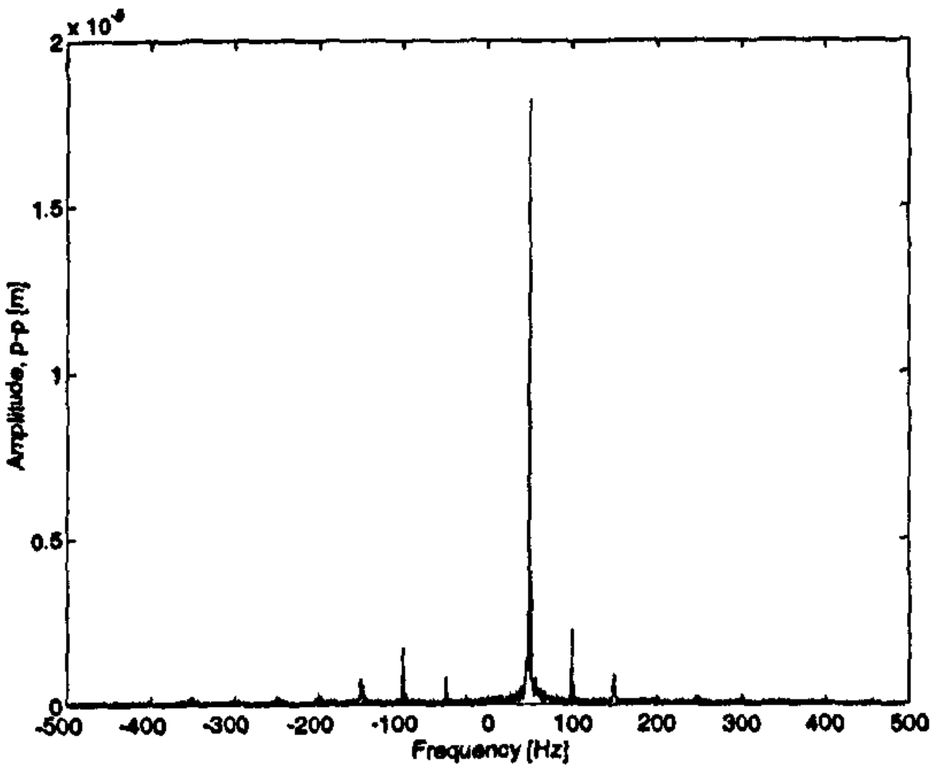
(c) 200 mg, Static 90°



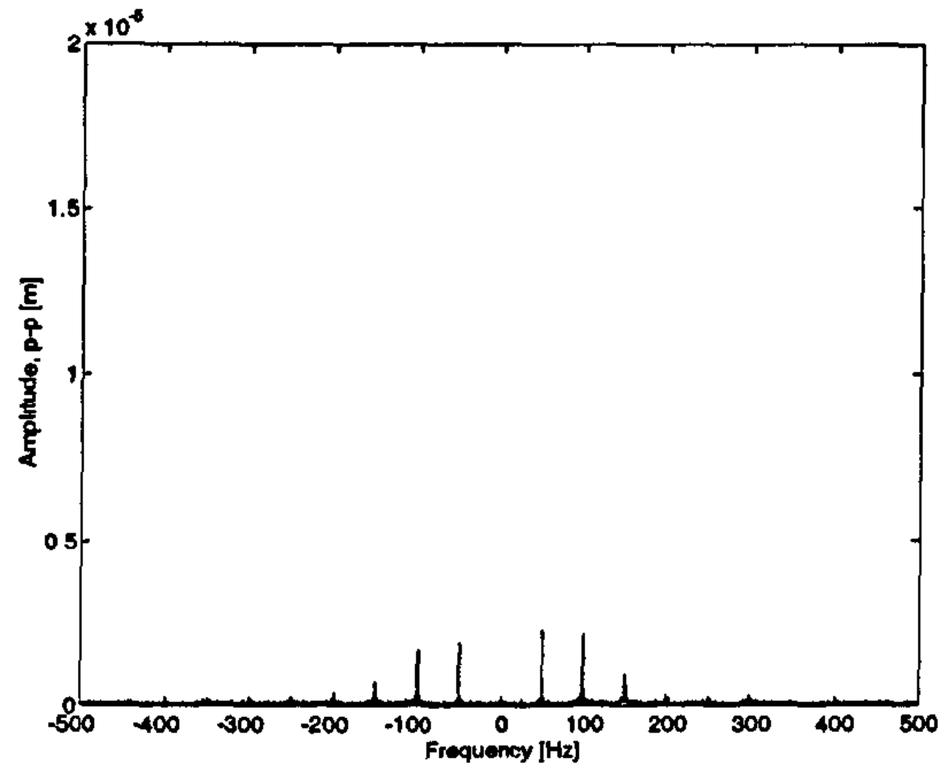
(d) 400 mg, Static 90°



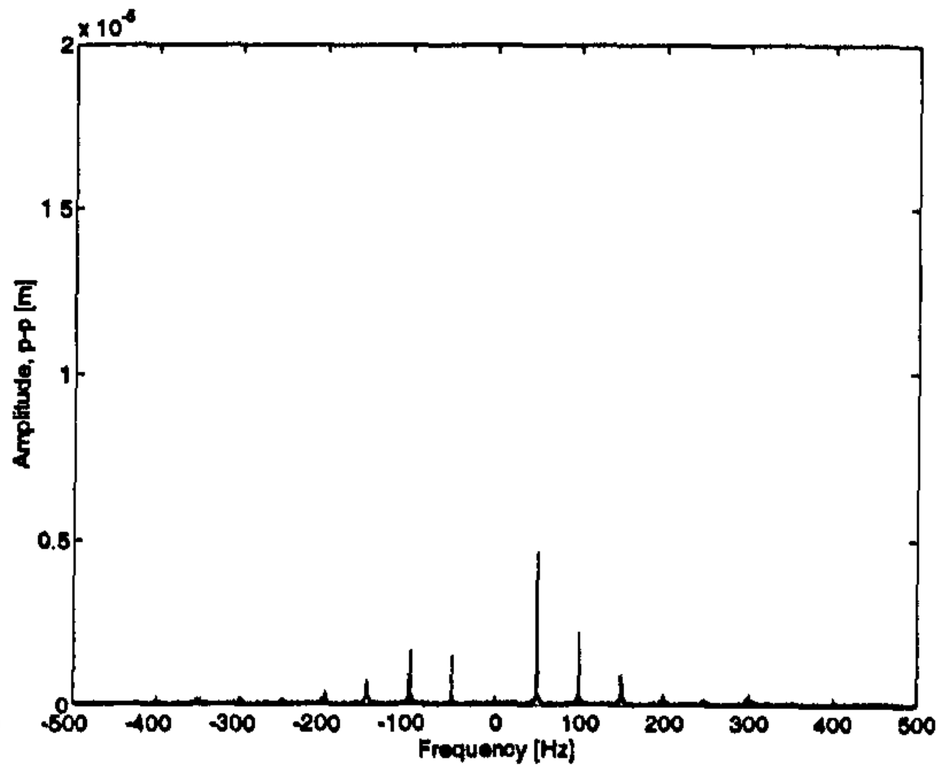
(e) 200 mg, Static 180°



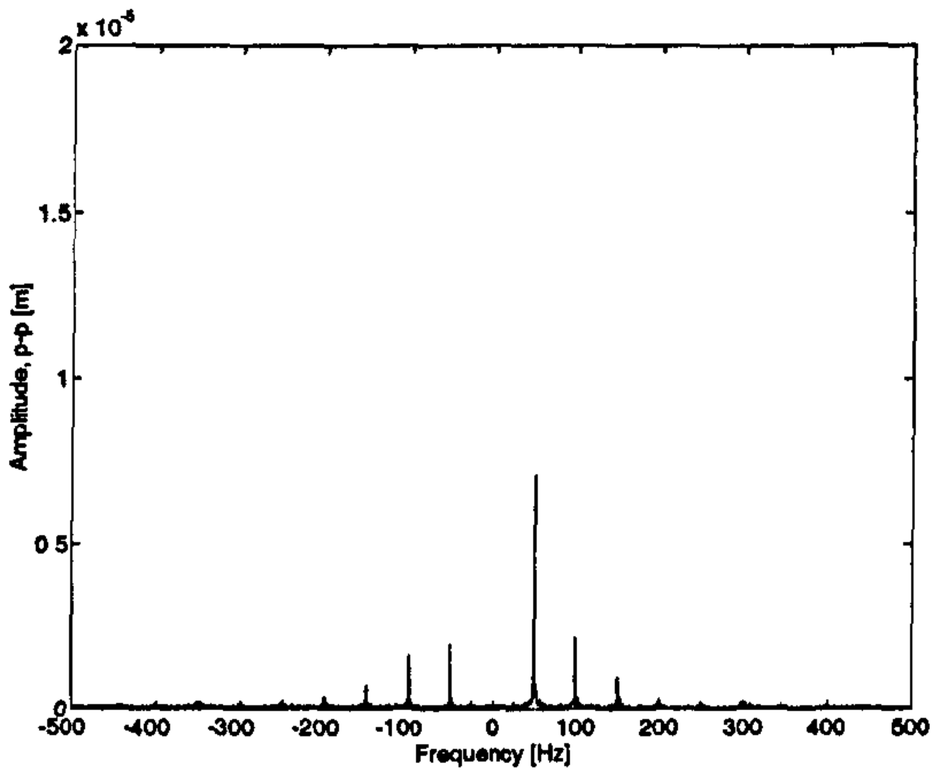
(f) 400 mg, Static 180°



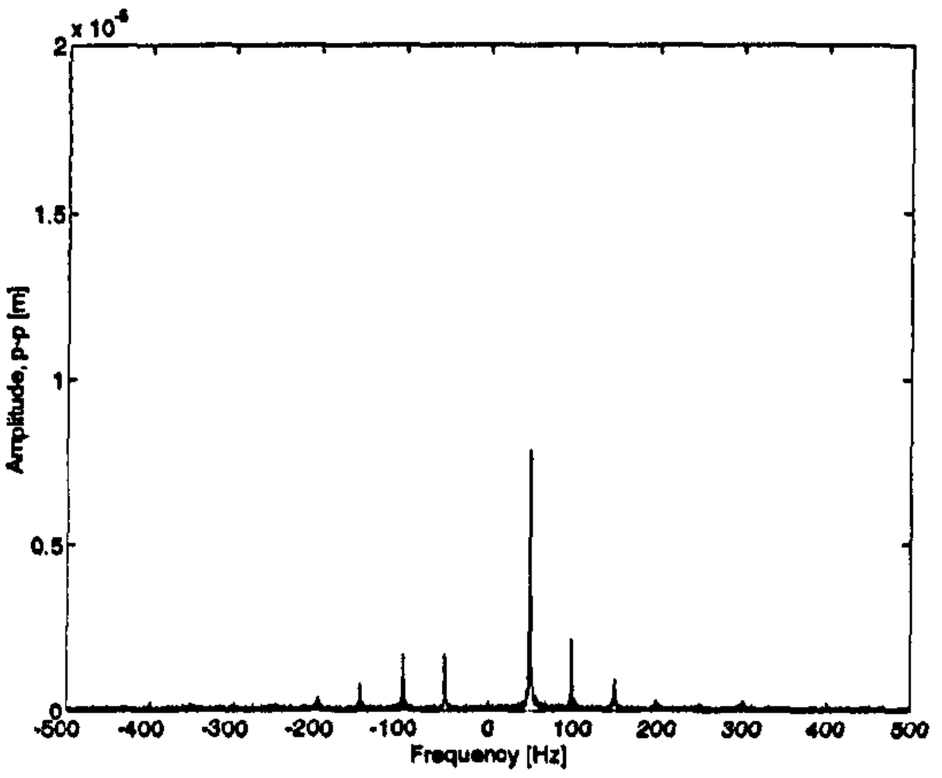
(g) 200 mg, Couple 0°



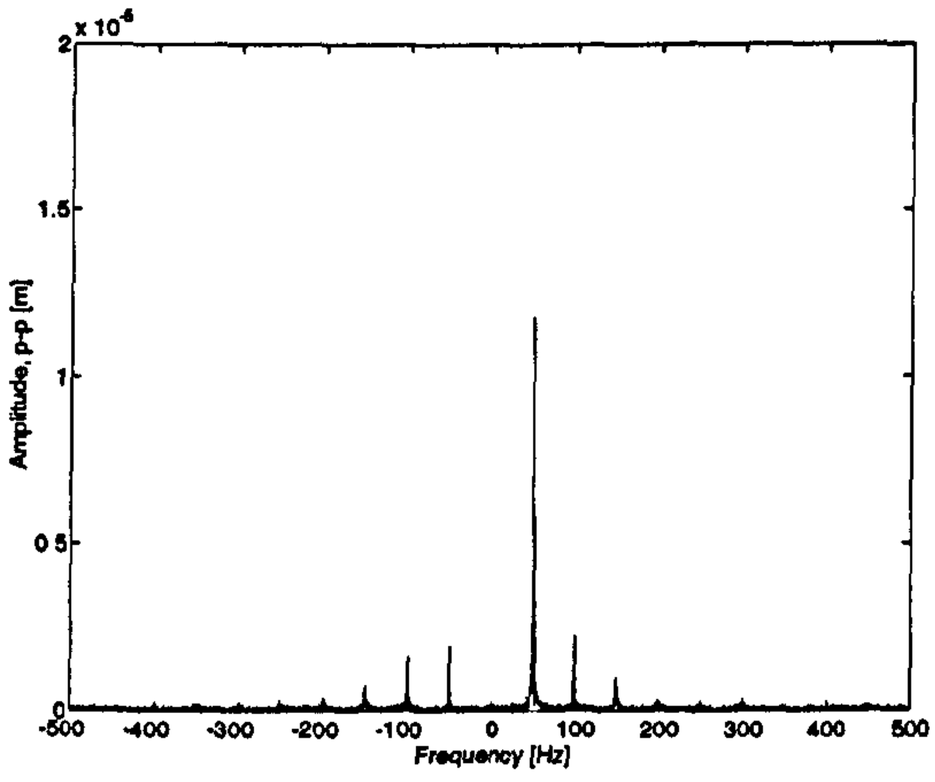
(h) 400 mg, Couple 0°



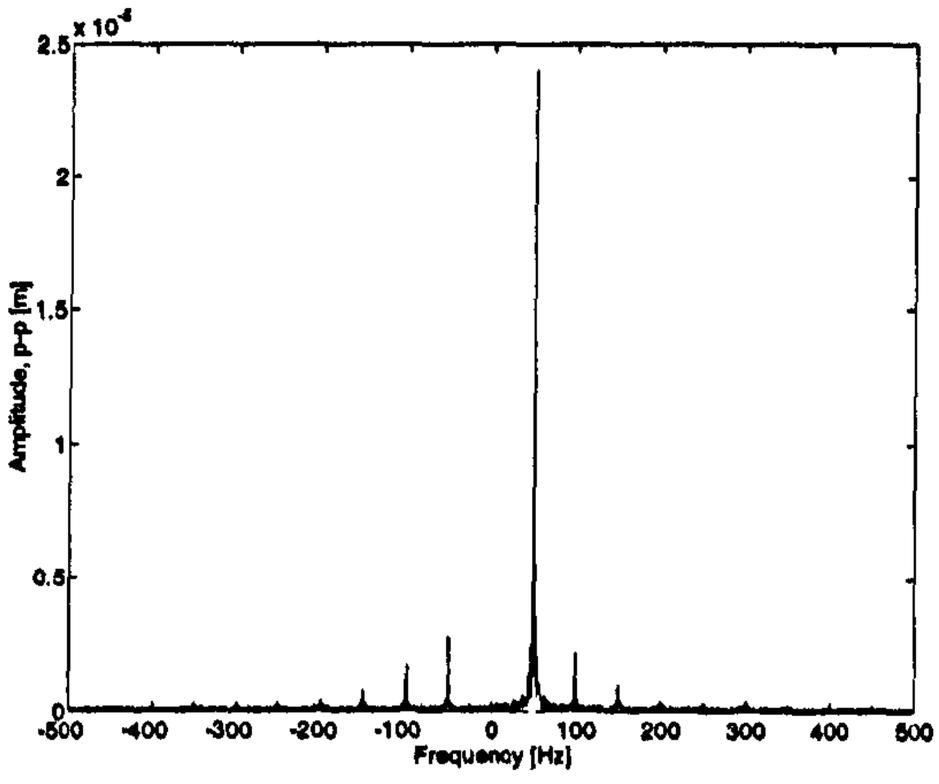
(i) 200 mg, Couple 90°



(j) 400 mg, Couple 90°



(k) 200 mg, Dynamic



(l) 400 mg, Dynamic

Fig 5.5.9 Effect of Unbalance on the Cracked Rotor System

5.6 Conclusions

With the cracked rotor rig, the following phenomena have been explored experimentally:

(i) effect of crack extent

(ii) effect of crack location

(iii) relationship between crack and unbalance

(iv) application of newly-developed crack detection techniques

• Effect of Crack Extent

The effect of crack extent on vibration characteristics has been investigated experimentally with 10 % and 20 % crack depths gradually introduced to a normal shaft. With the introduction of a crack, the 2Ω harmonic component starts to appear and induces a sub-resonance when the rotor is running up to its designated speed. From the rotor's steady-state response, the increase of $\pm 1\Omega$ components, together with higher harmonics, could be identified as being due to increased crack depth, as has been predicted with the new crack modelling concept presented in Chapter 3. This fact suggests that the $\pm 1\Omega$ vibration components also should be carefully inspected to increase the possibility of crack detection, which is unlikely with conventional crack detection methods that usually rely on only the 2Ω harmonic component.

• Effect of Crack Location

The sensitivity of the crack-related harmonics has been investigated experimentally with different crack locations (mid-span and outboard). As has been predicted and discussed in the analytical research, so also in the experiments, when the crack is located near the bearing, the crack-related higher harmonics (2Ω, 3Ω, $\cdots$) were revealed to be more sensitive - compared with the mid-span cracked rotor - due to the

effect of the support (or bearing) interacting with the rotor system. Also, in both cases, the growing property of the crack-related harmonics (according to the increase of crack depth) was identified as an important discriminating factor between cracks and other faults in the rotating machinery.

• Relationship between Crack and Unbalance

By using various forms of trial mass as a controlled unbalance, the effect of unbalance on the cracked rotor has been investigated for the 20 % cracked rotor in its steady-state condition as unbalance is the most common problem in rotating machinery. In all experimental cases studied, only the $\pm 1\Omega$ vibration components were changed with increase of the unbalance masses with virtually no influence on higher-harmonic vibration components, suggesting the independence of crack-related higher harmonics and the unbalance-related $\pm 1\Omega$ vibration components.

• Application of Developed Crack Detection Techniques

The new methods (or approaches) for crack detection have been applied to evaluate the performance when the methods are applied to measured vibration data.

For transient vibration data, the directional harmonic wavelet transform provided quite a compact information (in the time-*wavelet level* region) which is sensitive to local changes in the vibration response of the rotor system. As a result, the crack-induced sub- and fundamental resonances could have been accurately detected by applying the DHWT. Considering the fact that the crack-related resonances are the most representative symptoms used to detect cracks in operating rotors for run-up or run-down conditions, the DHWT technique is considered to be an important new tool for crack detection.

For steady-state vibration data, the DDVSA has been applied for both mid-span and outboard cracked rotors. In both cases, using the normal rotor's vibration signature as baseline data, the crack-related directional-difference vibration components ($\pm 1\Omega$, $\pm 2\Omega$, and $\pm 3\Omega$) were successfully extracted for increasing crack depth. With these directional-difference vibration signatures, it becomes possible to estimate the growth-rate of crack-related harmonics explicitly for reliable crack detection.

In both methods, the performance has been greatly enhanced by decomposing the vibration components from rotating machinery into co- and counter-rotating components, which is a major feature that enables one to overcome the limitations of existing conventional methods.

Chapter 6
Industrial Application Case Study

6.1 Introduction

In this chapter, in order to verify the field-applicability of the developed crack detection techniques, the performance of the methods has been evaluated with simulated vibration data of an industrial 250 MW high & intermediate pressure (HIP) steam turbine rotor model for power generation.

Generally, power industry turbomachines are supported by fluid-film bearings to ensure low level of vibration during operation. Due to this reason, the rotordynamic characteristics of turbomachines are strongly influenced by the bearings:

(i) as the stiffness of the rotor-bearing system is mainly determined by the bearing stiffnesses which act in series with shaft stiffness, and

(ii) the damping of the system is usually determined almost entirely by the bearing damping properties.

Due to the large amount of damping introduced by the bearings and its masking effect, the possibility of crack detection has always been limited with the conventional crack detection methods. In this regard, it is required to evaluate the performance of the developed crack detection techniques to check the applicability to such field situations.

6.2 Model Description

As an industrial case study model, the Inchon thermal power plant (250 MW generator output, operated by Korea Electric Power Corporation) No 1 High & Intermediate Pressure (HIP) steam turbine rotor has been selected. As presented in Table 6.2.1, the HIP turbine has total weight of 17.7 ton, total length of 6633 mm, and has 7 stages for the high-pressure and 5 stages for the intermediate-pressure turbine sections in one rotor structure. At the end of the high-pressure turbine section, the main oil pump (MOP) is connected, and the intermediate-pressure turbine is connected to one of two low-pressure turbines via a coupling. Also, the HIP turbine rotor is supported by two elliptical journal bearings, and one thrust bearing is installed at the intermediate-pressure turbine rotor section to support the axial-direction thrust force during operating conditions. In Fig 6.2.1, HIP turbine rotor model is presented in the form of a finite element model.

Table 6.2.1 Specifications of High & Intermediate Pressure Turbine

Component	Type	Dimension	No	Material
Rotor	hollow drum	No 1 Bearing Journal 280.0 mmϕ × 178.0 mm$L$ No 2 Bearing Journal 355.6 mmϕ × 228.6 mm$L$	1	1.25 % Cr 1.10 % Mo 0.25 % V Steel
Bearing	elliptical	No 1 Bearing Minimum Clearance: 0.18 mm No 2 Bearing Minimum Clearance: 0.24 mm	2	WJ2
Note	total weight total length 1st critical speed	17.7 ton 6633 mm 2270 rpm		

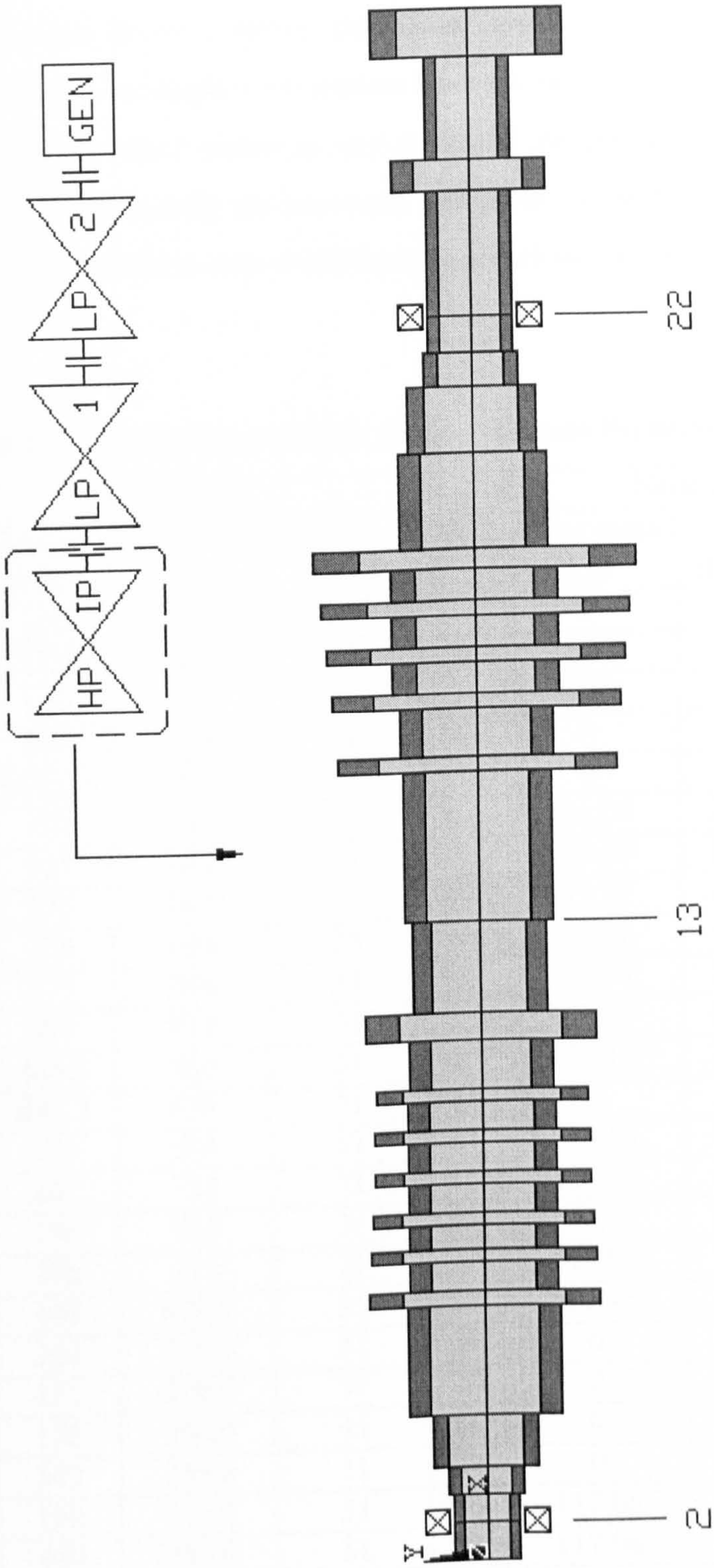


Fig 6.2.1 FE Model of the HIP Steam Turbine Rotor

To perform a vibration analysis, the model has been discretised into 25 beam elements, with 26 nodes. Hence, the model has total of 104 degrees of freedom (as the axial and torsional degrees of freedom have not been considered). The turbine blades have treated as added masses at each node and the gyroscopic effects have also been considered by including the transverse and polar moment of inertia into the analysis scheme. The structural data of HIP turbine model are presented in Table 6.2.2.

Table 6.2.2 Rotor Data of High & Intermediate Pressure Turbine

Element Data				Node Data			
No	length (mm)	outer dia. (mm)	inner dia. (mm)	No	added mass (kg)	I (kg mm^2)	J (kg mm^2)
1	160	280	68	1	0	0	0
2	117.98	280	31	2	0	0	0
3	110	320	31	3	0	0	0
4	220	450	31	4	0	0	0
5	500.02	650	31	5	0	0	0
6	185	644	31	6	231.05	2.053e7	4.090e7
7	157	644	31	7	181.09	1.572e7	3.135e7
8	175	644	31	8	175.27	1.502e7	2.995e7
9	175	644	31	9	169.48	1.437e7	2.867e7
10	175	644	31	10	164.92	1.384e7	2.760e7
11	297	614	31	11	131.78	1.098e7	2.192e7
12	446.7	568	31	12	453.11	3.773e7	7.412e7
13	681.3	638	31	13	0	0	0
14	271	664	31	14	380.53	4.469e7	8.914e7
15	201	714	31	15	386.72	4.914e7	9.803e7
16	196	714	31	16	450.71	6.036e7	1.204e8
17	206	714	31	17	519.03	7.261e7	1.448e8
18	446	629.6	31	18	696.45	1.041e8	2.074e8
19	280	559.6	31	19	0	0	0
20	152	399.6	31	20	0	0	0
21	158	355.6	31	21	0	0	0
22	542	355.6	31	22	0	0	0
23	126	355.6	31	23	117.08	0	0
24	440	355.6	31	24	117.08	0	0
25	215	473.13	31	25	307.67	0	0
				26	307.67	0	0

6.3 Fluid-Film Bearing Characteristics

The stiffness of the rotor-bearing system is mainly determined by the bearing stiffnesses which act in series with shaft stiffness. Also, the damping of the system is usually determined almost entirely by the bearing damping properties. Due to these reasons, the vibration characteristics of turbomachines are strongly influenced by the bearings which support the rotor.

In some types of fluid bearing, as well as in seals, cross-coupled stiffness and damping exist (which do not appear in ball bearings) in addition to the direct stiffness and damping effects. Also, this cross-coupling can have significant effects on the rotordynamic properties, especially whirl stability.

To analyse the dynamic behaviour of a rotor system supported by fluid-film bearings, the fluid-film pressure forces must be known a priori. Also, these forces can be described by using linearised stiffness and damping coefficients. To define the linearised stiffness and damping coefficients, static equilibrium position of the journal has to be calculated first.

6.3.1 Static Equilibrium of Journal supported by Fluid-Film Bearings

The static equilibrium position of the journal under a unidirectional load (such as rotor weight) can be calculated by setting components of the load equal to integrals of the hydrodynamic fluid-film pressure, p, over the surface of the journal. The distribution of p is obtained by solving the Reynolds equation under a boundary condition that applies for the pressure at the peripheries of the oil film. This condition is not fully known or settled yet, because of the complexity of rupture or cavitation of oil film. At present the most widely-accepted assumption on this condition is the

Reynolds boundary condition, which requires that the pressure gradient vanishes at the end of the positive pressure region.

Fig 6.3.1 shows a journal in its static equilibrium position, where the journal is supported by journal bearings and rotating with a constant rotational speed, Ω. The journal is assumed to be loaded vertically and downwards by an external force of constant magnitude, W. In its equilibrium position, the resultant force P of pressure p is balanced with the external load W. Generally, due to the asymmetrical distribution of p against the line $\overline{O_B O_J}$, the centre O_J of the journal does not move vertically or in the direction of the applied load, but shifts along a sort of semicircle when the load or rotational speed is changed.

For rotordynamic analysis, the equilibrium position is important as the starting point as the dynamic forces exerted by the bearing must be evaluated for motions away from the equilibrium position.

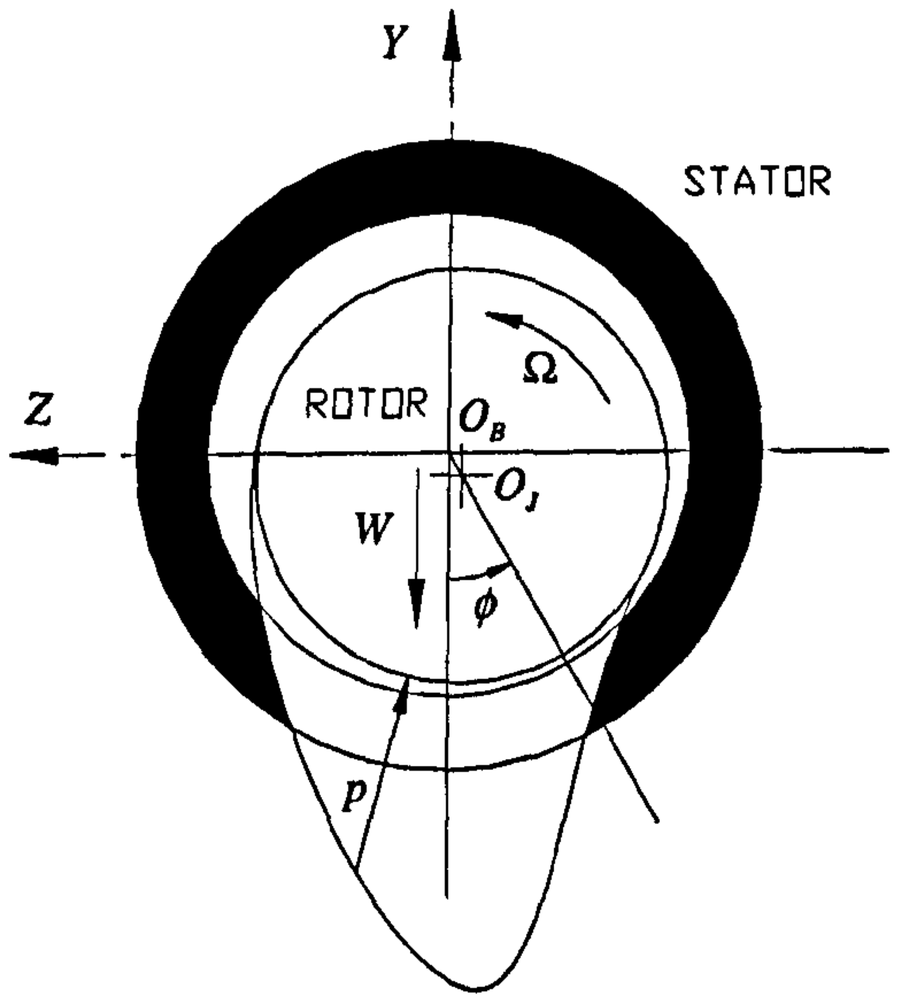


Fig 6.3.1 Static Equilibrium of Journal Bearing

6.3.2 Linearised Bearing Force Coefficients

When the centre of a rotor supported by a journal bearing moves (or vibrates) in the clearance circle, squeeze film pressure is also generated in addition to the wedge film pressure. These pressures give rise to non-linear spring and damping forces in the oil film as the resultant force of oil film pressure acting on the journal varies. The components F_y and F_z of oil film force can be expressed as functions of coordinates y and z of the journal centre O_J and its velocity components $\dot{y}$ and $\dot{z}$:

$$F_y = F_y(y,\ z,\ \dot{y},\ \dot{z}) \tag{6.3.1}$$

$$F_z = F_z(y,\ z,\ \dot{y},\ \dot{z}) \tag{6.3.2}$$

Functions on the right-hand side of equation (6.3.1) and (6.3.2) are not linear in each variable, but can be approximated with sufficient accuracy by a Taylor series of the 1st-order when vibration of the journal occurs in the vicinity of the static equilibrium position and both amplitude and velocity are negligibly small.

Thus, expressing oil film force as a vector:

$$\boldsymbol{F} = \begin{Bmatrix} F_y \\ F_z \end{Bmatrix} \tag{6.3.3}$$

Then, the following equations can be obtained:

$$\boldsymbol{F} = \boldsymbol{F}_0 + \Delta\boldsymbol{F} \tag{6.3.4}$$

$$\Delta\boldsymbol{F} = [\boldsymbol{k}]\begin{bmatrix} \Delta y \\ \Delta z \end{bmatrix} + [\boldsymbol{c}]\begin{bmatrix} \Delta\dot{y} \\ \Delta\dot{z} \end{bmatrix} \tag{6.3.5}$$

where the suffix '0' denotes static equilibrium and 'Δ' stands for small increments in the variables. Symbols $[\boldsymbol{k}]$ and $[\boldsymbol{c}]$ on the right-hand side of equation (6.3.5) are matrices with two rows and columns and are defined as follows:

$$[\boldsymbol{k}] = \begin{bmatrix} k_{yy} & k_{yz} \\ k_{zy} & k_{zz} \end{bmatrix} = \begin{bmatrix} \frac{\partial F_y}{\partial y} & \frac{\partial F_y}{\partial z} \\ \frac{\partial F_z}{\partial y} & \frac{\partial F_z}{\partial z} \end{bmatrix}_0 \tag{6.3.6}$$

as the spring coefficient matrix of oil film, and

$$[\boldsymbol{c}] = \begin{bmatrix} c_{yy} & c_{yz} \\ c_{zy} & c_{zz} \end{bmatrix} = \begin{bmatrix} \frac{\partial F_y}{\partial \dot{y}} & \frac{\partial F_y}{\partial \dot{z}} \\ \frac{\partial F_z}{\partial \dot{y}} & \frac{\partial F_z}{\partial \dot{z}} \end{bmatrix}_0 \tag{6.3.7}$$

as the damping coefficient matrix of oil film.

Here, the first suffix i ($= y$ or z) of elements k_{ij} and c_{ij} represents the direction of the oil film force, whereas the second, j ($= y$ or z, $\dot{y}$ or $\dot{z}$), represents the direction of displacement or the velocity of the journal centre.

Further, k_{ij} are the spring coefficients, and c_{ij} are the damping coefficients of the oil film. These coefficients are dimensional, and are usually made dimensionless as follows:

$$\boldsymbol{K} = \begin{bmatrix} K_{yy} & K_{yz} \\ K_{zy} & K_{zz} \end{bmatrix} = \frac{C_m}{W}[\boldsymbol{k}] \tag{6.3.8}$$

$$\boldsymbol{C} = \begin{bmatrix} C_{yy} & C_{yz} \\ C_{zy} & C_{zz} \end{bmatrix} = \frac{C_m \Omega}{W}[\boldsymbol{c}] \tag{6.3.9}$$

These dimensionless coefficients of the oil film force are functions of the Sommerfeld number S_o:

$$S_o = \frac{\mu \Omega D L}{\phi^2 W} \tag{6.3.10}$$

or the eccentricity ratio:

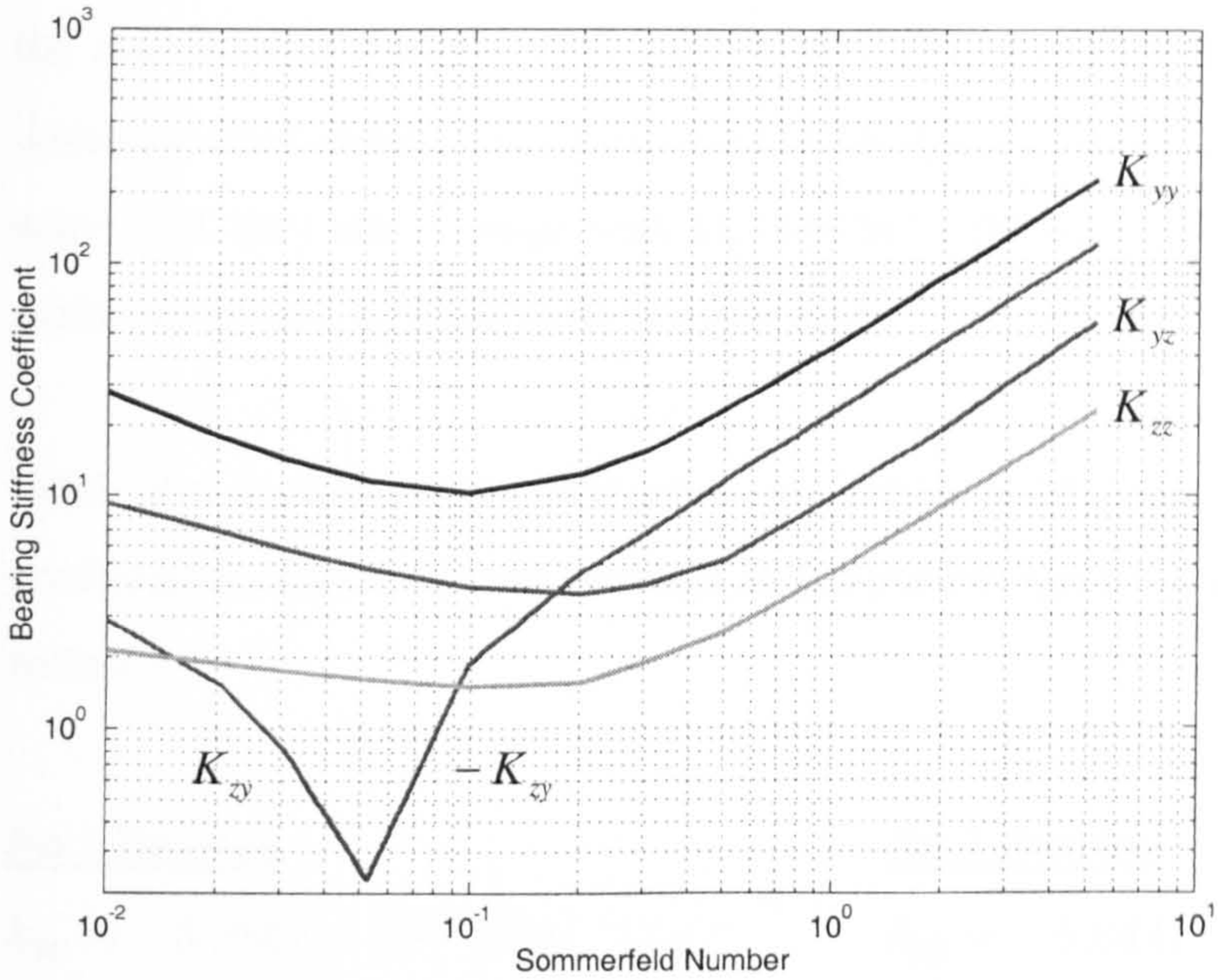
$$\epsilon = \varepsilon / C_a \tag{6.3.11}$$

for a given set of geometrical parameters of a bearing such as bearing length-to-diameter ($L:D$) ratio. They are also called dynamic characteristics of oil film in journal bearings or simply dynamic characteristics of journal bearings.

6.3.3 Characteristics of Elliptical Bearing

As the HIP steam turbine rotor is supported by two elliptical (or 2-lobe) bearings with different geometry, the rotordynamic analysis code VARS (refer to Chapter 3) has been updated to incorporate the complete modelling of fluid-film bearings. The updated code allows one to model virtually any type of fluid-film bearings, provided that the eccentricity, the attitude angle, and the eight bearing coefficients (four stiffness and four damping coefficients) are known functions of the Sommerfeld number. For every rotation speed (or for every time step), the bearing coefficients are estimated by the code which computes the working conditions of the bearings by solving a non-linear static problem and then linearising the behaviour of the bearing about the static equilibrium position. For elliptical bearings, the required data are available in the form of a table [133] where all data entries are provided in nondimensional parameters.

Fig 6.3.2 shows the elliptical (or 2-lobe) bearing data used in the simulation in the form of nondimensional parameters as functions of the Sommerfeld number. As can be seen in Fig 6.3.2-(a), there exist cross-coupled stiffnesses, k_{yz} and k_{zy}, which make the stiffness matrix non-symmetric and sometimes cause bearing instability known as oil whirl or oil whip.



(a) Bearing Stiffness Coefficients (nondimensional)

(b) Bearing Damping Coefficients (nondimensional)

Fig 6.3.2 Elliptical Bearing Characteristics

Moreover, each stiffness term changes its value with rotor's speed of rotation (Ω) as the Sommerfeld number S_o is a function of Ω as expressed in equation (6.3.10). For damping coefficients, the cross-coupled damping terms (c_{yz} and c_{zy}) are much the same, but they also change with Ω, together with the direct damping terms, which make the system analysis quite complicated.

With the specifications presented in Table 6.2.1, the stiffness and damping coefficients of the elliptical bearings at designated operating speed - 3600 rpm - are as follows:

No 1 Bearing

$k_{yy} = 5.2862 \times 10^9$ N/m
$k_{zz} = 0.6588 \times 10^9$
$k_{yz} = 1.5087 \times 10^9$
$k_{zy} = -2.1287 \times 10^9$
$c_{yy} = 1.7488 \times 10^7$ Ns/m
$c_{zz} = 0.3762 \times 10^7$
$c_{yz} = -0.3958 \times 10^7$
$c_{zy} = -0.3902 \times 10^7$

No 2 Bearing

$k_{yy} = 5.8442 \times 10^9$ N/m
$k_{zz} = 0.7277 \times 10^9$
$k_{yz} = 1.6628 \times 10^9$
$k_{zy} = -2.3610 \times 10^9$
$c_{yy} = 1.9348 \times 10^7$ Ns/m
$c_{zz} = 0.4169 \times 10^7$
$c_{yz} = -0.4410 \times 10^7$
$c_{zy} = -0.4349 \times 10^7$

6.4 Effect of Fluid-Film Bearings on Rotor Dynamics

The vibration of a rotor supported by journal bearings is much more complicated than that of one supported by ball bearings. This is mainly because the journal bearings significantly influence the motion of a rotor with considerable stiffness and damping which usually vary with operating speed of the rotor, while the ball bearing influences the vibration of a rotor only as a linear spring. In mathematical terms, the equations of motion of a rotor system supported by fluid-film bearings can be described as follows:

$$\boldsymbol{M}\,\ddot{\boldsymbol{q}}(t) + [\boldsymbol{C}_B(\Omega) + \boldsymbol{G}(\Omega)]\,\dot{\boldsymbol{q}}(t) + [\boldsymbol{K} + \boldsymbol{K}_B(\Omega)]\,\boldsymbol{q}(t) = \boldsymbol{F}(t) \tag{6.4.1}$$

where

$\boldsymbol{M}$	mass matrix of rotor
$\boldsymbol{C}_B(\Omega)$	bearing damping matrix, anisotropic & non-symmetric
$\boldsymbol{G}(\Omega)$	gyroscopic matrix, skew-symmetric
$\boldsymbol{K}$	stiffness matrix of rotor, becomes time-dependent, $\boldsymbol{K}(t)$, for cracked rotor
$\boldsymbol{K}_B(\Omega)$	bearing stiffness matrix, anisotropic & non-symmetric
$\boldsymbol{q}(t)$	displacement
$\boldsymbol{F}(t)$	external force

As can be noticed from the equation (6.4.1), almost all system properties (except mass) are changing with time (or speed), which makes the system non-linear.

Before dealing with the cracked rotor problem, the unbalance response of the HIP turbine rotor supported by elliptical fluid-film bearings has been investigated to understand its basic dynamic behaviour.

Fig 6.4.1 shows the elliptical vibration of the HIP rotor system excited by unbalance at its initial run-up stage. As can be been in the figure, the rotor orbit is vibrating horizontally due to the strong bearing stiffness anisotropy (as well as asymmetry) which might be expected from the stiffness characteristics presented previously in Fig 6.3.2-(a) which shows a smaller horizontal direction stiffness K_{zz} (i.e. more flexible in horizontal direction) than vertical direction stiffness K_{yy}.

At the resonance region, the change of whirl direction can be identified as Fig 6.4.2 shows. The change of whirl direction is; forward → backward → forward. Also, when the whirl direction is changing, a linear orbit can be identified (two linear orbits are marked with circles).

Fig 6.4.3 shows the vibration amplitude of the rotor during a run-up period and there exist double resonance peaks around the normalised rotational speed of $\Omega/\omega_s = 1.0$ (where ω_s is the reference natural frequency of the rotor system assumed to be rigidly supported) due to strong bearing stiffness anisotropy. The directional spectrogram in Fig 6.4.4 exhibits strong backward whirl component all through the run-up period also caused by strong bearing stiffness anisotropy which makes the motion of the shaft elliptical.

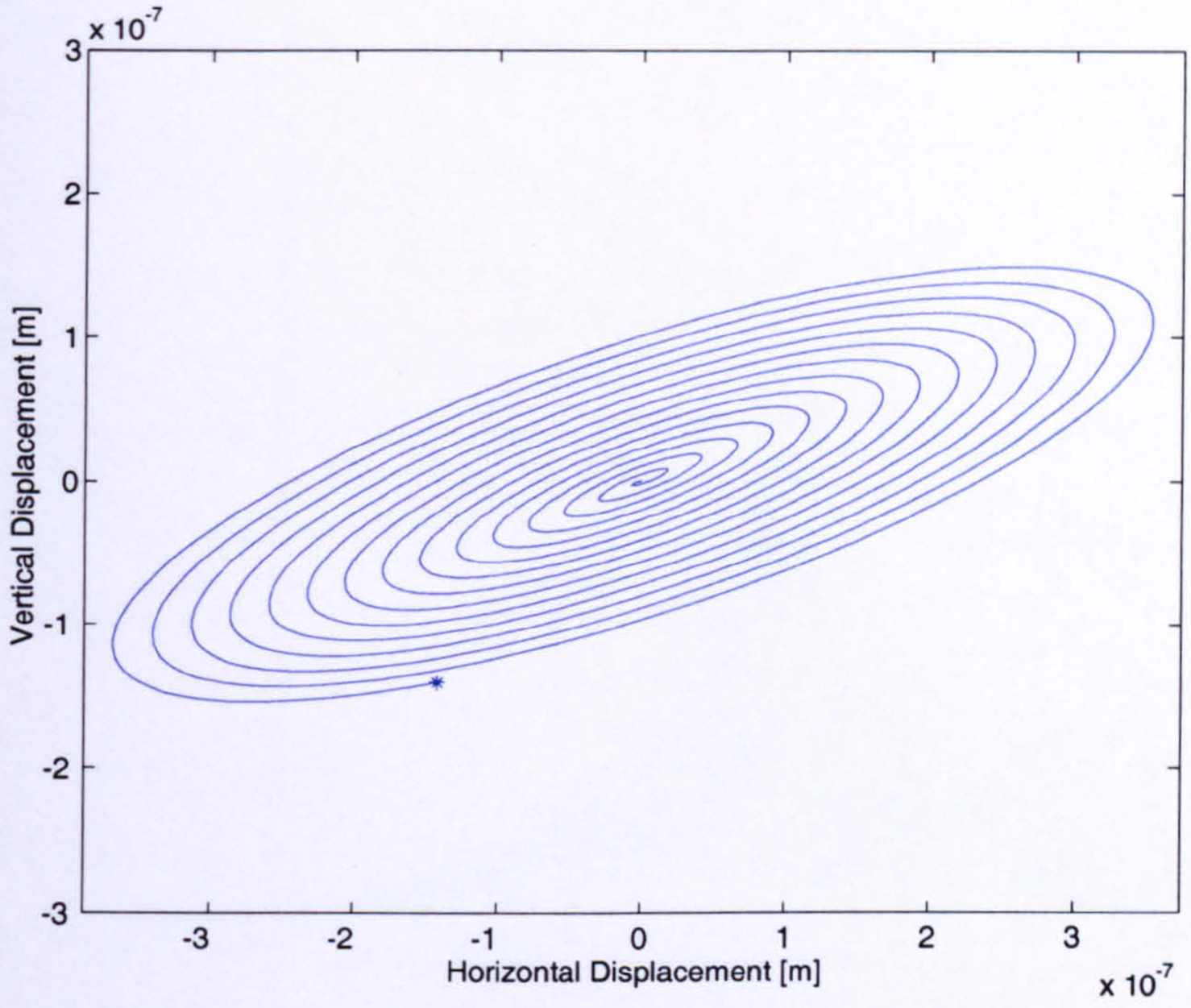


Fig 6.4.1 Elliptical Vibration (for Initial Run-up Stage)

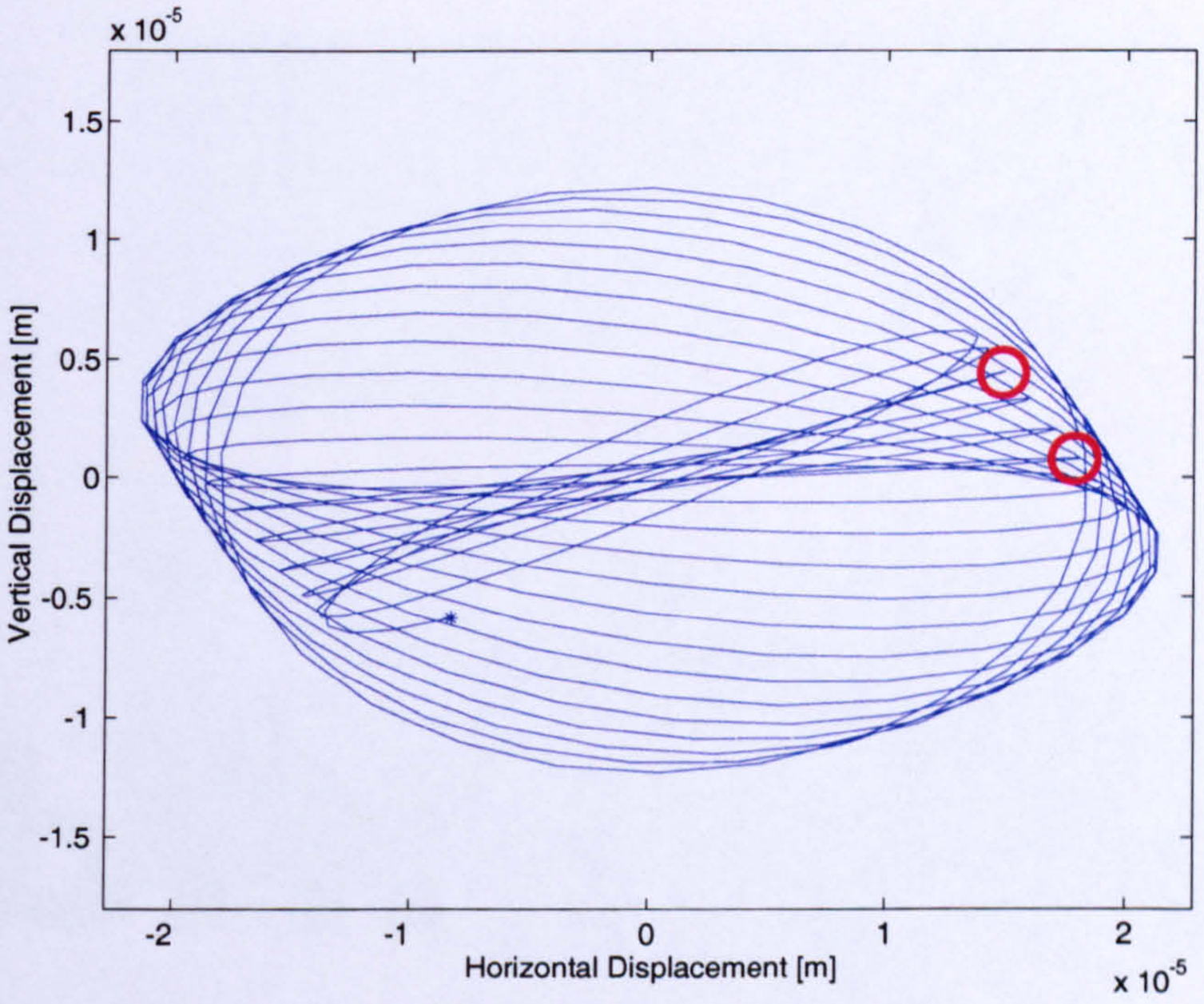


Fig 6.4.2 Forward and Backward Whirl at $\Omega/\omega_n = 1.0$

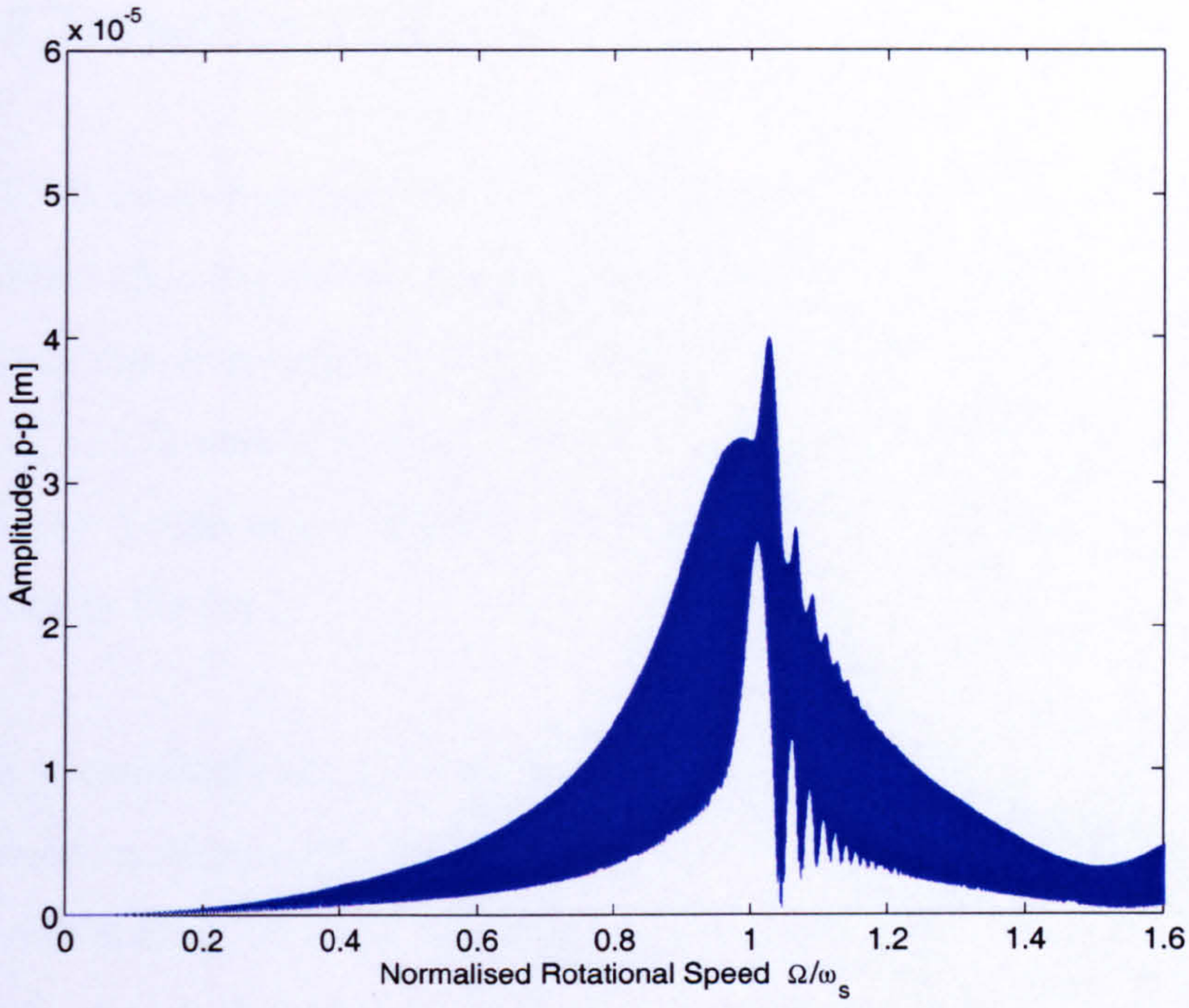


Fig 6.4.3 Unbalance Response

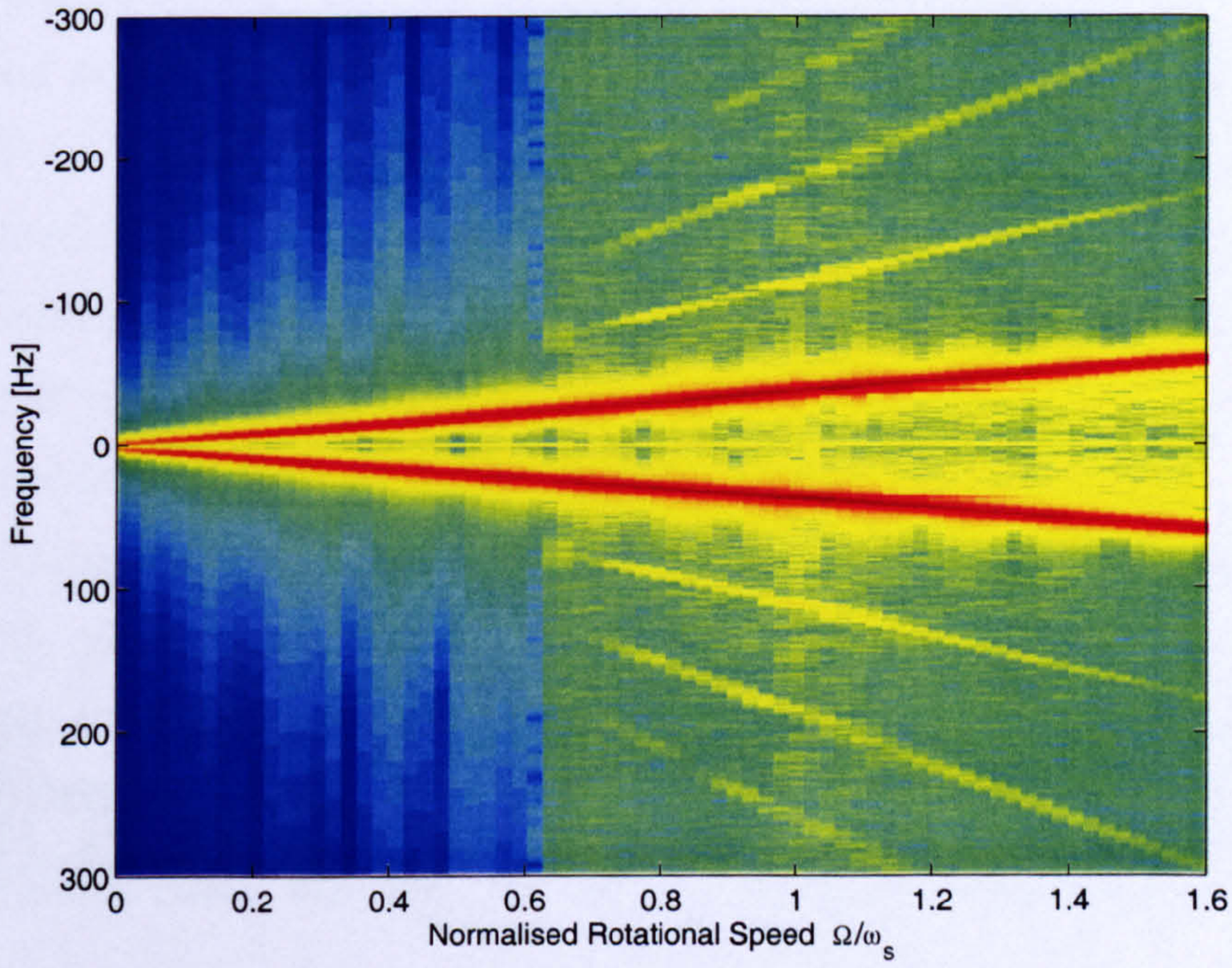


Fig 6.4.4 Unbalance Response in Speed-Frequency Distribution

6.5 Transient Vibration

A 10 % transverse crack has been induced to the HIP turbine rotor at mid-span (node number 13 in Fig 6.2.1). As can be seen in Fig 6.5.1, there now exist sub-resonances due to the occurrence of crack-related higher harmonics at the rotation speed of $\Omega/\omega_s = 1/3$ and $1/2$, while the unbalanced rotor has resonance only at the speed of $\Omega/\omega_s = 1$ (due to the synchronous 1Ω vibration component caused by unbalance) as shown in Fig 6.4.3.

The speed-frequency distribution in Fig 6.5.2 shows the existence of crack-related harmonics. Especially, -2Ω and -3Ω harmonic components are also very strong due to the bearing stiffness anisotropy. However, in the directional spectrogram (Fig 6.5.2), the crack-related resonances cannot clearly be identified due to the effect of substantial bearing damping which masks local changes in a vibration response.

The directional harmonic wavelet transform (DHWT) has been applied to the same set of data. As shown in Fig 6.5.3-(a), the sub-resonance at the rotation speed of $\Omega/\omega_s = 1/2$, and synchronous resonance at the speed of $\Omega/\omega_s = 1$, caused by the crack-related $+2\Omega$ and $+1\Omega$ harmonics respectively, can be clearly identified at wavelet level 10 (represents the frequency region where the natural frequency of the HIP rotor is included) in the forward directional wavelet map. In particular, in the backward directional wavelet map in Fig 6.5.3-(b), the recognisable sub-resonance (caused by -2Ω harmonic) at the speed of $\Omega/\omega_s = 1/2$ can be identified as well as the synchronous resonance (caused by -1Ω harmonic). This is considered to be invaluable information for crack detection as it will rarely exist in the vibration response of normal steam turbine rotors or hardly be generated by other common types of fault.

Under the effect of huge amounts of damping with fluid-film bearings (compared with that of the rotor supported by ball bearings), while the directional spectrogram has some resolution problem in identifying the crack-induced resonances, still the wavelet map could successfully detect the local changes (or resonances) caused by a crack. Hence, it can be concluded that the technique can be applied to the field situation where the vibration is usually suppressed by the large amount of damping level originated from the fluid-film bearings.

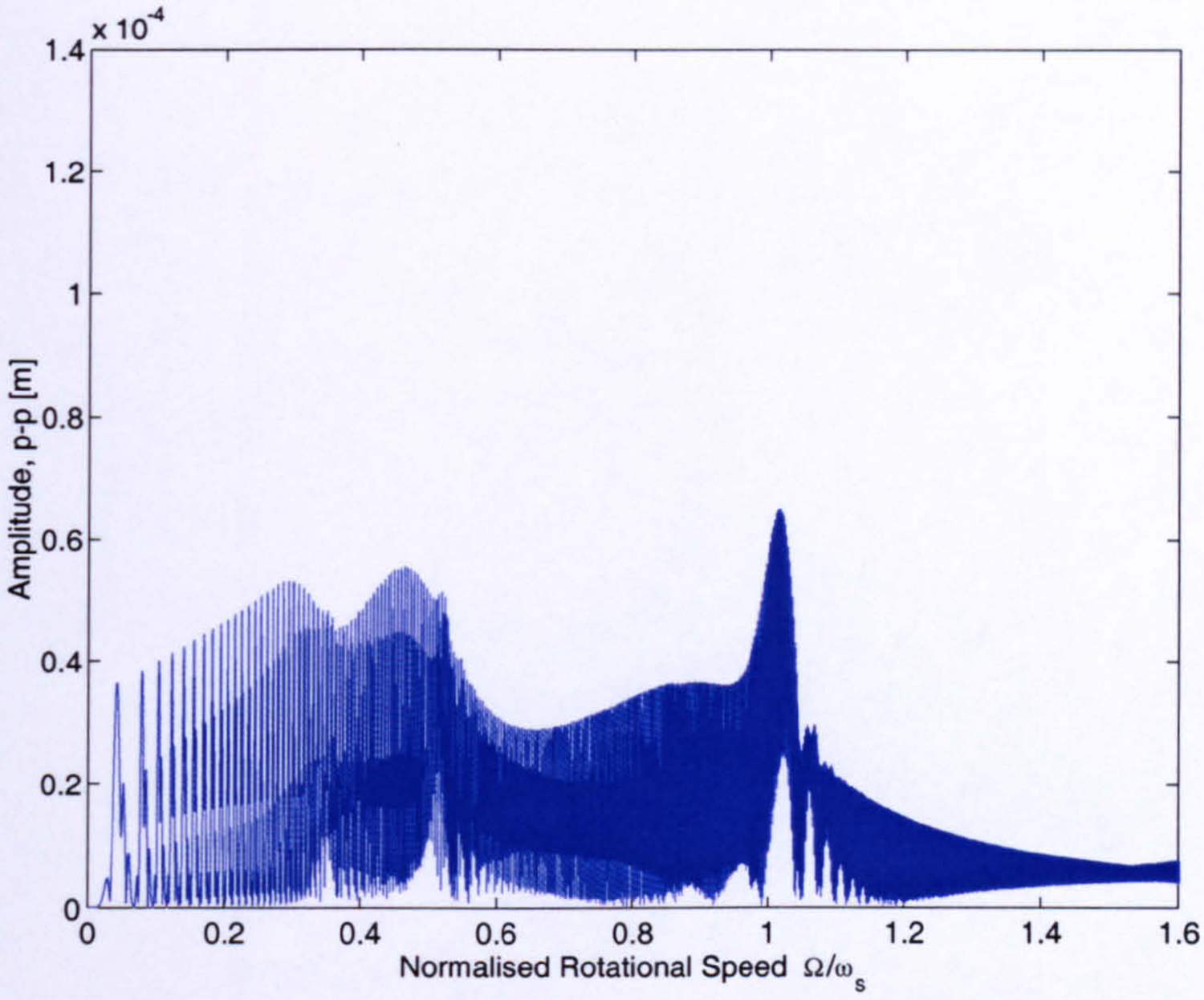


Fig 6.5.1 Vibration Amplitude of Cracked Rotor (10 %)

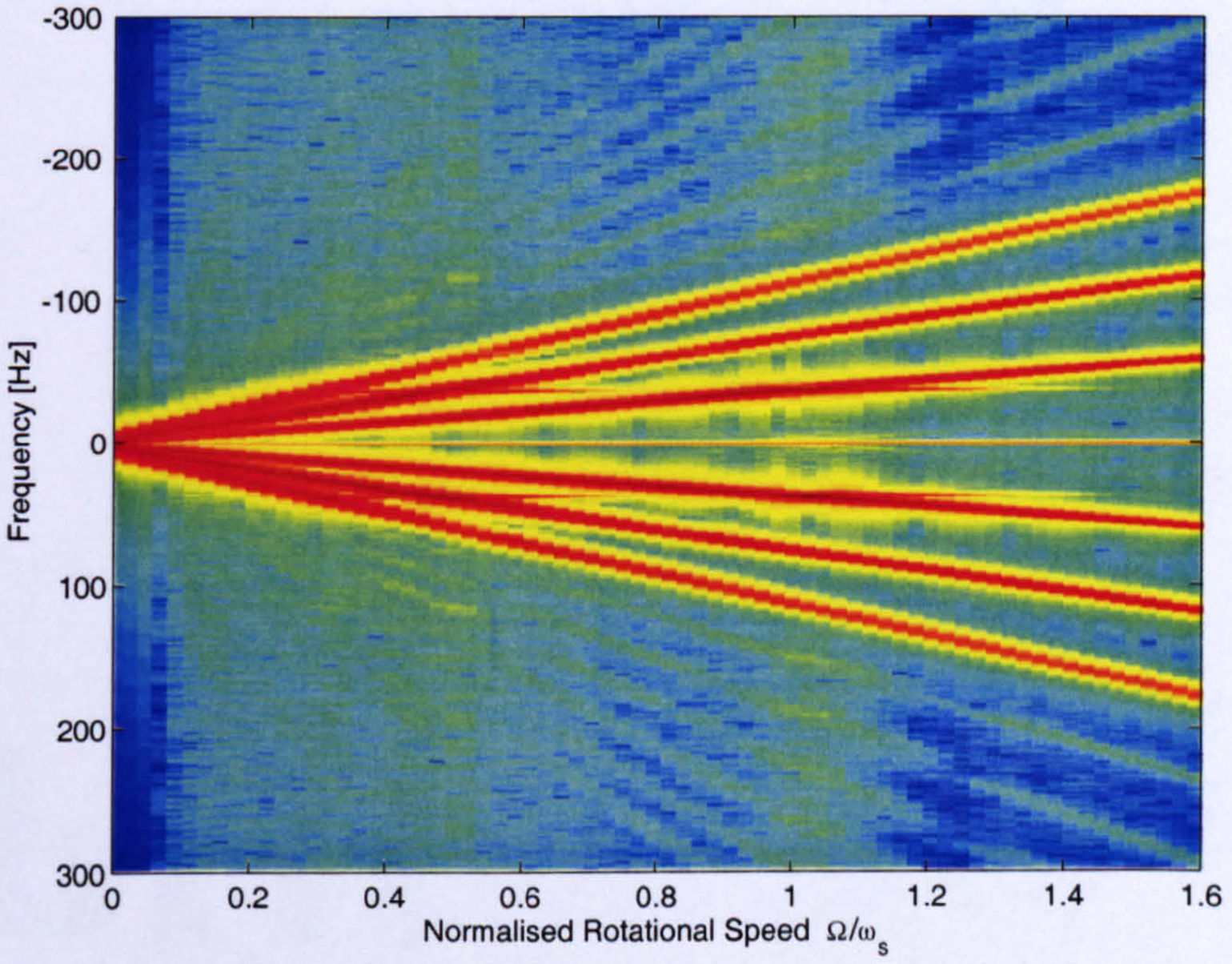
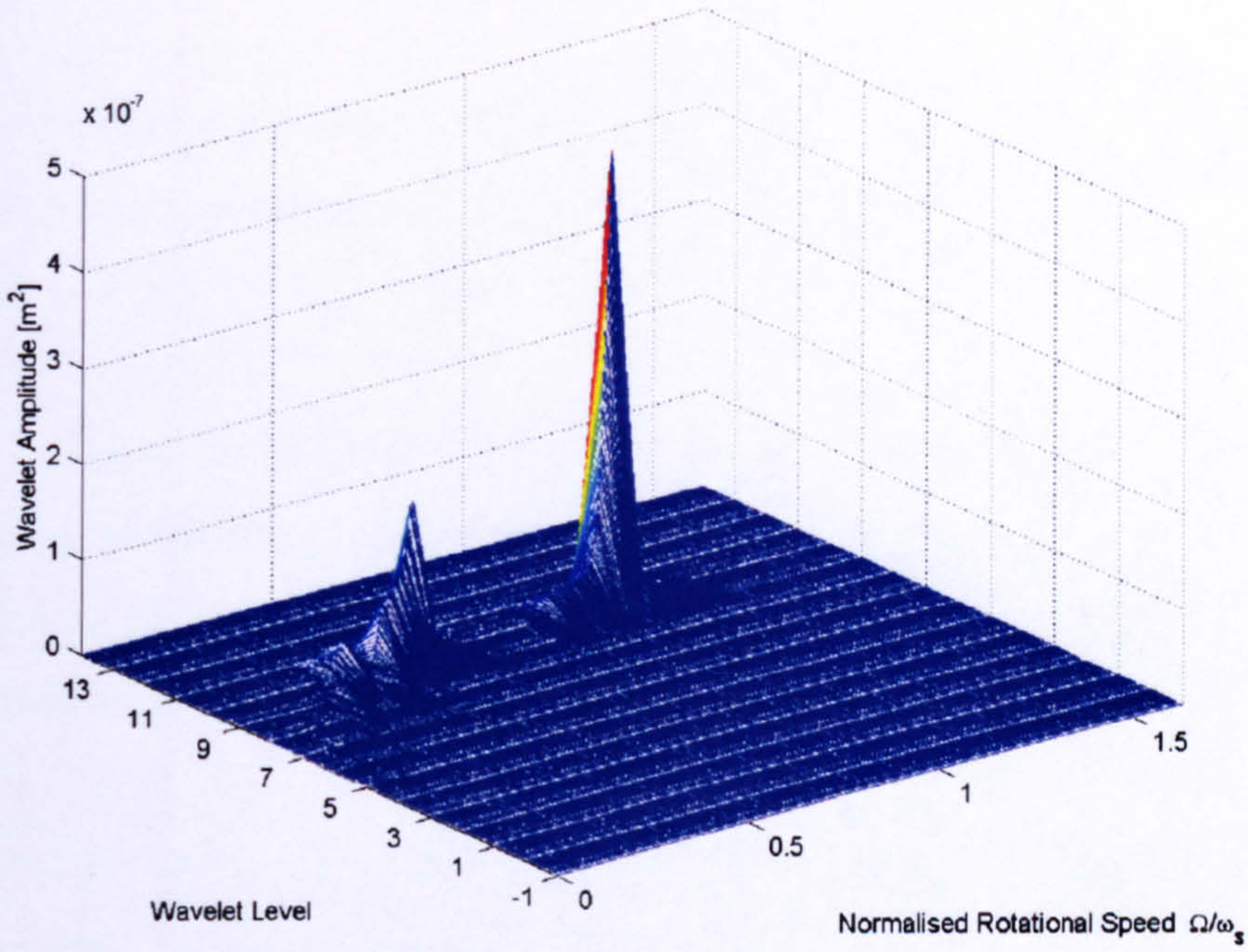
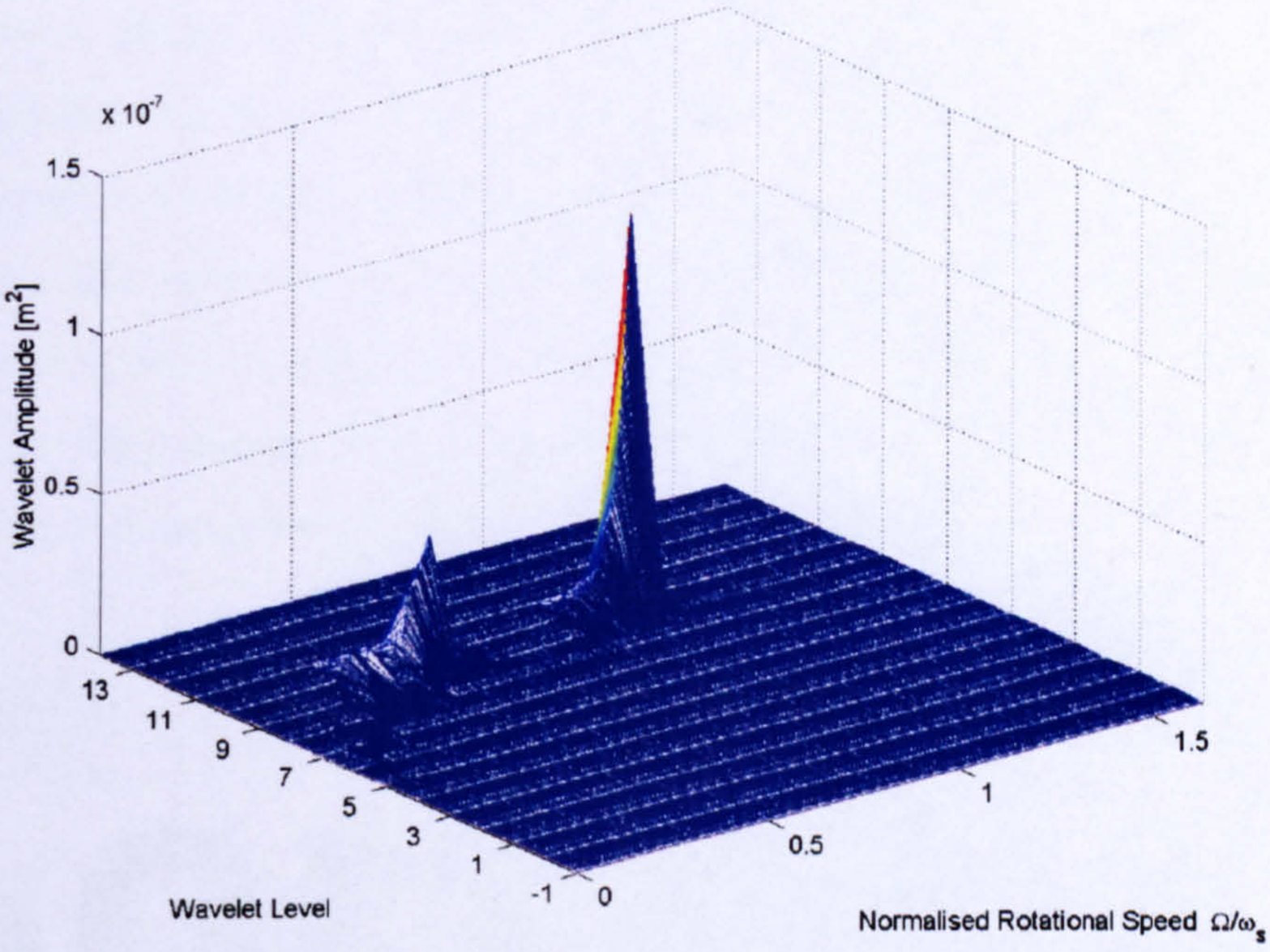


Fig 6.5.2 Speed-Frequency Distribution of Cracked Rotor (10 %)



(a) Forward Directional Wavelet Map



(b) Backward Directional Wavelet Map

Fig 6.5.3 Directional Wavelet Map of Cracked Rotor (10 %)

6.6 Steady Vibration

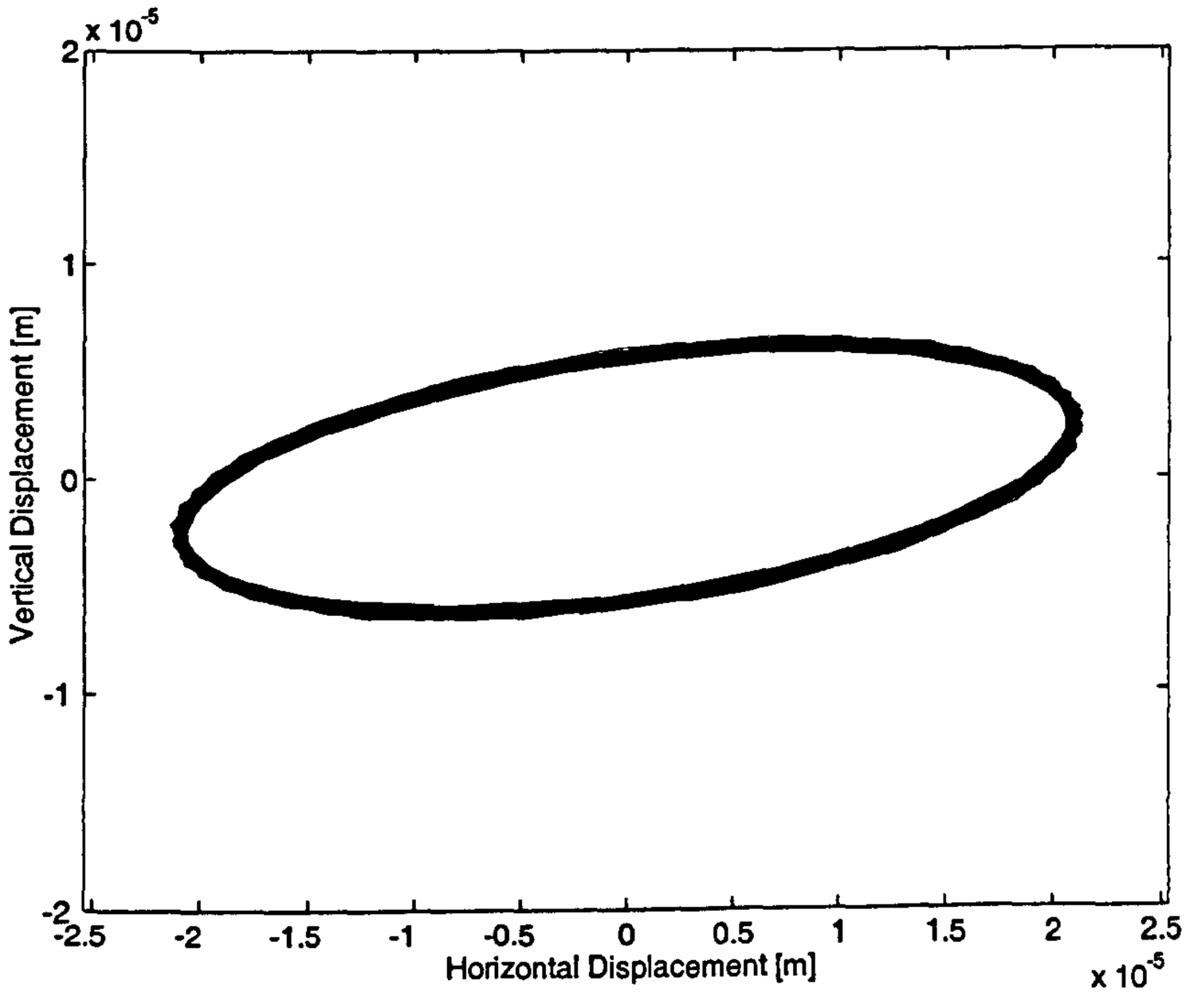
While the rotor is operating steadily at its designated speed (3600 rpm, or 60 Hz), the vibration has been computed at the location of No 1 bearing (node number 2 in the FE model).

Fig 6.6.1-(a) & (b) show an orbit of the normal rotor system with unbalance and its frequency components, respectively. Due to bearing stiffness anisotropy, the orbit exhibits an elliptical vibration, and in the directional frequency spectrum, a large backward whirl vibration component can be identified.

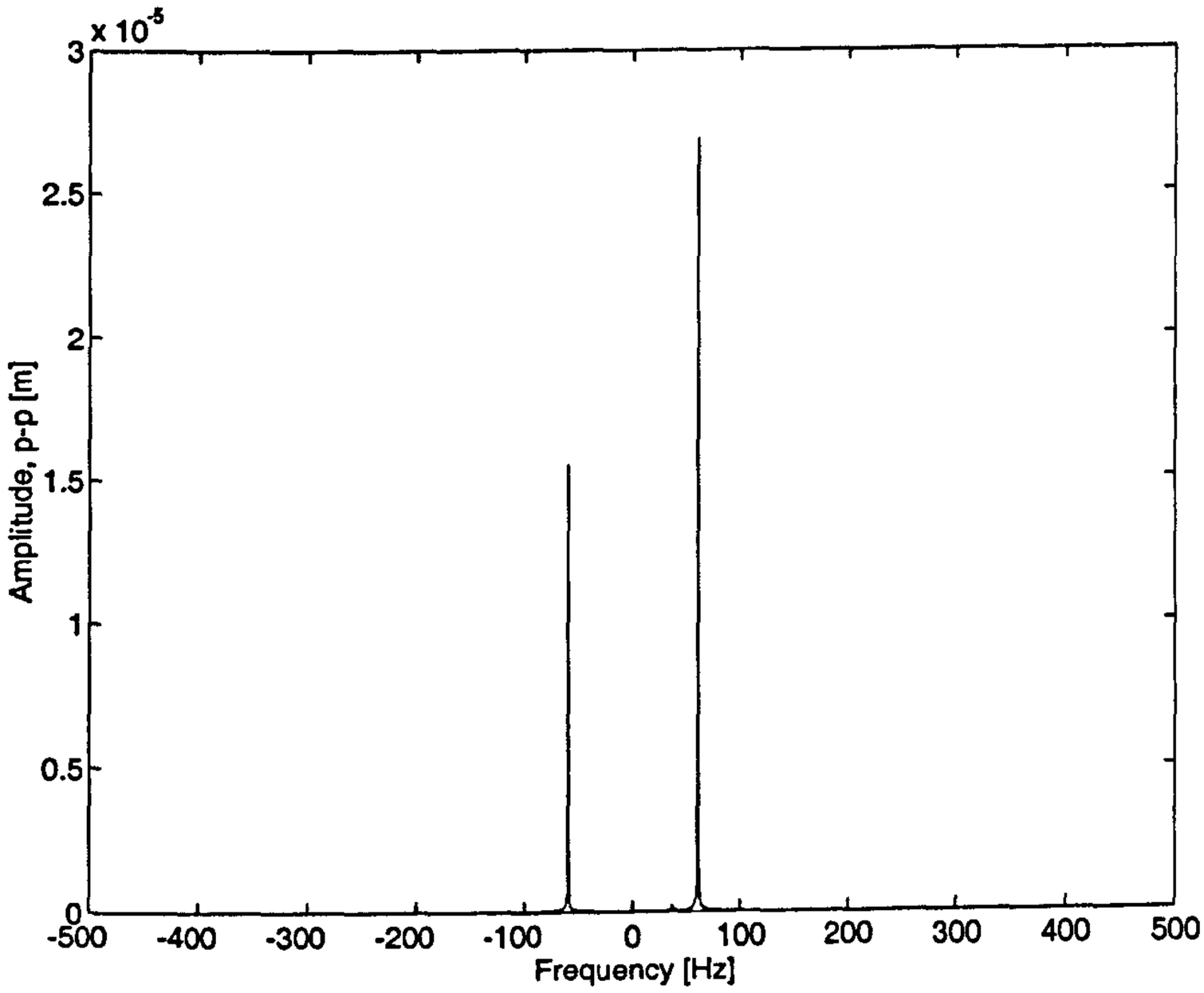
Fig 6.6.2-(a) & (b) show the orbit of a cracked rotor system and its frequency components. Unlike the case of an unbalanced rotor, the orbit of a cracked rotor exhibits quite a distortion due to a combination of shaft stiffness non-linearity (due to crack) and bearing stiffness anisotropy. As has already been identified in the transient vibration, strong $\pm 2\Omega$ and $\pm 3\Omega$ harmonics can be identified in addition to $\pm 1\Omega$ harmonics. As in the MDOF rotor system analysed in Chapter 3, the relative amplitude ratio of each crack-related harmonic component can be estimated to detect a crack after isolating the crack-related harmonics by applying DDVSA (directional-difference vibration signature analysis). In this case, i.e. the case of the HIP rotor system, the extended relationship should be applied to accommodate the effect of bearing stiffness anisotropy, i.e.:

$$\frac{S(\pm 1\Omega)_{\Delta j}}{S(\pm 1\Omega)_{\Delta k}} = \frac{S(\pm 2\Omega)_{\Delta j}}{S(\pm 2\Omega)_{\Delta k}} = \frac{S(\pm 3\Omega)_{\Delta j}}{S(\pm 3\Omega)_{\Delta k}} \tag{6.6.1}$$

Hence, by the estimation of the extended relationship with directional-difference harmonic components, the crack can be unambiguously identified as the crack has the relatively rapid growing property once it has been initiated.

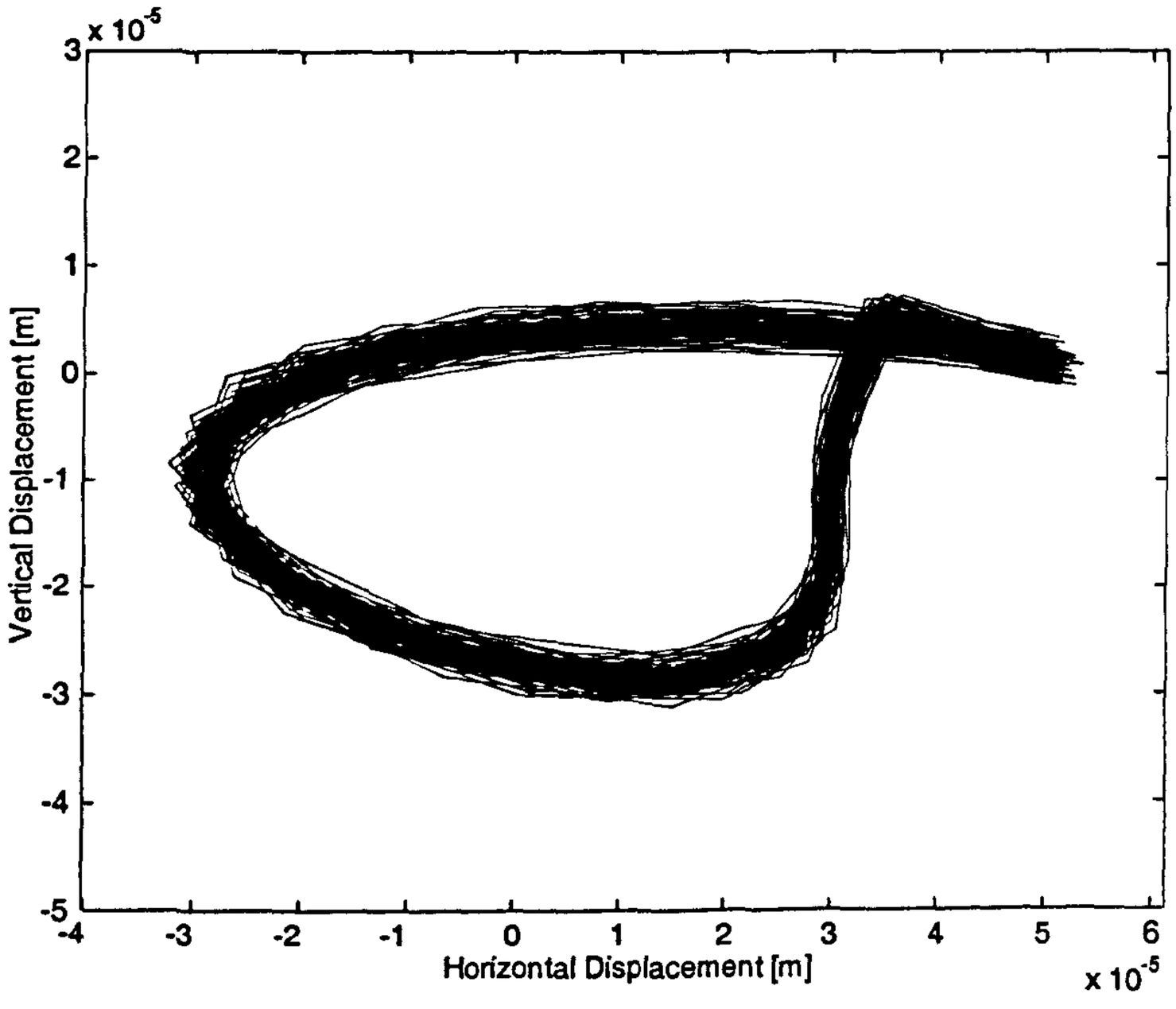


(a) Orbit

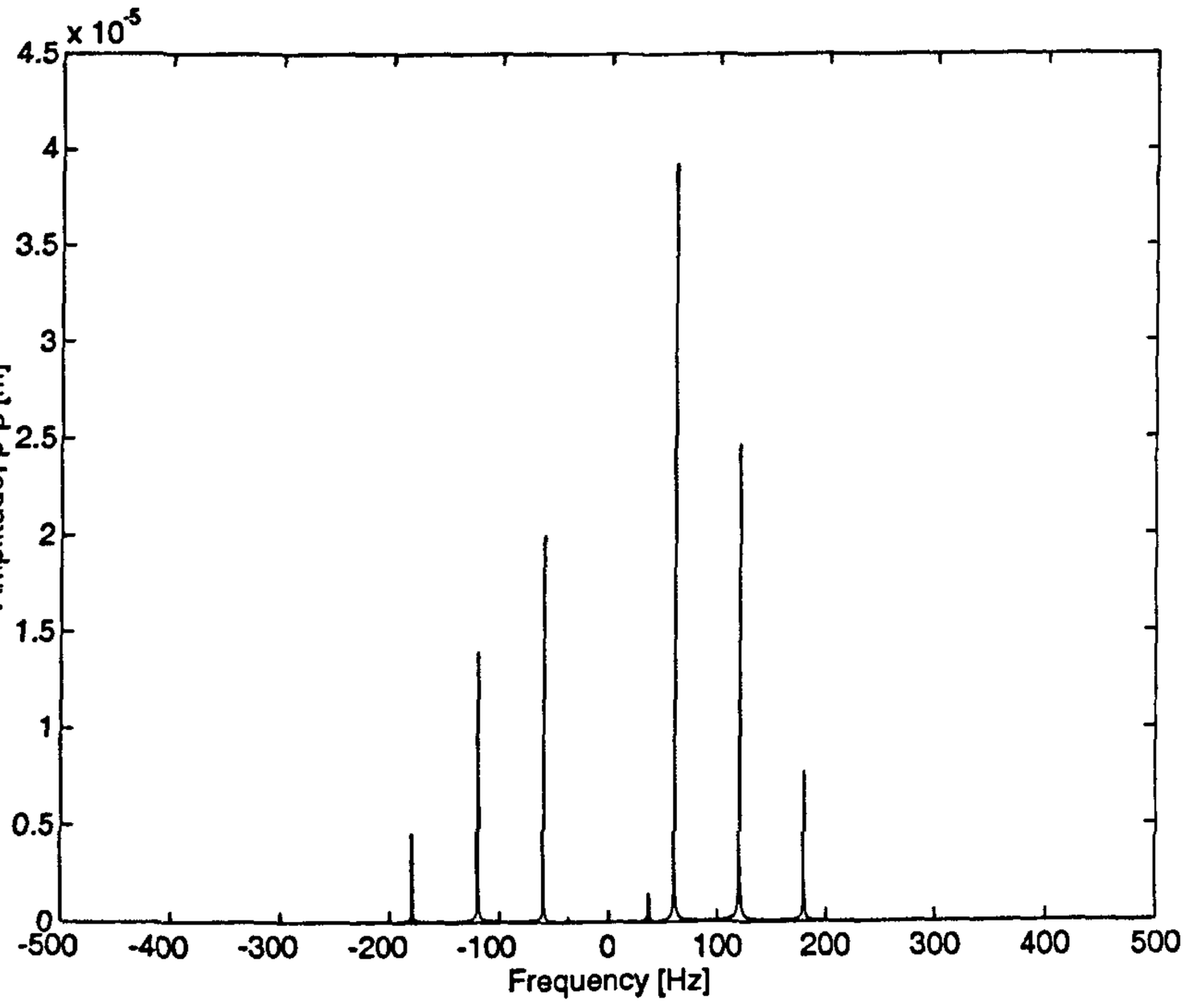


(b) Directional Frequency Spectrum

Fig 6.6.1 Unbalanced Rotor



(a) Orbit



(b) Directional Frequency Spectrum

Fig 6.6.2 Cracked Rotor (10 %)

6.7 Conclusions

The practical-applicability of the developed crack detection methods has been verified by demonstrating the improved performance with a numerical simulation based on the industrial 250 MW high & intermediate pressure (HIP) steam turbine rotor system, where the fluid-film bearings play a significant role in vibration characteristics due to strong bearing stiffness anisotropy and substantial damping.

To simulate the dynamic behaviour of the HIP turbine rotor system, the characteristics of fluid-film bearings have been investigated and the rotordynamic analysis code VARS (refer to Chapter 3) has been updated to incorporate the function of a complete modelling of any fluid-film bearing.

For transient vibration of a cracked HIP rotor, by applying the DHWT (Directional Harmonic Wavelet Transform), the crack-induced sub- and 1Ω-resonances can be clearly identified in the forward and backward directional wavelet maps, respectively. In particular, the considerable backward sub-resonance at $\Omega/\omega_n = 1/2$ caused by the -2Ω harmonic component has been identified to be invaluable information for crack detection as it will rarely exist in the vibration response of normal steam turbine rotors or hardly be generated by other common types of fault. Under the effect of a large amount of damping, the wavelet map could still detect the local changes (or resonances) caused by a crack successfully. Hence, it can be concluded that the technique can be applied to practical situations where the vibration is usually suppressed by the large amount of damping originating from the fluid-film bearings.

For steady-state vibration of a cracked HIP rotor, unlike the case of an unbalanced rotor which exhibits an elliptical orbit, quite a distorted orbit is expected due to combination of rotor stiffness non-linearity (due to crack) and bearing stiffness anisotropy. As has been found in the transient vibration case, strong $\pm 2\Omega$ and $\pm 3\Omega$

frequency components can be identified in addition to $\pm 1\Omega$ frequency components in the directional spectrum. In estimating the relative amplitude ratios of each directional-difference harmonic component for crack detection, the relationship of the harmonics amplitude ratio has been extended to accommodate the effect of bearing stiffness anisotropy. By estimating the extended relationship with crack-related directional-difference harmonic components, crack can be unambiguously identified as the crack has the relatively rapid growing property once it has been initiated.

Chapter 7
Conclusions

This chapter presents the overall conclusions and a summary of the specific contributions reported in this thesis. Also, recommendations for further research have been presented.

7.1 Conclusions

It is considered that the development of new crack detection methods for operating rotor systems need to reflect the industrial situation. For static structures, NDT techniques have been successfully applied for detecting and even for locating cracks. However, for most critical rotating machinery in the process industry, it is virtually impossible to apply these well-developed techniques, mainly due to inaccessibility under operating conditions. Usually, the instruments available for vibration measurements are only a pair of displacement probes at the bearing locations which are usually located at the ends of the shaft. Due to this fact, most crack detection techniques have been developed with the progress of signal processing techniques.

To date, it has been widely-accepted that the following items are the most promising symptoms which can be applied to detect cracks in operating rotor systems:

(i) crack-related harmonics for steady-state signals, and

(ii) resonances caused by the crack-related harmonics for run-up and run-down transient signals.

Among those options, existing crack detection strategies have been focused mainly on dealing with transient vibration data, rather than in the steady state, as more information is available in transient operating conditions. However, in analysing transient data, the methods based on existing signal processing techniques impose unwanted resolution problems in both time and frequency domains. Also, for steady-state conditions, the possibility of crack detection has always been limited by its reliance on the inspection of the 2Ω harmonic component caused by a crack, although considerable $\pm 1\Omega$ vibrations are also induced in the cracked rotor systems.

To overcome these limitations, two new methods have been developed in the present research for transient and steady-state conditions, respectively. For transient response data, the Directional Harmonic Wavelet Transform (DHWT) has been developed to improve the monitoring procedure for crack detection, based on harmonic wavelet transform theory. The performance of the DHWT has been demonstrated by application to the transient vibration response of the MDOF cracked rotor system. From the directional harmonic wavelet maps, the crack-related resonances could be clearly identified even with the existence of noise. Hence, the limitations imposed by the STFT, related to the resolution in the joint time-frequency domain, can be solved with this new method.

For steady-state conditions, that is, while the machine is operating at its designated speed, the most important indication of the presence of a crack is the initial appearance and/or a steady increase over time in $\pm 1\Omega$, 2Ω, 3Ω, and higher harmonics of lateral vibration. The appearance of an increase in $\pm 1\Omega$ and 2Ω harmonics is especially important because it is the main indication of the existence of a transverse crack. When a crack is relatively shallow, the increase in the 2Ω component is small

and is usually buried in the background noise. Probably due to this, the main concern in crack detection has focused on monitoring the crack-induced sub-resonances during the run-up or run-down periods. Furthermore, some finite levels of these harmonics are always present in rotating machines, even in a normal condition. To detect a crack using the crack-related harmonics, the other vibration components have to be eliminated from the overall vibration response. To isolate the crack-related harmonics from the overall vibration signature, an improved technique of vibration signature analysis called 'Directional-Difference Vibration Signature Analysis (DDVSA)' has been proposed and developed in this work. This technique enhances the conventional crack detection technique by using Directional-Difference Harmonics (DDH) and also by utilising predefined fault-related signatures obtained from an analytical model. This approach, in addition to reducing the effects of background noise, eliminates the harmonics which already exist in the normal rotor systems. By using 'directional-difference' information from the operating machines, it is possible to use both $\pm 1\Omega$ and 2Ω harmonics together as opposed to individually, as in the conventional approaches, which mainly rely on 2Ω harmonic component.

The enhanced performance of these new techniques has been shown via laboratory experiments with a 2-disk cracked rotor test rig. For transient data, the crack-induced resonances have been accurately detected by applying the DHWT, and for steady-state data, DDVSA enabled the isolation of crack-related harmonic components, leading to reliable crack detection. In both methods, the performance has been greatly enhanced by decomposing the vibration components from rotating machines into co- and counter-rotating components, which is a major feature that enables one to overcome the limitations of existing conventional methods.

Finally, the field-applicability of the developed methods has been confirmed by demonstrating the improved performance with the vibration data (simulated) for an industrial 250 MW high & intermediate pressure (HIP) steam turbine rotor model,

where the fluid-film bearings play an important role in vibration characteristics due to strong bearing stiffness anisotropy and substantial damping.

Throughout the research, it is concluded that the developed MDOF cracked rotor models are capable of accurately predicting the dynamic behaviour of cracked rotor systems, and the cracks in operating rotors can be identified reliably by applying the improved crack detection techniques (DHWT & DDVSA).

7.2 Summary of Comparison with Existing Methods

The following tables summarise comparison between the new methods (DHWT & DDVSA) and representative existing methods.

Table 7.2.1 Transient State

Feature/ Method	DHWT	HWT	DSTFT	STFT	WD
Directionality (FW/BW)	✓		✓		
High Resolution	✓	✓			✓
Sensitive to Local Changes	✓	✓			
Applicable to Rotating Machines	✓		✓		
Applicable to Long Time Data	✓	✓	✓	✓	

Table 7.2.2 Steady State

Feature/ Method	DDVSA	Imam et al [62]	Seibold et al [123]	Joh & Lee [67]	Bach & Markert [3]
Directionality (FW/BW)	✓			✓	
On-line	✓	✓	✓		✓
Unambiguous Detection	✓				
Crack Location			✓		✓
Data Type♦	TD/EE	TD/EE	TD/EA	FRF/EE	TD/AA

Notes for Table 7.2.2

[123] : limited to simple model & slow speed ($\Omega < 1000$ rpm)
[67] : requires controlled-excitation
[3] : restricted to simulation as yet

♦ Abbreviations used in Table 7.2.2

TD Time-Domain Response
FRF Frequency Response Function
EE Damaged Test/Undamaged Test Correlation
EA Damaged Test/Undamaged Analysis Correlation
AA Damaged Analysis/Undamaged Analysis Correlation

7.3 List of Contributions

The contributions made in this research can be briefly summarised as follows:

• Comparison of Cracked Rotor and Normal Rotor with Various Configurations

Comprehensive comparative research on the dynamic behaviour of cracked rotors and equivalent normal rotor systems with various different configurations (rotor asymmetry, bearing anisotropy, etc) has been performed to provide a basis for thorough understanding of the cracked rotor problem.

• Finite Element Modelling of Cracked Rotor

To overcome the limitations inherent in using simple rotor systems, a multi-degree-of-freedom (MDOF) rotor system with a transverse crack has been modelled based on the finite element method (FEM) and its dynamic characteristics have been investigated for both transient and steady-state conditions. Particularly, by positioning the crack at a node, the effect of the crack was more localised than the existing way of MDOF cracked rotor modelling where the crack is positioned at an element.

• Directional Harmonic Wavelet Transform

The Directional Harmonic Wavelet Transform Technique can accommodate the most characteristic feature of the rotating structures; namely, the existence of forward whirl and backward whirl components. With this new method, the local characteristics of non-stationary signals from rotating structures can be better observed by using the further-decomposed wavelets (even though wavelets are already decomposed from the original time signal), or directional-wavelets (FW Wavelet & BW Wavelet).

• Revisiting the Fast Fourier Transform

The classical FFT has been revisited, and the complex-data based FFT has been introduced as an effective way of obtaining the directional spectra. Also, the property of the complex-data based FFT has been explored in association with forward/backward whirl decomposition concept of rotordynamic theory on elliptical vibrations.

• Directional-Difference Vibration Signature Analysis

The DDVSA enables the use of synchronous harmonic component unlikely with existing methods. For industrial application, the systematic procedure for crack detection based on DDVSA has been presented and implemented with experimental data.

• Development of Data Acquisition System

A data acquisition system has been established for the experimental work. The subroutines enabling the data acquisition have been written in the MATLAB environment. They can control the data-capture of up to 16 channels at up to 100 kS/s (single-channel) simultaneously to the MATLAB workspace. The response channels can be low-pass filtered by a programmable, 8-pole, 16-channel filter with variable cut-off frequencies.

• Investigation of the Effect of Crack Location on Harmonics Sensitivity

The sensitivity of the crack-related harmonics has been investigated experimentally with different crack locations (thin slots made to simulate cracks at shaft mid-span and outboard, respectively). As has been predicted and discussed in the analytical

research, also in the experiments, when the crack is located near the bearing, the crack-related higher harmonics (2Ω, 3Ω, $\cdots$) were revealed to be more sensitive - compared with the mid-span cracked rotor - due to the effect of the support (or bearing) interacting with the rotor system.

• Investigation of the Effect of Unbalance on the Cracked Rotor System

By using various forms of trial mass as a controlled unbalance, the effect of unbalance on the cracked rotor has been investigated for 20 % crack in the steady-state condition. In all experimental cases attempted, the independence of crack-related higher harmonics and the unbalance-related 1Ω vibration component has been confirmed.

• Modelling of Fluid-film Bearings for Industrial Case Study

To accommodate the effect of the fluid-film bearings which support the HIP turbine rotor, a complete modelling of fluid-film bearings has been performed. For every rotation speed (or for every time step), the bearing coefficients can be estimated by the code which computes the working conditions of the bearings by solving a non-linear static problem and then linearising the behaviour of the bearing about the static equilibrium position.

• Modelling of HIP Steam Turbine Rotor System for Industrial Case Study

The 250 MW HIP (High & Intermediate Pressure) steam turbine rotor system has been modelled using the finite element method. A crack has been induced into the rotor and the dynamic behaviour has been analysed. In particular, the effect of fluid-film bearings has been investigated as the dynamic characteristics of such turbomachines are strongly influenced by the bearings on which the rotor operates.

7.4 Recommendations for Further Research

Regarding the further research on the identification of cracks in operating rotors, the following items would be recommended:

- Use of validated dynamic models for diagnostic purpose
- Development of expert systems for fault diagnosis of rotating machinery
- Identification of damping changes due to a crack, as an alternative parameter for crack detection

Also, the following items will be implemented by the author in the power industry:

- Application of DHWT to field vibration data
- Incorporation of DDVSA to the existing field vibration monitoring system

References

[1] Adams, R. D., Cawley, P., Pye, C. J., and Stone, B. J., *A vibration technique for non-destructively assessing the integrity of structures*, in Journal of Mechanical Engineering Science, IMechE, pp 93-100, 1978

[2] Allen, J. B. and Rabiner, L. R., *A unified approach to short-time Fourier analysis and synthesis*, in Proceedings of the IEEE, pp 1558-1564, 1977

[3] Bach, H. and Markert, R., *Determination of the fault position in rotors for the example of a transverse crack*, in International Workshop on Structural Health Monitoring, pp 325-335, 1997

[4] Bachschmid, N., Diana, G., and Pizzigoni, B., *The influence of unbalance on cracked rotors*, in International Conference on Vibrations in Rotating Machinery, IMechE, pp 193-198, 1984

[5] Bently, D. E. and Muszynska, A., *Detection of rotor cracks*, in Texas A&M Turbomachinery Symposium, pp 129-139, 1986

[6] Brutti, C., Salvini, P., Tripodi, P., and Vullo, V., *Theoretical analysis on dynamic behavior of cracked rotors*, in International Modal Analysis Conference, pp 976-981, 1984

[7] Bucher, I., Ewins, D. J., *Multidimensional decomposition of time-varying vibration response signals in rotating machinery*, in Journal of Mechanical Systems and Signal Processing, pp 577-601, 1997

[8] Bucher, I., Ewins, D. J., and Robb, D. A., *Modal testing of rotating structures: difficulties, assumptions, and practical approach*, in International Conference on Vibrations in Rotating Machinery, IMechE, pp 539-562, 1996

[9] Bucher, I., Ewins, D. J., Robb, D. A., and Schmiechen, P., *Multi-dimensional directional spectrograms and Campbell (ZMOD) diagrams for rotating machinery*, in ASME Design Engineering Technical Conferences, pp 1327-1334, 1995

[10] Bucher, I., Ewins, D. J., von Groll, G., and Schmiechen, P., *Directional and multi-dimensional spectrograms and Campbell diagrams: a diagnostic and surveillance tool for rotating machinery*, in International Conference on Acoustical & Vibratory Surveillance, Methods & Diagnostic Techniques, Society Française Ddes Mechanicies, pp 291-301, 1995

[11] Bucher, I. and Seibold, S., *Using combined temporal and spatial information in multi-hypothesis based damage detection*, in International Modal Analysis Conference, pp 870-876, 1997

[12] Cawley, P. and Adams, R. D., *The location of defects in structures from measurements of natural frequencies*, in Journal of Strain Analysis, pp 49-57, 1979

[13] Cawley, P. and Ray, R., *A comparison of the natural frequency changes produced by cracks and slots*, in Journal of Vibration, Acoustics, Stress, and Reliability in Design, pp 366-370, 1988

[14] Chen, Y. D., Du, R., and Qu, L. S., *Fault features of large rotating machinery and diagnosis using sensor fusion*, in Journal of Sound and Vibration, pp 227-242, 1995

[15] Childs, D., *Turbomachinery rotordynamics*, John Wiley & Sons, 1993

[16] Cohen, L., *Time-frequency distributions - a review*, in Proceedings of the IEEE, pp 941-981, 1989

[17] Collins, K. R., Plaut, R. H., and Wauer, J., *Detection of cracks in rotating Timoshenko shafts using axial impulses*, in Journal of Vibration and Acoustics, pp 74-78, 1991

[18] Darlow, M. S., Smalley, A. J., and Parkinson, A. G., *A unified approach to flexible rotor balancing: outline and experimental verification*, in International Conference on Vibrations in Rotating Machinery, IMechE, pp 437-444, 1980

[19] Davies, W. G. R., Lees, A. W., Mayes, I. W., Worsfold, J. H., and Crampton, F. J. P., *Vibrational problems in modern power station plant*, in International Conference on Vibrations in Rotating Machinery, IMechE, pp 215-222, 1976

[20] Davies, W. G. R. and Mayes, I. W., *The vibrational behavior of a multi-shaft, multi-bearing system in the presence of a propagating transverse crack*, in Journal of Vibration, Acoustics, Stress, and Reliability in Design, pp 146-153, 1984

[21] Diana, G., Bachschmid, N., and Angeli, F., *An on-line crack detection method for turbogenerator rotors*, in International Conference on Rotordynamics, JSME, pp 385-390, 1986

[22] Diana, G., Gasparetto, M., Cheli, F., Manenti, A., and Vania, A., *A diagnostic system to define malfunctioning conditions of a turbogenerator*, in International Conference on Rotordynamics, JSME, pp 367-372, 1986

[23] Dimarogonas, A. D., *Vibration of cracked structures: a state of the art review*, in Journal of Engineering Fracture Mechanics, pp 831-857, 1996

[24] Dimarogonas, A. D. and Massouros, G., *Torsional vibration of a shaft with a circumferential crack*, in Journal of Engineering Fracture Mechanics, pp 439-444, 1980

[25] Dimarogonas, A. D. and Paipetis, S. A., *Analytical methods in rotor dynamics*, Applied Science Publishers, pp 144-193, 1983

[26] Dimarogonas, A. D. and Papadopoulos, C. A., *Crack detection in turbine rotors*, in International Symposium on Transport Phenomena, Dynamics, and Design of Rotating Machinery, pp 227-239, 1988

[27] Dimarogonas, A. D. and Papadopoulos, C. A., *Vibration of cracked shafts in bending*, in Journal of Sound and Vibration, pp 583-593, 1983

[28] Doebelin, E. O., *Measurement systems: application and design*, McGraw-Hill, 1990

[29] Doebling, S. W., Farrar, C. R., Prime, M. B., and Shevitz, D. W., *Damage identification and health monitoring of structural and mechanical systems from changes in their vibration characteristics: a literature review*, in Los Alamos National Laboratory Report: LA-13070-MS, 1996

[30] Downham, E., *Vibration in rotating machinery: malfunction diagnosis - art & science*, in International Conference on Vibrations in Rotating Machinery, IMechE, pp 1-6, 1976

[31] Dynamic Testing Agency, *Primer on best practice in dynamic testing*, Chameleon Press, 1993

[32] Edwards, S., Lees, A. W., and Friswell, M. I., *Fault diagnosis of rotating machinery*, in Shock and Vibration Digest, pp 4-13, 1998

[33] Ehrich, F., *Handbook of rotordynamics*, McGraw-Hill, pp 4.40-4.66, 1992

[34] Ehrich, F., *Observations of subcritical superharmonic and chaotic response in rotordynamics*, in Journal of Vibration and Acoustics, pp 93-100, 1992

[35] Eisenmann, R. C. Sr. and Eisenmann, R. C. Jr., *Machinery malfunction diagnosis and correction*, Prentice-Hall, 1997

[36] Ewins, D. J., *Modal testing: theory and practice*, Research Studies Press, 1984

[37] Feldman, M. and Seibold, S., *Damage diagnosis of rotors: application of Hilbert transform and multihypothesis testing*, in Journal of Vibration and Control, pp 421-442, 1999

[38] Fox, C. H. J., *The location of defects in structures: a comparison of the use of natural frequency and mode shape data*, in International Modal Analysis Conference, pp 522-528, 1992

[39] Friswell, M. I., Penny, J. E. T., and Wilson, D. A. L., *Using vibration data and statistical measures to locate damage in structures*, in Journal of Analytical and Experimental Modal Analysis, pp 239-254, 1994

[40] Fritzen, C.-P., Seibold, S., and Buchen, D., *Application of filter techniques for damage detection in linear and nonlinear mechanical structures*, in International Modal Analysis Conference, pp 1874-1881, 1995

[41] Gasch, R., *A survey of the dynamic behaviour of a simple rotating shaft with a transverse crack*, in Journal of Sound and Vibration, pp 313-332, 1993

[42] Gasch, R., *Dynamic behaviour of a simple rotor with a cross-sectional crack*, in International Conference on Vibrations in Rotating Machinery, IMechE, pp 123-128, 1976

[43] Gasch, R., Person, M., and Weitz, B., *Dynamic behaviour of the Laval rotor with a cracked hollow shaft - a comparison of crack models*, in International Conference on Vibrations in Rotating Machinery, IMechE, pp 463-472, 1988

[44] Gasch, R. and Pfützner, H., *Rotordynamik eine einführung*, Springer-Verlag, 1975

[45] Genta, G., *A fast modal technique for the computation of the Campbell diagram of multi-degree-of-freedom rotors*, in Journal of Sound and Vibration, pp 385-402, 1992

[46] Genta, G., *Whirling of unsymmetrical rotors: a finite element approach based on complex co-ordinates*, in Journal of Sound and Vibration, pp 27-53, 1988

[47] Genta, G., Delprete, C., Tonoli, A., and Vadori, R., *Unbalance response of nonlinear asymmetric rotating systems*, in International Conference on Vibrations in Rotating Machinery, IMechE, pp 575-581, 1992

[48] Goldman, P. and Muszynska, A., *Application of full spectrum to rotating machinery diagnostics*, in Orbit, pp 17-21, March, 1999

[49] Grabowski, B., *The vibrational behavior of a turbine rotor containing a transverse crack*, in Journal of Mechanical Design, Vol. 102, pp 140-146, 1980

[50] Grabowski, B. and Mahrenholtz, O., *Theoretical and experimental investigations of shaft vibrations in turbomachinery excited by cracks*, in International Conference on Rotor Dynamics, IFToMM, pp 507-514, 1982

[51] Greenhill, L. M. and Cornejo, G. A., *Critical speeds resulting from unbalance excitation of backward whirl modes*, in ASME Design Engineering Technical Conferences, pp 991-1000, 1995

[52] Guang, M. and Gasch, R., *Stability and stability degree of a cracked flexible rotor supported on journal bearings*, in ASME Conference on Vibration of Rotating Systems, pp 305-323, 1993

[53] Hachmann, I. and Popp, K., *Detection of crack position and depth in rotating shafts*, in International Conference on Rotor Dynamics, IFToMM, pp 113-124, 1998

[54] Haisty, B. S., Duerr, R. E., and Springer, W. T., *Cracked beam modification element Part I: Theoretical Development*, in International Modal Analysis Conference, pp 1343-1348, 1988

[55] Haisty, B. S., Duerr, R. E., and Springer, W. T., *Cracked beam modification element Part II: Application*, in International Modal Analysis Conference, pp 1349-1354, 1988

[56] Hammond, J. K. and White, P. R., *The analysis of non-stationary signals using time-frequency methods*, in Journal of Sound and Vibration, pp 419-447, 1996

[57] He, J. and Ewins, D. J., *Analytical stiffness matrix correction using measured vibration modes*, in Journal of Analytical and Experimental Modal Analysis, pp 9-14, 1986

[58] Henry, T. A., *Monitoring rotating machinery to detect the growth of rotor cracks*, in Colloquium on the Design Applications and Maintenance of Large Industrial Drives, IEE, pp 37-44, 1978

[59] Henry, T. A. and Okah-Avae, B. E., *Vibrations in cracked shafts*, in International Conference on Vibrations in Rotating Machinery, IMechE, pp 15-19, 1976

[60] Huang, F. and Gu, S., *Application of high order cumulants to structure fault diagnosis*, in International Modal Analysis Conference, pp 1237-1240, 1993

[61] Huang, S. C., Huang, Y. M., and Shieh, S. M., *Vibration and stability of a rotating shaft containing a transverse crack*, in Journal of Sound and Vibration, pp 387-401, 1993

[62] Imam, I., Azzaro, S. H., Bankert, R. J., and Scheibel, J., *Development of an on-line rotor crack detection and monitoring system*, in Journal of Vibration, Acoustics, Stress, and Reliability in Design, pp 241-250, 1989

[63] Inagaki, T., Kanki, H., and Shiraki, K., *Response analysis of a general asymmetric rotor-bearing system*, in Journal of Mechanical Design, pp 147-157, 1980

[64] Inagaki, T., Kanki, H., and Shiraki, K., *Transverse vibrations of a general cracked rotor-bearing system*, in Journal of Mechanical Design, pp 345-355, 1982

[65] Ismail, F., Ibrahim, A., and Martin, H. R., *Identification of fatigue cracks from vibration testing*, in Journal of Sound and Vibration, pp 305-317, 1990

[66] Iwatsubo, T., Arii, S., and Oks, A., *Detection of a transverse crack in a rotor shaft by adding external force*, in International Conference on Vibrations in Rotating Machinery, IMechE, pp 275-282, 1992

[67] Joh, C.-Y. and Lee, C.-W., *Use of dFRFs for diagnosis of asymmetric/anisotropic properties in rotor-bearing system*, in Journal of Vibration and Acoustics, pp 64-69, 1996

[68] Jones, D. L. and Parks, T. W., *A resolution comparison of several time-frequency representations*, in IEEE Transactions on Signal Processing, pp 413-420, 1992

[69] Kam, T. Y. and Lee, T. Y., *Detection of cracks in structures using modal test data*, in Journal of Engineering Fracture Mechanics, pp 381-387, 1992

[70] Kavarana, F. H. and Kirk, R. G., *Cracked shaft detection using the unbalance excitation technique*, in Design Engineering Technical Conferences, pp 1001-1007, 1995

[71] Kiciñski, J. and Ostachowicz, W. M., *Nonlinear analysis of cracked rotors with multiple supports*, in Design Engineering Technical Conferences, pp 1283-1292, 1995

[72] Kim, J., *Lateral vibration analysis of turbine-rotor system using transfer matrix method*, MSc Thesis, Seoul National University, 1993

[73] Kim, J. and Ewins, D. J., *Monitoring transient vibrations in rotating machinery using wavelet analysis*, in International Workshop on Structural Health Monitoring, Stanford, USA, pp 287-297, September, 1999

[74] Kim, J. and Ewins, D. J., *Effect of crack locations on the vibration characteristics of MDOF rotor systems*, in International Conference on Noise and Vibration Engineering, Leuven, Belgium, September, 2000

[75] Knott, J. F., *Fundamentals of fracture mechanics*, Butterworth, 1973

[76] Kowal, M. G. and O'Brien, J. T. Jr., *Monitoring for shaft cracks on reactor recirculation pumps*, in Journal of Sound and Vibration, pp 12-17, 1989

[77] Krämer, E., *Dynamics of rotors and foundations*, Springer-Verlag, pp 329-347, 1993

[78] Kujath, M. R., *Identification of fractures in rotors*, in International Conference on Rotordynamics, JSME, pp 379-383, 1986

[79] Lalanne, M. and Ferraris, G., *Rotordynamics prediction in engineering*, John Wiley & Sons, 1998

[80] Lee, C.-W., *Vibration Analysis of Rotors*, Kluwer Academic Publishers, pp 296-303, 1993

[81] Liebowitz, H. and Claus, W. D., *Failure of notched columns*, in Journal of Engineering Fracture Mechanics, pp 379-383, 1968

[82] Liebowitz, H., Vanderveldt, H., and Harris, D. W., *Carrying capacity of notched column*, in Journal of Solids and Structures, pp 489-500, 1967

[83] Lin, R. M. and Ewins, D. J., *On the location of structural nonlinearity from modal testing - a feasibility study*, in International Modal Analysis Conference, pp 358-364, 1990

[84] Liu, B., Ling, S.-F., and Meng, Q, *Machinery diagnosis based on wavelet packets*, in Journal of Vibration and Control, pp 5-17, 1997

[85] MARS Project Final Technical Report, *Development of validated structural dynamic modelling and testing techniques for vibration predictions in rotating machinery*, 1996

[86] Mayes, I. W. and Davies, W. G. R., *A method of calculating the vibrational behaviour of coupled rotating shafts containing a transverse crack*, in International Conference on Vibrations in Rotating Machinery, IMechE, pp 17-27, 1980

[87] Mayes, I. W. and Davies, W. G. R., *Analysis of the response of a multi-rotor-bearing system containing a transverse crack in a rotor*, in Journal of Vibration, Acoustics, Stress, and Reliability in Design, pp 139-145, 1984

[88] Mayes, I. W. and Davies, W. G. R., *The vibrational behaviour of a rotating shaft system containing a transverse crack*, in International Conference on Vibrations in Rotating Machinery, IMechE, pp 53-64, 1976

[89] McFadden, P. D. and Wang, W. J., *Analysis of gear vibration signatures by the weighted Wigner-Ville distribution*, in International Conference on Vibrations in Rotating Machinery, IMechE, pp 387-393, 1992

[90] McGuire, P. M. and Price, D. W., *The development and practical application of rotordynamic analysis techniques for large steam turbine generators*, in International Conference on Vibrations in Rotating Machinery, IMechE, pp 655-664, 1988

[91] Mitchell, J. S., *Introduction to machinery analysis and monitoring*, Pennwell Books, 1993

[92] Moss, J. C. and Hammond, J. K., *A comparison between the modified spectrogram and the pseudo-Wigner-Ville distribution with and without modification*, in Journal of Mechanical Systems and Signal Processing, pp 243-258, 1994

[93] Muszynska, A., *Modal testing of rotor/bearing systems*, in Journal of Analytical and Experimental Modal Analysis, pp 15-34, 1986

[94] Muszynska, A., *Shaft crack detection*, in Machinery Dynamics Seminar, Canada, 1982

[95] Muszynska, A., Goldman, P., and Bently, D. E., *Torsional/lateral vibration cross-coupled responses due to shaft anisotropy: a new tool in shaft crack detection*, in International Conference on Vibrations in Rotating Machinery, IMechE, pp 257-262, 1992

[96] Natke, H. G. and Cempel, C., *Model-aided diagnosis of mechanical systems*, Springer, pp 210-213, 1997

[97] Nelson, H. D. and Nataraj, C., *The dynamics of a rotor system with a cracked shaft*, in Journal of Vibration, Acoustics, Stress, and Reliability in Design, pp 189-196, 1986

[98] Newland, D. E., *An introduction to random vibrations, spectral & wavelet analysis*, Longman, 1993

[99] Nilsson, L. R. K., *On the vibration behaviour of a cracked rotor-bearing system*, in International Conference on Rotor Dynamics, IFToMM, pp 515-524, 1982

[100] Nordmann, R. and Schöllhorn, K., *Identification of stiffness and damping coefficients of journal bearings by means of the impact method*, in International Conference on Vibrations in Rotating Machinery, IMechE, pp 231-238, 1980

[101] Pandey, A. K., Biswas, M., and Samman, M. M., *Damage detection from changes in curvature mode shapes*, in Journal of Sound and Vibration, pp 321-332, 1991

[102] Papadopoulos, C. A. and Dimarogonas, A. D., *Coupled longitudinal and bending vibrations of a cracked shaft*, in Journal of Vibration, Acoustics, Stress, and Reliability in Design, pp 1-8, 1988

[103] Papadopoulos, C. A. and Dimarogonas, A. D., *Coupled longitudinal and bending vibrations of a rotating shaft with an open crack*, in Journal of Sound and Vibration, pp 81-93, 1987

[104] Papadopoulos, C. A. and Dimarogonas, A. D., *Coupled vibration of cracked shafts*, in Journal of Vibration and Acoustics, pp 461-467, 1992

[105] Papadopoulos, C. A. and Dimarogonas, A. D., *Coupling of bending and torsional vibration of a cracked Timoshenko shaft*, in Ingenieur-Archiv, pp 257-266, 1987

[106] Papadopoulos, C. A. and Dimarogonas, A. D., *Stability of cracked rotors in the coupled vibration mode*, in Journal of Vibration, Acoustics, Stress, and Reliability in Design, pp 356-359, 1988

[107] Petroski, H. J., *Simple static and dynamic models for the cracked elastic beam*, in Journal of Fracture, pp 71-76, 1981

[108] Pusey, H. C., *Turbomachinery condition monitoring and failure prognosis technology*, in Sound and Vibration, pp 28-33, 1999

[109] Qian, G.-L., Gu, S.-N., and Jiang, J.-S., *The dynamic behaviour and crack detection of a beam with a crack*, in Journal of Sound and Vibration, pp 233-243, 1990

[110] Rajab, M. D. and Al-Sabeeh, A., *Vibrational characteristics of cracked shafts*, in Journal of Sound and Vibration, pp 465-473, 1991

[111] Randall, R. B., *Frequency analysis*, Brüel & Kjær, 1987

[112] Randall, R. B., *Hilbert transform techniques in machine diagnostics*, in International Conference on Rotordynamics, JSME, pp 409-414, 1986

[113] Rao, J. S., *Rotor Dynamics*, John Wiley & Sons, pp 187-195, 1991

[114] Ratan, S., Baruh, H., and Rodriguez, J., *On-line identification and location of rotor cracks*, in Journal of Sound and Vibration, pp 67-82, 1996

[115] Rice, J. R. and Levy, N., *The part-through surface crack in an elastic plate*, in Journal of Applied Mechanics, pp 185-194, 1972

[116] Richman, M. S., Parks, T. W., and Shenoy, R. G., *Discrete-time, discrete-frequency, time-frequency analysis*, in IEEE Transactions on Signal Processing, pp 1517-1527, 1998

[117] Rizos, P. F., Aspragathos, N., and Dimarogonas, A. D., *Identification of crack location and magnitude in a cantilever beam from the vibration modes*, in Journal of Sound and Vibration, pp 381-388, 1990

[118] Salawu, O. S. and Williams, C., *Structural damage detection using experimental modal analysis - A comparison of some methods*, in International Modal Analysis Conference, pp 254-260, 1993

[119] Sanderson, A. F. P., *The vibration behaviour of a large steam turbine generator during crack propagation through the generator rotor*, in International Conference on Vibrations in Rotating Machinery, IMechE, pp 263-273, 1992

[120] Schmalhorst, B. K., *Numerical simulation of cracked rotor's vibrations due to measured crack shapes*, in International Symposium on Transport Phenomena, Dynamics, and Design of Rotating Machinery, Part II, pp 211-225, 1988

[121] Schmied, J. and Krämer, E., *Vibrational behaviour of a rotor with a cross-sectional crack*, in International Conference on Vibrations in Rotating Machinery, IMechE, pp 183-192, 1984

[122] Seibold, S., *A multi-hypothesis approach to damage detection of rotating machinery*, in International Modal Analysis Conference, pp 863-869, 1997

[123] Seibold, S., Fritzen, C.-P., and Wagner, D., *Employing identification procedures for the detection of cracks in rotors*, in International Modal Analysis Conference, pp 1378-1384, 1995

[124] Seibold, S. and Weinert, K., *A time domain method for the localisation of cracks in rotors*, in Journal of Sound and Vibration, pp 57-73, 1996

[125] Sekhar, A. S., *Vibration characteristics of a cracked rotor with two open cracks*, in Journal of Sound and Vibration, pp 497-512, 1999

[126] Sekhar, A. S. and Prabhu, B. S., *Crack detection and vibration characteristics of cracked shafts*, in Journal of Sound and Vibration, pp 375-381, 1992

[127] Sekhar, A. S. and Prabhu, B. S., *Transient analysis of a cracked rotor passing through critical speed*, in Journal of Sound and Vibration, pp 415-421, 1994

[128] Sekhar, A. S. and Prabhu, B. S., *Vibration and stress fluctuation in cracked shafts*, in Journal of Sound and Vibration, pp 655-667, 1994

[129] Sekhar, A. S. and Prasad, P. B., *Dynamic analysis of a rotor system considering a slant crack in the shaft*, in Journal of Sound and Vibration, pp 457-474, 1997

[130] Shannon, R. A., *ADRE for Windows and full spectrum plots*, in Orbit, pp 29-31, March, 1999

[131] Shatoff, J., *Using vibration analysis to determine the dynamic health of turbine/generators*, in Power, pp 23-28, May, 1976

[132] Smith, D. M., *Recognition of the causes of rotor vibration in turbomachinery*, in International Conference on Vibrations in Rotating Machinery, IMechE, pp 1-4, 1980

[133] Someya, T., *Journal-bearing databook*, Springer-Verlag, 1988

[134] Southgate, C. B. and Tur, H., *Trouble shooting using modal testing - the case of the cracked centrifuge*, in International Modal Analysis conference, pp 1270-1276, 1988

[135] Söffker, D., Bajkowski, J., and Müller, P. C., *Crack detection in turbo rotors: vibration analysis and fault detection*, in ASME Conference on Vibration of Rotating Systems, pp 277-287, 1993

[136] Stewart, R. M., *Vibration analysis as an aid to the detection and diagnosis of faults in rotating machinery*, in International Conference on Vibrations in Rotating Machinery, IMechE, pp 223-229, 1976

[137] Sundermeyer, J. N. and Weaver, R. L., *On crack identification and characterization in a beam by non-linear vibration analysis*, in Journal of Sound and Vibration, pp 857-871, 1995

[138] Theis, W., *Längs- und torsionsschwingungen bei quer angerissenen rotoren: untersuchungen auf der grundlage eines rißmodells mit 6 balken-freiheitsgraden*, Reihe 11: Schwingungstechnik, Nr. 131, VDI Verlag, 1990

[139] Thomas, D. L., *Turbine generator vibration monitoring in the CEGB*, in International Conference on Rotordynamics, JSME, pp 361-366, 1986

[140] Thomas, D. L., *Vibration monitoring strategy for large turbogenerators*, in International Conference on Vibrations in Rotating Machinery, IMechE, pp 91-99, 1984

[141] Tondl, A., *Some problems of rotor dynamics*, Chapman & Hall, pp 70-113, 1965

[142] Vance, J. M., *Rotordynamics of turbomachinery*, John Wiley & Sons, 1987

[143] Wang, W. and Kirkhope, J., *New eigensolutions and modal analysis for gyroscopic/rotor systems, part 1: undamped systems*, in Journal of Sound and Vibration, pp 159-170, 1994

[144] Wang, W. and Kirkhope, J., *New eigensolutions and modal analysis for gyroscopic/rotor systems, part 2: perturbation analysis for damped systems*, in Journal of Sound and Vibration, pp 171-183, 1994

[145] Wauer, J., *Modelling and formulation of equations of motion for cracked rotating shafts*, in Journal of Solids and Structures, pp 901-914, 1990

[146] Wauer, J., *On the dynamics of cracked rotors: a literature survey*, in Journal of Applied Mechanics Reviews, pp 13-17, 1990

[147] Weaver, W. Jr., Timoshenko, S. P., and Young, D. H., *Vibration problems in engineering*, John Wiley & Sons, pp 474-478, 1990

[148] White, M. F., *Fault diagnosis in rotating machinery*, in International Conference on Rotordynamics, JSME, pp 391-395, 1986

[149] Wowk, V., *Machinery Vibration: Measurement & Analysis*, McGraw-Hill, 1991

[150] Xie, Y. M., *An assessment of time integration schemes for non-linear dynamic equations*, in Journal of Sound and Vibration, pp 321-331, 1996

[151] Yuen, M. M. F., *A numerical study of the eigenparameters of a damaged cantilever*, in Journal of Sound and Vibration, pp 301-310, 1985